Departamento de Física
Facultad de Ciencias Naturales y Exactas
Universidad del Valle
Ciudad Universitaria Meléndez

EXPLORATIONS IN THE DARK SIDE OF THE UNIVERSE

Universidad del Valle

Doctoral Candidate:
John Bayron Orjuela-Quintana

Supervisor: **César Alonso Valenzuela-Toledo**

EXPLORATIONS IN THE DARK SIDE OF THE UNIVERSE

JOHN BAYRON ORJUELA QUINTANA

THESIS DIRECTED BY:
CÉSAR ALONSO VALENZUELA-TOLEDO

A thesis submitted in partial fulfillment of the requirements for the degree of
Philosophy Doctor in SCIENCES - PHYSICS

May, 2024

Dedication

To my honey, my mommy, my supervisor...

I am a dreamer, they are my feet on earth...

Bayron

Preface

Outline

Throughout history, humans have exhibited an inexhaustible curiosity about their environment, its components, and abstractions. Science is the humankind instrument to convert this curiosity into knowledge. When the acquired knowledge is mastered, it evolves into wisdom. This practice has been the primary force propelling human progress since ancient times.

From the earliest advancements in geometry, arithmetic, and mechanics inscribed on stone tablets, laying the groundwork for architectural marvels, to the principles underpinning relativity and quantum mechanics, upon which technologies like the geo-positioning system (GPS) and magnetic resonance imaging (MRI) rely, science has never been the foremost priority of any civilization. However, while only a handful of passionate individuals have genuinely appreciated and delved into the sciences and their accomplishments, the fruits of their endeavors have benefited countless others. The contributions of these dedicated scientists have greatly enriched the vast reservoir of knowledge and wisdom that we now possess.

Cosmology, the exploration of our Universe as a physical system encompassing its origin, evolution, and ultimate fate, has been a source of fascination for numerous scientists. While we have reached a point where we possess paradigms to construct instruments for observation and theories to interpret much of the observable Universe, several details remain elusive, such as the principles behind the existence of dark matter and dark energy. As a cosmologist in 2024, with aspirations to attain a doctoral degree in Physics, I find myself pondering: "How can I honor the tireless efforts of my predecessors and current colleagues while contributing to the advancement of cosmology?" Regrettably, I have yet to discover a definitive answer to this question. Therefore, during my postgraduate studies, I have resolved to delve deeply into various topics, seeking novel techniques and approaches to unravel the profound mysteries of our Universe.

This dissertation comprises five chapters, each covering the topics I explored during my doctoral studies.

1. **Historical Introduction**
    - A concise overview of some of the most significant achievements by cosmologists spanning nearly a century following Albert Einstein's seminal paper, where the nascent general relativity theory was applied to formulate one of the first models of our Universe.
2. **Dark Energy**

- After introducing the concept of dark energy and its contemporary relevance, we will present some of the most pertinent techniques employed to investigate novel models of dark energy and explore their cosmological consequences. This chapter draws upon the following works:[1]

  [1] M. Álvarez, **J. B. Orjuela-Quintana**, Y. Rodriguez and C. A. Valenzuela-Toledo, *Einstein Yang-Mills Higgs dark energy revisited*, Class. Quant. Grav. **36**, 195004 (2019).

  [2] **J. B. Orjuela-Quintana**, M. Álvarez, C. A. Valenzuela-Toledo and Y. Rodriguez, *Anisotropic Einstein Yang-Mills Higgs Dark Energy*, JCAP **10**, 019 (2020).

  [3] A. Guarnizo, **J. B. Orjuela-Quintana** and C. A. Valenzuela-Toledo, *Dynamical analysis of cosmological models with non-Abelian gauge vector fields*, Phys. Rev. D **102**, no.8, 083507 (2020).

  [4] J. Motoa-Manzano, **J. Bayron Orjuela-Quintana**, T. S. Pereira and C. A. Valenzuela-Toledo, *Anisotropic solid dark energy*, Phys. Dark Univ. **32**, 100806 (2021).

  [5] **J. B. Orjuela-Quintana** and C. A. Valenzuela-Toledo, *Anisotropic k-essence*, Phys. Dark Univ. **33**, 100857 (2021).

  [6] S. García-Serna, **J. B. Orjuela-Quintana**, C. A. Valenzuela-Toledo and H. Ocampo-Durán, *Reconstructing the parameter space of nonanalytical cosmological fixed points*, Int. J. Mod. Phys. D **32**, no.11, 2350073 (2023).

  [7] D. Gallego, **J. B. Orjuela-Quintana** and C. A. Valenzuela-Toledo, *Anisotropic Dark Energy from String Compactifications*, JHEP **04** 131 (2024).

3. **Modified Gravity**

- The chapter thoroughly examines the most general Lagrangian incorporating second-order equations in terms of the metric, a scalar field, and a vector field, and several approximation schemes at the linear perturbative level. This analysis is grounded in the following references:

  [8] W. Cardona, **J. B. Orjuela-Quintana** and C. A. Valenzuela-Toledo, *An effective fluid description of scalar-vector-tensor theories under the sub-horizon and quasi-static approximations*, JCAP **08**, 059 (2022).

  [9] **J. B. Orjuela-Quintana** and S. Nesseris, *Tracking the validity of the quasi-static and sub-horizon approximations in modified gravity*, JCAP **08**, 019 (2023).

[1] The names of the co-authors are hyperlinked to their respective InSPIRE profiles.

4. **Inflation**

    - While the prevailing cosmological paradigm supports the inflationary theory, certain intricacies of this theory still elude complete understanding. This chapter draws upon:

        [3] A. Guarnizo, **J. B. Orjuela-Quintana** and C. A. Valenzuela-Toledo, *Dynamical analysis of cosmological models with non-Abelian gauge vector fields*, Phys. Rev. D **102**, no.8, 083507 (2020).

        [10] J. C. Bueno Sanchez, **J. B. Orjuela-Quintana** and C. A. Valenzuela-Toledo, *On the coupling of vector fields to the Gauss-Bonnet invariant*, Rev. Acad. Colomb. Cienc. Ex. Fis. Nat. **45**, 67-82 (2021).

5. **Machine Learning**

    - Machine learning has garnered significant attention from many cosmologists owing to its versatility. In this chapter, we explore its applications in symbolic regression problems. This chapter is based on:

        [11] **J. B. Orjuela-Quintana**, S. Nesseris and W. Cardona, *Using machine learning to compress the matter transfer function $T(k)$*, Phys. Rev. D **107**, no.8, 08 (2023).

        [12] **J. B. Orjuela-Quintana**, S. Nesseris and D. Sapone, *Machine learning unveils the linear matter power spectrum of modified gravity*, Phys. Rev. D **106**, no.6, 06 (2024)

6. **Concluding Remarks and Outlooks**

    - Concluding remarks concerning the work done during my studies, and perspectives for further developments related to my career.

Given the structure of this dissertation, numerous details will be omitted, and only the primary conclusions will be presented. Interested readers can find further information in the corresponding published works.

Keywords: Cosmology, Dark Energy, Modified Gravity, Inflation, Machine Learning.

Acknowledgements

Financial and facilities support undoubtedly plays a vital role in advancing scientific endeavors. I extend appreciation to all grant providers and Institutions who supported my dissertation research, enabling scientific exploration and discovery:

1. COLCIENCIAS–DAAD—110278258747 RC- 774-2017.

2. COLCIENCIAS—123365843539 RC-FP44842-081-2014.

3. COLCIENCIAS—110671250405 RC-FP44842-103-2016.

4. Vicerrectoría de Investigaciones - Universidad del Valle Grant No. 71220.

5. Patrimonio Autónomo - Fondo Nacional de Financiamiento para la Ciencia, la Tecnología y la Innovación Francisco José de Caldas (MINCIENCIAS - COLOMBIA) Grant No. 110685269447 RC-80740-465-2020, projects 69723 and 69553.

6. Departamento de Física, Universidade Estadual de Londrina.

7. Instituto de Física Téorica UAM-CSIC, in Universidad Autonóma de Madrid.

Contents

Chapter1

Cosmology: History and Current Understanding

The field of cosmology as a physical science is relatively recent. Prior to the remarkable observational breakthroughs at the end of the past century, cosmological theories were largely speculative, grounded in intuitive reasoning. Ranging from religious interpretations to mathematical constructs within the paradigms of Newtonian mechanics or General Relativity (GR), these theories lacked empirical validation. Observational evidence was limited to discerning the dynamics of the Universe primarily within the nearest extragalactic systems.

During a period marked by intense astronomical exploration, E. Hubble's groundbreaking discovery of the expansion of the Universe in 1929 marked a significant milestone [13]. Prior to Hubble's announcement, the prevailing model, introduced by A. Einstein in 1917 [14], depicted an infinite Universe characterized by a homogeneous, isotropic, and quasi-static distribution of matter, where gravity's attractive force was counterbalanced by the cosmological constant Λ. However, alternative proposals emerged soon after Einstein's pioneering work. W. de-Sitter, for instance, identified vacuum solutions within GR that pointed to an expanding Universe [15–17]. Between 1922 and 1924, A. A. Friedman delineated solutions depicting expanding universes with unbounded open geometries and closed geometries, the latter characterized by expansion to a maximum radius followed by collapse to a singularity [18, 19]. G. Lemaître demonstrated that Friedman's solutions yielded a linear velocity-distance relation locally, suggesting that the recession of astronomical objects could be attributed to the cosmic expansion [20].

Hubble's revelation of an expanding Universe is a milestone in the history of cosmology. By 1935, H. P. Robertson [21–23] and A. Walker [24] independently established that the metric for a homogeneous and isotropic Universe must adhere to the form:

$$ds^2 = -dt^2 + a^2(t)\left(\frac{dr^2}{1-Kr^2} + r^2d\theta^2 + \sin^2\theta d\phi^2\right) \tag{1.0.1}$$

where (r, θ, ϕ) denote the standard spherical coordinates, $K = -1, 0, 1$ distinguishes between open, flat, and closed geometries, and the dynamics of expansion are encapsulated in the scale factor $a(t)$.

Another significant leap forward came with the discovery of the cosmic microwave background (CMB). The origin of the chemical elements was supposed to have occurred in an epoch when the Universe was extremely hot and dense, as needed for the nucleosynthesis to take place. This scenario, known as the Big-Bang model, required that the early universe was dominated by radiation. The Universe cools as it is expanding and eventually, the radiation fluid would decouple from the first atoms and follow free paths. These primordial photons should be present in the Universe today as a nearly isotropic thermal background following a black body distribution whose temperature was estimated to be around 5 K [25–29]. This Big-Bang relic was found serendipitously by A. Penzias and R. Wilson in 1965. Penzias and Wilson were employed by Bell Laboratories to investigate radio transmissions from communication satellites. However, they found a persistent "excess antenna temperature" isotropically distributed about 3.5 K at 7.35 cm [30]. R. Dicke and his collaborators visited Penzias and Wilson at Bell Labs and correctly recognized the "problem" as the missing piece of the Big-Bang puzzle, the CMB [31].

With the identification of the CMB, the Copernican principle expanded to cosmological scales, asserting that we are not privileged observers within the Universe. This assumption, known as the cosmological principle, posits that the Universe is homogeneous and isotropic, the same around each point in every direction, on cosmological scales, rendering our observations objective. This assertion, once a hypothesis, became an empirical reality. Notably, Penzias and Wilson's work marked the first cosmological breakthrough to be honored with a Nobel Prize, highlighting the transformative impact of their discovery. During Hubble's times, astronomy and cosmology were not yet fully recognized as branches of physics, which contributed to Hubble not being considered for the Nobel Prize despite his monumental contributions. It wasn't until the late 1950s that these fields gained acceptance, by which time Hubble had passed away, and the Nobel Prize cannot be awarded posthumously.

The Cosmic Background Explorer (COBE), launched by NASA in 1989, marked the first dedicated space mission aimed at studying the CMB. In 1992, the teams overseeing the Differential Microwave Radiometer (DMR) and the Far Infrared Absolute Spectrophotometer (FIRAS) experiments aboard the COBE satellite reported significant findings regarding the CMB. They revealed that the CMB constitutes a thermal bath of photons at approximately 2.7 K, with slight fluctuations or anisotropies on the order of 10^{-5} [32, 33]. For their pioneering work, the leaders of these experiments, G. Smoot and J. C. Mather, were awarded the Nobel Prize in 2006, with the committee acknowledging that "these measurements [COBE-project] also marked the inception of cosmology as a precise science" [34]. Moreover, the COBE team reported a spectral index of the temperature power spectrum around 1, offering initial confirmation of predictions stemming from inflationary cosmology.

Numerous other discoveries and observations have played pivotal roles in advancing cosmology. These include the identification of dark matter [35–37], the observation of baryonic acoustic oscillations [38], the determination of the Universe's age [39], the confirmation of spatial flatness [40], and the mapping of galaxy distributions on large scales by projects like the Sloan Digital Sky Survey [41].

Of particular significance are the observations on supernovae, which revealed the accelerated expansion of the Universe. Independently, the High-z Supernova Search Team, led by B. P. Schmidt and A. Riess, and the Supernova Cosmology Project, led by S. Perlmutter, made this groundbreaking discovery [42, 43]. This finding suggested two potential explanations: the presence of an exotic cosmological fluid with negative pressure, termed dark energy, capable of exerting a repulsive gravitational force, or the limitations of General Relativity at cosmological scales. In recognition of their contributions, the leaders of these projects were awarded the Nobel Prize in 2011.

Future missions, such as the Cosmic Origins Explorer (CORE) by the European Space Agency (ESA), and Pixie and LiteBIRD by NASA, are poised to explore these mysteries further [44–46]. Additionally, projects like Euclid by ESA and the Dark Energy Spectroscopic Instrument (DESI) aim to measure various cosmological parameters with unprecedented precision [47, 48]. These endeavors promise to deepen our understanding of the cosmos and address lingering questions in the field of cosmology.

The profound importance of Cosmology in driving forward contemporary fundamental physics is evident through the multitude of esteemed prizes bestowed upon contributions in this field, such as the Gruber Prize and the Breakthrough Prize in Fundamental Physics. Of particular note is the 2019 Nobel Prize conferred upon Jim Peebles for his "theoretical discoveries in physical cosmology." Additionally, substantial resources are allocated to observational and theoretical projects, further underscoring the significance and impact of Cosmology in scientific advancement.

We find ourselves amidst what is often termed the "Golden Era" of cosmology, a period ripe with opportunity to delve into one of humanity's most ancient inquiries: What is the Universe?

CHAPTER 2

Dark Energy

2.1 Introduction

The current Universe is expanding at an accelerated rate. This fact was first discovered in type Ia supernovae (SNe Ia) surveys [49–51] and later confirmed by several other observations like large scale structures (LSS) [52, 53], cosmic microwave background (CMB) [39, 54], and baryon acoustic oscillations (BAO) measurements [55, 56]. Observations also show that our expanding Universe is highly homogeneous, isotropic and spatially flat at cosmological scales [57–59]. However, the origin of this accelerated expansion is yet to be known.

This phenomenon resurrected the Einstein's *"biggest blunder"* and has consolidated the cosmological constant Λ as a key element in the best cosmological description of our Universe: the Standard Cosmological Model [60]. In this standard model, nearly 95% of the energy budget of the Universe is distributed between two components, around 25% is attributed to a cold dark matter (CDM) component, while 70% is in the form of Λ which is the responsible for speeding up the expansion rate. The homogeneous and isotropic background geometry is described by the flat Friedman-Lemaître-Robertson-Walker (FLRW) metric.

Despite its general success, however, there are still some challenges that the standard cosmological model, also known as ΛCDM, has to overcome in order to become the correct theory describing the cosmological evolution of our Universe. One of the theoretical difficulties is the own nature of Λ, since if it is associated with the vacuum energy density of the Universe, the value predicted by the theory and the value obtained from observations differs by several tens orders of magnitude [61, 62]. This is known as the cosmological constant problem. On the observational side, pretty interesting discrepancies in cosmological parameters are challenging the standard model of cosmology ΛCDM [39, 63]. Low red-shift measurements of pulsating (Cepheid variables) and exploding stars (Supernovae type Ia) allow a determination of the Hubble constant H_0 which disagrees ($\approx 5\sigma$) with the value inferred by the Planck Collaboration in the context of the ΛCDM model [64–66]. A similar situation involves the strength of matter clustering parameterized as S_8. The ΛCDM value obtained from CMB anisotropies differs ($2-3\sigma$) when compared to S_8 values determined by probes such as weak lensing and galaxy clustering [67–80]. Although Big Bang nucleosynthesis (BBN) is a key ingredient in the standard cosmological model, there is a factor of ≈ 3.5 discrepancy between the theoretically expected abundance of lithium-7 and the observationally inferred abundance obtained from absorption spectroscopy of metal-poor stars in the galactic halo [81–86]. By measuring the sky-averaged 21 cm brightness temperature at red-shift $z \approx 20$, the EDGES experiment indicates a value for the baryon temperature cooler than expected in ΛCDM [87, 88]. However, a recent analysis bears out earlier concerns and shows no evidence for non-standard cosmology [89].

These exemplifying discordances could be due to unaccounted for systematic errors in analyses of current data sets, but thus far different analyses do not show a preference for this explanation. There exists also the very interesting possibility that the lack of agreement in some cosmological parameters measured by different experiments could also be due to a misunderstanding of the underlying physics. In other words, data would be hinting at new physics not taken into consideration within the standard cosmological model [90, 91].

The profuse search for alternatives to the cosmological constant has basically split into two categories: the introduction of non-standard forms of matter and modifications to the Einstein gravity. On the one hand, it is expected that new kinds of matter with the right properties (e.g., a negative equation of state implying some violation of the energy conditions) will be discovered in laboratories. For instance, new particles in more complete theories of fundamental interactions could dominate the energy content at late-times, avoid fine-tuning issues and be the reason why the Universe is speeding up [92–94]. These exotic matter fields are collectively known as dark energy (DE). On the other hand, GR might require modifications despite its success [95, 96], making plausible to consider modified gravity (MG) theories (for a review on DE and MG models see, for instance, [60]).

In this chapter, we will explore several proposals intending to improve our understanding of the role of different fields, such as vector fields, non-abelian gauge fields, p-forms, among others, and the impact of the underlying metric describing the geometry of our Universe in the late-time expansionary dynamics of our Universe.

2.1.1 Preliminaries

In this section, we give some details about one of the specific techniques typically used in the analysis of theoretical proposals to explain the current accelerated expansion of the Universe.

Dynamical Systems

One of the most powerful tools used in the analysis of the parameter space of a theoretical proposal is the dynamical system technique [94, 97, 98]. In the realm of cosmology, this technique consists of recasting the equations of motion of the fields in terms of dimensionless variables, which are typically chosen from the first Friedman equation. This yields a set of autonomous first-order differential equations whose stationary solutions lie in the phase space of the dynamical variables. This technique has been widely used in cosmology (see e.g., Refs. [1–4, 99–101])

In a nutshell, the autonomous set can be schematically represented as

$$\{x_i' = f_i(x_1, \dots, x_n; a_1, \dots, a_k) \,|\, i = 1, \dots, n\}, \tag{2.1.1}$$

where the prime denotes the derivative with respect to the number of e-folds, and f_i is an algebraic expression in terms of the n variables x_j and the k parameters a_j of the model. The possible stationary states of this set, i.e., where $\{x_i' = 0 \mid i = 1, \dots, n\}$, define the so-called fixed points of the system, which can be found by solving the set of algebraic equations given by $\{f_i(x_1, \dots, x_n; a_1, \dots, a_k) = 0 \,|\, i = 1, \dots, n\}$. Usually, these algebraic equations are analytically solvable. The solutions correspond to expressions for the variables in terms of the parameters, allowing a full characterization of the parameter space of the model.

Once the stationary states have been located in the parameter of the model, their stability should be analyzed. In general terms, this stability can be analyzed by assuming a small perturbation around each fixed point. Up to linear order, this yield to a system of differential equations for the perturbations vector

$$\delta\mathcal{X}' = \mathbb{J}\,\delta\mathcal{X}, \tag{2.1.2}$$

where $\mathcal{X}$ denotes the perturbations of the variables x_j around an arbitrary fixed point, and $\mathbb{J}$ is known as the Jacobian matrix.[1] Therefore, when evaluating on the fixed point, and upon solving the last equation, the stability of the fixed point is completely determined by the sign of the real part of the eigenvalues of the Jacobian matrix. We say that a fixed point is an attractor, or sink, if the real part of all these eigenvalues are negative. If there is a mix of positive and negative eigenvalues in a point, that point is called a saddle. If the real part of all the eigenvalues are positive the fixed point is called a repeller or source. For a review with further discussions and applications of dynamical systems in cosmology, see to Ref. [99].

[1] The Jacobian matrix for a set of n equations of the form $x_i' = f_i(x_1, \dots, x_n)$ is defined as $J_{ij} \equiv \frac{\partial f_i}{\partial x_j}$.

Conventions

Here, we establish some conventions used throughout this chapter, unless explicitly mentioned.

- The Einstein-Hilbert action is defined as

$$S = \int \sqrt{-g} \left[\frac{m_{\mathrm{P}}^2}{2} R + \mathcal{L} \right], \tag{2.1.3}$$

  where g is the determinant of the metric $g^{\mu\nu}$, m_{P} is the reduced Planck mass, R is the Ricci scalar, and $\mathcal{L}$ is the Lagrangian of matter.

- The scalar field of a theory will be denoted as ϕ or φ, and the vector field will be denoted as A_μ.

- For any field, namely a scalar, vector, 2-form, its potential is typically denoted as V.

- The canonical kinetic term X of the scalar field, the strength tensor $F_{\mu\nu}$ associated to the vector field, and its Hodge dual $\tilde{F}^{\mu\nu}$ are defined as

$$X \equiv -\frac{1}{2} g^{\mu\nu} \nabla_\mu \phi \nabla_\nu \phi, \qquad F_{\mu\nu} \equiv \nabla_\mu A_\nu - \nabla_\nu A_\mu, \quad \tilde{F}^{\mu\nu} \equiv \frac{1}{2} \varepsilon^{\mu\nu\alpha\beta} F_{\alpha\beta}, \tag{2.1.4}$$

  where $\epsilon^{\mu\nu\alpha\beta}$ is the totally antisymmetric tensor density.

- Greek indices run from 0 to 3 and latin indices run from 1 to 3.

- When a function depends on several fields, e.g., $f \equiv f(\phi, X, \ldots)$, its derivatives will be denoted using subscripts, for instance

$$f_\phi \equiv \frac{\partial f}{\partial \phi}, \quad f_X \equiv \frac{\partial f}{\partial X}.$$

- The flat Friedman-Lemaître-Robertson-Walker (FLRW) metric always reads

$$\mathrm{d}s^2 = -\mathrm{d}t^2 + a(t)^2 \delta_{ij} \mathrm{d}x^i \mathrm{d}x^j, \tag{2.1.5}$$

  where $a(t)$ is the scale factor which is a function of the time t only, and x^i denotes the spatial Cartesian coordinates (i.e., $\{x, y, z\}$). Therefore, we do not consider curvature in this work.

- An overdot denotes derivative with respect to the time t. A prime denotes a derivative with respect to the number of e-folds, $\mathrm{d}N \equiv H \mathrm{d}t$, where $H \equiv \dot{a}/a$ is the Hubble parameter.

- The axially symmetric Bianchi-I spacetime, with a residual isotropy in the (y, z) plane is given by
$$\mathrm{d}s^2 = -\mathrm{d}t^2 + a(t)^2 \left[e^{-4\sigma(t)}\mathrm{d}x^2 + e^{2\sigma(t)} \left(\mathrm{d}y^2 + \mathrm{d}z^2\right)\right] , \tag{2.1.6}$$
where σ denotes the geometrical shear.

- A configuration for the vector field compatible with the symmetries of the Bianchi-I metric in Eq. (2.1.6) is
$$A_\mu = (0, A(t), 0, 0) . \tag{2.1.7}$$

- When a function depends on time, or redshift, the subscript i means that the corresponding quantity is evaluated at some time in the deep radiation epoch, while the subscript 0 means that that quantity is evaluated at present.

- The density parameter Ω related to a fluid with density ρ is defined as
$$\Omega \equiv \frac{\rho}{3m_\mathrm{P}^2 H^2}, \tag{2.1.8}$$
Generally, the density parameters of radiation, matter, and dark energy fluids will be denoted as Ω_r, Ω_m, and Ω_DE, respectively.

- Round brackets enclosing space-time indices mean a standard symmetrization: $B_{(\mu}C_{\nu)} \equiv (B_\mu C_\nu + B_\nu C_\mu)/2$

- The symbols $\wedge$ and $\vee$ stands for the logic "AND" and "OR", respectively.

Some of these conventions are pretty standard and will not be stated again in next chapters. However, we will state new conventions if required.

2.2 k-essence

2.2.1 Introduction

The search for alternatives to the ΛCDM model is generally split into two broad categories: modified gravity theories and dynamical dark energy. Recent observations, like the detection of gravitational waves [102], have put some models based on modifications to GR under serious observational pressure [103–107]. These modifications to gravity or dark energy fields are usually studied in a flat FLRW background, assuring a homogeneous and isotropic background evolution. However, the CMB anomalies (if they exist) imply a violation of the Universe's isotropy at large scales, meaning that a geometry different to that described by the FLRW metric should be considered [108–110]. It has been remarked that some of these CMB anomalies could be explained by the introduction of an anisotropic late-time accelerated expansion[2] [111–113].

Among the proposals for anisotropic dark energy, we can find models that include vector fields [114–121], p-forms [122–124], non-Abelian gauge fields [1–3, 125], or inhomogeneous fields [4, 112, 126]. Although the most popular models of dark energy are based on homogeneous scalar fields (quintessence) [92, 94, 127, 128], it is known that this kind of fields alone cannot source anisotropic stress, meaning that any initial spatial shear would be quickly damped and the Universe will isotropize. However, in Ref. [117] was shown that if this quintessence is coupled to the canonical kinetic term of a vector field, anisotropic late-time solutions are possible. This study was extended to the inflationary context in Ref. [129], by considering the same coupling but to a non-canonical kinetic term for the scalar field (the so called k-inflation). In this case, it was shown that anisotropic inflationary solutions are a general property of the coupled k-inflation model. Here, inspired by Refs. [117, 129], we analyze the late-time cosmology of a non-canonical scalar field coupled to the kinetic term of a vector field; i.e. we study the *coupled k-essence model*. We find that, as in the inflationary case, anisotropic solutions are a generality of the model. In particular, we study three concrete models: the dilatonic ghost condensate (DGC), the Dirac Born Infeld (DBI) field with exponentials throat and potential, and the canonical scalar field with exponential potential for completeness; whose isotropic dynamics have been extensively studied in the literature (see Refs. [130–139], for example).

2.2.2 General Model

Consider the following Lagrangian:

$$\mathcal{L} \equiv -\frac{1}{4} f^2(\phi) F_{\mu\nu} F^{\mu\nu} + \mathcal{P}(\phi, X) + \mathcal{L}_m + \mathcal{L}_r, \tag{2.2.1}$$

where $\mathcal{P}$ is the Lagrangian of the k-essence scalar field. The function $f(\phi)$ is the coupling of the k-essence field to the vector field.

Upon varying with respect to the metric $g^{\mu\nu}$, we find that the energy-momentum tensor of the model will have separated contributions from the vector field and the scalar field, respectively given as

$$T^{\phi}_{\mu\nu} \equiv \mathcal{P}_X \nabla_\mu \phi \nabla_\nu \phi + \mathcal{P} g_{\mu\nu}, \qquad T^{A}_{\mu\nu} \equiv f^2(\phi) F_{\mu\rho} F_{\nu}{}^{\rho} - \frac{1}{4} g_{\mu\nu} f^2(\phi) F_{\sigma\rho} F^{\sigma\rho}, \tag{2.2.2}$$

[2] We want to mention that some of these anomalies could be also the result of an unknown primordial mechanism acting during inflation [10].

Varying the Lagrangian in Eq. (2.2.1) with respect to ϕ and A_ν, we get the equations of motion for the k-essence field and the vector field respectively as:

$$\nabla_\mu \left(\mathcal{P}_X \nabla^\mu \phi\right) + \mathcal{P}_\phi - \left(2\frac{f_\phi}{f}\right)\frac{f^2(\phi)}{4}F_{\mu\nu}F^{\mu\nu} = 0, \qquad \nabla_\mu \left(f^2(\phi)F^{\mu\nu}\right) = 0. \tag{2.2.3}$$

The Lagrangian (2.2.1) considers the interaction between a scalar field and a vector field. The introduction of such vector field violates rotational invariance.[3] In the following, we derive the dynamical equations of motion for the model in the specific anisotropic background in Eq. (2.1.6) using the vector field profile in Eq. (2.1.7), while the scalar field is only a function of time in order to preserve homogeneity.

The energy density and pressure of the vector field (ρ_A and p_A) and the k-essence field (ρ_ϕ and p_ϕ) are obtained from Eqs. (2.2.2) as

$$\rho_A \equiv \frac{1}{2}f^2(\phi)\frac{\dot{A}^2 e^{4\sigma}}{a^2}, \quad p_A \equiv \frac{1}{3}\rho_A, \quad \rho_\phi \equiv 2X\mathcal{P}_X - \mathcal{P}, \quad p_\phi \equiv \mathcal{P}. \tag{2.2.4}$$

From the gravitational field equations, the Friedman equations and the evolution equation of the geometrical shear are

$$3m_{\rm P}^2 H^2 = \rho_A + \rho_\phi + \rho_m + \rho_r + 3m_{\rm P}^2\dot{\sigma}^2, \tag{2.2.5}$$

$$-2m_{\rm P}^2\dot{H} = 2X\mathcal{P}_X + \frac{4}{3}\rho_A + \rho_m + \frac{4}{3}\rho_r + 6m_{\rm P}^2\dot{\sigma}^2, \tag{2.2.6}$$

$$3m_{\rm P}^2\ddot{\sigma} + 9m_{\rm P}^2 H\dot{\sigma} = 2\rho_A. \tag{2.2.7}$$

In Eq. (2.2.7), we can identify that the matter source for the shear is the energy density of the vector field. Although this source is different from zero even in the case when there is no coupling to the scalar field; i.e. when $f(\phi) = 1$, we will see later that it is precisely this interaction which allows late-times anisotropic solutions with interesting oscillatory behaviors.

It is known that isotropic k-essence models allow for scaling solutions whenever the Lagrangian has the form

$$\mathcal{P}(\phi, X) \equiv XG(Y), \quad Y \equiv Xe^{\lambda\phi/m_{\rm P}}, \tag{2.2.8}$$

where λ is a constant [60]. Here, we assume this form of the Lagrangian, and then the equation of motion of the scalar field is simplified as

$$\ddot{\phi} + 3HQ\mathcal{P}_X\dot{\phi} + Q(\mathcal{P}_{X\phi} - \mathcal{P}_\phi) - 2Q\frac{f_\phi}{f}\rho_A = 0, \tag{2.2.9}$$

[3] We want to stress that a vector field *does respect* isotropy if only the temporal component is considered [100, 140].

where $Q(Y) \equiv (2X\mathcal{P}_{XX} + \mathcal{P}_X)^{-1}$.

Our next task will be to recast the background equations in an autonomous system and find their fixed points, in order to know the asymptotic behavior of the model [97]. Therefore, we introduce the following dimensionless variables:

$$x \equiv \frac{\dot{\phi}}{\sqrt{6}m_{\rm P}H}, \quad z^2 \equiv \frac{\rho_A}{3m_{\rm P}^2H^2}, \quad \Sigma \equiv \frac{\dot{\sigma}}{H}, \tag{2.2.10}$$

such that the first Friedman equation (2.2.5) becomes the constraint

$$1 = x^2\left[2\mathcal{P}_X(Y) - G(Y)\right] + z^2 + \Omega_m + \Omega_r + \Sigma^2, \tag{2.2.11}$$

from which, we can write Ω_m in terms of the other variables. From the second Friedman equation in Eq. (2.2.6), we compute the deceleration parameter

$$q = \frac{1}{2}\left[1 + 3x^2G(Y) + z^2 + \Omega_r + 3\Sigma^2\right]. \tag{2.2.12}$$

For the dark sector, we define the density and pressure of dark energy as

$$\rho_{\rm DE} \equiv \rho_A + \rho_\phi + 3m_{\rm P}^2\dot{\sigma}^2, \quad p_{\rm DE} \equiv p_A + p_\phi + 3m_{\rm P}^2\dot{\sigma}^2, \tag{2.2.13}$$

and thus the equation of state of dark energy, $w_{\rm DE} \equiv p_{\rm DE}/\rho_{\rm DE}$, is given by

$$w_{\rm DE} = -1 + \frac{2}{3}\frac{3x^2\mathcal{P}_X + 2z^2 + 3\Sigma^2}{x^2(\mathcal{P}_X + G_1) + z^2 + \Sigma^2}. \tag{2.2.14}$$

Note that with this choice of including the geometrical shear in $\rho_{\rm DE}$ and $p_{\rm DE}$ we can write the continuity equation of dark energy as

$$\dot{\rho}_{\rm DE} + 3H\left(\rho_{\rm DE} + p_{\rm DE}\right) = 0, \tag{2.2.15}$$

which is the usual form. In the case that this anisotropic contribution is not consider in the definition of the density and pressure of dark energy, we would obtain an equation of the form $\dot{\rho}_{\rm DE} + 3H\left(\rho_{\rm DE} + p_{\rm DE}\right) \propto \dot{g}_{ij}\Pi^{ij}$, where Π^{ij} is the trace-free part of the energy-momentum tensor.

We want to write the autonomous set of equations for the dynamical variables in Eq. (2.2.10). Therefore, it is necessary to choose a specific coupling. To ease the computations we consider an exponential function of the form

$$f(\phi) = f_0 e^{-\mu\phi/m_{\rm P}}, \tag{2.2.16}$$

where μ is a constant. By taking the derivative of the dimensionless variables with respect to the number of e-folds, $\mathrm{d}N \equiv H\mathrm{d}t$, we get the following autonomous system:

$$x' = x(q+1) - \frac{\sqrt{6}}{2}\lambda x^2 - \frac{\sqrt{6}}{2}Q\left[\sqrt{6}x\mathcal{P}_X - \lambda x^2\left(\mathcal{P}_X + G_1\right) + 2\mu z^2\right], \tag{2.2.17}$$

$$z' = z(q-1) + \sqrt{6}\mu x z - 2z\Sigma, \tag{2.2.18}$$

$$\Sigma' = \Sigma(q-2) + 2z^2, \tag{2.2.19}$$

$$\Omega_r' = 2\Omega_r(q-1). \tag{2.2.20}$$

We note that this system of differential equations is not closed since the function Y is not written in terms of the variables. For this function, it is necessary to choose a specific variable depending on the form of the Lagrangian in order to avoid possible singularities in the system, which are related to the term $x^2\left[2\mathcal{P}_X(Y) - G(Y)\right]$ in Eq. (2.2.11).

2.2.3 Specific Models

In Ref. [5], we studied three models: quintessence, dilatonic ghost condensate (DGC), and the Dirac-Born-Infeld (DBI) model.

Anisotropic Quintessence

In this case, the Lagrangian is

$$\mathcal{P}(\phi, X) \equiv X - c\, m_{\mathrm{P}}^4 e^{-\lambda\phi/m_{\mathrm{P}}}, \tag{2.2.21}$$

with c a constant. We have that $\mathcal{P}_X = 1$, while the function characterizing the Lagrangian is

$$G(Y) = 1 - c\frac{m_{\mathrm{P}}^4}{Y}. \tag{2.2.22}$$

We note that the term $x^2(2\mathcal{P}_X - G)$ in the Friedman constraint (2.2.11) can yield singularities depending on the variables we choose to define Y. In this case, we can use the dimensionless variable[4]

$$y \equiv c_y \frac{m_{\mathrm{P}}\, e^{-\lambda\phi/2m_{\mathrm{P}}}}{\sqrt{3}H}, \tag{2.2.23}$$

where $c_y \equiv c^{1/2}$, such that

$$x^2\left(2\mathcal{P}_X - G\right) = x^2 + y^2. \tag{2.2.24}$$

[4]We want to stress that avoiding singularities in the Friedman constraint by choosing a suitable variable is extremely important, since some fixed points could be "hidden" in these divergences [141].

The evolution equation of this new variable is

$$y' = y(q+1) - \frac{\sqrt{6}}{2}\lambda x y. \tag{2.2.25}$$

We found two fixed points relevant for the late-time accelerated expansion phase: one isotropic and another anisotropic. The isotropic DE point is denoted as (*DE-1*) and the anisotropic one is denotes as (*DE-2*).

In (*DE-1*) only two variables are different form zero:

$$x = \frac{\lambda}{\sqrt{6}}, \quad y = \sqrt{1 - \frac{\lambda^2}{6}}, \quad w_{\text{eff}} = w_{\text{DE}} = -1 + \lambda^2/3. \tag{2.2.26}$$

This point is an accelerated solution for $\lambda^2 < 2$, as expected. The stability of the point, however, change with the introduction of the parameter μ. Computing the eigenvalues of the Jacobian matrix evaluated at the point, we found that this point serves as an attractor of the system whenever

$$\lambda^2 < 2 \quad \wedge \quad \mu \leq \frac{4 - \lambda^2}{2\lambda}. \tag{2.2.27}$$

Note that $\lambda \approx 0$ in order to have $w_{\text{DE}} \approx -1$, as required by observations [39].

For the anisotropic point (*DE-2*), the values of the variables are

$$\begin{aligned}
x &= \frac{2\sqrt{6}\,(\lambda + 2\mu)}{8 + (\lambda + 2\mu)(\lambda + 6\mu)}, \\
y &= \frac{\sqrt{6(8 - (\lambda - 6\mu)(\lambda + 2\mu))(2 + \mu(\lambda + 2\mu))}}{8 + (\lambda + 2\mu)(\lambda + 6\mu)}, \\
z &= \frac{\sqrt{3(8 - (\lambda - 6\mu)(\lambda + 2\mu))(\lambda^2 + 2\mu\lambda - 4)}}{8 + (\lambda + 2\mu)(\lambda + 6\mu)}, \\
\Sigma &= 2\frac{\lambda^2 + 2\mu\lambda - 4}{8 + (\lambda + 2\mu)(\lambda + 6\mu)},
\end{aligned} \tag{2.2.28}$$

with $\Omega_r = 0$, $\Omega_m = 0$, and

$$w_{\text{DE}} = -1 + \frac{4\lambda(\lambda + 2\mu)}{8 + (\lambda + 2\mu)(\lambda + 6\mu)}. \tag{2.2.29}$$

This point is a viable cosmological solution in the following region of the parameter space $\{\lambda, \mu\}$

$$\lambda < \sqrt{2} \quad \wedge \quad \mu \geq \frac{4 - \lambda^2}{2\lambda}. \tag{2.2.30}$$

We see that the condition on μ, in this case, is exactly the opposite of the condition on μ for

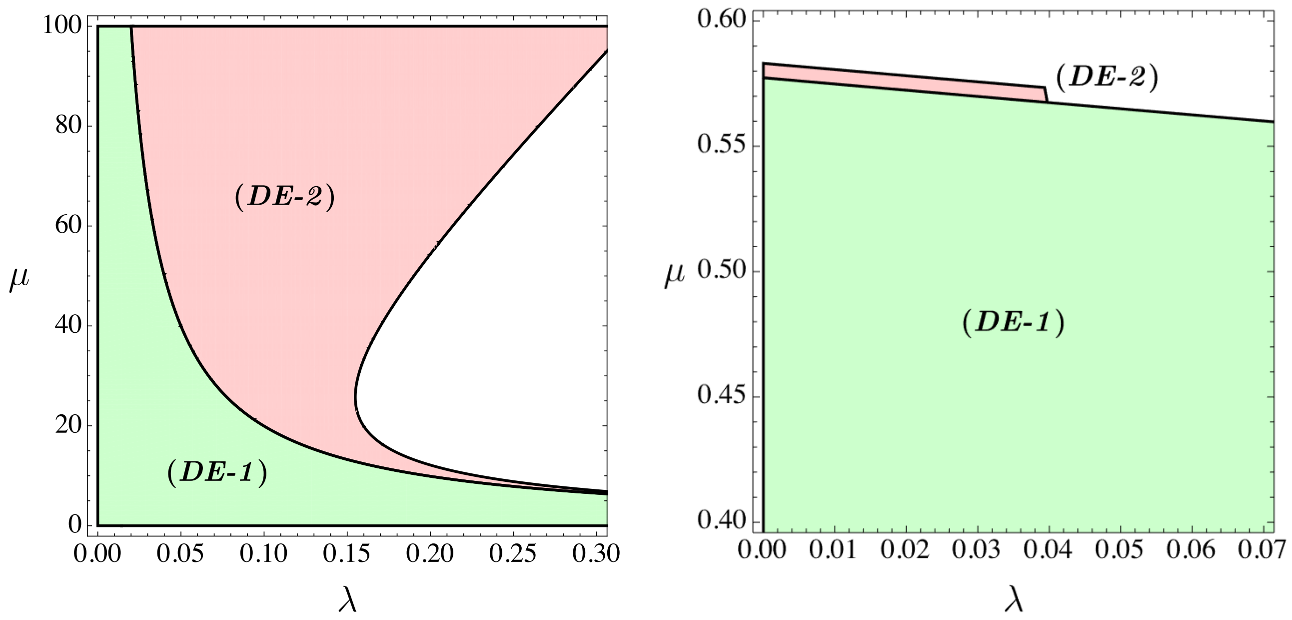

Figure 2.2.1: Stability regions for the dark energy dominated points (*DE-1*) and (*DE-2*). Each color represents a $\{\lambda, \mu\}$ parameter region where the indicated fixed point is an attractor with $-1 \leq w_{\rm DE} \leq -0.95$ and the shear is small $\Sigma \leq 10^{-3}$. (Left) For the anisotropic quintessence model, these regions are separated by the bifurcation curve $2\lambda\mu = 4 - \lambda^2$. (Right) For the DGC model, the region for anisotropic attractors is clearly far smaller than that admitting isotropic solutions.

the isotropic point in Eq. (2.2.27). This means that when the anisotropic point (*DE-2*) is an accelerated solution, the isotropic point (*DE-1*) is a saddle. Also note that, since an equation of state of dark energy near to -1 requires[5] $\lambda \ll \mu$, then this point needs a large μ. This can be clarified by noting that a small shear, as also required by observations [142, 143], can be satisfied if $\mu \gg \lambda$. Assuming the later, the shear and the equation of state of dark energy can be approximated to first order by

$$\Sigma \approx \frac{\lambda}{3\mu} - \frac{2}{3\mu^2}, \quad w_{\rm DE} \approx -1 + \frac{2\lambda}{3\mu}, \tag{2.2.31}$$

We verified that under these conditions, (*DE-2*) is also the attractor of the system. Therefore, for small λ and *large* μ this point is an accelerated solution with $w_{\rm DE} \approx -1$, a small shear, and it is an attractor

[5]There is another possibility, namely, $\lambda \sim -2\mu$, but we do not pursue this rather fine-tuned case.

Anisotropic Dilatonic Ghost Condensate

Next, we study the dilatonic ghost condensate (DGC) model whose Lagrangian reads

$$\mathcal{P}(\phi, X) \equiv -X + b\, e^{\lambda\phi/m_{\rm P}} \frac{X^2}{m_{\rm P}^4}, \tag{2.2.32}$$

and thus we have $\mathcal{P}_X(Y) = -1 + 2b\,Y/m_{\rm P}^4$, while the function characterizing the Lagrangian is

$$G(Y) = -1 + b\frac{Y}{m_{\rm P}^4}, \tag{2.2.33}$$

where b is a constant. From the later we get $G_1(Y) = 1 + G(Y)$ and $Q = [5 + 6G(Y)]^{-1}$.

In order to avoid possible singularities in the "troublesome term" in the Friedman constraint (2.2.11); namely, $(2\mathcal{P}_X - G)$, we define a new dimensionless variable[6]

$$l \equiv c_l \frac{\sqrt{3}H\, e^{\lambda\phi/2m_{\rm P}}}{m_{\rm P}} \propto \frac{1}{y}, \tag{2.2.34}$$

with $c_l = b^{1/2}$, such that

$$2\mathcal{P}_X - G = -1 + 3l^2x^2. \tag{2.2.35}$$

The evolution equation for this new variable is

$$l' = \frac{\sqrt{6}}{2}\lambda l x - l(q+1). \tag{2.2.36}$$

The fixed points are now obtained by setting all the derivatives of the variables to zero in the autonomous set, and their stability can be investigated by perturbing the autonomous set around them, considering the variable l instead of y.

In this case as well, two DE fixed points where found: an isotropic point denoted as (*DE-1*) and an anisotropic point denoted as (*DE-2*).

(*DE-1*) corresponds to the usual isotropic dark energy fixed point in the DGC model, in which the variables take the following values:

$$x = \frac{1}{2}\left(-\sqrt{\frac{3}{2}}\lambda + \sqrt{8 + \frac{3\lambda^2}{2}}\right), \quad l = \sqrt{\frac{1}{4} + \frac{3\lambda^2}{16} + \frac{3\lambda^4}{128} + \frac{\lambda(16+3\lambda^2)^{3/2}}{128\sqrt{3}}},$$

$$w_{\rm eff} = w_{\rm DE} = -1 + \frac{\lambda}{6}\left(-3\lambda + \sqrt{48 + 9\lambda^2}\right), \tag{2.2.37}$$

[6] If we had chosen to continue the computations with y instead of considering the new variable l, we would have found divergences in the points where $l = 0$.

where the other variables are zero. This point is an accelerated solution for

$$\lambda^2 < 2/3, \tag{2.2.38}$$

as expected [60]. Applying the linear stability formalism, we found that for $\lambda \geq 0$ the eigenvalues of the Jacobian matrix are all negative whenever

$$\lambda^2 < 2/3 \quad \wedge \quad \mu \leq -\frac{\lambda}{4} + \frac{\sqrt{16+3\lambda^2}}{4\sqrt{3}}. \tag{2.2.39}$$

Note that $\lambda \approx 0$ in order to have $w_{\rm DE} \approx -1$, implying $\mu \lesssim 1/\sqrt{3}$.

In (*DE-2*), the values of the variables are

$$\begin{aligned}
x &= 2\sqrt{6}\frac{2\lambda + 2\mu - \sqrt{8+\lambda^2-4\lambda\mu-8\mu^2}}{-8+3\lambda^2+12\lambda\mu+12\mu^2}, \\
\Sigma &= \frac{8-3(\lambda+2\mu)\left(-\lambda+\sqrt{8+\lambda^2-4\lambda\mu-8\mu^2}\right)}{-8+3(\lambda+2\mu)^2},
\end{aligned}$$

$$\begin{aligned}
l &= \frac{1}{8\sqrt{6}}\Big\{9\lambda^4 - 10\lambda^3\mu + \lambda^2(80-124\mu^2) - 8\lambda\mu(19\mu^2-14) + 32(\mu^4+\mu^2-2) \\
&\quad + \sqrt{8+\lambda^2-4\lambda\mu-8\mu^2}\left[9\lambda^3 + 10\lambda^2\mu + \lambda(40-36\mu^2) + 8\mu(6-5\mu^2)\right)\Big\}^{1/2} \\
z &= \frac{1}{3(\lambda+2\mu^2)}\Bigg\{-96 - \frac{3}{2}\left[-9\lambda^4 + 30\lambda^3\mu + 96\mu^2 + 20\lambda^2(4+9\mu^2) + 8\lambda\mu(21\mu^2-10)\right] \\
&\quad + \sqrt{8+\lambda^2-4\lambda\mu-8\mu^2}\left[\frac{27}{2}\lambda^3 + 72\mu - 9\lambda^2\mu - 108\mu^3 + \lambda(60-126\mu^2)\right]\Bigg\}^{1/2},
\end{aligned} \tag{2.2.40}$$

and

$$w_{\rm DE} = -1 + 4\lambda\frac{2\lambda^2+2\mu^2-\sqrt{8+\lambda^2-4\lambda\mu-8\mu^2}}{-8+3(\lambda+2\mu)^2}. \tag{2.2.41}$$

An equation of state of dark energy near to -1 requires $\lambda \sim 0$. The region of existence where this point exists as an accelerated solution, $-1 \leq w_{\rm DE} < -1/3$, is given by[7]

$$\lambda < 2\sqrt{2/39} \quad \wedge \quad -\frac{\lambda}{4} + \frac{\sqrt{16+3\lambda^2}}{4\sqrt{3}} \leq \mu \leq -\frac{\lambda}{4} + \frac{\sqrt{16+3\lambda^2}}{4}. \tag{2.2.42}$$

[7]Note that we concentrate in no-ghost solutions. In the canonical scalar field case, it was not necessary to consider this explicitly since the equation of state of dark energy (2.2.29) cannot cross the phantom line.

A small shear, as mandatory by observations ($|\Sigma_0| \leq 10^{-3}$) [142, 143], requires μ to be near to its lower bound; i.e. $1/\sqrt{3} \lesssim \mu$, which is exactly the opposite of the condition on μ for the isotropic point (*DE-1*) in Eq. (2.2.39). As in the canonical scalar field case, this means that when the anisotropic point (*DE-2*) is an accelerated solution, the isotropic point (*DE-1*) is a saddle. In this case, it was not possible to obtain an analytic expression for the eigenvalues of $\mathbb{J}$ due to the complicated algebraic terms for the variables. However, we can investigate them numerically. In Fig. 2.2.1, we can see that the two possible dark energy points are separated by a bifurcation curve, and that, for the DGC model, the region where the anisotropic solution exists as an attractor is small in comparison with the region for the isotropic point. This implies that a viable cosmological evolution with a strong coupling regime between the scalar field and the vector field is not possible. Hence for instance, if we choose parameters such that (*DE-2*) is the attractor, the system will spend a large amount of time around the saddle isotropic (*DE-1*), reaching the anisotropic solution in the far-far future.

Anisotropic Dirac Born Infeld Field

At last, we study the Dirac Born Infeld (DBI) model whose Lagrangian reads

$$\mathcal{P}(\phi, X) \equiv -\frac{1}{h(\phi)}\sqrt{1-2h(\phi)X} + \frac{1}{h(\phi)} - V(\phi), \tag{2.2.43}$$

and thus we have $\mathcal{P}_X \equiv \gamma = (1-2hX)^{-1}$, while the function characterizing the Lagrangian is

$$G(Y) = -\left(\frac{m^4}{Y}\right)\frac{1}{\gamma} - \left(\frac{M^4}{Y}\right), \tag{2.2.44}$$

where $h = h(\phi)$ and $V = V(\phi)$ are functions of the scalar field ϕ, and m and M are mass coefficients. The function $G(Y)$ so defined requires

$$h(\phi) \equiv \frac{1}{m^4}e^{\lambda\phi/m_{\rm P}}, \quad V(\phi) \equiv m^4(1+\eta)e^{-\lambda\phi/m_{\rm P}}, \tag{2.2.45}$$

where we have defined

$$m^4 \equiv c_m^2 m_{\rm P}^4,\ M^4 \equiv c_M^2 m_{\rm P}^4,\ \eta \equiv \frac{c_M^2}{c_m^2}, \tag{2.2.46}$$

with c_m and c_M constants.

Possible singularities in the "troublesome term" $x^2(2\mathcal{P}_X - G)$ can be avoided if we use both variables y and l, such that

$$x^2(2\mathcal{P}_X - G) = \frac{2\eta\, x^2 - y^2\left(\eta + \sqrt{1-2l^2x^2}\right)}{-1+2l^2x^2}. \tag{2.2.47}$$

In this case, it is not possible to obtain analytical fixed points in general. In the following, we attach to the procedure of Ref. [129] in order to find the dark energy dominated points. At very late-times, dark energy dominates and the contributions of radiation and matter to the total density are negligible. Therefore, we consider $\Omega_r = \Omega_m = 0$, and then, from the constraint in Eq. (2.2.11), we can write the variable z in terms of x, y, and Σ. The fixed points of this simplified system are found by setting $x' = 0$, $\Sigma' = 0$, and $y' = 0$ in Eqs. (2.2.17), (2.2.19), and (2.2.25). We obtain:

- (*DE-1*) Isotropic point

$$\mathcal{P}_X = \frac{\lambda}{\sqrt{6}x}, \quad G_1 = \frac{1}{x^2} - \frac{\lambda}{\sqrt{6}x}, \quad z = 0, \quad \Sigma = 0, \tag{2.2.48}$$

- (*DE-2*) Anisotropic point

$$\mathcal{P}_X = \frac{(\lambda + 2\mu)\left(2\sqrt{6} - x(\lambda + 6\mu)\right)}{8x}, \quad G_1 = \frac{12 + x^2\lambda(\lambda + 2\mu) - \sqrt{6}x(3\lambda + 2\mu)}{8x^2},$$

$$\Sigma = -1 + \frac{\sqrt{6}}{4}x(\lambda + 2\mu). \tag{2.2.49}$$

In both cases we have

$$w_{\text{DE}} = -1 + \sqrt{\frac{2}{3}}\lambda x, \tag{2.2.50}$$

and thus accelerated solutions obey

$$0 \leq x < \frac{\sqrt{6}}{3\lambda}. \tag{2.2.51}$$

In the next subsections, we will study each point apart.

- **(*DE-1*): Isotropic Dark Energy**

  In this case, it is possible to find explicit expressions for the variables x and y:

$$x = \frac{\lambda\left(-\lambda^2 \pm \sqrt{36 + 12\eta\lambda^2 + \lambda^4}\right)}{2\sqrt{6}(3 + \eta\lambda^2)}, \quad y = \frac{\sqrt{2}x\lambda}{\sqrt{\lambda^2 - 6x^2}}. \tag{2.2.52}$$

The minus solution in the variable x does not correspond to an accelerated solution, hence we only consider the solution with the plus sign. This point is an accelerated solution when

$$\lambda > 0 \quad \wedge \quad \eta > \frac{\lambda^4 - 12}{4\lambda^2}. \tag{2.2.53}$$

Note that, with respect to the other models studied, in this case we can get $w_{\text{DE}} \approx -1$ for $\lambda = \mathcal{O}(10)$ and large η. For instance, if $\lambda = 1$, $\eta > 3297$ for $-1 \leq w_{\text{DE}} < -0.99$.

- **(*DE-2*): Anisotropic Dark Energy**

In the isotropic case, the variable x can be obtained from a second order algebraic equation which has analytic solutions. However, in the anisotropic case, we get a complex algebraic equation for x which is *not* analytically solvable for general values of λ, η, and μ. Therefore, it is impossible to find explicit expressions for the variables. However, we do find bounds for them in order to discriminate cosmologically viable solutions.

The tighter bound we found for x is given by

$$\frac{2\sqrt{6}}{3(\lambda+2\mu)} < x < \frac{2\sqrt{6}}{\lambda+6\mu}. \tag{2.2.54}$$

A cosmologically viable anisotropic accelerated solution must fulfill that $w_{\rm DE} \approx -1$ and $|\Sigma_0| \leq 10^{-3}$ [39, 142, 143]. We can see that, if we take x equal to its lower bound then

$$w_{\rm DE} = -1 + \frac{4\lambda}{3(\lambda+2\mu)}, \quad \Sigma = 0. \tag{2.2.55}$$

Therefore, we have to choose the parameters λ and μ such that x approximates its lower bound, and also $\mu \gg \lambda$. We get the compatibility conditions

$$\mu > \frac{2\sqrt{\lambda^4+12\eta\lambda^2+36}-\lambda^2}{6\lambda}, \quad \lambda < \sqrt{2\eta+2\sqrt{3+\eta^2}}, \tag{2.2.56}$$

where we assumed that x is equal to the lower bound of Eq. (2.2.54). These results assure that $\mu \gg \lambda$. Note that this procedure considers a general k-essence field.

2.2.4 Oscillatory Behavior of $w_{\rm DE}$ and Σ

In this section, we will confirm some of the conclusions drawn from the dynamical system analysis. We will concentrate in the anisotropic quintessence model in order to keep simple our presentation. More details and a similar numerical analysis for the DGC and DBI models can be found in the corresponding article (Ref. [5]).

Now, we solve numerically the autonomous set in Eqs. (2.2.17)-(2.2.20) and (2.2.25). We assume that, prior to the radiation epoch, the Universe underwent an inflationary period which perfectly smoothed any initial spatial shear or inhomogeneities. Therefore, we choose $\Sigma_i = 0$ as an initial condition, such that the starting point for any cosmological trajectory is from the isotropic radiation point. We will choose parameters λ and μ such that the attractor point is given by (*DE-2*). In particular, we have chosen $\lambda = 0.1$, and $\mu = 10^3$ from the bound in

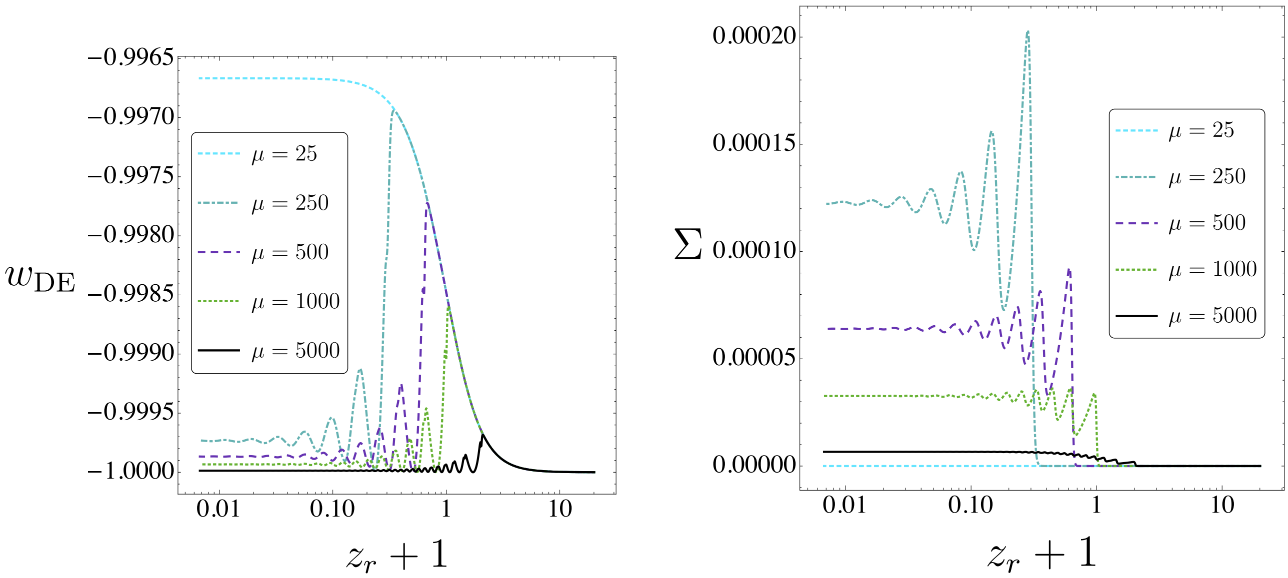

Figure 2.2.2: (Left) Evolution of the equation of state of dark energy $w_{\rm DE}$ and (Right) the shear around $z_r = 0$ for different values of the parameter μ, while λ is fixed and the initial conditions are the same given in Eq. (2.2.57).

Eq. (2.2.30). Having this in mind, we set

$$x_i = 10^{-15}, \quad y_i = 2\times 10^{-14}, \quad z_i = 10^{-12}, \quad \Sigma_i = 0, \quad \Omega_{r_i} = 0.99995, \tag{2.2.57}$$

as initial conditions at redshift $z_r = 6.57 \times 10^7$, and we have integrated the system up to $z_r \to -1$.

In Figs. 2.2.2, we show the late-time evolution of the equation of state of dark energy and the shear for a fixed $\lambda = 0.1$ and varying μ. We can see that the equation of state of dark energy is very close to -1 and that Σ is within the observational bound today, namely, $|\Sigma_0| \leq 10^{-3}$ [142, 143]. We also see an interesting behavior of the equation of state and the shear: they oscillate. This can be understood as follows. Note that when $\mu = 25$, there is no oscillations in $w_{\rm DE}$ since in this case the system spend more time in the saddle isotropic point (*DE-1*). For larger values of μ the coupling of the vector field to the scalar field is stronger, and the contribution of the vector field to the density is greater. It is possible to show that at some late-time, the density of the vector field is comparable to the kinetic energy of the scalar field, i.e., $z \approx x$, and hence the scalar field obeys the equation of a constant forced and damped harmonic oscillator. For the quintessence field we tacitly find:

$$\ddot{\phi}(t) + \gamma\dot{\phi}(t) + \omega_0^2\phi(t) = F_0, \tag{2.2.58}$$

which corresponds to the equation of motion of a damped harmonic oscillator with damping γ

(which is the usual Hubble friction), frequency ω_0^2, driven by a constant force F_0. These terms are given by

$$\gamma \equiv 3H, \quad \omega_0^2 \equiv 3\lambda(\lambda+\mu)H^2, \quad F_0 \equiv \lambda\frac{V_0}{m_{\rm P}}. \tag{2.2.59}$$

Hence we see that, when the coupling parameter μ is small, the frequency of the oscillator is $\omega_0^2 \approx 3\lambda^2 H^2$ and of course $\gamma \gg \omega_0$, given that $\lambda \approx 0$, and thus the oscillator is overdamped. That is the reason why we need a large μ to see oscillations. Even more, we can give an estimate of how large μ has to be in order to see critically damped oscillations; i.e. when $\gamma^2 = 4\omega_0^2$. Using $\lambda = 0.1$ we get $\mu = 7.4$. We confirmed that, using the same initial conditions in Eq. (2.2.57), a very small oscillation occurs in $w_{\rm DE}$ for $\mu = 8$ at redshift $z_r \approx -1 + e^{-8}$.

2.2.5 Conclusions

In this work, we have studied the background cosmological evolution of a k-essence field coupled to the canonical kinetic term of an abelian vector field, extending to late-times the work of Ref. [129] where inflationary solutions were found. We assumed three specific realizations of the k-essence field, namely: the dilatonic ghost condensate, the Dirac Born Infeld field, and the canonical scalar field for completeness.

By using a dynamical system approach, we were able to show that each of these models has an anisotropic dark energy dominated point which can be an attractor. The dynamical system also allowed us to find the available space parameter for each anisotropic solution to be cosmologically viable. For the quintessence field, an equation of state of dark energy near to -1 and a small shear as required by observations [39, 142, 143], need $\mu \gg \lambda$ and $\mu \gg 1$ (see the left panel of Fig. 2.2.1). For the DGC model, the requirements are $\lambda \ll 1$ and $\mu \gtrsim 1/\sqrt{3}$ (see the right panel Fig. 2.2.1), while for the DBI field we found that λ can be greater than 1 ($\lambda = \mathcal{O}(10)$, for instance) given that $\eta, \mu \gg 1$ [see the bounds in Eqs. (2.2.56)].

We solved numerically the autonomous set of equations corresponding to each model, verifying that a correct expansion history is reproduced, and that the anisotropic dark energy dominated points (*DE-2*) are indeed attractors of the systems. For every case studied, we set the initial conditions in the deep radiation epoch [$z_r = \mathcal{O}(10^7)$] and assumed a zero initial shear ($\Sigma_i = 0$). For the quintessence and the DBI field, we found that $w_{\rm DE}$ and Σ oscillate at late-times until they reach their values in the attractor (*DE-2*). We show that for parameters $\lambda \ll 0$ and $\mu \gg \lambda$ and $\mu \gg 1$, the system is underdamped, making possible to see these oscillations around nowadays. In the uncoupled case ($\mu = 0$), these oscillations are overdamped and thus it is extremely hard to see them. On the other hand, for the DGC model we found that the shear today (and for the near future) would be effectively zero, because the isotropic and anisotropic point are very near in the phase space. This implies that the cosmological trajectories will spend at large amount of time around the isotropic point before reach the anisotropic attractor. This also implies that no oscillations of the fields are expected to be seen.

The non-negligible shear and the oscillatory behavior of the fields, w_{DE}, and Σ, are notorious properties of this coupled k-essence model. However, the observable imprints of these models which could be compared with CMB or SN Ia measurements are yet to be done. We leave a detailed study of this subject for a future work.

2.3 Tachyonic Scalar Field

2.3.1 Introduction

As exemplified in the latter section with the fixed points of the DBI model, there are some cases where analytical solutions to the autonomous system are not available, forbidding a complete examination of the parameter space. For instance, if any of the equations $f_i = 0$ involves a polynomial of degree greater than 4 in the dynamical variables, this implies that analytical solutions do not exist due to the fundamental theorem of Galois theory [144].

Although analytical fixed points are not available in all cases, it is still possible to solve numerically the algebraic set $\{f_i(x_1, \ldots, x_n) = 0 \mid i = 1, \ldots, n\}$ [see Eq. (2.1.1)] assuming specific values for the parameters. In this work, we put forward a general framework to determine the stability of these "numerical fixed points" given a finite portion of the parameter space. In the particular case of a scalar field coupled to a vector field evolving in an anisotropic background, our numerical scheme allows us to estimate the attraction region in the parameter space of anisotropic accelerated solutions which do not have analytical counterparts. For this model, we numerically solve the corresponding autonomous set assuming some values of the parameters, finding general agreement with the asymptotic behaviors predicted for the numerical fixed points.

2.3.2 Dynamical Systems: Numerical Approach

In this section, we describe our general framework to analyze the stability properties of a region in the parameter space of a model with no analytical fixed points. Assuming an autonomous system of n differential equations, as in Eq. (2.1.1), our numerical scheme relies on the following steps:

1. Choice of a representative region in the parameter space of the model.

This can be done by defining an interval for each parameter, i.e., $a_{i_{\min}} < a_i < a_{i_{\max}}$ for $i = 1, \ldots, k$, such that the Cartesian product of these intervals build a portion of the parameter space. The length of each interval should take into consideration relevant physical conditions of the model and the symmetries of the autonomous system.

2. Setting of physical constraints to discriminate between cosmologically viable and non-viable fixed points.

These constraints are required to ensure that the numerical solutions of the autonomous set are related to some physically interesting properties of the model. For instance, imposing the condition $w_{\rm eff} < -1/3$, where $w_{\rm eff}$ is the effective equation of state, implies that any found solution describes an expanding universe at an accelerated rate. Other conditions have to be satisfied for the consistency of the theory, for instance, the density parameters must take on nonnegative values. Numerical solutions meeting all the chosen conditions are called "cosmologically viable". Otherwise, they are cataloged as "non-viable solutions" and discarded. Note that all the cosmologically viable solutions coming from the same set of parameters are physically indistinguishable.

3. Stochastic search of viable solutions in the chosen region in the parameter space.

A large number N of random points in the parameter space $\{a_1, \dots a_k\}$ is generated. The corresponding fixed points for each set of parameters are found by numerically solving the system of algebraic equations $\{f_i(x_1, \dots, x_n) = 0 \mid i = 1, \dots, n\}$.[8] Then, the chosen physical constraints in the previous step are evaluated for all the solutions, such that those which fulfill them are cataloged as "viable solutions" and the others are discarded. In our case of interest, all the viable points will correspond to accelerated solutions of the system, i.e., Dark Energy (DE) dominated points.

4. Stability analysis of the region of viable points.

In general, the stability of a fixed point can be determined by computing the real part of the eigenvalues of the Jacobian matrix evaluated in the point. When all the corresponding eigenvalues are negative, we say that the fixed point is an attractor. When all of them are positive, the fixed point is a source or repeller. If there is a mix of negative and positive eigenvalues, then the fixed point is a saddle.

In the cosmological context, a proper expansion history requires the existence of at least three fixed points as follows: *i*) a radiation dominated point which can be a saddle or a source, *ii*) a saddle matter dominated point, and *iii*) a DE dominated point that can be an attractor of the system.

[8]This can be done using the default numerical methods in the `NSolve` of `Mathematica`, for example.

Note that for a given point in the parameter space, there could exist several fixed points with their own stability; for example, the three stages of dominance (radiation, matter, and DE epochs) should exist for a given set of parameters in order for the model to be able to reproduce a correct expansion history. Therefore, it is necessary to compute all the available Jacobian matrices (and their eigenvalues) for each set of parameters yielding cosmologically viable solutions. Since viable solutions from a given set of parameters have the same physical characteristics, the stability of the point in the parameter space is determined by the most stable point, that is:

- If all eigenvalues of at least one of the matrices are negative, then this point is an attractor and the other possible fixed points are discarded.
- If all eigenvalues of all matrices are positive, then the stability corresponds to a repeller.
- If the stability is not an attractor neither a repeller in the sense described above, one or more matrices have a mix of positive and negative eigenvalues, and the stability is of a saddle point.

Here, we are mainly interested in DE dominated attractor points. Therefore, once an attractor is found, the computation of the Jacobian matrices for the given set of parameters is stopped, just to proceed to another point in the parameter space.

In the following section, we will illustrate the numerical method described here by analyzing the asymptotic behavior of a specific model, prioritizing the search of DE domination points.

2.3.3 Illustration of the Method

Tachyon field in an anisotropic background

The Lagrangian of our template model is given by

$$\mathcal{L} \equiv -V(\phi)\sqrt{1+\partial_\mu\phi\partial^\mu\phi} - \frac{1}{4}f(\phi)F^{\mu\nu}F_{\mu\nu}, \tag{2.3.1}$$

where $f(\phi)$ is a coupling function between ϕ and A_μ.

As pointed out in Refs. [129] and [5], a full analytical description of the dynamical system is impossible for some non-canonical scalar field models in a Bianchi-I background, such as the Dirac-Born-Infeld (DBI) field. Since the Lagrangian of the DBI model shares some similarities with the Lagrangian in Eq. (2.3.1), we expect that the dynamical system of this model also lacks of a full analytical description. We will explicitly show that the anisotropic dark energy attractor of our model cannot be studied analytically and use the numerical framework explained in Sec. 2.3.2 to reconstruct a portion of its parameter space.

Dynamical System

Following the standard procedure [98], we derive the evolution equations of the model by varying the action from the Lagrangian in Eq. (2.3.1) with respect to the metric, the scalar field and the vector field. After these variations, we replace the Bianchi I metric given in Eq. (2.1.6), and the ansatz for the fields in Eq. (2.1.7) obtaining:

$$3m_{\rm P}^2H^2 = \frac{1}{2}f\frac{e^{4\sigma}\dot{A}^2}{a^2} + \frac{V}{\sqrt{1-\dot{\phi}^2}} + \rho_m + \rho_r + 3m_{\rm P}^2\dot{\sigma}^2, \tag{2.3.2}$$

$$-2m_{\rm P}^2\dot{H} = \dot{\phi}^2\frac{V}{\sqrt{1-\dot{\phi}^2}} + \frac{2}{3}f\frac{e^{4\sigma}\dot{A}^2}{a^2} + \frac{4}{3}\rho_r + \rho_m + 6m_{\rm P}^2\dot{\sigma}^2, \tag{2.3.3}$$

$$\ddot{\sigma} + 3H\dot{\sigma} = \frac{e^{4\sigma}f\dot{A}^2}{3a^2m_{\rm P}^2}, \tag{2.3.4}$$

$$\frac{\ddot{\phi}}{1-\dot{\phi}^2} = \frac{\sqrt{1-\dot{\phi}^2}f_{,\phi}}{2Va^2}e^{4\sigma}\dot{A}^2 - \frac{V_{,\phi}}{V} - 3H\dot{\phi}, \tag{2.3.5}$$

$$\frac{\ddot{A}}{\dot{A}} = -\frac{\mathrm{d}}{\mathrm{d}t}\ln\left(afe^{4\sigma}\right). \tag{2.3.6}$$

Equations (2.3.2) and (2.3.3) correspond to the first and second Friedman equations, Eq. (2.3.4) is the evolution equation for the geometrical shear, and Eqs. (2.3.5) and (2.3.6) are the equations of motion for the scalar and vector fields, respectively. The above equations can be recast in terms of the following dimensionless variables

$$x \equiv \dot{\phi}, \quad y^2 \equiv \frac{V(\phi)}{3m_{\rm P}^2H^2}, \quad z^2 \equiv \frac{1}{2}f(\phi)\frac{e^{4\sigma}\dot{A}^2}{3m_{\rm P}^2H^2a^2}, \quad \Sigma \equiv \frac{\dot{\sigma}}{H}.$$

The first Friedman equation in Eq. (2.3.2) becomes the constraint

$$1 = \frac{y^2}{\sqrt{1-x^2}} + z^2 + \Sigma^2 + \Omega_m + \Omega_r, \tag{2.3.7}$$

while from the second Friedman equation in Eq. (2.3.3) we can compute the deceleration parameter $q \equiv -1 - \dot{H}/H^2$ obtaining

$$q = \frac{1}{2}\left[1 - 3\sqrt{1-x^2}y^2 + z^2 + \Omega_r + 3\Sigma^2\right]. \tag{2.3.8}$$

We can easily integrate Eq. (2.3.6) such that for the vector field degree of freedom we have

$$\dot{A} = c\frac{e^{-4\sigma}}{af}, \tag{2.3.9}$$

where c is a constant. From the Friedman equations (2.3.2) and (2.3.3), we can identify the density and pressure of dark energy, which can be written in terms of the dimensionless variables as

$$\rho_{\rm DE} \equiv 3m_{\rm P}^2 H^2\left(\frac{y^2}{\sqrt{1-x^2}} + z^2 + \Sigma^2\right), \quad p_{\rm DE} \equiv 3m_{\rm P}^2 H^2\left(-y^2\sqrt{1-x^2} + \frac{1}{3}z^2 + \Sigma^2\right), \tag{2.3.10}$$

respectively. Now, the equation of state of DE, $w_{\rm DE} \equiv p_{\rm DE}/\rho_{\rm DE}$, is given by

$$w_{\rm DE} = -1 + \frac{2}{3}\frac{\frac{3}{2}\frac{x^2y^2}{\sqrt{1-x^2}} + 2z^2 + 3\Sigma^2}{\frac{y^2}{\sqrt{1-x^2}} + z^2 + \Sigma^2}. \tag{2.3.11}$$

In order to calculate the evolution equations for the dimensionless variables, we differentiate each variable in Eq. (2.3.7) with respect to the number of e-folds. We get

$$x' = \sqrt{3}\left(1-x^2\right)\left[\frac{\sqrt{1-x^2}}{y}\beta z^2 - \sqrt{3}x - \alpha y\right], \tag{2.3.12}$$

$$y' = y\left[\frac{\sqrt{3}}{2}\alpha y x + q + 1\right], \tag{2.3.13}$$

$$z' = z(q-1) - 2z\Sigma - \frac{\sqrt{3}}{2}\beta x y z, \tag{2.3.14}$$

$$\Sigma' = \Sigma(q-2) + 2z^2, \tag{2.3.15}$$

$$\Omega_r' = 2\Omega_r(q-1), \tag{2.3.16}$$

where

$$\alpha(t) \equiv m_{\rm P}\frac{V_{,\phi}}{V^{3/2}}, \quad \beta(t) \equiv m_{\rm P}\frac{f_{,\phi}}{f\sqrt{V}}. \tag{2.3.17}$$

The last equations can be easily integrated when α and β are constants. Under this assumption, we get that the potential $V(\phi)$ and the coupling function $f(\phi)$ are given by expressions of the form[9]

$$V(\phi) \propto 1/(\alpha\phi)^2, \quad f(\phi) \propto (\alpha\phi)^{2\beta\phi/|\alpha\phi|}, \tag{2.3.18}$$

which correspond to common power law expressions typically used in the literature [145, 146].

[9] In the case of varying α and β, the autonomous set is not closed and we would be forced to introduce more dimensionless variables to close the system. Thus, we choose α and β constant to keep our presentation simple.

Analytical Fixed points

The asymptotic behavior of the autonomous system in Eqs. (2.3.12)-(2.3.16) is encoded in its fixed points, which can be found by setting $x' = 0$, $y' = 0$, $z' = 0$, $\Sigma' = 0$, and $\Omega_r' = 0$. This yields a set of algebraic equations given by

$$0 = \left(-1 + x^2\right)\left\{\alpha^2 y^4 + 2\sqrt{3}\alpha x y^3 + 3x^2y^2 + \beta^2 x^2 z^4 - \beta^2 z^4\right\}, \tag{2.3.19}$$

$$0 = y\Big\{9\left(x^2-1\right)y^4 + \left(3\Sigma^2 + \Omega_r + z^2 + 3\right)^2 + 3\alpha^2x^2y^2 \tag{2.3.20}$$
$$+ 2\sqrt{3}\alpha x y\left(3\Sigma^2 + \Omega_r + z^2 + 3\right)\Big\},$$

$$0 = z\Big\{3\beta^2x^2y^2 + \left[\Sigma(3\Sigma-4) + \Omega_r + z^2 - 1\right]^2 + 9\left(x^2-1\right)y^4\Big\} \tag{2.3.21}$$
$$- 2\sqrt{3}\beta x y\left[\Sigma(3\Sigma-4) + \Omega_r + z^2 - 1\right]$$

$$0 = 9\Sigma^6 + \Sigma^4\left(6\Omega_r + 6z^2 - 18\right) + 24\Sigma^3z^2 + 16z^4 + \Sigma\left(8z^4 + 8\Omega_r z^2 - 24z^2\right) \tag{2.3.22}$$
$$+ \Sigma^2\Big\{9\left(x^2-1\right)y^4 + \Omega_r^2 - 6\Omega_r + z^4 + 2\Omega_r z^2 - 6z^2 + 9\Big\}$$

$$0 = \Omega_r\left\{9\left(x^2-1\right)y^4 + \left(3\Sigma^2 + \Omega_r + z^2 - 1\right)^2\right\}, \tag{2.3.23}$$

where we have replaced the expression for q in terms of the dynamical variables given in Eq. (2.3.8), and some algebraic manipulations have been performed. Notice that these equations compose a polynomial system of degree greater than 4, since Eq. (2.3.22) is an equation of degree 6 in the variable Σ. This means that the system is not analytically solvable in general due to the fundamental theorem of Galois theory [144]. Nonetheless, in the case $\Sigma = 0$, equation (2.3.22) implies $z = 0$, and Eq. (2.3.21) is trivially satisfied. This is consistent with the fact that the vector field is the source of the anisotropy, as it can be seen in Eq. (2.3.4). The simplified Eqs. (2.3.19), (2.3.20) and (2.3.23) compose a system of degree reduced to 4, and thus analytical solutions exist.

In order to do some analytical progress, in the following we neglect anisotropy, i.e., we consider $\Sigma = 0$ and $z = 0$, and study the fixed points of the simplified system in Eqs. (2.3.19), (2.3.20) and (2.3.23) relevant for the radiation era ($\Omega_r \simeq 1$, $w_{\text{eff}} \simeq 1/3$), the matter era, ($\Omega_m \simeq 1$, $w_{\text{eff}} \simeq 0$) and an isotropic DE era ($\Omega_{\text{DE}} \equiv \rho_{\text{DE}}/3m_{\text{P}}^2H^2 \simeq 1$, $w_{\text{eff}} < -1/3$).

- (*DE-I*) Isotropic DE dominance:

$$x = \mp\frac{\alpha\sqrt{\sqrt{36+\alpha^4} - \alpha^2}}{3\sqrt{2}}, \quad y = \pm\frac{\sqrt{\sqrt{36+\alpha^4}-\alpha^2}}{\sqrt{6}}, \quad z = 0, \quad \Sigma = 0, \tag{2.3.24}$$

with $\Omega_{\text{DE}} = 1$, $\Omega_m = 0$, $\Omega_r = 0$ and

$$w_{\text{DE}} = -1 + \frac{1}{18}\alpha^2\left(-\alpha^2 + \sqrt{36+\alpha^4}\right). \tag{2.3.25}$$

Since $w_{\rm DE} = w_{\rm eff}$ in this point, the condition for accelerated expansion ($w_{\rm eff} < -1/3$) is satisfied when

$$|\alpha| < 3^{1/4}\sqrt{2} \approx 1.86121. \tag{2.3.26}$$

In this case, the eigenvalues are given by large expressions which we do not present in order to keep our presentation simple. In summary, we find that just one eigenvalue depends on α and β, while the remaining four eigenvalues depend only on α. These four later eigenvalues, namely, $\lambda_{1,2,3,4} < 0$ in the region where (*DE-I*) is an accelerated solution. The fifth eigenvalue, λ_5, is negative when $\alpha = 0$ or in the regions

$$0 < \alpha \quad \wedge \quad \beta < -\frac{\alpha}{3} + \frac{2}{3}\sqrt{\frac{36+\alpha^4}{\alpha^2}}, \tag{2.3.27}$$

$$\alpha < 0 \quad \wedge \quad \beta > -\frac{\alpha}{3} - \frac{2}{3}\sqrt{\frac{36+\alpha^4}{\alpha^2}}. \tag{2.3.28}$$

Therefore, (*DE-I*) is an attractor in these regions. By looking at Eqs. (2.3.12)-(2.3.16), we note that the autonomous system is invariant under the transformation $\{x \to -x, \alpha \to -\alpha, \beta \to -\beta\}$. This symmetry is reflected in Eqs. (2.3.27) and (2.3.28).

Numerical Fixed points

As shown in the last section, the set of algebraic equations in Eqs. (2.3.19)-(2.3.23) does not have analytical solutions when $\Sigma \neq 0$. Therefore, our numerical setup can be useful for further analysis of the model.

Despite early anisotropies being expected to be insignificant given the homogeneity of the CMB [59], late-time anisotropies sourced by a dark energy component are not discarded by observations [142, 143]. In the last section, we analytically found an isotropic dark energy-dominated point (*DE-I*). Then, our numerical search will be focused on anisotropic accelerated solutions. Moreover, it is possible to find initial conditions, in the deep radiation epoch, ensuring a proper radiation era followed by a standard matter era. Hence, in the following, we will neglect the radiation component, i.e., $\Omega_r = 0$. This assumption will simplify our numerical treatment.

Now, we proceed with the implementation of the numerical setup explained in Sec. 2.3.2. Firstly, we have to choose a specific window parameter where the stochastic search will be performed. Having in mind that $|\alpha| < 1.86121$ for (*DE-I*) being an accelerated solution, we choose $\alpha \in [-30, 30]$ and $\beta \in [0, 30]$; more precisely,

$$\{\alpha, \beta\} \in [-30, 30] \times [0, 30]. \tag{2.3.29}$$

Note that unlike α, β takes on nonnegative values since the autonomous system enjoys the sym-

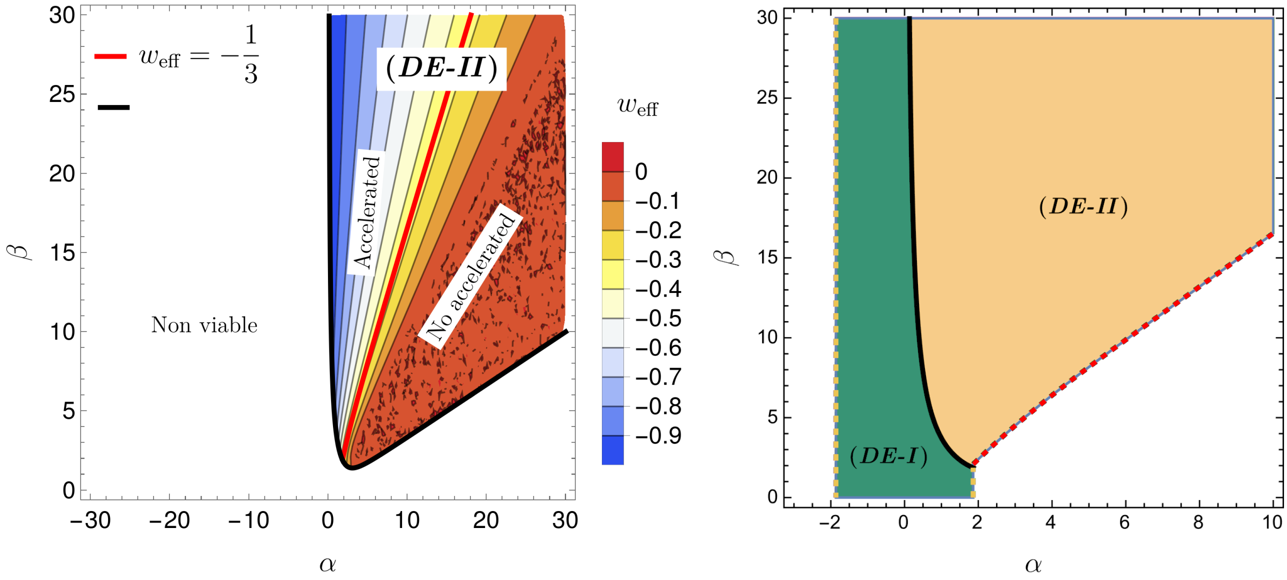

Figure 2.3.1: (Left) Region in the parameter space where the stochastic search was performed. This region is divided in "non-viable" solutions and (*DE-II*). Points in (*DE-II*) match the physical constraints in Eq. (2.3.30). These regions are separated by the black curve whose expression is given in Eq. (2.3.31). The red line represents the points for which $w_{\rm eff} = -1/3$, which further divides (*DE-II*) into two regions: accelerated solutions and non-accelerated solutions. (Right) Regions where (*DE-I*) and (*DE-II*) are attractors and accelerated solutions. The black line is the bifurcation curve given in Eq. (2.3.31).

metry $\{x \to -x, \alpha \to -\alpha, \beta \to -\beta\}$. Secondly, we impose the following physically motivated conditions

$$0 \leq \Omega_m \leq 1, \quad 0 \leq \Omega_{\rm DE} \leq 1. \tag{2.3.30}$$

Therefore, any point in the parameter space is cataloged as a "non-viable solution" if all the found fixed points do not obey these physical constraints. If at least one of the corresponding fixed points meets all the conditions, the point is cataloged as a "viable solution". Now, we generate $N \sim 10^4$ random points in the region specified in Eq. (2.3.29). For each of this points, the set of algebraic equations in Eqs. (2.3.19)-(2.3.22) is solved, considering $\Omega_r = 0$, using the `NSolve` command of `Mathematica`.[10] The code for solving $\sim 10^4$ algebraic systems takes approximately 45 minutes running on 136 parallelized mixed physical cores. This code is available on GitHub.[11]

The results of code runs are depicted in the left panel of Fig. 2.3.1, which we explain in the following. If all the solutions for a given point in the region in Eq. (2.3.29) do not satisfy the

[10]Note that our numerical scheme is not tied to the `Mathematica` software or to the `NSolve` command. This step, namely, the solution of the algebraic equations, can be done using any other coding language or algebraic system solver.

[11]https://github.com/sagaser/Numerical-dynamical-analysys

physical conditions in Eq. (2.3.30), this point in the parameter space is allocated in the white region called "non viable". The points filling this region are cosmologically irrelevant. In turn, if at least one of the solutions for a given point matches all the physical constraints, this point is allocated in the "viable region" which is called (*DE-II*). We found that these regions, non viable and (*DE-II*), are separated by the curve

$$\beta = -\frac{\alpha}{3} + \frac{2}{3}\sqrt{\frac{36+\alpha^4}{\alpha^2}}, \tag{2.3.31}$$

which is the same curve dividing the regions where (*DE-I*) is an accelerated solution [see Eqs. (2.3.27) and (2.3.28)]. Region (*DE-II*) can be further divided into "accelerated" and "non accelerated" solutions by the line $w_{\text{eff}}(\alpha,\beta) = -1/3$. The color code in the left panel of Fig. 2.3.1 shows that it is possible to get $w_{\text{eff}} \sim -1$ for some values of α and β. The existence of (*DE-I*) and the "accelerated" region in (*DE-II*) ensures an expanding universe at an accelerated rate, which can be isotropic or anisotropic.

The stability of (*DE-II*) can be determined following the step 4 in Sec. 2.3.2. We compute all the available Jacobian matrices (and their eigenvalues) for each of the points in (*DE-II*). We expect that at least a portion of the "accelerated" region in (*DE-II*) could be an attractor of the system. As mentioned in Sec. 2.3.2, a point in the parameter space yield attractor solutions if all the eigenvalues of at least one of the corresponding Jacobian matrices are negative. We found that this attractor condition is obeyed by all the points in (*DE-II*). Therefore, (*DE-II*) is an attractor inside its own region of existence. We summarize the possible attractors of the system in the right panel of Fig. 2.3.1. In this figure, we find out that Eq. (2.3.31) is the bifurcation curve that separates both attractors.

2.3.4 Conclusions

In this work, we have put forward a numerical method to explore the parameter space of a cosmological model when no analytical fixed points are available. We applied our method to a specific model of anisotropic dark energy based on the interaction between a scalar tachyon field and a vector field in a Bianchi I background. We have explicitly shown that the anisotropic attractor of the system has no analytical description, given that the degree of the algebraic system from which this point must be computed is greater than 4 [see Eqs. (2.3.19)-(2.3.22)]. However, when the anisotropy is neglected, the system is reduced to a system of degree 4 and thus analytical solutions exist, which we presented in Eqs. (2.3.24). In particular, our method allowed us to find the parameter space of the model where anisotropic accelerated solutions exist as attractors of the system, which we plot in Fig. 2.3.1. In the corresponding work (Ref. [6]), we checked the consistency of the method by numerically solving the full autonomous system in Eqs. (2.3.12)-(2.3.16) for a particular set of initial conditions, but we do not show it here to keep our presentation simple. As a last remark, we would like to stress on the generality of our method, as explained in Sec. 2.3.2, i.e., in principle, it can be applied to any DE scenario.

2.4 Inhomogeneous Scalar Fields

2.4.1 Introduction

An anisotropic dark energy can be realized by considering a homogeneous but spatially anisotropic metric, together with a suitable arrangement of the fields driving the expansion of the universe which are typically only time-dependent [2, 3, 115–117, 122–124]. Nonetheless, in Refs. [147, 148], it was shown that a triad of scalar fields with spatially constant but nonzero gradients can generate a homogeneous and isotropic energy-momentum tensor, i.e. invariant under translations and spatial rotations. This triad, known as “solid”, is given by

$$\phi^I \equiv x^I, \quad I \in \{1,2,3\}, \tag{2.4.1}$$

where ϕ^I is a scalar field and x^I is a comoving cartesian coordinate. The solid configuration for inhomogeneous scalar fields is similar to other configurations for different fields. For instance, the cosmic triad for vector and nonabelian gauge vector fields [114, 125, 149–151], the U(1) triad of homogeneous scalar fields [152], and the recent Higgs triad [2], among others.

In Refs. [147], an isotropic energy-momentum tensor is achieved since the Lagrangians constructed from each of the three scalar fields are equal, while in Ref. [148] it is assumed that the scalar fields possess an internal SO(3) symmetry such that the ansatz in Eq. (2.4.1) is invariant under combined spatial and internal rotations. In Refs. [153, 154], it was shown that the solid configuration in Eq. (2.4.1) can support *prolonged anisotropic inflationary* solutions[12]. In this work, we show that this characteristic behavior is also present at late-times for most of the parameter space of the model and thus the final stage of the Universe can be an anisotropic accelerated expansion, even if the initial spatial shear is set to zero. Nonetheless, there is a particular region in the parameter space of the model where the Universe becomes isotropic, meaning that the solid does not source the shear, which then eventually vanishes. For completeness, we also show that dark energy dominance is possible when the background metric is homogeneous and isotropic.

[12]Other scenarios of anisotropic inflation have been studied, see for instance [155–161].

2.4.2 General Model

We call a "solid" the specific configuration of three inhomogeneous scalar fields given by Eq. (2.4.1).[13]. We thus opt for studying the simple action

$$S = \int \mathrm{d}^4x\sqrt{-g}\left[\frac{m_{\mathrm{P}}^2}{2}R - \sum_I F^I\left(X^I\right) + \mathcal{L}_m + \mathcal{L}_r\right], \tag{2.4.2}$$

where F^I is the Lagrangian characterizing the dynamics of the scalar field ϕ^I, whose argument is the canonical kinetic-type term

$$X^I \equiv g^{\mu\nu}\nabla_\mu\phi^I\nabla_\nu\phi^I. \tag{2.4.3}$$

This action is an extension to the late-time cosmology of the model studied in Ref. [147] in the inflationary context.

Varying the action in Eq. (2.4.2) with respect to the space-time metric $g^{\mu\nu}$, we get the gravitational field equations $m_{\mathrm{P}}^2 G_{\mu\nu} = T_{\mu\nu}$, with $T_{\mu\nu}$ the total energy tensor given by

$$T_{\mu\nu} = 2\sum_I F_{X^I}\nabla_\mu\phi^I\nabla_\nu\phi^I - g_{\mu\nu}\sum_I F^I + T^m_{\mu\nu} + T^r_{\mu\nu}, \tag{2.4.4}$$

where we have used the shorthand notation $F_{X^I} \equiv \frac{\mathrm{d}F^I}{\mathrm{d}X^I}$. Varying the action with respect to ϕ^I, we get the equation of motion

$$\nabla_\mu(F_{X^I}\nabla^\mu\phi^I) = 0. \tag{2.4.5}$$

Background Equations of Motion

Since we are interested in anisotropic deformations sourced by the solid, we adopt the geometry of a homogeneous but anisotropic Bianchi-I metric as in Eq. (2.1.6). In Ref. [147], it was shown that the action in Eq. (2.4.2) can be compatible with the symmetries of the FLRW metric if the three Lagrangians F^I are identical; i.e. $F^I = F$ and thus $\sum_I F^I = 3F$. However, in the Bianchi-I background in Eq. (2.1.6), the canonical kinetic-type terms read

$$X^1(t) = \frac{e^{4\sigma(t)}}{a^2(t)}, \quad X^2(t) = X^3(t) = \frac{e^{-2\sigma(t)}}{a^2(t)}, \tag{2.4.6}$$

[13] Even more general configurations can be studied, like the "supersolids" in Ref. [162]

and the requirement for the Lagrangians F^I in this case is

$$\sum_I F^I\left(X^I\right) = F^1\left(X^1\right) + 2F^2\left(X^2\right). \tag{2.4.7}$$

The Friedman equations read

$$3m_{\rm P}^2 H^2 = F^1 + 2F^2 + 3m_{\rm P}^2\dot{\sigma}^2 + \rho_m + \rho_r, \tag{2.4.8}$$

$$-2m_{\rm P}^2\dot{H} = \frac{2}{3}X^1 F_{X^1} + \frac{4}{3}X^2 F_{X^2} + \rho_m + \frac{4}{3}\rho_r + 6m_{\rm P}^2\dot{\sigma}^2, \tag{2.4.9}$$

$$\ddot{\sigma} + 3H\dot{\sigma} = \frac{2}{3m_{\rm P}^2}\left(X^2 F_{X^2} - X^1 F_{X^1}\right). \tag{2.4.10}$$

We define the density and pressure of dark energy by

$$\rho_{\rm DE} \equiv F^1 + 2F^2 + 3m_{\rm P}^2\dot{\sigma}^2,$$
$$p_{\rm DE} \equiv \frac{1}{3}(2x_1 - 3)F^1 + \frac{2}{3}(2x_2 - 3)F^2 + 3m_{\rm P}^2\dot{\sigma}^2,$$

where we have defined the quantities

$$x_1 \equiv \frac{X^1 F_{X^1}}{F^1}, \quad x_2 \equiv \frac{X^2 F_{X^2}}{F^2}, \tag{2.4.11}$$

which characterize the form of the Lagrangians F^1 and F^2, respectively.

The set of Eqs. (2.4.8)-(2.4.10) describes the cosmological background dynamics. In the next section, we will study the asymptotic behavior of this set of equations through a dynamical system analysis [97, 163].

2.4.3 Autonomous System

In order to proceed, we introduce the following dimensionless variables

$$f_1^2 \equiv \frac{F^1}{3m_{\rm P}^2 H^2}, \quad f_2^2 \equiv \frac{F^2}{3m_{\rm P}^2 H^2}, \quad \Omega_m \equiv \frac{\rho_m}{3m_{\rm P}^2 H^2}, \quad \Omega_r \equiv \frac{\rho_r}{3m_{\rm P}^2 H^2}, \quad \Sigma \equiv \frac{\dot{\sigma}}{H}, \tag{2.4.12}$$

such that the first Friedman equation (2.4.8) becomes the constraint

$$\Omega_m = 1 - f_1^2 - 2f_2^2 - \Sigma^2 - \Omega_r. \tag{2.4.13}$$

Changing the cosmic time t for the number N of e-folds, the background equations (2.4.8)-(2.4.10) are replaced by the autonomous system

$$f_1' = f_1 \left[q + 1 - x_1 (1 - 2\Sigma)\right], \tag{2.4.14}$$
$$f_2' = f_2 \left[q + 1 - x_2 (1 + \Sigma)\right], \tag{2.4.15}$$
$$\Sigma' = \Sigma(q-2) - 2\left(x_1 f_1^2 - x_2 f_2^2\right), \tag{2.4.16}$$
$$\Omega_r' = 2\Omega_r (q-1), \tag{2.4.17}$$

where the deceleration parameter, $q \equiv -a\ddot{a}/\dot{a}^2$, is given by

$$q = \frac{1}{2}\left[1 + (2x_1 - 3)f_1^2 + 2(2x_2 - 3)f_2^2 + 3\Sigma^2 + \Omega_r\right]. \tag{2.4.18}$$

The dark sector is characterized by its equation of state $w_{\rm DE} \equiv p_{\rm DE}/\rho_{\rm DE}$, which in terms of the dynamical variables reads

$$w_{\rm DE} = -1 + \frac{2}{3}\frac{x_1 f_1^2 + 2x_2 f_2^2 + 3\Sigma^2}{f_1^2 + 2f_2^2 + \Sigma^2}, \tag{2.4.19}$$

and its density parameter $\Omega_{\rm DE} \equiv \rho_{\rm DE}/3m_{\rm P}^2 H^2$.

It is necessary to choose the specific Lagrangians F^1 and F^2 in order to get a closed autonomous system. In this case, the simplest model is obtained when x_1 and x_2 are constants, which corresponds to a power law model

$$F^1 \propto (X^1)^n, \quad F^2 \propto (X^2)^m \quad \Rightarrow \quad x_1 = n, \quad x_2 = m. \tag{2.4.20}$$

We will see that this simple choice is enough to get interesting behaviors.

Fixed Points and Stability

The fixed points of the system can be obtained by setting $f_1' = 0$, $f_2' = 0$, $\Sigma' = 0$, and $\Omega_r' = 0$ in equations (2.4.14)-(2.4.17) and their stability can be analyzed using the linear theory.

• **(*DE*-1) Anisotropic dark energy scaling with F^1:** This is the first solution corresponding to an anisotropic dark energy dominated universe. The variables take on the values

$$f_1 = \frac{\sqrt{3(3+n)(1-n)}}{3-n}, \quad \Sigma = \frac{2n}{n-3}, \quad w_{\rm eff} = w_{\rm DE} = -1 + \frac{2n(1+n)}{3-n}, \tag{2.4.21}$$

while the other variables are zero.

If we now impose the conditions $f_1^2 \geq 0$, $-1 \leq w_{\rm DE} < -1/3$, and $|\Sigma_0| < \mathcal{O}(0.001)$ – the latter being necessary for having accelerated solutions[14] – we find the following regions of existence

$$0 \leq n < 0.535184, \quad \forall m. \tag{2.4.22}$$

Note that if $n = 0$, then $\Sigma = 0$ given that the Lagrangian F^1 becomes a cosmological constant. We find that the eigenvalues of the corresponding Jacobian matrix in this point are negative in the region of existence given in Eq. (2.4.22) and

$$m \geq n \left(\frac{1+n}{1-n} \right). \tag{2.4.23}$$

Therefore, we conclude that (*DE-1*) is an attractor inside the region of existence in Eq. (2.4.22) whenever Eq. (2.4.23) is obeyed.

- **(*DE*-2) Anisotropic dark energy with F^2:** The variables take on the values

$$f_2 = \frac{\sqrt{3(3/2-m)}}{3-m}, \quad \Sigma = \frac{m}{3-m}, \quad w_{\rm eff} = w_{\rm DE} = -1 + \frac{2m}{3-m}, \tag{2.4.24}$$

while the other variables are zero. Imposing the conditions $f_2^2 \geq 0$ and $-1 \leq w_{\rm DE} < -1/3$, we arrive at the following region of existence

$$0 \leq m < 0.75, \quad \forall n. \tag{2.4.25}$$

Note that if $m = 0$, then $\Sigma = 0$ given that the Lagrangian F^2 becomes a cosmological constant.

We find that the eigenvalues of the corresponding Jacobian matrix in this point are negative in the region of existence given by Eq. (2.4.25) and

$$n \geq \frac{m}{1-m}. \tag{2.4.26}$$

Thus, (*DE-2*) is an attractor inside the region of existence in Eq. (2.4.25) when Eq. (2.4.26) is satisfied.

[14] We concentrate in no-phantom solutions; i.e. $w_{\rm DE} \geq -1$, although this possibility has not been discarded by observations yet [39].

• **($\boldsymbol{DE}$-3) Anisotropic dark energy scaling with F^1 and F^2:** This is the only solution in which dark energy scales with both F^1 and F^2. The variables are given by

$$f_1 = \frac{\sqrt{3(m-n+mn)}}{m+2n}, \quad f_2 = \frac{\sqrt{3\left[n(n+1)+m(n-1)\right]}}{\sqrt{2}(m+2n)}, \quad \Sigma = \frac{n-m}{m+2n},$$

$$w_{\text{eff}} = w_{\text{DE}} = -1 + \frac{2mn}{m+2n}. \tag{2.4.27}$$

By demanding that both f_1^2 and f_2^2 are positive, and that $-1 \leq w_{\text{DE}} < -1/3$, we arrive at two possible regions for the parameters m and n:

$$(I) : 0 < n < 0.535184 \ \wedge \ \frac{n}{1+n} \leq m < n\left(\frac{1+n}{1-n}\right), \tag{2.4.28}$$

$$(II) : 0.535184 \leq n < 3 \ \wedge \ \frac{n}{1+n} \leq m < \frac{2n}{3n-1}. \tag{2.4.29}$$

Notice that the cases $m = 0$ and $n = 0$ are not allowed in the region of existence.

Note that in the region of existence of (DE-3) there is the possibility that $n = m$, implying that $\Sigma = 0$. This follows since, in the case $n = m$, $f_1 = f_2$ and therefore $F^1 = F^2$ by the definition of the variables. This implies that the right-hand side of Eq. (2.4.10) is zero, and thus the shear decays since the solid is not sourcing it. In other words, the shear is dynamically erased given that the Lagrangians behave in the same way. On the other hand, and as we will see later, the shear grows at late-times even if it is set to zero as the initial condition, since the solid sources it given that the Lagrangians F^I behave in different ways, i.e. when $n \neq m$.

The eigenvalues of the Jacobian matrix in this fixed point are given by too long algebraic expressions involving the parameters n and m. We omit them here since only the sign of the real part of the eigenvalues is relevant to the stability analysis. We investigated the parameter window, inside the regions of existence, and we found that the four corresponding eigenvalues are negative inside the whole region of existence of the point; i.e. when (*DE-3*) exists, it *is* an attractor.

From the previous analysis, it is clear that the three dark energy dominated points can be attractors. In Fig. 2.4.1, we plot the $\{m, n\}$ parameter space where each dark energy dominated point is an attractor. We can see that these regions are separated by bifurcation curves (black solid lines), meaning that they are mutually excluded. This ensures that the system has only one dark energy attractor for a particular set of parameters $\{m, n\}$. This leave the case $n = m$ as the only possibility to get an isotropic Universe, since the points (*DE-1*) and (*DE-2*) are saddle while (*DE-3*) is the global attractor under this condition.

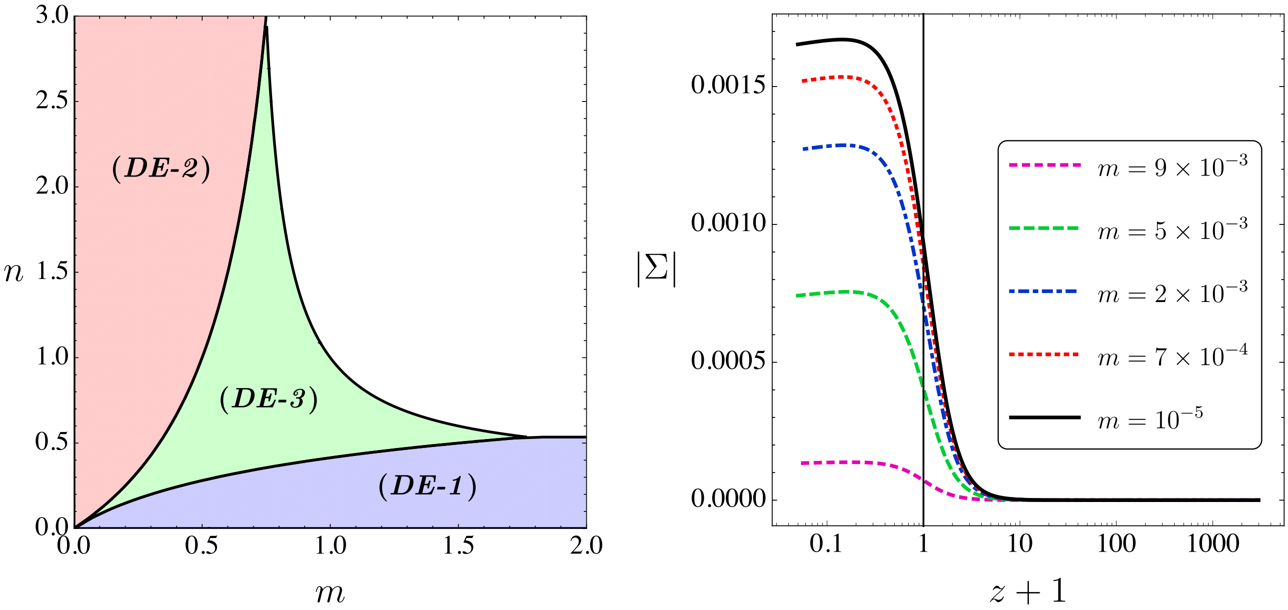

Figure 2.4.1: (Left) Stability regions for the dark energy dominated points. Each color represents a $\{m, n\}$ parameter region where the indicated fixed point is an attractor. These three regions are separated by bifurcations curves (black solid lines), i.e. they are mutually excluded. (Right) Evolution of the shear Σ around $z = 0$ for different values of the parameter m, while n is fixed and the initial conditions are the same given in Eq. (2.4.30). The thin vertical line signals the value of the shear today.

2.4.4 Observational Signatures

From the magnitude-redshift data of SNe Ia, the analysis of Ref. [142] showed that the present value of the spatial shear is constrained to be $|\Sigma_0| \lesssim \mathcal{O}(0.01)$. More recently, the authors of Ref. [143] used a combination of the observational Hubble data $H(z)$ and SNe Ia measurements to put the tighter bound of $|\Sigma_0| \lesssim \mathcal{O}(0.001)$. Similarly, future weak-lensing measurements with the Euclid satellite are expected to reach a similar sensitivity level of $|\Sigma_0| \lesssim \mathcal{O}(0.008)$ [164]. In order to investigate the evolution of the shear at late-times when dark energy is able to effectively source it, in the following, we numerically solve the autonomous system in Eqs. (2.4.14)-(2.4.17)

We assume that, prior to the radiation epoch, the Universe underwent an inflationary period which perfectly smoothed any initial spatial shear or inhomogeneities. Moreover, we will choose parameters m and n such that the attractor point is given by (*DE-2*). Since $\Sigma_i = 0$, it is natural to assume that the contributions to the energy budget coming from the variables f_1 and f_2 are the same at the starting point. Having this in mind, we have chosen

$$\Omega_{r_i} = 0.99995, \quad f_{1_i} = f_{2_i} = 10^{-14}, \quad \Sigma_i = 0 \tag{2.4.30}$$

as initial conditions at the redshift $z = 7.25 \times 10^7$, and we have integrated the system up to $z \to -1$. Since observations favor an equation of state of dark energy close to -1, from Eq. (2.4.25) we have to choose $m \approx 0$.

We have investigated the evolution of Σ taking this initial conditions with $n = 10^{-2}$ and considering different values for the parameter m in such a way that (DE-2) is the only attractor of the system. The results are shown in the right panel of Fig. 2.4.1, where we can see that $|\Sigma|$ starts to grow around $z = 10$. The values predicted for the present spatial shear are $|\Sigma_0| \leq 9.4 \times 10^{-4}$, corresponding to the black solid curve in Fig. 2.4.1, which are in agreement with the observational bounds $|\Sigma_0| \leq \mathcal{O}(0.001)$ [142, 143]. We want to stress that, even for $\Sigma_i = 0$, the final state of the Universe is an anisotropic accelerated expansion.

For the set of parameters and initial conditions used in Fig. 2.4.1, we can see that $|\Sigma_0|$ is within these bounds, although it can take greater values in the future cosmological evolution.

An anisotropic dark energy has the potential for breaking of statistical isotropy and explain of some of the large scale CMB anomalies. In particular, anisotropic pressure can induce peculiar velocity flows, anisotropy in the SNe Ia data, and significant CMB dipole and quadrupole [112] fluctuations. The main observational effect of an anisotropic shear is its contribution to the CMB temperature anisotropies. This contribution is introduced through the redshift at last scattering surface, which becomes anisotropic. Considering only large-scale fluctuations, this can be quantified as [122, 165]:

$$\left|\frac{\delta T}{T}(\hat{\boldsymbol{n}})\right| \lesssim |\sigma_0 - \sigma_{\rm dec}| \,, \tag{2.4.31}$$

where $\delta T/T$ is the CMB temperature anisotropies, $\hat{\boldsymbol{n}}$ is the unit vector along the line-of-sight, and $\sigma_{\rm dec}$ is the value of the geometrical shear at the time of decoupling ($z \simeq 1090$). Since $\sigma' = \Sigma$, we can obtain the values for the geometrical shear by numerical integration. For the cases with the largest and smallest shear today, as depicted in Fig. 2.4.1, and using the same initial conditions of Eq. (2.4.30), we obtain

$$\text{largest } \Sigma_0: \; |\sigma_0 - \sigma_{\rm dec}| \approx 5 \times 10^{-4}, \tag{2.4.32}$$

$$\text{smallest } \Sigma_0: \; |\sigma_0 - \sigma_{\rm dec}| \approx 3 \times 10^{-5}, \tag{2.4.33}$$

which are in qualitative agreement with the conservative bound $|\sigma_0 - \sigma_{\rm dec}| < 10^{-4}$ [39], thus, a solid anisotropic dark energy could alleviate the observed CMB quadrupole anomaly.

2.4.5 Conclusions

In this work we studied a set of three scalar fields with a constant but nonvanishing spatial gradients as a source of anisotropic dark energy. This particular set of inhomogeneous scalar fields, known as "solid", has been used in the inflationary context showing interesting features at the perturbative level [147, 148]. It was also shown that anisotropic inflationary solutions are possible [153, 154]. Here, we have investigated the late-time dynamics of the solid in a Bianchi-I expanding universe. Through a dynamical system analysis, we showed that for a particular power-law model, the solid can generate an anisotropic late-time accelerated expansion, being this epoch an attractor of the system for suitable values of the free parameters of the model (see Fig. 2.4.1). In these regions, the cosmological evolution starts in a radiation-dominance epoch, followed by a matter-dominance epoch, and ending in a possible anisotropic dark energy-dominated period which can be realized by three different points, whose attractor regions are separated by bifurcation curves, i.e. they are mutually excluded. Nonetheless, we found that in the particular case when $n = m$ the Universe isotropizes provided that the Lagrangians F^I evolve in the same way.

The dynamical analysis was complemented with a numerical integration of the dynamical system. The parameters were fixed in such a way that (*DE-2*) was the only attractor point and the equation of state of dark energy was close to -1 as expected from observations [39]. The initial conditions were chosen in the deep radiation era (redshift $z = 7.25 \times 10^7$) and assuming a zero spatial shear ($\Sigma_i = 0$). We found that the spatial shear differs sensibly from zero at around $z = 10$, taking nonnegligible values nowadays but within the observational bounds $|\Sigma_0| \lesssim \mathcal{O}(0.001)$ [142, 143]. The numerical solution also showed a nearly constant equation of state of dark energy, $w_{\rm DE}$, that only changed about $\sim 0.001\%$ from its value at $z = 7.25 \times 10^7$ to its final value in the far future ($z \to -1$). We verified that similar behaviors are obtained if the parameters are chosen to establish (*DE-1*) or (*DE-3*) as the attractor points.

The nonvanishing shear after the radiation-dominated epoch leaves imprints on CMB and SNe Ia data. In particular, the shear affects the CMB quadrupole temperature anisotropy through the standard Sachs-Wolfe formula. We showed that the change of the spatial shear from decoupling to today can be compatible with the CMB quadrupole data. In particular, if $|\sigma_0 - \sigma_{\rm dec}|$ is of order 10^{-4}, there may be an interesting possibility for addressing the CMB quadrupole anomaly.

2.5 Non-Abelian Gauge Vector Fields

2.5.1 Introduction

As already mentioned, the most popular models to account for the current accelerated expansion of the Universe are based on single scalar fields. Despite the successes of these theories, other interesting alternatives, built with different types of fields, have been also explored [122–124, 160, 166–181]. Between these proposals, non-Abelian gauge fields have recently attracted a lot of attention since they could link cosmology with the phenomenology of particle physics [167]. The cosmological dynamics of these fields have been extensively discussed in the literature [1, 2, 118, 120, 125, 151, 182–199]. For instance, the late-time accelerated expansions can be uniquely explained by non-Abelian gauge vector fields as in Ref. [125] where the "gaugessence" model was proposed. It was shown that for several sets of initial conditions and parameters there exists a period of accelerated expansion. In this work, we generalize this model by considering the effect of a mass term for the gauge vector field in the late-time cosmological evolution. We show in particular that accelerated expansion is an "effective" attractor. We also study the equation of state of dark energy, showing different behaviors to those found in Ref. [125] that allow distinguishing this model from other dark energy proposals. We also address some differences between this model and the usual quintessence models.

Several observational indications are suggesting that the present Universe is undergoing an anisotropic accelerated expansion [142, 143, 200, 201]. Regarding gauge vector fields, in Ref. [185] was shown that an axially symmetrical massless gauge vector field isotropizes during the inflationary expansion, and thus any initial anisotropy is quickly dilute. However, this scenario has not been studied in the frame of the late-time accelerated expansion where other conclusions or interesting features can be reached. Here we consider the dynamics of an axially symmetrical gauge field in a homogeneous but anisotropic background and numerically investigate the possibility to get a non-negligible contribution to the current spatial shear.

2.5.2 Background Dynamics

In Ref. [125] the action

$$S = \int \mathrm{d}^4x\sqrt{-\tilde{g}}\left[\frac{m_{\mathrm{P}}^2}{2}R - \frac{1}{4}F^a{}_{\mu\nu}F_a{}^{\mu\nu} + \frac{\kappa}{96}\left(\tilde{F}_a{}^{\mu\nu}F^a{}_{\mu\nu}\right)^2 - \frac{1}{2}m_a^2A^a{}_\mu A_a{}^\mu\right], \tag{2.5.1}$$

was studied in the context of dark energy. Here, $\tilde{g}$ its determinant of the metric, κ is a positive-definite constant with dimensions $[\,m_{\mathrm{P}}^{-4}\,]$, m_a is a constant mass term, $F^a{}_{\mu\nu}$ is the field strength tensor

$$F^a_{\ \mu\nu} \equiv \partial_\mu A^a_{\ \nu} - \partial_\nu A^a_{\ \mu} + g\,\varepsilon^a_{\ bc} A^b_{\ \mu} A^c_{\ \nu}\,, \tag{2.5.2}$$

of a non-Abelian gauge vector field $A^a_{\ \mu}$ with mass m_a, g is the SU(2) coupling constant and $\varepsilon^a_{\ bc}$ being the Levi-Civita symbol. The dual of the strength tensor is defined as usual by

$$\tilde{F}_a^{\ \mu\nu} \equiv \frac{1}{2}\varepsilon^{\mu\nu\rho\sigma} F^a_{\ \rho\sigma}\,, \tag{2.5.3}$$

In that work it was shown that, for several sets of initial conditions and parameters, the dynamics of the non-Abelian gauge field can account for the late-time accelerated expansion of the Universe. Here we extend the model by considering the effect of the mass term in the cosmological evolution and use a dynamical system approach to fully describe the late-time behaviour of the expansion. In particular, we explicitly show that dark energy domination is indeed an attractor and give the full parameter space of the theory, complementing the results given in Ref. [125].

Varying the action in Eq. (2.5.1) with respect to the metric $g^{\mu\nu}$ we obtain the energy tensor for the gauge sector as

$$T_{\mu\nu} = F^a_{\ \mu\rho} F^a_{\ \nu\sigma} g^{\sigma\rho} + m^2 A^a_{\ \mu} A^a_{\ \nu} - g_{\mu\nu}\left[\frac{1}{4}F_a^{\ \rho\sigma} F^a_{\ \rho\sigma} + \frac{\kappa}{96}\left(\tilde{F}_a^{\ \rho\sigma} F^a_{\ \rho\sigma}\right)^2 + \frac{1}{2}m^2 A_a^{\ \lambda} A^a_{\ \lambda}\right]. \tag{2.5.4}$$

In the following, we will assume a flat FLRW metric. An ansatz for the massive gauge vector field consistent with the symmetries of this spacetime is [149]

$$A^a_{\ 0} \equiv 0, \quad A^a_{\ i} \equiv a(t)\psi(t)\delta^a_{\ i}, \tag{2.5.5}$$

where $\psi(t)$ is a scalar field. As a shorthand notation, we define $\phi(t) \equiv a(t)\psi(t)$. Isotropy also requires that the gauge fields have identical masses, i.e. $m_1 = m_2 = m_3 = m$. In order to reproduce the known expansion history of the Universe, let us define the density and pressure of dark energy as

$$\rho_{\rm DE} = \rho_{\rm YM} + \rho_\kappa + \rho_A, \quad p_{\rm DE} = \frac{1}{3}\rho_{\rm YM} - \rho_\kappa - \frac{1}{3}\rho_A, \tag{2.5.6}$$

where

$$\rho_{\rm YM} \equiv \frac{3}{2}\left(\frac{\dot{\phi}^2}{a^2} + \frac{g^2\phi^4}{a^4}\right), \quad \rho_\kappa \equiv \frac{3}{2}\kappa g^2 \frac{\phi^4\dot{\phi}^2}{a^6}, \quad \rho_A \equiv \frac{3}{2}\frac{m^2\phi^2}{a^2}. \tag{2.5.7}$$

The Friedmann equations become

$$3m_{\rm P}^2 H^2 = \frac{3}{2}\left[\frac{\dot{\phi}^2}{a^2} + \frac{g^2\phi^4}{a^4} + \kappa g^2 \frac{\phi^4\dot{\phi}^2}{a^6} + \frac{m^2\phi^2}{a^2}\right] + \rho_m + \rho_r, \tag{2.5.8}$$

$$2m_{\rm P}^2\dot{H} = -2\left[\frac{\dot{\phi}^2}{a^2} + \frac{g^2\phi^4}{a^4} + \frac{1}{2}\frac{m^2\phi^2}{a^2} + \frac{1}{2}\rho_m + \frac{2}{3}\rho_r\right]. \tag{2.5.9}$$

Varying the action in Eq. (2.5.1) with respect to $A^a{}_\nu$ we get

$$0 = \nabla_\mu\left[F_a{}^{\mu\nu} - \frac{\kappa}{12}\left(\tilde{F}_d{}^{\rho\sigma}F^d{}_{\rho\sigma}\right)\tilde{F}_a{}^{\mu\nu}\right] - m^2 A_a{}^\nu - g\varepsilon_c{}^{ab}A^c{}_\mu\left[F_b{}^{\mu\nu} - \frac{\kappa}{12}\left(\tilde{F}_d{}^{\rho\sigma}F^d{}_{\rho\sigma}\right)\tilde{F}_b{}^{\mu\nu}\right], \tag{2.5.10}$$

and thus the gauge field equation of motion is given by

$$0 = \frac{\ddot{\phi}}{a}\left(1 + \kappa g^2\frac{\phi^4}{a^4}\right) + \frac{H\dot{\phi}}{a}\left(1 - 3\kappa g^2\frac{\phi^4}{a^4}\right) + \frac{2g^2\phi^3}{a^3}\left(1 + \kappa\frac{\dot{\phi}^2}{a^2}\right) + m^2\frac{\phi}{a}. \tag{2.5.11}$$

These equations are complemented by the usual continuity equations for the barotropic fluids.

Proceeding as usual, from the Friedmann equation in Eq. (2.5.8) we define the dimensionless variables

$$x \equiv \frac{1}{\sqrt{2}m_{\rm P}}\frac{\dot{\phi}}{aH}, \quad y \equiv \frac{1}{\sqrt{2}m_{\rm P}}\frac{g\,\phi^2}{a^2H}, \quad w \equiv \frac{1}{\sqrt{2}m_{\rm P}}\frac{m\phi}{aH}, \quad z \equiv \frac{1}{\sqrt{2}m_{\rm P}}\frac{\phi}{a}. \tag{2.5.12}$$

Hence Eq. (2.5.8) becomes a constraint from which we can write Ω_m in terms of the other variables as

$$\Omega_m = 1 - x^2(1 + 4\alpha z^4) - y^2 - w^2 - \Omega_r, \tag{2.5.13}$$

where α is a dimensionless parameter defined as $\alpha \equiv m_{\rm P}^4\,\kappa g^2$. Using the equation of motion in Eq. (2.5.11), the continuity equation for radiation fluid, and the constraint in Eq. (2.5.13), the autonomous set of equations reads

$$x' = xq - \left(1 + 4\alpha z^4\right)^{-1}\left[2\frac{y^2}{z} + 8\alpha x^2 z^3 + x\left(1 - 12\alpha z^4\right) + \frac{w^2}{z}\right], \tag{2.5.14}$$

$$y' = y\left(2\frac{x}{z} + q - 1\right), \tag{2.5.15}$$

$$w' = w\left(\frac{x}{z} + q\right) \tag{2.5.16}$$

$$z' = x - z, \tag{2.5.17}$$

$$\Omega_r' = 2\Omega_r\left(q - 1\right), \tag{2.5.18}$$

where the deceleration parameter $q \equiv -1 - \dot{H}/H^2$ is obtained from Eq. (2.5.9) as

$$q = \frac{1}{2}\left[1 + x^2\left(1 - 12\alpha z^4\right) + y^2 - w^2 + \Omega_r\right]. \tag{2.5.19}$$

From this deceleration parameter, we can define the effective equation of state $w_{\rm eff} \equiv \frac{2q-1}{3}$

which in terms of the dimensionless variables reads

$$w_{\text{eff}} = \frac{1}{3}\left[x^2\left(1-12\alpha z^4\right)+y^2-w^2+\Omega_r\right], \tag{2.5.20}$$

which completely characterizes the evolution of the average scale factor $a(t)$. The dark sector is characterized by the density parameter $\Omega_{\text{DE}} \equiv \rho_{\text{DE}}/\left(3m_{\text{P}}^2H^2\right)$ and the equation of state $w_{\text{DE}} \equiv p_{\text{DE}}/\rho_{\text{DE}}$:

$$\Omega_{\text{DE}} = x^2\left(1+4\alpha z^4\right)+y^2+w^2, \quad w_{\text{DE}} = \frac{1}{3}\frac{x^2\left(1-12\alpha z^4\right)+y^2-w^2}{x^2\left(1+4\alpha z^4\right)+y^2+w^2}. \tag{2.5.21}$$

Note that the dynamical system analysis has revealed that only the combination of the parameters κ and g through α is relevant for the dynamics of the model.

Dynamical Analysis

In what follows, we study the fixed points relevant for the dark energy era ($\Omega_{\text{DE}} \simeq 1, w_{\text{eff}} < -1/3$).

- (DE) Dark energy dominance

$$x = z = \sqrt{\frac{\sqrt[3]{\alpha}f_\alpha^2-\sqrt[3]{3}}{2f_\alpha\sqrt[3]{9\alpha^2}}}, \quad y=0, \quad w=0, \quad \Omega_r=0, \tag{2.5.22}$$

with $\Omega_{\text{DE}} = 1$, $\Omega_m = 0$ and

$$w_{\text{DE}} = -1+\frac{2f_\alpha}{9}\left[\sqrt[3]{\frac{3}{\alpha}}+\sqrt[3]{\frac{\alpha}{3}}f_\alpha\left(18-f_\alpha^3\right)\right], \quad f_\alpha \equiv \left(9+\sqrt{81+\frac{3}{\alpha}}\right)^{1/3}. \tag{2.5.23}$$

This point corresponds to an accelerated expansion solution if $w_{\text{DE}} < -1/3$, which implies that $\alpha > 1$. Since observations favor $w_{\text{DE}} \approx -1$ [39], from Eq. (2.5.23), for example, $-1 \leq w_{\text{DE}} < -0.99$ implies $\alpha > 5.88148 \times 10^5$. We conclude that the dark energy component can behave in agreement with the observational bounds for large α.

Now, we proceed to discuss the stability of this fixed point by analyzing the sign of the eigenvalues $\lambda_{1,2,3,4,5}$. In this case, the eigenvalues are very long quantities, therefore, we investigate the stability of the point by plotting them as functions of α for large values of this parameter. In Fig. 2.5.1, we can see that $\lambda_{1,2} > 0$ while the other eigenvalues are negative such that this point corresponds to a saddle in the phase space $\{x, y, w, z, \Omega_r\}$. We verified that $\lambda_1 \to 0$, $\lambda_2 \to 0$, $\lambda_3 \to -4$, $\lambda_4 \to -3$ and $\lambda_5 \to -3$ when $\alpha \to \infty$. Although in general this point is not an attractor, as usual in dark energy models, this is not a problem for the theory. Moreover, we argue that (DE) is indeed an attractor in the relevant physical space.

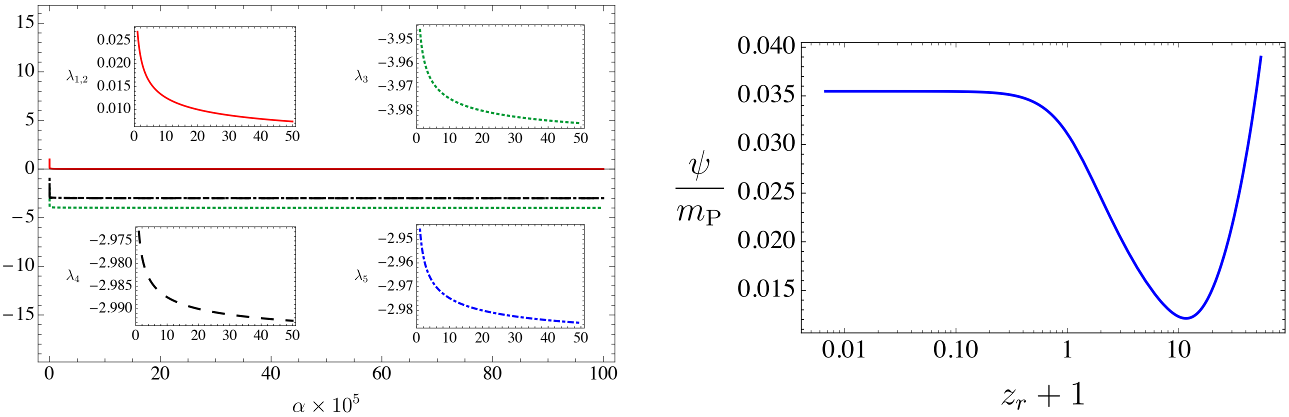

Figure 2.5.1: (Left) The five eigenvalues of the Jacobian matrix. The fixed point is a saddle $\lambda_{1,2} > 0$ and $\lambda_{3,4,5} < 0$. However, this point is an attractor in the relevant physical space. The scale for α is the same for all the plots. (Right) Evolution of the gauge field during the dark energy dominated period. The gauge field ψ reaches a constant value at late-times, where $\dot{\psi} = 0$, and it becomes an effectively cosmological constant.

The eigenvector associated with λ_1 is $(0, 1, 0, 0, 0)$ while the eigenvector of λ_2 is $(0, 0, 1, 0, 0)$, such that this point is a repeller in the y and w directions, i.e. the variables y and w run away from zero. In this point we have $x = z$, which implies $y \propto \psi^2/H \propto 1/H$, given that $\dot{\psi} = 0$ and $\psi = \text{const}$. Now, since H decreases with the expansion, the variable y increases in the same proportion. Therefore, we realize that $\lambda_1 > 0$ is needed for the theory to be consistent. The same argument follows for $\lambda_2 > 0$ since $w \propto \psi/H$. Therefore, we conclude that this point is a physical attractor but a saddle in the state space spanned by the chosen variables. This is not surprising since the phase space $\{x, y, w, z, \Omega_r\}$ is not compact, hence there will not be necessarily a source point and an attractor point in the phase space [163]. These arguments are further supported by numerical results in the next subsection.

2.5.3 Dark energy equation of state

We proceed to solve the autonomous set of equations (2.5.14) to (2.5.18) through a numerical integration. Based in the dynamical system analysis, the initial conditions are chosen in the deep radiation era. Explicitly we choose

$$\alpha = 10^9, \quad x_i = 3 \times 10^{-30}, \quad z_i = 1.1 \times 10^5, \quad y_i = 0.001, \quad \Omega_{r_i} = 0.99998. \tag{2.5.24}$$

The Friedman equation (2.5.13) forbids arbitrary values for the mass of the gauge fields. Note that there exist a relation between the variables w and z:

$$\frac{w^2}{z^2} = \frac{m^2}{H^2} \equiv \omega. \tag{2.5.25}$$

For the chosen initial conditions, we find that for $\Omega_{m_i} > 0$ we have $\omega_i < 1.57025 \times 10^{-15}$, so we choose

$$\omega_i = 5 \times 10^{-29}, \tag{2.5.26}$$

corresponding to $\Omega_{m_i} = 1.9 \times 10^{-5}$ at the redshift $z_r = 2.18 \times 10^8$.

From the numerical solution we can say that, at late-times, the dark sector behaves very similar to a cosmological constant once the κ-term is dominating the energy budget, as depicted in the right panel of Fig. 2.5.1. However, in order to thoroughly characterize the behaviour of this sector, it is necessary to study the evolution of its equation of state.

Because of the Friedmann constraint in Eq. (2.5.13), the values of the variables w_i and y_i are determined by ω_i [see Eq. (2.5.26)]. In Fig. 2.5.2 we plot $w_{\rm DE}$ for several values of ω_i. For $z_r > 10^4$ we see that $w_{\rm DE} \approx 1/3$, meaning that the dark sector behaves as a radiation fluid at early times. This is expected since the Yang-Mills term is dominating over the dark components during this period, so this term can contribute to the early relativistic degrees of freedom as claimed in Ref. [125]. We also see that for $\omega_i \neq 0$ it is possible that the mass term dominates the dark sector implying $w_{\rm DE} \approx -1/3$. This is a new behaviour with respect to the results given in Ref. [125]. As a comment, a fluid with equation of state equal to $-1/3$ cannot drive accelerated expansion. However, there is no transition period from decelerated expansion to accelerated expansion in our model, because dust is the dominant fluid when $w_{\rm DE} \approx -1/3$ and thus $w_{\rm eff} \approx 0$. Note that in all of the cases, the final stage of the Universe is dark energy domination, which is reached at different cosmological epochs, depending on the value of ω_i. This behaviour takes place due to modifications in the Hubble parameter since a change in ω implies a change in H/g as we will see later.

In the left panel of Fig. 2.5.2, we see that $w_{\rm DE}$ has some peaks around $z_r = 10$. This is because, around this time, the gauge field reaches its minimum magnitude, as can be seen in the right panel of Fig. 2.5.1. We want to stress that this particular behaviour of $w_{\rm DE}$ is a distinctive property found in this model that was not reported in Ref. [125].

As expected $-1 < w_{\rm DE} < 1/3$, contrasting with the equation of state of any quintessence model where $-1 < w_{\rm DE} < 1$. The main difference is in the so-called "kination" period, which corresponds to the epoch when the kinetic term of the quintessence field dominates over its potential. This period must be prior to the radiation dominance epoch since the energy density of the quintessence field decays as a^{-6} [60]. As a comment, some authors claim that this kination period could be very useful in the study of the reheating process (see e.g. Refs. [202–207]).

The dark energy dominated period runs from $z_r \approx 0.3$ on into the future. During this epoch (right panel of Fig. 2.5.1), the gauge field decays until it reaches a minimum and after that a constant value, when its speed goes to zero, as expected since $x = z$ in the point (DE) (dark energy dominance). The asymptotic value of the gauge field is $\psi \approx 0.0354378\, m_{\rm P}$, in agreement with $\sqrt{2}\,z = 0.0354917$ which is the value in the attractor point (DE).

We also can perform a rough estimation of the parameters κ and g by noting the relation

$$\frac{H}{g} = \frac{\sqrt{2}z^2}{y} m_{\mathrm{P}}. \tag{2.5.27}$$

Replacing the values of these variables at present, i.e., y_0 and z_0, we get

$$\frac{H_0}{g} = \frac{\sqrt{2}z_0^2}{y_0} m_{\mathrm{P}} \approx 0.042\, m_{\mathrm{P}}, \tag{2.5.28}$$

and using the observational value $H_0 \approx 10^{-61} m_{\mathrm{P}}$ [39] we find

$$g \approx 2.38 \times 10^{-60}, \quad \kappa \approx 1.76 \times 10^{130} m_{\mathrm{P}}^{-4}. \tag{2.5.29}$$

This calculation shows that the gauge coupling g is extremely small (the order of 10^{-60}), while the parameter κ is extremely large (the order of $10^{130} m_{\mathrm{P}}^{-4}$).

2.5.4 Anisotropic Massless Case

So far, we have discussed systems embedded in an FLRW metric. It was shown that any early background spatial shear is extremely damped within a few e-folds during the inflationary phase driven by this kind of non-abelian gauge fields [185]. In contrast, the vector gauge field acquires a constant magnitude in the late-time cosmological expansion. This suggests that the gauge field could support an anisotropic expansion. In the following, we investigate this possibility where, by simplicity, we only consider massless gauge fields.

We assume a homogeneous but anisotropic spacetime described by the axially symmetric Bianchi-I metric. An appropriate axially symmetric ansatz for the gauge field is

$$A^a{}_0(t) = 0, \quad A^a{}_i(t) = e^a{}_i(t)\psi_i(t), \tag{2.5.30}$$

where

$$e^1{}_1(t) = e^{\alpha(t)-2\sigma(t)}, \quad e^2{}_2(t) = e^3{}_3(t) = e^{\alpha(t)+\sigma(t)}, \tag{2.5.31}$$

$$\psi_1(t) = \frac{\psi(t)}{\lambda^2(t)}, \quad \psi_2(t) = \psi_3(t) = \lambda(t)\psi(t), \tag{2.5.32}$$

with $\lambda(t)$ a function parametrizing the deviation from the isotropic configuration of the gauge field. This kind of ansatz has been used in other works where the dynamics of gauge fields in anisotropic backgrounds is studied (see Refs. [185, 186, 190]).

Employing the axial ansatz, and assuming massless gauge vector fields, i.e. $m_a = 0$, the

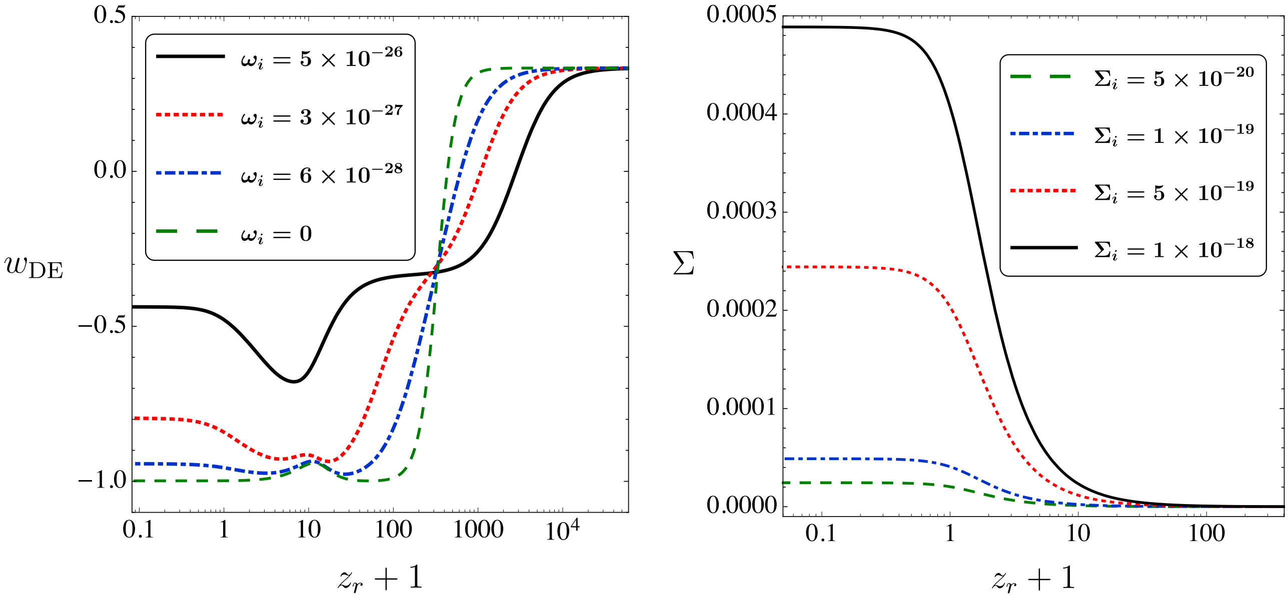

Figure 2.5.2: (Left) Evolution of $w_{\rm DE}$ for different ω. Arbitrary values of ω are not viable since they do not yield to a correct expansion history of the Universe. The initial state corresponds to "dark radiation", and the final stage to dark energy. The values of α, x, z, y and Ω_r are the same used in the numerical analysis section. (Right) Evolution at late-times of the shear. The initial conditions were chosen in the deep radiation epoch, corresponding to the same ones used in the isotropic model with $l = 1 - 10^{-20}$ and $s = 10^{-20}$, while Σ_i varies. Even a small deviation from the isotropic initial conditions yields to a non-negligible anisotropic contribution to the present Universe density budget.

density and pressure coming from the Yang-Mills term are

$$\rho_{\rm YM} = \frac{1}{2\lambda^4}\left[\frac{\dot\phi}{a} - 2\frac{\phi}{a}\left(\dot\sigma + \frac{\dot\lambda}{\lambda}\right)\right]^2 + \lambda^2\left[\frac{\dot\phi}{a} + \frac{\phi}{a}\left(\dot\sigma + \frac{\dot\lambda}{\lambda}\right)\right]^2 + \frac{g^2\phi^4}{2a^4}\frac{2+\lambda^6}{\lambda^2}, \tag{2.5.33}$$

and $p_{\rm YM} = \rho_{\rm YM}/3$. For the κ-term, we have $p_\kappa = -\rho_\kappa$ with ρ_κ given by Eq. (2.5.7) meaning that this term does not introduce anisotropies in the energy tensor.

The corresponding Friedmann equations are

$$3m_{\rm P}^2(H^2 - \dot\sigma^2) = \rho_{\rm YM} + \rho_\kappa + \rho_r + \rho_m, \quad m_{\rm P}^2(\dot H + 3\dot\sigma^2) = -\left[\frac{2}{3}\rho_{\rm YM} + \frac{2}{3}\rho_r + \frac{1}{2}\rho_m\right], \tag{2.5.34}$$

$$m_{\rm P}^2(\ddot\sigma + 3H\dot\sigma) = \frac{1}{3\lambda^4}\left[\frac{\dot\phi}{a} - 2\frac{\phi}{a}\left(\dot\sigma + \frac{\dot\lambda}{\lambda}\right)\right]^2 - \frac{g^2\phi^4}{3a^4}\frac{1-\lambda^6}{\lambda^2} - \frac{\lambda^2}{3}\left[\frac{\dot\phi}{a} + \frac{\phi}{a}\left(\dot\sigma + \frac{\dot\lambda}{\lambda}\right)\right]^2. \tag{2.5.35}$$

The axial ansatz in the equations of motion for the gauge field components yields to two related equations given by

$$
\begin{aligned}
0 &= \frac{\ddot{\phi}}{a}\left[1+\frac{1}{3}\kappa g^2\frac{\phi^4}{a^4}\frac{2+\lambda^6}{\lambda^2}\right]+H\frac{\dot{\phi}}{a}\left[1-\kappa g^2\frac{\phi^4}{a^4}\frac{2+\lambda^6}{\lambda^2}\right]-2\frac{\phi}{a}\left(\dot{\sigma}^2-\frac{\dot{\lambda}^2}{\lambda^2}\right)+\frac{2}{3}\frac{g^2\phi^3}{a^3}\frac{1+2\lambda^6}{\lambda^4}\\
&+\frac{2}{3}\kappa g^2\frac{\phi^3\dot{\phi}^2}{a^5}\frac{2+\lambda^6}{\lambda^2}, \qquad (2.5.36)\\
0 &= \frac{\ddot{\lambda}}{\lambda}+2\frac{\dot{\phi}}{\phi}\frac{\dot{\lambda}}{\lambda}+\ddot{\sigma}-\dot{\sigma}^2+H\left(\dot{\sigma}+\frac{\dot{\lambda}}{\lambda}\right)+\frac{g^2\phi^2}{a^2}\frac{1+\lambda^6}{\lambda^4}+\frac{\ddot{\phi}}{\phi}\left(1+\kappa g^2\frac{\phi^4}{\lambda^2a^4}\right)\\
&+\frac{H\dot{\phi}}{\phi}\left(1-3\kappa g^2\frac{\phi^4}{\lambda^2a^4}\right). \qquad (2.5.37)
\end{aligned}
$$

The value of the present shear is constrained to be $|\Sigma_0| \leq \mathcal{O}(0.001)$ [142, 143]. More restricted bounds are expected from future observational missions like Euclid [47]. Since observations rule out high anisotropies, we are interested in anisotropic solutions near to the isotropic solutions obtained in the last section. Therefore, we rewrite the system using the same expansion variables defined in Eqs. (2.5.12). The dynamical degrees of freedom involving the anisotropy in the gauge field and the background are encoded in the variables

$$
l \equiv \lambda^2, \quad s \equiv \frac{\dot{\lambda}}{\lambda H}, \quad \Sigma \equiv \frac{\dot{\sigma}}{H}, \qquad (2.5.38)
$$

such that, the isotropic limit corresponds to $l = 1$, $s = 0$ and $\Sigma = 0$. In this case, the dynamical systems technique provides an autonomous set very hard to deal with. Instead of looking for the fixed points of the whole system, we numerically integrate the system around the isotropic solutions found in the last section. Explicitly, we use the same initial conditions of the isotropic case, with $\omega_i = 0$, and assume that

$$
l_i = 1 - 10^{-20}, \quad s_i = 10^{-20}, \qquad (2.5.39)
$$

at $z_r = 2.18 \times 10^8$, while Σ_i varies two orders of magnitude from a very small value. As seen in the right panel of Fig. 2.5.2, even a small deviation from the initial conditions used in the isotropic model yields a non-negligible amount of anisotropy in the present Universe. The values obtained are within the observational bounds, explicitly we found $|\Sigma_0| < 5 \times 10^{-4}$.

The equation of state of dark energy is also modified by the anisotropy in the following way:

$$
w_{\rm DE} = \frac{p_{\rm DE}}{\rho_{\rm DE}} = \frac{1}{3}\frac{\Omega_{\rm YM} - 3\Omega_\kappa + 3\Sigma^2}{\Omega_{\rm YM} + \Omega_\kappa + \Sigma^2}, \qquad (2.5.40)
$$

where $\Omega_{\rm YM} \equiv \rho_{\rm YM}/3m_{\rm P}^2H^2$ and $\Omega_\kappa \equiv \rho_\kappa/3m_{\rm P}^2H^2$ are the density parameters for the Yang-Mills and κ-terms, respectively. However, since $\Sigma^2 \ll \Omega_\kappa, \Omega_{\rm YM}$ during the whole expansion history, the contribution of the shear is always negligible in comparison to the other dark components and thus the changes are not noticeable. We want to stress that, although the asymptotic behaviour of the model remains unknown, this model could support a late-time anisotropic expansion observable nowadays. It is possible that the Universe lose its anisotropic hair in the future, as it is the case presented e.g. in Ref. [2]. We left a better exploration of the cosmological consequences of this model for a future work.

2.5.5 Conclusions

In this work, we studied non-Abelian gauge vector fields endowed with SU(2) group representation as the unique source of dark energy. Regarding the late-time accelerated expansion, we were able to show that the dark energy domination period is the only physical attractor of the theory, and thus confirming the results in Ref. [125] where only some particular sets of initial conditions and parameters were studied. We also generalized the model of Ref. [125] by introducing a mass term to the dynamics. We found that this term yields to new behaviors in the equation of state of dark energy $w_{\rm DE}$. For instance, some peculiar peaks around the redshift $z_r = 10$ were observed (see Fig. 2.5.2). By noting that the gauge field acquires a constant magnitude in the attractor point, we studied the same action but in a homogeneous and anisotropic axially symmetrical Bianchi-I background. The dynamical system of the model is very cumbersome hence we opted for numerical integration of the autonomous set. Since observations rule out high anisotropies [142, 143] we set the initial conditions near to the isotropic solutions. We found that, starting from a highly isotropic Universe, the gauge field can support a late-time anisotropic expansion, given that the spatial shear evaluated today is within the observational bounds. A more rigorous treatment on anisotropic models of dark energy driven for non-Abelian gauge fields is left for future works.

2.6 Einstein Yang-Mills Higgs Model: SU(2) Case

2.6.1 Introduction

The profuse search for modification to the standard cosmological model has been focused primarily in scalar field replacing the cosmological constant. In contrast, little has been done in the search for a mechanism that mimics the cosmological constant while involving standard forms of matter that minimally couple to the gravity described by GR. Inspired in the Standard Model of Particle Physics (SM) (see, for example, Refs. [208, 209]), the Einstein Yang-Mills Higgs action was introduced in Refs. [210, 211] in order to study its role in the description of the primordial inflationary period. Many years later, M. Rinaldi studied such an action in Ref. [191] arguing that a late period of accelerated expansion was possible due to the complex doublet nature of the Higgs field, charged under the SU(2) gauge symmetry[15]. In summary, Rinaldi believed to have shown that, when considering the effect of gravity, the Higgs complex field rotates about the axis of the Mexican hat potential, away from the minimum of its potential but slowly chasing it, giving way to an slowly-varying effective cosmological constant much in the same way as in the *"spintessence"* scenario [214]. Despite the fact that the Yang-Mills fields, charged under SU(2), were considered, Rinaldi neglected the interaction between them and the Higgs field, arriving to the conclusion that the former behaved as a pure radiation fluid. Later on, in Ref. [192], the same author took into account such an interaction, but this time in the SO(3) representation for the Higgs field, arriving to similar conclusions as in Ref. [191][16]. Our purpose in this paper is to seriously consider this interaction in the SU(2) representation for the Higgs field and determine the extent to which it affects the dark energy mechanism.

2.6.2 Importance of the Yang-Mills Higgs interaction

The Einstein Yang-Mills Higgs action [191, 210, 211] borrows some elements from the SM (see, for example, Refs. [208, 209]) such as the SU(2) gauge invariance – and, therefore, the existence of three gauge bosons – and the presence of a Higgs complex doublet. It also involves non-interacting radiation and matter fluids, and the gravity is described by the General Relativity. Its action is given by

$$\mathcal{L} = -\frac{1}{4}F_a{}^{\mu\nu}F^a{}_{\mu\nu} - (D^\mu\Phi)^\dagger(D_\mu\Phi) - V(\Phi^2), \tag{2.6.1}$$

$F^a_{\mu\nu}$ is the non-Abelian gauge field strength tensor defined by

$$F^a{}_{\mu\nu} \equiv \partial_\mu A^a{}_\nu - \partial_\nu A^a{}_\mu + \gamma\epsilon^a{}_{bc}A^b{}_\mu A^c{}_\nu, \tag{2.6.2}$$

$A^a{}_\mu$ representing the vector fields, γ being the SU(2) group coupling constant, and ϵ_{abc} being the three-dimensional Levi-Civita symbol, D_μ is the gauge covariant derivative defined by

$$D_\mu \equiv \nabla_\mu - i\gamma\frac{\sigma_c}{2}A^c{}_\mu, \tag{2.6.3}$$

[15]It is worth stressing that this Higgs is not the one of the SM whose discovery in 2012 was reported in Refs. [212, 213].

[16]A careful analysis of Ref. [192] shows that its assumption of a homogeneous and isotropic background is incorrect, the latter being actually described by an axisymmetric Bianchi I metric at best [2] (M. Álvarez, Y. Rodríguez and M. Rinaldi, private communications).

∇_μ being the space-time covariant derivative and σ_c denoting the Pauli matrices, Φ is the Higgs complex doublet described as

$$\Phi \equiv \begin{pmatrix} \Phi_1 \\ \Phi_2 \end{pmatrix} = \begin{pmatrix} \phi_1 + i\psi_1 \\ \phi_2 + i\psi_2 \end{pmatrix}, \tag{2.6.4}$$

ϕ_1, ϕ_2, ψ_1 and ψ_2 being real scalar fields, $V(\Phi^2)$ is the usual Higgs Mexican hat potential given by

$$V(\Phi^2) \equiv \frac{\lambda}{4}(\Phi^2 - \Phi_0^2)^2, \tag{2.6.5}$$

λ being the quartic coupling constant and Φ_0 denoting the Higgs field configuration at the minimum of its potential.

A FLRW configuration of spacetime requires a homogeneous arrangement of fields and an isotropic energy-momentum tensor. The latter is defined as

$$T_{\mu\nu} \equiv 2\frac{\partial \mathcal{L}}{\partial g^{\mu\nu}} - g_{\mu\nu}\mathcal{L}, \tag{2.6.6}$$

From the definition in Eq. (2.6.6), it is obvious that the second term on the right member of the equation vanishes for $\mu\nu = \mu i$, with $\mu \neq i$, i.e., this term neither contributes to the momentum density nor to the anisotropic stress. What it is not obvious is whether the first term on the right member of the equation contributes to these physical quantities. A simple but delicate calculation shows that this first term is given by

$$2\frac{\partial \mathcal{L}}{\partial g^{\mu\nu}} = -F^a{}_{\mu\rho}F_a{}^\rho{}_\nu - 2(D_{(\mu}\Phi)^\dagger(D_{\nu)}\Phi). \tag{2.6.7}$$

A close examination of the ij components reveals that the only way to avoid anisotropic stress is by employing the *"cosmic triad"* configuration[17] for the gauge fields:

$$A^a_\mu = f\delta^a_\mu. \tag{2.6.8}$$

In fact,

$$2\frac{\partial \mathcal{L}}{\partial g^{\mu\nu}}\bigg|_{\mu\nu=ij} \supset \delta_{ij}\left(\dot{f}^2 - 2\frac{\gamma^2 f^4}{a^2} - \frac{1}{2}\gamma^2\Phi^2 f^2\right), \tag{2.6.9}$$

when the cosmic triad is employed. However, we see that this is insufficient to avoid a contribution to the momentum density:

$$2\frac{\partial \mathcal{L}}{\partial g^{\mu\nu}}\bigg|_{\mu\nu=0i} = -\frac{1}{4}\gamma f\, \mathrm{Im}(\dot{\Phi}^\dagger\sigma_i\Phi). \tag{2.6.10}$$

[17]For other applications of the cosmic triad to dark energy, see Refs. [114, 125, 196].

The origin of this contribution is, clearly, the interaction between the Yang-Mills fields and the Higgs field and, since it imposes severe restrictions on the Higgs doublet, *it cannot be neglected* as was done in Ref. [191]. Such restrictions are the following:

$$\begin{aligned}
\mathrm{Im}(\dot{\Phi}_1^*\Phi_2 + \dot{\Phi}_2^*\Phi_1) &= 0, \\
\mathrm{Re}(\dot{\Phi}_1^*\Phi_2 - \dot{\Phi}_2^*\Phi_1) &= 0, \\
\mathrm{Im}(\dot{\Phi}_1^*\Phi_1 - \dot{\Phi}_2^*\Phi_2) &= 0,
\end{aligned} \tag{2.6.11}$$

which are equivalent to

$$\begin{aligned}
\dot{\phi}_1\psi_2 - \dot{\psi}_1\phi_2 + \dot{\phi}_2\psi_1 - \dot{\psi}_2\phi_1 &= 0, \\
\dot{\phi}_1\phi_2 + \dot{\psi}_1\psi_2 - \dot{\phi}_2\phi_1 - \dot{\psi}_2\psi_1 &= 0, \\
\dot{\phi}_1\psi_1 - \dot{\psi}_1\phi_1 - \dot{\phi}_2\psi_2 + \dot{\psi}_2\phi_2 &= 0.
\end{aligned} \tag{2.6.12}$$

Thus, the additional condition to avoid an anisotropic energy-momentum tensor is to fix the gauge so that

$$\Phi(t) \equiv \begin{pmatrix} \phi(t) \\ 0 \end{pmatrix}, \tag{2.6.13}$$

with ϕ being a real scalar field[18]. This conclusion is clearly at odds with the claims in Ref. [191] since any evolution of the Higgs field that involves a rotation around the axis of the Mexican hat potential, as in the spintessence model [214], will immediately produce a huge amount of anisotropy in disagreement with observations.

It is worth stressing that if it were not for the presence of the gauge fields and their interaction with the Higgs field, the energy-momentum tensor would be isotropic no matter the chosen gauge for the Higgs field. In connection with this, we know that there are no preferred directions associated to scalar fields, so that cosmological models based solely on homogeneous versions of them always produce both background and statistical isotropy[19]. In contrast, it is clear that vector fields enjoy inherent preferred directions, so that cosmological models based solely on them produce a huge amount of both background and statistical anisotropy unless the cosmic triad configuration is employed [215]; this is the case of models like vector inflation [150], and gauge-flation [151, 193].

Will this conclusion throw away the possibility of a dark energy mechanism for the Einstein Yang-Mills Higgs action? The answer is no, as we will see in the following sections.

[18] Any gauge transformation of this configuration satisfies as well the restrictions in Eq. 2.6.12.

[19] Inhomogeneous scalar fields can drive a homogeneous but anisotropic universe if extra symmetries are added, as in the solid inflation model [148, 153].

2.6.3 Dynamical System Analysis

Equations of Motion

Once the cosmic triad configuration has been employed, as in Eq. (2.6.8), and the gauge for the Higgs field has been fixed, as in Eq. (2.6.13), the gravitational field equations in the FLRW background are the following:

$$
\begin{aligned}
H^2 &= \frac{1}{3m_{\mathrm{P}}^2}\left[\frac{3}{2}\frac{\dot{f}^2}{a^2}+\dot{\phi}^2+\frac{3}{2}\frac{\gamma^2 f^4}{a^4}+\frac{3}{4}\frac{\gamma^2\phi^2 f^2}{a^2}+V(\phi^2)+\rho_r+\rho_m\right], &(2.6.14)\\
\dot{H} &= -\frac{1}{2m_{\mathrm{P}}^2}\left[2\frac{\dot{f}^2}{a^2}+2\dot{\phi}^2+2\frac{\gamma^2 f^4}{a^4}+\frac{\gamma^2\phi^2 f^2}{2a^2}+\frac{4}{3}\rho_r+\rho_m\right], &(2.6.15)
\end{aligned}
$$

These equations are complemented by the field equations of motion obtained by varying the action with respect to $A^a{}_\mu$ and Φ and replacing the field configurations and the FLRW metric:

$$
\ddot{f}+H\dot{f}+2\frac{\gamma^2 f^3}{a^2}+\frac{\gamma^2 f\phi^2}{2}=0, \quad \ddot{\phi}+3H\dot{\phi}+\frac{3}{4}\frac{\gamma^2 f^2\phi}{a^2}+\frac{dV(\phi)}{d\phi}=0. \tag{2.6.16}
$$

One of these four equations is redundant but, nevertheless, keeping the four equations will be useful for the construction and analysis of the autonomous dynamical system in the following section.

An important aspect of Eq. (2.6.16) is that it reveals the existence of a potential for the gauge field. This potential is clearly a product of the interaction between the gauge field and the Higgs field and cannot be neglected. As we will see, $f=0$ minimizes this potential; this is in agreement with the usual assumption in standard particle physics of assigning a vanishing vacuum expectation value to the gauge fields. On the other hand, the same interaction between the gauge field and the Higgs field is the responsible for the existence of an effective potential for the Higgs field [see Eq. (2.6.16)] that produces an accelerated expansion period despite the fact the Mexican hat potential is not flat enough. This kind of effective potentials is ubiquitous when dealing with multiple types of fields (see e.g. Ref. [216]).

Dynamical system

With the purpose of analyzing the dynamical behaviour of the physical quantities in this scenario, we can construct an autonomous dynamical system by defining the following dimensionless dynamical quantities:

$$
x\equiv\frac{\dot{f}}{\sqrt{2}am_{\mathrm{P}}H}, \quad y\equiv\frac{\gamma f^2}{\sqrt{2}a^2 m_{\mathrm{P}}H}, \quad w\equiv\frac{\gamma f\phi}{2am_{\mathrm{P}}H}, \quad z\equiv\frac{\dot{\phi}}{\sqrt{3}m_{\mathrm{P}}H},
$$

$$v \equiv \frac{1}{m_{\rm P}H}\sqrt{\frac{V(\phi)}{3}}, \quad r \equiv \frac{1}{m_{\rm P}H}\sqrt{\frac{\rho_r}{3}}, \quad m \equiv \frac{1}{m_{\rm P}H}\sqrt{\frac{\rho_m}{3}}, \quad l \equiv \frac{\sqrt{2}am_{\rm P}}{f}. \tag{2.6.17}$$

Thus, the Friedmann equation in Eq. (2.6.14) becomes the constraint equation

$$x^2 + y^2 + w^2 + z^2 + v^2 + r^2 + m^2 = 1, \tag{2.6.18}$$

from which we can write the m variable as a function of the other variables.

Exchanging the cosmic time by the number of e-folds N, and taking into account Eqs. (2.6.15)-(2.6.18), we can write the evolution equations for each independent dimensionless variable as follows:

$$\begin{aligned}
x' &= x(q-1) - l(2y^2 + w^2), &(2.6.19)\\
y' &= y(2xl + q - 1), &(2.6.20)\\
w' &= w(xl + q) + \frac{\sqrt{3}}{2}lyz, &(2.6.21)\\
z' &= z(q-2) - wl\left(2\alpha v + \frac{\sqrt{3}}{2}y\right), &(2.6.22)\\
v' &= v(q+1) + \alpha lwz, &(2.6.23)\\
r' &= r(q-1), &(2.6.24)\\
l' &= l(1 - lx), &(2.6.25)
\end{aligned}$$

where a prime means a derivative with respect to N, $q \equiv -\ddot{a}a/\dot{a}^2$ is the deceleration parameter which is given by

$$q = \frac{1}{2}(1 + x^2 + y^2 - w^2 + 3z^2 - 3v^2 + r^2), \tag{2.6.26}$$

and α is the positive dimensionless constant defined by $\alpha \equiv \sqrt{\lambda/2\gamma^2}$. This autonomous dynamical system is similar to the one obtained by Rinaldi in Ref. [192] where he studied the Einstein Yang-Mills Higgs action with the Higgs field in the SO(3) representation; however, the conclusions obtained in this section differ in some important aspects from his.

It is important to notice that, although the variables in Eq. (2.6.17) are the ones that describe the dynamical system, the actual quantities we are interested in are the physical ones, i.e., the physical vector field f/a, its speed $(f/a)'$, the Higgs field ϕ, its speed ϕ', and the deceleration parameter q [already shown in Eq. (2.6.26)]:

$$\frac{f/a}{m_{\rm P}} = \frac{\sqrt{2}}{l}, \quad \frac{(f/a)'}{m_{\rm P}} = \sqrt{2}\left(x - \frac{1}{l}\right), \quad \frac{\phi}{m_{\rm P}} = 2\frac{w}{yl}, \quad \frac{\phi'}{m_{\rm P}} = \sqrt{3}z. \tag{2.6.27}$$

- **Dark energy critical point**:

$$\{x = 0, \quad y = 0, \quad w = 0, \quad z = 0, \quad v = 1, \quad r = 0, \quad l = 0\}$$

For this point, $q = -1$, which means dark energy domination. This, in turn, implies that the Hubble parameter is almost constant in the surroundings of the point. Thus, from the eigenvalues and eigenvectors, we can conclude that the point is an attractor in the $\{x, y, w, z, v, r\}$ space, which is what matters when calculating the deceleration parameter. We can also conclude that the Higgs field approaches a constant value, because $v = 1$ is a v-direction attractor, but it does it in a decelerated way, because $z = 0$ is a z-direction attractor, that the radiation, pure and dark, approaches zero because $x = 0$, $y = 0$, and $r = 0$ are attractors in the x direction, the y direction, and the r direction respectively, and that the physical vector field approaches zero, because $y = 0$ is a y-direction attractor, but it does it in a decelerated way (in magnitude) because $x = 0$ is a x-direction attractor while $l = 0$ is a l-direction repeller.

Notice that neither the critical points nor the stability criteria depend on the value of α. Moreover, the dark energy critical point is the only attractor in the $\{x, y, w, z, v, r\}$ space.

2.6.4 Global Evolution

We will now proceed to present a numerical solution whose initial conditions are in agreement with the present observed values for the density parameters (see Refs. [39, 217]). We know that, today, the pure radiation density parameter defined as $\Omega_r \equiv \rho_r/3m_{\rm P}^2H^2$ has a value $\Omega_{r_0} \simeq 10^{-4}$ while the matter density parameter, defined as $\Omega_m \equiv \rho_m/3m_{\rm P}^2H^2$ has a value $\Omega_{m_0} \simeq 0.31$. This implies the following initial values for the r and m dimensionless variables:

$$r_0 = 10^{-2}, \quad m_0 = 0.557. \tag{2.6.28}$$

We also know, from the previous section, that the final stage of the evolution of the Einstein Yang-Mills Higgs system is the dark energy dominated period (dark energy critical point) where the energy budget is dominated by the Higgs potential energy, parameterized by the dimensionless variable v. Thus, and having in mind the values and stability properties for all the variables in the dark energy critical point and the constraint equation in Eq. (2.6.18), we have chosen the following initial conditions for the other dimensionless variables that characterize the system under study:

$$x_0 = 10^{-18}, \quad y_0 = 10^{-18}, \quad w_0 = 10^{-18}, \quad z_0 = 10^{-18}, \quad v_0 = 0.831, \quad l_0 = 10^2. \tag{2.6.29}$$

Another motivation to choose these initial conditions has to do with the total length of the radiation dominated period,[20] from the end of the kination dominated period to the time of matter-radiation equality:

$$\Delta N_{\rm rad} \approx -\frac{1}{2}\ln\left(\frac{\sqrt{\Omega_{m_0}}H_0(1+z_{r_{\rm eq}})^{3/2}}{H_{\rm end}}\right), \tag{2.6.30}$$

where $z_{r_{eq}}$ is the redshift at matter-radiation equality and $H_{\rm end}$ is the Hubble parameter at the end of the kination dominated period. Since nucleosynthesis has to occur during the radiation dominated period, $H_{\rm end} \gtrsim 10^{-45} m_{\rm P}$. Additionally, the constraint on the tensor to scalar ratio [218] gives the upper bound $H_{\rm end} \lesssim 10^{-2} m_{\rm P}$ when the reheating is instantaneous and the length of the kination dominated period is considered to vanish. These two bounds, together with Eq. (2.6.30), lead to $13 \lesssim \Delta N_{\rm rad} \lesssim 62$. As we will see, the above initial conditions lead to a cosmological dynamics consistent with the latter constraint.

We have numerically solved the system of equations given by Eqs. (2.6.19)-(2.6.25) assuming a realistic value for the α parameter, $\alpha = 1$.[21] This allows us to plot the evolution of the deceleration parameter q and the effective equation of state parameter $\omega_{\rm eff}$ given by $\omega_{\rm eff} = (2q-1)/3$; such plots are shown in Figs. 2.6.1. As observed, the system exhibits four stages of evolution: the kination dominated period, the radiation dominated period, the matter dominated period, and, finally, the dark energy dominated period. Except for the first one, the other periods and their relative order are in agreement with the standard cosmology (see Ref. [217]); nevertheless, a kination dominated period previous to the radiation dominated one is absolutely beneficial for a successful reheating mechanism if the inflaton is only coupled to matter gravitationally [207]. We can also confirm that the kination dominated period is an attractor towards the past (a repeller or source), the radiation and matter dominated periods are metastable (saddle points), and the dark energy dominated period is an attractor (a sink). The dark components (Yang-Mills + Higgs) support the kination dominated period in early times as well as the dark energy dominated period in the present and future, similarly to what happens with most of the quintessence models [60].

We have checked that the changes in Figs. 2.6.1 are negligible when increasing or decreasing x_0 and y_0. However, an increment in the value of w_0 does modify the figures, shortening the radiation dominated period while lengthening the kination dominated one without modifying the length of the matter dominated period; a similar behaviour has been found for changes in z_0, l_0, or α. It is remarkable that the behaviour in these plots is consistent with the redshift at the matter-radiation equality, $z_{r_{\rm eq}} = 3390$ [39, 60, 217]; it is also consistent with the constraint

[20] See Appendix A of the reference corresponding to this work [1].

[21] This is the order of magnitude obtained when calculating α in the SM.

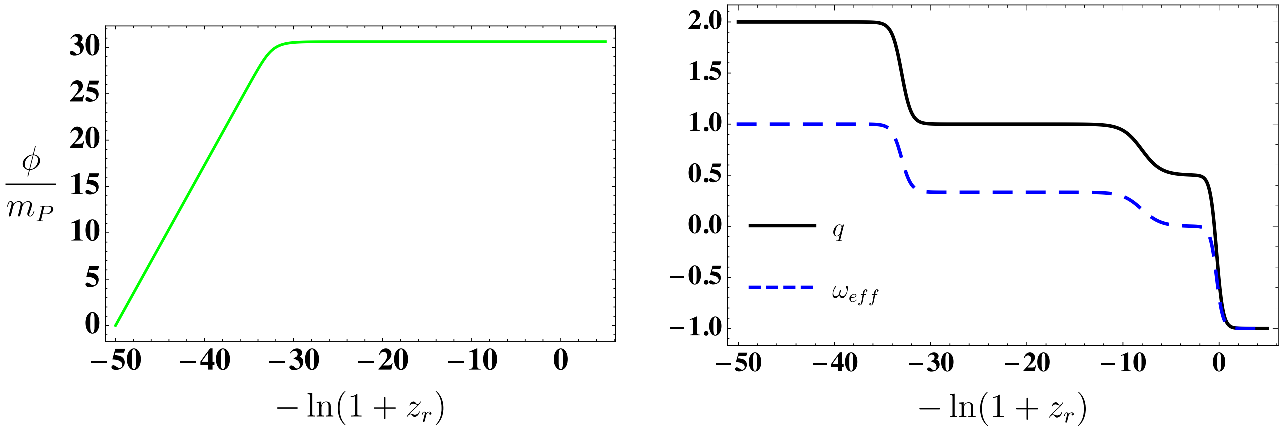

Figure 2.6.1: Global evolution of the Einstein Yang-Mills Higgs system. The Higgs field moves away from the minimum of its potential, being hold towards an asymptotic finite value by its interaction with the Yang-Mills fields. The physical vector field, which represents the Yang-Mills fields, starts from a huge value and decreases towards zero, it being its asymptotic value. It is the interaction between these two types of fields that lifts the Higgs field and keeps it away from its minimum. This, in turn, produces the dark energy dominated period.

on the length of the radiation dominated period given above Eq. (2.6.30).

We can take a global look at the evolution of the physical quantities described in Eqs. (2.6.27). We can conclude that *the Higgs field moves away from the minimum of its potential towards an asymptotic finite value, being hold by its interaction with the Yang-Mills fields which do not allow it to roll down the Mexican hat potential.* (see the left panel of Fig. 2.6.1); of course, since it is approaching an asymptotic value, its movement is decelerated. In contrast, *the physical vector field, which represents the Yang-Mills fields, starts from a huge value and decreases towards zero, it being its asymptotic value*; its movement, of course, is decelerated (in magnitude).

It is worth mentioning that if the cosmic triad were actually zero, the interaction term in Eq. (2.6.16) would disappear and the Higgs field would go to the minimum of its potential, which is indeed the behaviour, for instance, in the SM; no late accelerated expansion period would be generated in this case. However, when recognizing that the gauge field does have a potential, and that it rolls down towards the minimum of this potential, the interaction between the gauge field and the Higgs field always survives because the evolution for f/a becomes asymptotic banning f/a to reach zero and approaching ϕ to a non-vanishing asymptotic value (see Fig. 2.6.1). This asymptotic behaviour reveals that the accelerated expansion period is eternal which is welcome, although not necessary, in a dark energy scenario.

Some implications for particle physics

We have discovered that the Higgs field in this scenario is not in the minimum of its potential but is hold towards a finite asymptotic value $\phi_{\rm asymp}$. Thus, its mass today as well as the Yang-Mills fields' receive a contribution which is proportional to $\phi_{\rm asymp}$. Moreover, in contrast to the SM, the Yang-Mills fields in this scenario do get a vacuum expectation value which approaches zero but never reaches it, so the Higgs mass and theirs also receive a contribution which is proportional to f_0/a_0. Let's remember that, in the SM, the Higgs mass m_ϕ is proportional to the quartic coupling constant λ whereas the Yang-Mills fields' m_{A_μ} is proportional to the SU(2) group coupling constant γ through the following relations that involve the vacuum expectation value of the Higgs field ϕ_0 [208, 209]:

$$m_\phi \sim \sqrt{\lambda}\phi_0 \sim \alpha\gamma\phi_0, \quad m_{A_\mu} \sim \gamma\phi_0. \tag{2.6.31}$$

In the present scenario:

$$m_\phi \sim \gamma\sqrt{\alpha^2\phi^2_{\rm asymp} + \frac{3}{8}\frac{f_0^2}{a_0^2}}, \quad m_{A_\mu} \sim \gamma\sqrt{\phi^2_{\rm asymp} + 4\frac{f_0^2}{a_0^2}}. \tag{2.6.32}$$

where, according to Figs. 2.6.1, $\phi_{\rm asymp} \approx 30 m_{\rm P}$ and $f_0/a_0 \approx 10^{-2} m_{\rm P}$. On the other hand, from the dimensionless parameters in Eq. (2.6.17), we can obtain an expression for the Hubble parameter:

$$\frac{H}{m_{\rm P}} = \sqrt{2}\frac{\gamma}{yl^2}, \tag{2.6.33}$$

which can be used in conjunction with the measured value for the Hubble parameter today $H_0 \sim 10^{-61} m_{\rm P}$ [39] to obtain $\gamma \sim 10^{-75}$. The present values of the Yang-Mills fields ${A^a}_\mu$ and the Higgs field ϕ are then $m_{A_\mu} \sim m_\phi \sim 10^{-74} m_{\rm P} \sim 10^{-47}$ eV. These are just figures since the actual values depend on the chosen initial conditions; however, they give us a notion of how small γ, m_ϕ and m_{A_μ} must be.

There are at least two ways of interpreting these results: *i*) the extremely low value for γ is a manifestation of the unsolved cosmological constant problem [61] so that the scenario discussed in this paper is just a 'rephrasing' of such a difficult and fundamental problem in a more comprehensive particle physics context[22], or *ii*) this scenario is promising but requires some modification in order to have interactions beyond gravity between the ${A^a}_\mu$ and ϕ and the particles of the SM, and mass values for the ${A^a}_\mu$ and ϕ not so extremely low so that they can be scanned in future particle physics experiments.

[22] It is very suggestive, however, that radiative corrections proportional to γ do not enter in conflict with the measured value of Λ.

2.6.5 Conclusions

M. Rinaldi's idea [191] of studying the role, for dark energy, of the Higgs field and the Yang-Mills fields in a SM-like action with Einstein gravity is very clever since it avoids the usual ways of research in the dark energy subject while feeding the analysis with well established and tested ideas from particle physics. We have shown that the interaction between the Higgs field and the Yang-Mills fields is fundamental for the success of this scenario, it being the key element that drives an asymptotic state that corresponds to the late accelerated expansion of the Universe. Such an interaction is so important that, despite the fact that the Higgs field is a scalar and the Yang-Mills fields are in the cosmic triad configuration, the setup is highly anisotropic unless the gauge for the Higgs field is fixed so that the latter moves along a straight direction in the field space. There can be no rotation around the axis of the Mexican hat potential and, therefore, this scenario differs completely from the "spintessence" one (see Ref. [214]); it is even different to the scenario in Ref. [192], where the SO(3) representation of the Higgs field is employed, since such a scenario is absolutely inconsistent with a homogeneous and isotropic universe [2]. The usual stages in the evolution of the postinflationary universe are successfully reproduced.

In addition, it is desirable that such a modification can explain the origin and nature of the dark matter and that implements interactions between the visible sector and the new one described in this paper, beyond the gravitational one, that allows us to test this scenario both from astronomical observations and in particle physics experiments. We think this scenario represents a step towards a successful merging of cosmology and well-tested particle physics phenomenology.

2.7 Einstein Yang-Mills Higgs Model: SO(3) Case

2.7.1 Introduction

In an attempt to describe the dark energy mechanism using matter fields included in the Standard Model of Particle Physics [209], the Higgs dark energy model was proposed in [191]. In that model, a complex Higgs doublet charged under the SU(2) gauge group drives the accelerated expansion by rotating around the minimum of its potential, in the same way as in the "spintessence" scenario [214]. This is possible by neglecting the interaction between the Higgs doublet and the gauge vector fields. Nonetheless, it was shown in [1] that if this interaction is properly considered, it yields to inconsistencies with the Friedmann-Lemaître-Robertson-Walker (FLRW) spacetime. These problems can be alleviated by gauge fixing the Higgs field, allowing a new dark energy mechanism and drastically changing the conclusions of the original work [1].[23]

In [192], the same author of [191] studied the Einstein Yang-Mills Higgs (EYMH) model, which is essentially the Higgs dark energy model but this time in the SO(3) representation instead of the SU(2) one, concluding that the Higgs field can also support the late accelerated expansion of the Universe. Although the author did take into account the interaction between the Higgs field and the gauge vector fields, we are going to show in this work that it is precisely this interaction term that plagues the EYMH model with several inconsistencies with the symmetries of the FLRW spacetime which cannot be avoided by fixing the gauge of the Higgs field as in [1]. Nevertheless, although the EYMH model is not compatible with the FLRW universe, it could fit in a homogeneous but anisotropic Bianchi-I background. We expected a non-negligible contribution of the spatial shear to the dark energy content due to the vector nature of the theory, as has been shown in other works where vector fields, gauge fields or p-forms have been used [115, 122, 219]. In this paper, we are going to show that the final state of the Universe is an eternal isotropic accelerated expansion; however, the anisotropic shear today can get appreciable values which can fit in the data analysis [142, 143] or that could be observed by future missions like ESA's Euclid [47].[24]

2.7.2 Incompatibility of the EYMH Model with an Isotropic Universe

The General Model

The EYMH model involves a Higgs field interacting with a gauge field whose dynamics is given by a Yang-Mills term. Both, the Higgs field and the gauge fields are minimally coupled to the gravity which, in turn, is described by the Einstein's General Relativity theory. The EYMH action, in the SO(3) representation, is

$$\mathcal{L} = -\frac{1}{4}F^a{}_{\mu\nu}F_a{}^{\mu\nu} - \frac{1}{2}D_\mu\mathcal{H}^a D^\mu\mathcal{H}_a - V\left(\mathcal{H}^2\right) \tag{2.7.1}$$

where $F^a{}_{\mu\nu}$ is the SO(3) gauge field strength tensor given by

$$F^a{}_{\mu\nu} \equiv \nabla_\mu A^a{}_\nu - \nabla_\nu A^a{}_\mu + g\varepsilon^a{}_{bc}A^b{}_\mu A^c{}_\nu, \tag{2.7.2}$$

[23]Refs. [182, 183] had already shown that appropriately fixing the gauge for the Higgs field makes the system compatible with a FLRW background although the incompatibility is restored by introducing the U(1) gauge interaction. Regarding the dark energy scenario, either the authors of these works did not consider it or the introduction of the U(1) interaction precluded such a possibility. We acknowledge M. Rinaldi for bringing these papers to our attention.

[24]The same conclusion has been reached in Ref. [220] in the framework of the Einstein-aether scalar field theory.

$A^a{}_\mu$ representing the gauge fields, g being the SO(3) group coupling constant, $\varepsilon^a{}_{bc}$ being the Levi-Civita symbol, D_μ being the SO(3) gauge covariant derivative defined by

$$D_\mu \mathcal{H}^a \equiv \nabla_\mu \mathcal{H}^a + g\varepsilon^a{}_{bc} A^b{}_\mu \mathcal{H}^c, \tag{2.7.3}$$

which is applied to the Higgs triplet $\mathcal{H}$:

$$\mathcal{H} \equiv (\mathcal{H}_1 \quad \mathcal{H}_2 \quad \mathcal{H}_3)^{\mathrm{T}}, \tag{2.7.4}$$

where $\mathcal{H}^a = \mathcal{H}_a$ are real scalar fields, $V(\mathcal{H}^2)$ is the symmetry breaking potential

$$V(\mathcal{H}^2) \equiv \frac{\lambda}{4}\left(\mathcal{H}^2 - \mathcal{H}_0^2\right)^2, \tag{2.7.5}$$

with λ being the quartic coupling constant, $\mathcal{H}_0$ being the Higgs vacuum value, and $\mathcal{L}_m$ and $\mathcal{L}_r$ being the Lagrangian densities for perfect fluids of matter and radiation respectively.

In the following subsections, we are going to assume that $g_{\mu\nu}$ corresponds to the homogeneous and isotropic FLRW metric and develop the equations of motion for this model employing two different formalisms.

The Reduced Action

The symmetries of the spacetime are encoded in the metric. Once these symmetries have been identified, for instance homogeneity and isotropy in a FLRW universe, the matter content has to obey the same symmetries in order to have consistent equations. This consistency between geometry and matter allows one to identify the non-dynamical degrees of freedom in the Lagrangian describing the theory, resulting in a "smaller" physical phase space. This Lagrangian written in terms of only the dynamical degrees of freedom yields to what is known as the "reduced action" [221].

The EYMH action in the SO(3) representation, as a mechanism for the late accelerated expansion, was originally proposed in [192] (see [210, 211] for primordial inflation). In that work, the author employed the reduced theory and a dynamical system analysis which allowed him to conclude that the only attractor of the theory is characterized by a dark energy dominance. In what follows, we have used the reduced action formalism to get the equations of motion of the model, thus reproducing some of the computations worked out in [192].

Since the Universe is highly homogeneous, isotropic and spatially flat [39], it is assumed that the background is described by the FLRW metric

$$\mathrm{d}s^2 \equiv -N^2(t)\mathrm{d}t^2 + a^2(t)\delta_{ij}\mathrm{d}x^i\mathrm{d}x^j, \tag{2.7.6}$$

where $N(t)$ is the lapse function. As shown in [114, 149], an ansatz for the gauge vector fields obeying the symmetries of this spacetime is

$$A_0^a(t) \equiv 0, \quad A^a{}_i \equiv a(t)\psi(t)\delta^a{}_i, \tag{2.7.7}$$

where $\psi(t)$ is a scalar field. As a shorthand notation we define $\phi(t) \equiv a(t)\psi(t)$. By replacing this ansatz, the Higgs triplet and the FLRW metric in the action (2.7.1), we get:

$$S_{\rm red} = \int \mathrm{d}tNa^3 \left[\frac{m_{\rm P}^2}{2}R(N,a) + \frac{3}{2}\frac{\dot{\phi}^2}{N^2a^2} - \frac{3}{2}\frac{g^2\phi^4}{a^4} + \frac{1}{2}\frac{\dot{\mathcal{H}}^2}{N^2} - \frac{g^2\phi^2\mathcal{H}^2}{a^2} - V(\mathcal{H}^2)\right], \tag{2.7.8}$$

which corresponds to the reduced action of the model as presented in [192].

Varying (2.7.8) with respect to $N(t)$ we have obtained the first Friedmann equation:[25]

$$3m_{\rm P}^2H^2 = \frac{3}{2}\frac{\dot{\phi}^2}{a^2} + \frac{3}{2}\frac{g^2\phi^4}{a^4} + \frac{1}{2}\dot{\mathcal{H}}^2 + \frac{g^2\phi^2\mathcal{H}^2}{a^2} + V + \rho_m + \rho_r, \tag{2.7.9}$$

where we have added the densities for matter and radiation, respectively. The second Friedmann equation comes after variation of (2.7.8) with respect to $a(t)$:

$$-2m_{\rm P}^2\dot{H} = 2\frac{\dot{\phi}^2}{a^2} + 2\frac{g^2\phi^4}{a^4} + \dot{\mathcal{H}}^2 + 2\frac{g^2\phi^2\mathcal{H}^2}{3a^2} + \rho_m + \frac{4}{3}\rho_r. \tag{2.7.10}$$

The equations of motion for the gauge field and the Higgs field are obtained upon variation of (2.7.8) with respect to $\phi(t)$ and $\mathcal{H}_a(t)$:

$$\ddot{\phi} + H\dot{\phi} + \frac{2g^2\phi^3}{a^2} + \frac{2g^2\mathcal{H}^2\phi}{3} = 0, \tag{2.7.11}$$

$$\ddot{\mathcal{H}}^a + 3H\dot{\mathcal{H}}^a + \frac{2g^2\phi^2\mathcal{H}^a}{a^2} + \frac{\mathrm{d}V}{\mathrm{d}\mathcal{H}_a} = 0, \tag{2.7.12}$$

respectively. In principle, Eqs. (2.7.9)-(2.7.12) describe the dynamics of the system in a proper way; we are going to show in the next subsection, however, that this model is indeed incompatible with a FLRW spacetime because the Higgs triplet cannot obey the same symmetries of this spacetime.

Einstein Equations and Inconsistencies of the Model

In general, the dynamics of the background universe (geometry + matter content) is encoded in the Einstein equations. In principle, this set of equations exhibits ten degrees of freedom;

[25] Where we assume $N(t) = 1$, once the variational principle is applied.

however, some of them are non dynamical and yield redundant equations of motion. It is possible to find the true dynamical degrees of freedom by eliminating the non-dynamical ones in all the equations, thus removing the redundancies [222]. As it is well known, the Einstein equations read $m_{\rm P}^2 G_{\mu\nu} = T_{\mu\nu}$, where $T_{\mu\nu}$ is the momentum-energy tensor, which is defined as

$$T_{\mu\nu} \equiv g_{\mu\nu}\mathcal{L} - 2\frac{\delta\mathcal{L}}{\delta g^{\mu\nu}}. \tag{2.7.13}$$

The model is consistent whenever $G_{\mu\nu}$ and $T_{\mu\nu}$ enjoy the same group of symmetries. Clearly, the first term of the right member of (2.7.13) exhibits the same symmetries of the metric $g_{\mu\nu}$. However, it is not obvious whether the second term of such a member also exhibits them; we are going to show that this is not the case.

The second term of the right hand side in (2.7.13) is given by

$$2\frac{\delta\mathcal{L}}{\delta g^{\mu\nu}} = -F^a{}_{\mu\rho}F_a{}^\rho{}_\nu - D_\mu\mathcal{H}^a D_\nu\mathcal{H}_a. \tag{2.7.14}$$

Replacing $g_{\mu\nu}$ by the FLRW metric, the cosmic triad ansatz (2.7.7), and the Higgs triplet in (2.7.14), we can see that there are off-diagonal terms in $T_{\mu\nu}$ since

$$2\frac{\delta\mathcal{L}}{\delta g^{\mu\nu}}\bigg|_{\mu\nu=0i} = g\,\phi\,\varepsilon_{aib}\dot{\mathcal{H}}^a\mathcal{H}^b. \tag{2.7.15}$$

This contribution to the momentum density is the first inconsistency of the model. Also, from (2.7.14), we have recognized a second problem

$$2\frac{\delta\mathcal{L}_{\rm mat}}{\delta g^{\mu\nu}}\bigg|_{\mu\nu=i\neq j} = g^2\phi^2\mathcal{H}_i\mathcal{H}_j, \tag{2.7.16}$$

which implies a contribution to the anisotropic stress. These off-diagonal terms in $T_{\mu\nu}$, whose origins are in the interaction between the gauge vector fields and the Higgs triplet, are clearly at odds with the energy tensor of a perfect fluid in the FLRW universe. Moreover, additional difficulties emerge from the equations of motion of the gauge fields. Varying the action (2.7.1) with respect to $A^a{}_\mu$ we have got

$$\nabla_\mu F_a{}^{\mu\nu} - g\varepsilon^b{}_{ca}F_b{}^{\mu\nu}A^c{}_\mu - g\varepsilon^b{}_{ac}g^{\mu\nu}D_\mu\mathcal{H}_b\mathcal{H}^c = 0, \tag{2.7.17}$$

such that, after having replaced the FLRW metric, the ansatz (2.7.7) and the Higgs triplet, we have obtained

$$\begin{aligned}
\ddot{\phi} + H\dot{\phi} + \frac{2g^2\phi^3}{a^2} + g^2\phi\left(\mathcal{H}_2^2 + \mathcal{H}_3^2\right) = 0,\ a, i = 1,\\
\ddot{\phi} + H\dot{\phi} + \frac{2g^2\phi^3}{a^2} + g^2\phi\left(\mathcal{H}_1^2 + \mathcal{H}_3^2\right) = 0,\ a, i = 2,\\
\ddot{\phi} + H\dot{\phi} + \frac{2g^2\phi^3}{a^2} + g^2\phi\left(\mathcal{H}_1^2 + \mathcal{H}_2^2\right) = 0,\ a, i = 3,
\end{aligned} \tag{2.7.18}$$

meaning that the gauge fields $A^a{}_i \equiv \phi(t)\delta^a{}_i$ do not evolve in the same way, implying that the isotropy in the model is dynamically broken. Again, this problem comes from the interaction between the gauge fields and the Higgs fields.

Similar irregularities were found in the EYMH model charged under the SU(2) group [1, 182, 183]. There, the authors showed that such a model can be compatible with a FLRW spacetime, once the cosmic triad (2.7.7) is employed, and the gauge of the Higgs doublet is suitable fixed. However, that strategy does not apply here since any gauge for the Higgs triplet yields to trouble with the FLRW universe. For instance, if we choose the gauge where all the components of the Higgs triplet are equal, there is no contribution to the momentum density and each gauge field evolves in the same way, but the contribution to the anisotropic stress does not vanish.

Although the EYMH model charged under the SO(3) group is incompatible with the FLRW spacetime, this does not rule it out as a possible model for dark energy. A naive solution to avoid the contributions to the momentum density and anisotropic stress is fixing the gauge of the Higgs triplet as

$$\mathcal{H}(t) \equiv (\Phi(t),\ 0,\ 0)\,, \tag{2.7.19}$$

with $\Phi(t)$ being a scalar field. However, the model is still inconsistent since the diagonal terms in the energy tensor are not equal:

$$\begin{aligned}
T_{11} &= a^2\left(\frac{1}{2}\frac{\dot{\phi}}{a^2} + \frac{1}{2}\frac{g^2\phi^4}{a^4} + \frac{1}{2}\dot{\Phi}^2 - \frac{g^2\phi^2\Phi^2}{a^2} - V\right),\\
T_{22} = T_{33} &= a^2\left(\frac{1}{2}\frac{\dot{\phi}}{a^2} + \frac{1}{2}\frac{g^2\phi^4}{a^4} + \frac{1}{2}\dot{\Phi}^2 - V\right);
\end{aligned} \tag{2.7.20}$$

of course, the interaction term is the responsible for the different components.

As shown above, the gauge where the Higgs triplet has only one component generates anisotropy but no other undesirable effect. This anisotropy perfectly fits in an axially symmetric Bianchi-I universe as seen in (2.7.20). Therefore, we turn our attention to consider the EYMH model, in the SO(3) representation, in an anisotropic Universe and search for the conditions under which non-negligible spatial shear contributions to the late accelerated expansion are obtained.

2.7.3 Anisotropic Model

Equations of Motion

Consider the axially symmetric Bianchi-I metric. To be consistent with the symmetries of this metric, the ansatz (2.7.7) is replaced by a more suitable axially symmetric ansatz [186]. We have chosen ${A^a}_0(t) \equiv 0$ and

$$ {A^1}_1(t) \equiv I(t), \quad {A^2}_2(t) = {A^3}_3(t) \equiv J(t), \tag{2.7.21} $$

while the other components of the fields are set to zero.[26] We have also used the shorthand notation

$$ G_1 \equiv \sqrt{g^{11}}, \; G_2 \equiv \sqrt{g^{22}} = \sqrt{g^{33}}. \tag{2.7.22} $$

The gauge of the Higgs field is fixed as in (2.7.19). As mentioned before, this choice assures no contributions either to the momentum density or to the anisotropic stress, while generating two different pressures.

Using the configurations for the Higgs Fields (2.7.19) and the gauge fields (2.7.21), together with the Einstein equations, we can write the first Friedmann equation ($m_{\rm P}^2 G_{00} = T_{00}$) as

$$ 3m_{\rm P}^2 H^2 = \rho_r + \rho_m + \rho_{\rm DE}, \quad \rho_{\rm DE} \equiv \rho_{\rm YM} + \rho_{\mathcal{H}} + 3m_{\rm P}^2 \dot{\sigma}^2, \tag{2.7.23} $$

is the density of the dark energy split into the contributions from the Yang-Mills term $\rho_{\rm YM}$ and the Higgs field $\rho_{\mathcal{H}}$. The latter are given by

$$ \rho_{\rm YM} \equiv \frac{1}{2}(G_1 \dot{I})^2 + (G_2 \dot{J})^2 + g^2 (G_1 I)^2 (G_2 J)^2 + \frac{1}{2} g^2 (G_2 J)^4, \tag{2.7.24} $$

$$ \rho_{\mathcal{H}} \equiv \frac{1}{2}\dot{\Phi}^2 + g^2 \Phi^2 (G_2 J)^2 + V. \tag{2.7.25} $$

On the other hand, for the second Friedmann equation ($m_{\rm P}^2 \operatorname{Tr}(G_{ij}) = \operatorname{Tr}(T_{ij})$) we have got

$$ -2m_{\rm P}^2 \dot{H} = 3m_{\rm P}^2 H^2 + \frac{1}{3}\rho_r + p_{\rm DE}, \tag{2.7.26} $$

[26] Other possible ansatz have been employed in [185, 190, 219].

where $p_{\rm DE}$ is the pressure of the dark energy given by

$$p_{\rm DE} \equiv \frac{1}{3}\rho_{\rm YM} + \frac{1}{2}\dot{\Phi}^2 - \frac{1}{3}g^2(G_2J)^2\Phi^2 - V + 3m_{\rm P}^2\dot{\sigma}^2, \tag{2.7.27}$$

and for the spatial shear $(G^2{}_2 - G^1{}_1 = (T^2{}_2 - T^1{}_1)/m_{\rm P}^2)$

$$3m_{\rm P}^2(\ddot{\sigma} + 3H\dot{\sigma}) = (G_1\dot{I})^2 - (G_2\dot{J})^2 + g^2(G_2J)^4 - g^2(G_1I)^2(G_2J)^2 + g^2\Phi^2(G_2J)^2. \tag{2.7.28}$$

Having replaced the field configurations in (2.7.17), we have got the equations of motion for the gauge fields

$$0 = (G_1\ddot{I}) + (H + 4\dot{\sigma})(G_1\dot{I}) + 2g^2(G_2J)^2(G_1I), \tag{2.7.29}$$

and

$$0 = (G_2\ddot{J}) + (H - 2\dot{\sigma})(G_2\dot{J}) + g^2(G_2J)(G_1I)^2 + g^2(G_2J)^3 + g^2(G_2J)\Phi^2. \tag{2.7.30}$$

Having performed a variation of the action (2.7.1) with respect to $\mathcal{H}^a$ and replaced the field configurations, we have got the equation of motion for the Higgs field

$$\ddot{\Phi} + 3H\dot{\Phi} + 2g^2(G_2J)^2\Phi + \frac{dV}{d\Phi} = 0\,. \tag{2.7.31}$$

The set of Eqs. (2.7.23), (2.7.26), (2.7.28), (2.7.29), (2.7.30), and (2.7.31) describe the cosmological evolution. The asymptotic behaviour of this set of dynamical equations can be studied through a dynamical system analysis [97, 163] (see also Ref. [223]), this being an approach that we are going to illustrate in the following section.

Dynamical System Analysis

We have introduced the following dimensionless variables

$$x \equiv \frac{1}{\sqrt{3}m_{\rm P}}\frac{(G_1\dot{I})}{H}, \quad y \equiv \frac{1}{\sqrt{3}m_{\rm P}}\frac{(G_2\dot{J})}{H}, \quad z \equiv \frac{1}{\sqrt{6}}\frac{\dot{\Phi}}{H}, \quad w \equiv \frac{1}{\sqrt{3}m_{\rm P}}\frac{g(G_2J)\Phi}{H}, \tag{2.7.32}$$

$$v \equiv \frac{1}{m_{\rm P}H}\sqrt{\frac{V}{3}}, \quad \xi \equiv \frac{\sqrt{3}m_{\rm P}}{(G_2J)}, \quad p \equiv \sqrt{\frac{g}{\sqrt{3}m_{\rm P}H}}(G_1I), \quad s \equiv \sqrt{\frac{g}{\sqrt{3}m_{\rm P}H}}(G_2J), \quad \Sigma \equiv \frac{\dot{\sigma}}{H},$$

such that the first Friedmann equation (2.7.23) becomes the constraint

$$\Omega_r = 1 - \frac{1}{2}x^2 - y^2 - \frac{1}{2}s^2\left(s^2 + 2p^2\right) - z^2 - v^2 - w^2 - \Sigma^2 - \Omega_m. \tag{2.7.33}$$

The set of background equations of motion (2.7.26), (2.7.28), (2.7.29), (2.7.30), and (2.7.31) is replaced by the autonomous set

$$x' = x(q-1-2\Sigma) - 2p\,\xi\, s^3, \tag{2.7.34}$$

$$y' = y(q-1+\Sigma) - \xi\,(p^2 s^2 + s^4 + w^2), \tag{2.7.35}$$

$$z' = z(q-2) - w\,\xi\,(\sqrt{2}s^2 + \alpha v), \tag{2.7.36}$$

$$w' = w(q + y\,\xi - \Sigma) + \sqrt{2}\,\xi\, z s^2, \tag{2.7.37}$$

$$v' = v(q+1) + \alpha w z\,\xi, \tag{2.7.38}$$

$$\xi' = \xi\,(1 - y\,\xi + \Sigma), \tag{2.7.39}$$

$$p' = \frac{1}{2}p(q-1+4\Sigma) + s x\,\xi, \tag{2.7.40}$$

$$s' = \frac{1}{2}s(q-1+2y\,\xi - 2\Sigma), \tag{2.7.41}$$

$$\Sigma' = \Sigma(q-2) + s^2(s^2-p^2) + w^2 - y^2 + x^2, \tag{2.7.42}$$

$$\Omega_m' = 2\Omega_m\,(q-1/2)\,, \tag{2.7.43}$$

where the deceleration parameter q is given by

$$q \equiv -1 - \frac{\dot{H}}{H^2} = 1 - 2v^2 - w^2 + z^2 - \frac{1}{2}\Omega_m + \Sigma^2, \tag{2.7.44}$$

and α is a positive dimensionless constant defined by $\alpha \equiv \sqrt{2\lambda/g^2}$. The deceleration parameter, or equivalently the effective equation of state $w_{\text{eff}} \equiv (2q-1)/3$, characterizes the evolution of the average scale factor $a(t)$.

Although the variables (2.7.32) describe the autonomous set, the relevant quantities we have been interested in are the physical fields, i.e. the physical gauge vector fields

$$\psi_1 \equiv \frac{(G_1 I)}{m_{\text{P}}} = \frac{\sqrt{3}p}{s\,\xi}, \quad \psi_2 \equiv \frac{(G_2 J)}{m_{\text{P}}} = \frac{\sqrt{3}}{\xi}, \tag{2.7.45}$$

their speeds

$$\begin{aligned} \psi_1' &\equiv \frac{(G_1 I)'}{m_{\text{P}}} = \psi_1(2\Sigma - 1) + \sqrt{3}x, \\ \psi_2' &\equiv \frac{(G_2 J)'}{m_{\text{P}}} = \psi_2(y\,\xi - 1 - \Sigma), \end{aligned} \tag{2.7.46}$$

and the Higgs field and its speed

$$\frac{\Phi}{m_{\rm P}} = \frac{\sqrt{3}w}{s^2\,\xi}, \quad \frac{\Phi'}{m_{\rm P}} = \sqrt{6}z. \tag{2.7.47}$$

Besides the behaviour of each field, the dark sector as a whole can be characterized by its density parameter $\Omega_{\rm DE} \equiv \rho_{\rm DE}/3m_{\rm P}H^2$ and its equation of state $w_{\rm DE} \equiv p_{\rm DE}/\rho_{\rm DE}$.

In the following, we are going to discuss the fixed points relevant to the dark energy era ($\Omega_{\rm DE} \simeq 1, w_{\rm eff} < -1/3$).

Dark energy dominance

- Isotropic dark energy (*DE-1*):

$$x = 0, \quad y = 0, \quad \xi = 0, \quad p = 0, \quad s = 0, \quad z = 0, \quad w = 0, \quad v = 1, \quad \Sigma = 0. \tag{2.7.48}$$

In this point we have $w_{\rm eff} = w_{\rm DE} = -1$, $\Omega_{\rm DE} = 1$, and $\Omega_m = 0$, corresponding to an accelerated expansion solution where the Universe is filled by the Higgs potential. This is a saddle point with only one positive eigenvalue, while the other eigenvalues are negative. The eigenvector associated to this positive eigenvalue indicates that $\xi = 0$ is a repeller in the ξ-direction, meaning that the gauge field ψ_2 is decreasing in magnitude. Note that $w_{\rm eff}$ does not depend on ξ, consequently $w_{\rm eff} = -1$ is an attractor since all the other variables are attracted to their corresponding values in the point. Hence, we say that (*DE-1*) is an "*effective attractor*". Also notice that the shear Σ is diluted in the point, i.e. the model does not support an anisotropic dark energy final state. This is consistent with the fact that the gauge fields, ψ_1 and ψ_2, and their speeds decay to zero in the point, implying that the interaction between the Higgs field and the gauge fields vanishes, and so does the anisotropic shear which is supported by this interaction. We have also been able to infer that the Higgs field Φ is attracted in a decelerated way (in magnitude) towards a constant value, since $z = 0$ in the point.

We want to stress that, although the final state of the Universe is characterized by an isotropic accelerated expansion, this does not rule out an observable anisotropic dark energy today. In the following, we are going to present the results of the numerical integration of the autonomous set, in order to see a particular trajectory of the Universe, and look for initial conditions yielding to a significant anisotropic contribution to the dark energy components nowadays.

Numerical Solution

We have performed a numerical integration of the autonomous system. In particular, we have chosen[27] $\alpha = 1$ and

$$x_i = y_i = \xi_i = 10^{-8},\ p_i = s_i = 10^{-12},\ z_i = w_i = 10^{-12},\ v_i = 2\times 10^{-14},\ \Sigma_i = 10^{-20}, \quad (2.7.49)$$

and $\Omega_{m_i} = 4.99\times 10^{-5}$, $\quad \Omega_{r_i} = 0.99995$ as initial conditions at redshift $z_r = 6.566\times 10^7$, well within the deep radiation era. The Universe is supposed to have undergone an inflationary phase prior to this epoch, therefore the initial value for the spatial shear is very close to zero. The initial values of the other fields have been chosen so that the dark components provide a subdominant contribution to the radiation era, while obeying the Friedmann constraint (2.7.33).

From the dimensionless variables (2.7.32), we have been able to obtain an expression for the Hubble parameter:

$$\frac{H}{m_{\rm P}} = \frac{\sqrt{3}\,g}{s^2\,\xi^2}, \quad (2.7.50)$$

where using $H_0 \sim 10^{-61} m_{\rm P}$ and the values of s and ξ evaluated today, we have got for the SU(2) coupling parameter $g \sim 10^{-88}$. Then, from the parameter $\alpha \equiv \sqrt{2\lambda/g^2}$ we have got $\lambda \sim 10^{-176}$. We want to stress that these values for g and λ are just figures since their actual values depend on the chosen initial conditions; however, they give us a notion of how small they must be.

Anisotropic Shear Today

Observationally, from data analysis of type Ia supernovae, the value of the present shear is constrained to be $|\Sigma_0| \leq \mathcal{O}(0.001)$ [142, 143]. However, it is expected future missions like Euclid [47] to impose more restricted bounds on the anisotropic contribution from the dark energy content. In this subsection, we are going to explore the behaviour of the anisotropic shear for different initial conditions, and show that the predicted values by our model around the present time, $z_r = 0$, are well within the present bounds. In order to do so, we have fixed the values for the variables as in (2.7.49), except for the variable w which we have varied in a consistent manner with the Friedmann constraint (2.7.33), the general behaviour of the density parameters, and the effective equation of state described in the previous subsection. As seen in the right panel of Fig. 2.7.1, the shear vanishes in the future in all the cases studied, being consistent with the dynamical system analysis. We can also see that around the end of the matter epoch ($z_r + 1 \approx 10$) the shear grows to appreciable values, its contribution being non negligible around today ($z_r + 1 = 1$). For instance, for $w_i = 10^{-8}$ we have got $\Sigma_0 \approx 2.1\times 10^{-5}$,

[27] This is the order of magnitude obtained when calculating α, based on the Standard Model of Particle Physics [209].

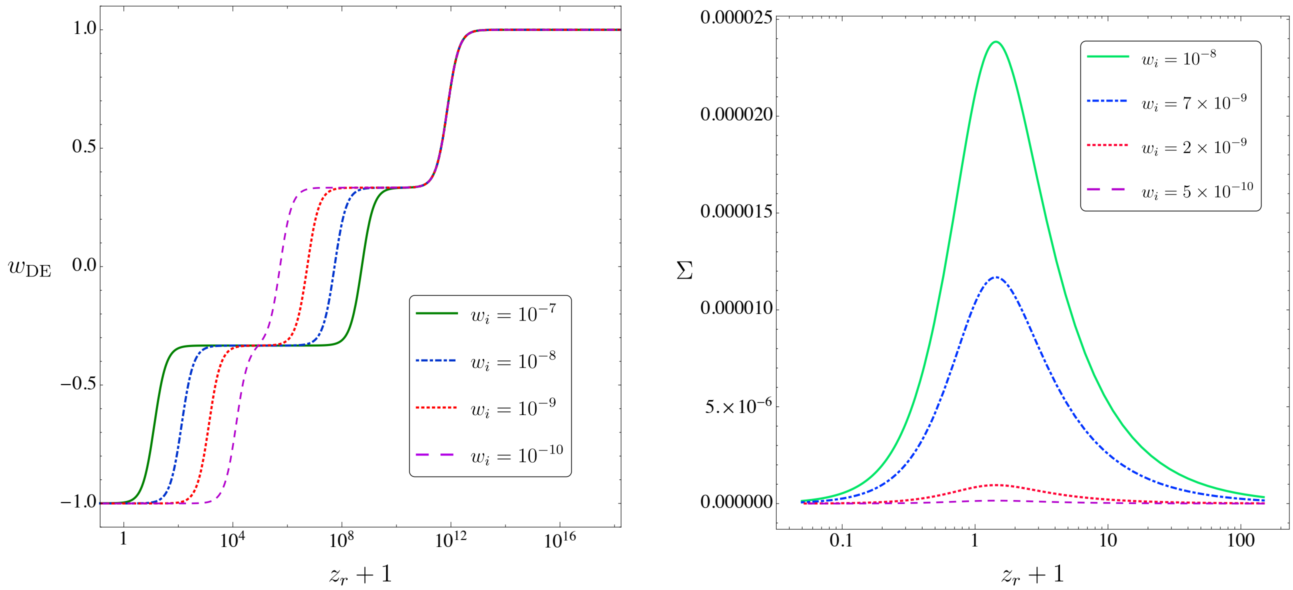

Figure 2.7.1: (Left) Cosmological evolution of the equation of state of dark energy $w_{\rm DE}$ for different values of the interaction variable w. In all the cases, the final stage is $w_{\rm DE} \simeq -1$, and there are also three other stages characterized by $w_{\rm DE} \simeq 1$, $w_{\rm DE} \simeq 1/3$ and $w_{\rm DE} \simeq -1/3$. (Right) Evolution of the shear Σ around $z_r = 0$ for different values of the interaction variable w. The shear vanishes in the future in all the cases; however, there are initial conditions yielding to observable values of anisotropic dark energy.

and for $w_i = 5 \times 10^{-10}$ we have got $\Sigma_0 \approx 1.3 \times 10^{-7}$. Therefore, although the Universe loses its hair in the future, it could have an observable hair today; similar conclusions have been obtained in [220] in the framework of the Einstein-aether scalar field theory.

Equation of State for Dark Energy

To end this section, we are going to discuss the cosmological evolution of the equation of state for dark energy $w_{\rm DE}$ for different initial conditions. Given that the amount of anisotropic shear is mainly supported by the interaction term encoded in the variable w, we are going to explore the behaviour of $w_{\rm DE}$ with respect to this variable, since we have been interested in the particular trajectories where Σ_0 is non negligible. Therefore, we fix the initial conditions as in (2.7.49) in the deep radiation era and vary w_i in a consistent way as described in the previous subsection. In the left panel of Fig. 2.7.1, we can see that $w_{\rm DE}$ is characterized by four stages which we are going to describe in the following.

At very high redshifts, $z_r > 10^{12}$, we have $w_{\rm DE} \simeq 1$, meaning that the dark sector behaves as a "stiff fluid" [224]. During this period, the dark sector is dominated either by the kinetic term of the Higgs field in the variable z, phase known as "kination", or by the shear Σ. After this phase, $w_{\rm DE} \simeq 1/3$ during the radiation domination, so the dark sector behaves as a "dark radiation" fluid [125]. The length of this period depends on the value of w: it increases by decreasing w. After this phase, $w_{\rm DE} \simeq -1/3$, indicating the transition from decelerated to accelerated expansion. This period exists for some values of w_i. This transition phase can be long enough to lasts until the end of the matter era, which has the potential to affect the process of structure formation [225]. At the end, in all the cases, the final stage is given by $w_{\rm DE} \simeq -1$, where the symmetry breaking potential dominates and the Higgs field reaches a constant value away from its vacuum value, driving this way an eternal accelerated expansion as an effective cosmological constant.

2.7.4 An Isotropic Possibility: The Higgs Triad

As explained in previous sections, a Higgs triplet is inconsistent with the symmetries of the FLRW spacetime. However, there could exist specific arrangements of several fields allowing a homogeneous and isotropic configuration compatible with a FLRW universe. Examples of such arrangements are: a large number of vectors fields pointing at random directions as in vector inflation [150], the cosmic triad for vector fields charged under some internal symmetry group [114, 120, 149, 151, 189, 196], three inhomogeneous scalar fields as in solid inflation [147, 148], and three U(1) scalar fields as in charged-vector inflation [152]. Based on these works, we propose the "*Higgs triad*" as a possible configuration consistent with the homogeneity and isotropy of the FLRW metric.

The Higgs triad consists of three SO(3) Higgs fields with the following inner structure

$$\mathcal{H}^I \equiv \begin{pmatrix} \Phi \\ 0 \\ 0 \end{pmatrix}, \; \mathcal{H}^{II} \equiv \begin{pmatrix} 0 \\ \Phi \\ 0 \end{pmatrix}, \; \mathcal{H}^{II} \equiv \begin{pmatrix} 0 \\ 0 \\ \Phi \end{pmatrix}, \tag{2.7.51}$$

i.e. three Higgs fields with the same magnitude and mutually orthogonal in the manifold associated to the SO(3) group. Each Higgs field comes with its respective gauge vector field, whose dynamics is given by its own Yang-Mills term, and its particular SO(3) gauge coupling. However, in order to keep the isotropy, it is mandatory to consider the same cosmic triad (2.7.7) for each gauge vector field, and the same group coupling constant g.

Under the conditions mentioned above, the EYMH model matches with a FLRW background. The equations of motion are equivalent to those obtained when the reduced action is used, which were first reported in [192]. Nonetheless, we want to stress that the original model in [192] is physically different to the one we are presenting here, since only one Higgs triplet with all its inner components being different is considered there, which yields to the inconsistencies discussed in previous sections.

2.7.5 Conclusions

In this paper, we have investigated the EYMH model charged under the SO(3) gauge symmetry as a mechanism for the late accelerated expansion. The same model was originally studied in [192] using the reduced Lagrangian method and a dynamical system analysis. This approach allowed the author of that work to conclude that the model is characterized by a unique accelerated attractor where the potential of the Higgs triplet dominates. However, using the whole set of Einstein equations, we have shown that the equations of motion presented in [192] are indeed inconsistent with a FLRW background. This is because the interaction between the gauge components of the Higgs field and the gauge vector field serves as source of momentum density, anisotropic stress or anisotropic shear. Similar inconsistencies were found in [1, 182, 183]. There, the authors studied the EYMH model charged under the SU(2) gauge symmetry, and they found that it is possible to eliminate the inconsistencies by fixing the gauge of the Higgs doublet. However, this is not possible here where the SO(3) gauge group is considered.

In consequence, we have turned our attention to the EYMH model in the SO(3) representation, embedded in a homogeneous but anisotropic axially symmetric Bianchi-I background. We have worked out the respective equations of motion, and treated them using a dynamical system approach. We have found that the only attractor of the theory corresponds to an isotropic accelerated expansion where the Higgs field reaches a constant value, different to its vacuum value, such that the dominating Higgs potential behaves as an effective cosmological constant. This result was expected since the interaction term vanishes, which is the support for the spatial shear. However, this does not exclude an observable amount of shear today and, as we have shown above, the model can support non-negligible anisotropies today (for instance, $\Sigma_0 \sim 10^{-5}$) depending on the initial values (in the deep radiation epoch) of the expansion variable w associated to the interaction term. We remark that the values predicted by our model are in agreement with several observational bounds [142, 143]. Therefore, we conclude that although the Universe loses most of its hair, a small amount could be observable today. We have also found that the equation of state of dark energy $w_{\rm DE}$ transits through several characteristic stages depending on the value of w. For some values of w, during the matter epoch ($z_r < 50$) $w_{\rm DE} \neq -1$, suggesting that the process of structure formation might be affected [225].

2.8 String Compactifications

2.8.1 Introduction

Despite the potential conceptual challenges surrounding its compatibility with accelerated universes [226, 227], superstring theory provides a top-down approach that serves as both a playground for model construction and a guiding principle in ensuring consistency within possible ultraviolet completions that incorporate quantum gravity. Remarkably, the phenomenology of string theory has made significant strides over recent decades, offering a wealth of insights into potential fields and their interactions. Although precise and exact outcomes remain elusive due to the intricacies of transitioning from the 10-dimensional theory to the 4-dimensional effective description, guidelines have surfaced, exemplified by the *swampland conjectures* [228–232]. These conjectures shed light on what can be anticipated from theories aiming for a coherent ultraviolet completion that encompasses gravity.[28]

Scalar fields are pervasive in effective 4-dimensional theories derived from string theory. They describe various couplings (e.g., dilaton modulus), internal dimensions' size and shape (e.g., Kähler modulus), brane locations, and more. Thus, the simplest scenarios involve single scalar field models. Encouragingly, several positive results have already been achieved. For instance, there are potential UV descriptions of generalizations of the Chaplygin gas derived from D-branes [234–236], stringy axions [237–239], and early dark energy scenarios like the one presented in Ref. [240].

Additionally, there are multifield scenarios, as seen in references such as [241–246]. In many cases, multifield scenarios address issues present in the single field case and include elements like the axionic superpartner for scalar fields. These multifield situations are not only more natural due to the expectation of many scalar fields in UV completions but also align with the *swampland conjectures*. These conjectures demand very steep scalar potentials, often in conflict with working scenarios of quintessence. Interestingly, a non-trivial curvature in the scalar field manifold can evade such constraints, as shown in Ref. [247] (see also Ref. [248]), and permit behaviours resembling inflation [238, 245, 249–251]. An interesting situation of multifield dynamics can simultaneously address the puzzle of dark matter, as shown for example in Ref. [252] and, recently in Ref. [251, 253]. The former work builds on a string inspired model of the dilaton that couples with a hidden sector, but does no regard its superpartner. This is done in Ref. [254] (also in Ref. [255] with more involved kinetic mixings) where, however, no any other energy components are included. This system, together with a barotropic perfect fluid is instead studied in Refs. [256, 257] and with a direct universal coupling in Ref. [258].

Vector fields are, indeed, a more intrinsic component of nature than scalar fields and are anticipated to be inherent in any extension of the standard model. The issue of consistency becomes less straightforward in this context, owing to the potential emergence of ghost fields. Nevertheless, substantial progress has been made in comprehending a bottom-up approach

[28]The pursuit of incorporating any model within the framework of string theory is more than an academic exercise; it emerges as an essential endeavour. This arises from the likelihood that explaining an accelerated epoch necessitates substantial contributions from a microscopic description that goes beyond the effective field theory approximation for point particles [233].

for constructing effective Lagrangians involving these fields, as discussed in references such as [100, 140, 259–263], facilitating a broad spectrum of cosmological investigations.

In the line of the present study, dynamical dark energy scenarios have been formulated, wherein vector fields play a pivotal role. For example, Refs. [1, 3, 192] introduces vector fields associated with an $SO(3)$ symmetry, forming what is termed the *cosmic triad*, first proposed in [114]. This scenario allows for isotropic solutions, while also accommodating situations with a preferred direction, as explored in Refs. [2, 4], considering a Bianchi I spacetime as the background. A simpler scenario involves a $U(1)$ gauge symmetry, where even general scalar-vector-tensor analyses have been conducted, for example in Refs. [8, 264]. Motivated by UV considerations, studies have delved into specific constructions, including the work of Thorsrud et al. in Ref. [117], who investigated the cosmological implications of a scalar field with an exponentially field-dependent gauge kinetic function inspired by dilaton field couplings. A detailed analysis of this model was subsequently undertaken in Ref. [5], exploring alternative kinetic term structures for the scalar field.

The primary objective of our current investigation is to explore the simplest yet least constrained model inspired by string theory compactifications. Specifically, we consider two scalar fields associated with a complex modulus and a $U(1)$ vector field, where the gauge kinetic function is dependent on the modulus. The analysis leads to study a dynamical system dependent on three parameters, resulting in four fixed points. One of these fixed points involves only one scalar field, reproducing models initially studied in this type of scenario [265] but which is in tension with the *swampland* constraints on the steepness of the potential. Two other fixed points are inherited from previous models [5, 256], which involve only a pair of fields in the model. Additionally, a completely novel fixed point is discovered in which all three fields play a role. We pay special attention to the cases where the vector field has a non-trivial role. We find that it is possible to describe the observed cosmology, albeit in a parameter space challenging to justify from superstring compactifications.

2.8.2 Scalar Multifield model from string compatifications

Much in the spirit of inflationary models, our main concern will be with the scalar sector whose dynamics are expected to lead to a dynamical equation of state that hopefully presents a late-time accelerated expansion epoch. The dynamics of the scalar sector are mainly encoded in the scalar potential, which in supergravity can be split into two components: the F-term and D-term contributions. The former has the following general structure [266]

$$V_F = e^{K/m_{\mathrm{P}}^2}\left(K^{I\bar{J}}(D_I W)(\bar{D}_{\bar{J}}\bar{W}) - \frac{3}{m_{\mathrm{P}}^2}W\bar{W}\right), \tag{2.8.1}$$

where $K = K(\bar{\Phi}^{\bar{I}}, \Phi^I)$ is the Kähler potential and $W = W(\Phi^I)$ is the superpotential. Here, I and J range over the complete set of chiral superfields, and the bar symbol representing the conjugate quantities; therefore, the superpotential is a holomorphic function for the chiral superfields, while the Kähler potential is a real one. Additionally, using the shorthand notation $\partial_I f \equiv \frac{\partial f}{\partial \Phi^I}$, we define $K_{I\bar{J}} \equiv \frac{\partial^2 K}{\partial \Phi^I \partial \bar{\Phi}^{\bar{J}}}$, and its inverse $K^{I\bar{K}} K_{J\bar{K}} = \delta^I_J$. The covariant derivative is defined as

$$D_I W = W_I + \frac{1}{m_{\mathrm{P}}} K_I W.$$

On the other hand, the D-term contribution has to do with the gauge symmetries,

$$V_D = \frac{1}{2} \mathrm{Re}(f^{AB}) D_A D_B, \tag{2.8.2}$$

with f^{AB} the inverse of f_{AB}, the gauge kinetic function (more on it below), while

$$D_A = i X^I_A \partial_I K, \tag{2.8.3}$$

where X^I_A are the, in general, field-dependent Killing vectors associated with the gauge symmetry A. In other words, a transformation associated with real parameters λ^A induces one on the chiral superfields given by $\delta\phi^i = \lambda^A X^i_A$, such that D_A is a gauge-invariant combination of charged fields.

While string compactifications exhibit a diverse array of scalar fields, the most distinctive aspect of four-dimensional effective supersymmetric theories is the presence of moduli fields, characterizing flat directions within the field space. This peculiarity motivates their incorporation into string-inspired model constructions for slow-roll inflationary and quintessence scenarios (for a review and specific instances, see [267] and references therein.) The underlying rationale for this behaviour lies in the moduli fields serving as superpartners to compactified p-forms potentials with gauge freedom, represented by $C_p \to C_p + \mathrm{d}A_{p-1}$, which manifests as shift symmetries. Denoting the scalar component of our chiral modulus superfield as $\Psi = s + \mathrm{i}\sigma$ with s and σ being real, the axionic symmetry $\sigma \to \sigma + c$ is reflected in the Kähler potential as a dependency in the form

$$K(\bar{\Phi}^{\bar{I}}, \Phi^I) = K(\bar{\Psi} + \Psi, \bar{\Phi}^{\bar{M}}, \Phi^M) = K(s, \bar{\Phi}^{\bar{M}}, \Phi^M),$$

with M ranging over all chiral fields but the modulus, while the superpotential should be modulus-independent, i.e.,

$$W(\Phi^I) = W_0(\Phi^M).$$

In light of these considerations, the F-term scalar potential adopts the following expression:

$$V_F = e^{K(s,\bar{\Phi}^{\bar{M}},\Phi^M)/m_{\rm P}^2}\left[K^{M\bar{N}}(D_M W_0)(\bar{D}_{\bar{N}}\bar{W}_0) + \frac{1}{m_{\rm P}^2}\frac{|K_\Psi|^2}{K_{\Psi\bar{\Psi}}}|W_0|^2 - \frac{3}{m_{\rm P}^2}|W_0|^2\right]. \tag{2.8.4}$$

We further simplify by considering that the structure of the Kähler potential is of the form

$$K(s,\bar{\Phi}^{\bar{M}},\Phi^M) = K(s) + \mathcal{K}(\bar{\Phi}^{\bar{M}},\Phi^M). \tag{2.8.5}$$

Consequently, the scalar potential takes the following general form:

$$V_F = e^{K(s)/m_{\rm P}^2}\left(\mathcal{F} + \mathcal{G}\frac{|K_\Psi|^2}{K_{\Psi\bar{\Psi}}}\right) \tag{2.8.6}$$

with modulus-independent functions

$$\mathcal{F} = e^{\mathcal{K}(\bar{\Phi}^{\bar{M}},\Phi^M)/m_{\rm P}^2}\left(K^{M\bar{N}}(D_M W_0)(\bar{D}_{\bar{N}}\bar{W}_0) - \frac{3}{m_{\rm P}^2}|W_0|^2\right),$$

and

$$\mathcal{G} = e^{\mathcal{K}(\bar{\Phi}^{\bar{M}},\Phi^M)/m_{\rm P}^2}\frac{|W_0|^2}{m_{\rm P}^2}.$$

A typical form for the modulus Kähler potential is given by a logarithmic dependency

$$K(s) = -p\ln\left(\frac{2s}{m_{\rm P}^2}\right)m_{\rm P}^2, \tag{2.8.7}$$

with p a real constant, such that

$$K_\Psi = -\frac{p}{2s}m_{\rm P}^2, \quad K_{\Psi\bar{\Psi}} = \frac{p}{(2s)^2}m_{\rm P}^2,$$

and

$$V_F = \frac{m_{\rm P}}{(2s)^p}\left(\mathcal{F} + p\mathcal{G}\right) \equiv \frac{1}{s^p}\mathcal{V}_{0,F}, \tag{2.8.8}$$

with $\mathcal{V}_{0,F}$ a s-independent function. Given that $\mathcal{V}_{0,F}$ depends on all other fields, we examine the scenario wherein all fields except s have previously been determined and stabilised through dynamics investigated over the last two decades, as illustrated for instance in [268–274]. In this context, we treat $\mathcal{V}_{0,F}$ as a non-vanishing constant.

Now, let us explore the D-term contribution. For it we restrict to the simplest case of a single $U(1)$ sector beyond the Standard Model symmetries and examine two cases. In the first case, we assume that the Killing vectors are independent of moduli and $X^\Psi = 0$, indicating that Ψ is neutral, resulting in

$$V_D = \frac{\frac{1}{2}D^2}{\mathrm{Re}(f(\Psi))}, \tag{2.8.9}$$

where the numerator is s-independent and its value is fixed by the stabilization of all other fields. Here the dependency on s will appear in the gauge kinetic function, as discussed below.

A second possibility is one of a pseudo-anomalous $U(1)$ sector, for which the field appearing as the gauge kinetic function develops a non-linear transformation with a constant Killing vector $X^\Psi = i\delta$ [275–277]. This induces a field-dependent Fayet-Ilioupoulus term of the form

$$D = iX^N K_N - \delta K_\Psi = iX^N K_N - \frac{p\delta}{2s}m_{\mathrm{P}}^2, \tag{2.8.10}$$

using the logarithmic dependency introduced above. Regarding the case on which the component $iX^N K_N = 0$ once the rest of the fields are fixed[29] and the D-term scalar potential reduces to

$$V_D = \frac{(p\delta)^2}{4s^2\mathrm{Re}(f(\Psi))}m_{\mathrm{P}}^4. \tag{2.8.11}$$

In order to be explicit we use a linear dependency for the gauge kinetic function, namely $f(\Psi) = \Psi/m_{\mathrm{P}}$, leading to the following general structure for the D-term scalar potential

$$V_D = \frac{\mathcal{V}_{0,D}}{s^n}m_{\mathrm{P}}^{4+n}, \tag{2.8.12}$$

with $n = 1$ and 3 respectively in the two cases and $\mathcal{V}_{0,D} = \frac{1}{2m_{\mathrm{P}}^4}D^2$ in the former case and $\mathcal{V}_{0,D} = \frac{(p\delta)^2}{4m_{\mathrm{P}}^2}$ in the pseudo-anomalous one.

The kinetic part is dictated solely by the Kähler potential and is given by

$$\mathcal{L}_{\mathrm{kin}} = -K_{I\bar{J}}\partial_\mu\Phi^I\partial^\mu\bar{\Phi}^{\bar{J}}, \tag{2.8.13}$$

thus $K_{I\bar{J}}$ is the metric of the field space so the consideration done in (2.8.5) means that the scalar manifold in the moduli sector factorises. Using the considerations above we get the following explicit kinetic term for the scalar fields

$$\mathcal{L}_{\mathrm{kin}} = -\frac{pm_{\mathrm{P}}^2}{(2s)^2}\partial_\mu s\partial^\mu s - \frac{pm_{\mathrm{P}}}{(2s)^2}\partial_\mu\sigma\partial^\mu\sigma. \tag{2.8.14}$$

[29] As discussed in [278], the presented scenario is considered unnatural. Nonetheless, in this context, we adhere to and illustrate this particular possibility.

Or, defining a canonical normalised field $\phi_1 = \sqrt{\frac{p}{2}}\ln(s/m_{\rm P})m_{\rm P}$ and renaming $\phi_2 = \sigma$,

$$\mathcal{L}_{\rm kin} = -\frac{1}{2}\partial_\mu\phi_1\partial^\mu\phi_1 - \frac{p}{4}e^{-\sqrt{2/p}\phi_1/m_{\rm P}}\partial_\mu\phi_2\partial^\mu\phi_2. \tag{2.8.15}$$

In terms of these fields the scalar potential takes the form

$$V = \mathcal{V}_{0,F}e^{-\sqrt{2p}\phi_1/m_{\rm P}} + \mathcal{V}_{0,D}e^{-n\sqrt{2p}\phi_1/m_{\rm P}}. \tag{2.8.16}$$

This result, motivates the study of a general two-field model of the form

$$\mathcal{L} = -\frac{1}{2}\partial_\mu\phi_1\partial^\mu\phi_1 - \frac{1}{2}f^2(\phi_1)\partial_\mu\phi_2\partial^\mu\phi_2 - V(\phi_1), \tag{2.8.17}$$

with exponential functions, as was done in [256]. In the following section, we will study the cosmological dynamics encoded in this model.

Cosmological setup

In a flat, homogeneous, and isotropic Friedman-Lemaître-Robertson-Walker (FLRW) spacetime, described by the metric

$$\mathrm{d}s^2 = -\mathrm{d}t^2 + a^2(t)\delta_{ij}\mathrm{d}x^i\mathrm{d}x^j, \tag{2.8.18}$$

where $a(t)$ is the cosmic time-dependent scale factor, the Lagrangian (2.8.17) regarding homogeneous fields, yields the following equations of motion:

$$\ddot{\phi}_1 + 3H\dot{\phi}_1 + V_{\phi_1} - f f_{\phi_1}\dot{\phi}_2^2 = 0, \qquad \ddot{\phi}_2 + 3H\dot{\phi}_2 + 2\frac{f_{\phi_1}}{f}\dot{\phi}_1\dot{\phi}_2 = 0, \tag{2.8.19}$$

where the subscript ϕ_1 denotes derivatives with respect to this field. To investigate the resulting cosmology, these equations must be coupled with the Einstein equation of motion $M_{\rm P}^2 G_{\mu\nu} = T_{\mu\nu}$. The contribution of these scalar fields to the energy-momentum tensor is expressed as

$$\begin{aligned} T^{(\phi)}_{\mu\nu} \equiv -\frac{2}{\sqrt{-g}}\frac{\delta(\sqrt{-g}\mathcal{L})}{\delta g^{\mu\nu}} =& -\nabla_\mu\phi_1\nabla_\nu\phi_1 - f^2(\phi_1)\nabla_\mu\phi_2\nabla_\nu\phi_2 \\ & - g_{\mu\nu}\left(-\frac{1}{2}\nabla_\alpha\phi_1\nabla^\alpha\phi_1 - \frac{1}{2}f^2(\phi_1)\nabla_\alpha\phi_2\nabla^\alpha\phi_2 - V(\phi_1)\right). \end{aligned} \tag{2.8.20}$$

For homogeneous fields, the density and pressure are specifically given by

$$\rho_\phi \equiv T^{(\phi)}_{00} = \frac{1}{2}\dot{\phi}_1^2 + \frac{1}{2}f^2(\phi_1)\dot{\phi}_2^2 + V, \qquad p_\phi \equiv \frac{1}{3}\mathrm{tr}\,T^{(\phi)}_{ij} = \frac{1}{2}\dot{\phi}_1^2 + \frac{1}{2}f^2(\phi_1)\dot{\phi}_2^2 - V. \tag{2.8.21}$$

However, for a more realistic scenario, additional components must be considered in the universe's energy budget. These contributions are represented by two perfect fluids, each following radiation and matter equations of state. Consequently, the complete energy-momentum tensor is formulated as

$$T_{\mu\nu} = T^{(\phi)}_{\mu\nu} + T^{(m)}_{\mu\nu} + T^{(r)}_{\mu\nu}, \tag{2.8.22}$$

and the dynamics for these two sectors adhere to the conservation of their energy-momentum tensors, i.e., $\nabla^\mu T^{(r)}_{\mu\nu} = 0$ and $\nabla^\mu T^{(m)}_{\mu\nu} = 0$, expressed explicitly as

$$\dot{\rho}_r + 4H\rho_r = 0, \qquad \dot{\rho}_m + 3H\rho_m = 0. \tag{2.8.23}$$

In light of these considerations, the Friedman equations from the Einstein field equations take the form

$$3M_{\rm P}^2 H^2 = \rho_\phi + \rho_m + \rho_r, \qquad -2M_{\rm P}^2 \dot{H} = \rho_\phi + p_\phi + \rho_m + \frac{4}{3}\rho_r. \tag{2.8.24}$$

As proposed in the preceding section and elucidated in Sec. 2.8.4, superstring theory likely necessitates the coupling function and potential to conform to the expressions given in (2.8.15) and (2.8.16),[30] explicitly represented as

$$f(\phi_1) \equiv f_0 e^{-\nu\phi_1/M_{\rm P}}, \qquad V(\phi_1) \equiv V_0 e^{-\lambda\phi_1/M_{\rm P}}, \tag{2.8.25}$$

where f_0 and V_0 are constants, and the parameters $\lambda = \sqrt{2p}$ and $\nu = \sqrt{2/p}$ are determined by the integer p.[31] Nevertheless, in the subsequent analysis, we treat λ and ν as arbitrary and examine the parameter space of the model yielding to viable cosmologies. Subsequently, we comment on the discrete parameter space favoured by string theory.

Dynamical Analysis

Unveiling the cosmological dynamics of the model requires solving Eqs. (2.8.19), (2.8.23) and (2.8.24) given some parameters and initial conditions. However, we can extract information of the asymptotic behaviour of the model encoded in its fixed points [97]. To do so, we recast these equations in terms of the following dimensionless variables

$$x_1 \equiv \frac{\dot{\phi}_1}{\sqrt{6}HM_{\rm P}}, \quad x_2 \equiv \frac{f(\phi_1)\dot{\phi}_2}{\sqrt{6}HM_{\rm P}}, \quad y \equiv \frac{\sqrt{V}}{\sqrt{3}HM_{\rm P}}, \quad \Omega_m \equiv \frac{\rho_m}{3M_{\rm P}^2H^2}, \quad \Omega_r \equiv \frac{\rho_r}{3M_{\rm P}^2H^2}. \tag{2.8.26}$$

[30] In the following we consider that only one of the contributions to the scalar potential (2.8.16) is present. More precisely we take the D-term contribution to vanish, being at least as constrained as the F-term counterpart, as will be shown below.

[31] In the case of the D-term scalar potential $\nu = n\sqrt{2/p}$ and a second integer is to be regarded.

The first Friedman equation (2.8.24) reduces to the constraint equation

$$1 = x_1^2 + x_2^2 + y^2 + \Omega_m + \Omega_r, \tag{2.8.27}$$

and the continuity equations in Eq. (2.8.23) and the equations of motion for the scalar fields in Eq. (2.8.19) are replaced by the following closed autonomous system

$$x_1' = x_1(1+q) + \sqrt{\frac{3}{2}}\left(\lambda y^2 - 2\nu x_2^2 - \sqrt{6}x_1\right), \tag{2.8.28}$$

$$x_2' = x_2(1+q) + x_2\left(\sqrt{6}\nu x_1 - 3\right), \tag{2.8.29}$$

$$y' = y\left(1 + q - \frac{\sqrt{6}}{2}\lambda x_1\right), \tag{2.8.30}$$

$$\Omega_r' = 2\,(q-1)\,\Omega_r, \tag{2.8.31}$$

where a prime denotes a derivative with respect to the number of e-folds, which is related to the cosmic time by $\mathrm{d}N \equiv H\mathrm{d}t$. The deceleration parameter, $q \equiv -a\ddot{a}/\dot{a}^2$, is written in terms of these variables as

$$1 + q = -\frac{\dot{H}}{H^2} = \frac{1}{2}\left(3x_1^2 + 3x_2^2 - 3y^2 + \Omega_r + 3\right). \tag{2.8.32}$$

The fixed points of this system are computed by solving the algebraic system resulting from $x_1' = 0$, $x_2' = 0$, $y' = 0$, and $\Omega_r' = 0$. We characterise the physical meaning of these fixed points by computing the effective equation of state and the equation of state of dark energy

$$w_{\mathrm{eff}} \equiv \frac{p_{\mathrm{tot}}}{\rho_{\mathrm{tot}}} = -1 - \frac{2}{3}\frac{\dot{H}}{H^2}, \qquad w_{\mathrm{DE}} \equiv \frac{p_\phi}{\rho_\phi} = -1 + \frac{2\,(x_1^2 + x_2^2)}{x_1^2 + x_2^2 + y^2}, \tag{2.8.33}$$

where $\rho_{\mathrm{tot}} \equiv \rho_\phi + \rho_m + \rho_r$ and $p_{\mathrm{tot}} = p_\phi + \rho_r/3$. Here, we focus on accelerated solutions driven by dark energy, i.e., fixed points where $w_{\mathrm{eff}} < -1/3$ and $w_{\mathrm{DE}} < -1/3$. Additionally, notice that the autonomous system exhibits the following symmetries:

$$\{x_1, \lambda, \nu\} \to \{-x_1, -\lambda, -\nu\}, \quad x_2 \to -x_2, \quad y \to -y. \tag{2.8.34}$$

Therefore, without loss of generality we restrict ourselves to solutions with $x_2, y \geq 0$ and consider non-negative values of the parameters λ and ν while leaving free x_1. Under these

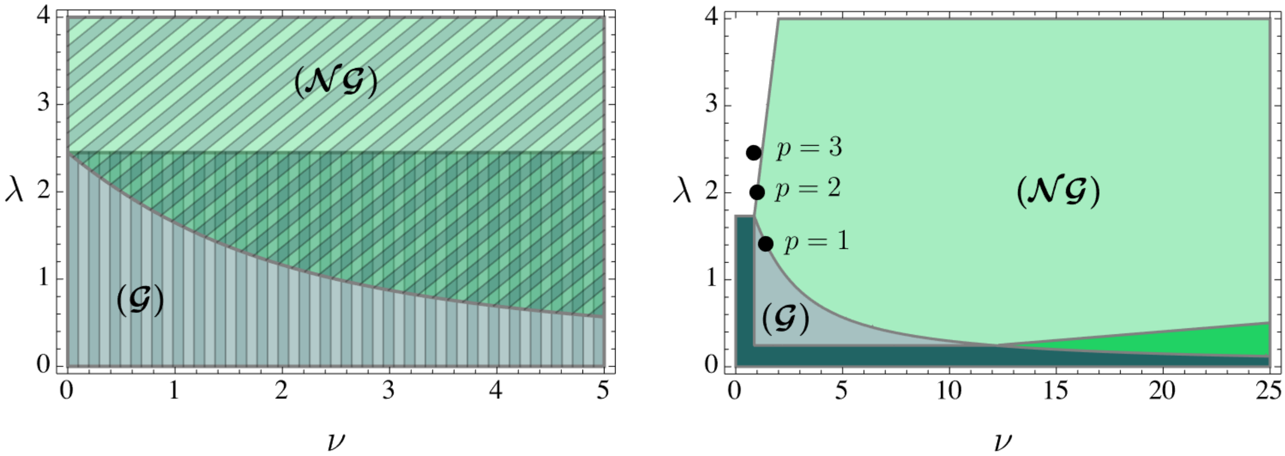

Figure 2.8.1: (Left) Existence (real valued variables) regions of $(\mathcal{G})$ and $(\mathcal{NG})$ in the parameter space $\{\nu, \lambda\}$. (Right) Attraction regions of these points. The darker regions correspond to the regions where $w_{\rm DE} \sim -1$, which in general require $\nu \gg \lambda$ for both points, although $(\mathcal{G})$ can be a suitable accelerated attractor for any ν given that $\lambda \ll 1$ as in the usual quintessence scenario. We can see that the values of λ and ν predicted by string theory happen to fall outside the region associated with stable and viable accelerated attractors.

conditions we obtained just two possible accelerated solutions:

$$\mathcal{G}: x_1 = \frac{\lambda}{\sqrt{6}}, \quad x_2 = 0, \quad y = \sqrt{1 - \frac{\lambda^2}{6}}, \quad \Omega_r = 0, \quad w_{\rm DE} = -1 + \frac{\lambda^2}{3}, \tag{2.8.35}$$

$$\mathcal{NG}: \tag{2.8.36}$$

$$x_1 = \frac{\sqrt{6}}{\lambda + 2\nu}, \; x_2 = \frac{\sqrt{\lambda^2 + 2\nu\lambda - 6}}{\lambda + 2\nu}, \; y = \sqrt{\frac{2\nu}{\lambda + 2\nu}}, \; \Omega_r = 0, \; w_{\rm DE} = -1 + \frac{2\lambda}{\lambda + \nu}.$$

These points were called "geodesic" $(\mathcal{G})$ and "non-geodesic" $(\mathcal{NG})$ solutions in Ref. [256], since they are related to the "curvature" in the field space of the scalar fields.

In the left panel of figure 2.8.1, we show the existence region of the points $(\mathcal{G})$ and $(\mathcal{NG})$, defined as the parameter space regions $\{\nu, \lambda\}$ where the variables in the fixed points [Eqs. (2.8.35) and (2.8.36)] attain real values. On the other hand, in the right panel of figure 2.8.1, we show the parameter space where these points emerge as attractors of the system, i.e., their corresponding regions of attraction. We particularly emphasize the subregions associated with an accelerated epoch, meeting the condition $-1 \leq w_{\rm eff} \leq -0.98$. Recalling that $\lambda = \sqrt{2p}$ and $\nu = \sqrt{2/p}$ are demanded by string theory, we depict the points for some values of p, observing that none of them describes a scenario of late-time accelerated expansion in agreement with current observations. This clearly indicates that the current state of the universe is challenging to explain within the framework of this model, as derived from string compactifications. To grasp this, observe that as p increases, the steepness of the potential for ϕ_1 also intensifies, necessitating a more pronounced interplay with ϕ_2, given by a larger ν parameter, as depicted in the figure. However, ν decreases with increasing p, creating a tension between these two requirements. This possibility was identified in Ref. [256] as a regime of "large curvature" in the scalar fields space. However, as illustrated in Figure 2.8.1, the parameter values required by string theory lie outside the regions where the model exhibits viable cosmological attractors.

2.8.3 Scalar multifield coupled to a vector field

While currently challenging to justify the existence of accelerated solutions in the multi-field model that align with observations, alternative mechanisms may potentially broaden the model's parameter space. For example, in Refs. [1, 2, 5, 122, 248], it was demonstrated that steep potentials, such as Higgs-like or exponential potentials resembling that in Eq. (2.8.25) with $\lambda^2 > 2$, can yield stable accelerated solutions when supported by the presence of other fields, including non-abelian $SU(2)$ vector fields, abelian $U(1)$ vector fields, or 2-form fields. In this section, we explore how this possibility holds true for the scalar multifield model.

Cosmological setup

Here, inspired by Ref. [5] where it was shown that a vector field coupled to a scalar field yields anisotropic accelerated attractors even for a steep exponential potential, we explore a scenario involving a coupling between the scalar field responsible for the accelerated expansion, denoted as ϕ_1, and a vector field represented by A_μ. The Lagrangian of this extended model reads

$$\mathcal{L} = -\frac{1}{2}\partial_\mu\phi_1\partial^\mu\phi_1 - \frac{1}{2}f^2(\phi_1)\partial_\mu\phi_2\partial^\mu\phi_2 - V(\phi_1) - \frac{1}{4}h^2(\phi_1)F_{\mu\nu}F^{\mu\nu}, \tag{2.8.37}$$

where $F_{\mu\nu} \equiv \nabla_\mu A_\nu - \nabla_\nu A_\mu$ is the strength tensor associated to the vector field, and $h^2(\phi_1)$ is the field dependent coupling to the gauge kinetic function. First of all, the energy-momentum tensor in Eq. (2.8.22) is extended by a contribution from the gauge sector which reads

$$T^{(A)}_{\mu\nu} = h^2(\phi_1)\left[F_{\mu\alpha}F^{\alpha}_{\ \nu} - \frac{1}{4}g_{\mu\nu}F_{\alpha\beta}F^{\alpha\beta}\right]. \tag{2.8.38}$$

In a FLRW spacetime, all the components of $F_{\mu\nu}$ are zero since only a time-dependent time-like vector field keeps the isotropy of the background [116]. Nonetheless, there is a recent increase in the amount of evidence suggesting that the Universe could not be as isotropic as thought [279–282]. Therefore, as in Ref. [5], we adopt an anisotropic Bianchi-I metric with a residual symmetry in the y-z plane[32] and a spatial-like vector field with only one component aligned

[32] This selection, chosen for its simplicity, is not lacking in generality. In fact, as demonstrated in Ref. [283], it was shown that the most general configuration for the space-like vector field and the Bianchi-I metric can be

with the x axis. Explicitly

$$\mathrm{d}s^2 = -\mathrm{d}t^2 + a^2(t)\left[e^{-4\sigma}\mathrm{d}x^2 + e^{2\sigma}(\mathrm{d}y^2 + \mathrm{d}z^2)\right], \qquad A_\mu = (0, A(t), 0, 0), \tag{2.8.39}$$

where $a(t)$ in this case represents an overall scale factor, and the anisotropy is encoded in the geometric shear $\sigma(t)$. Using this metric and this vector field profile, we distinguish the vector field contributions to the density and pressure

$$\rho_A = \frac{1}{2}h^2(\phi_1)\frac{\dot{A}^2 e^{4\sigma}}{a^2}, \qquad p_A = \frac{1}{3}\rho_A. \tag{2.8.40}$$

From the Einstein equations, besides the Friedman equations which will take into account the contribution of the vector field to the stress-energy tensor, we have the corresponding equation for the evolution of the geometric shear[33]

$$\begin{aligned} 3M_\mathrm{P}^2 H^2 &= \rho_A + \rho_\phi + \rho_m + \rho_r + 3M_\mathrm{P}^2\dot{\sigma}^2, && (2.8.41)\\ -2M_\mathrm{P}^2\dot{H} &= \frac{4}{3}\rho_A + \dot{\phi}_1^2 + f^2\dot{\phi}_2^2 + \rho_m + \frac{4}{3}\rho_r + 6M_\mathrm{P}^2\dot{\sigma}^2, && (2.8.42)\\ \ddot{\sigma} &= -3H\dot{\sigma} + \frac{2}{3M_\mathrm{P}^2}\rho_A. && (2.8.43) \end{aligned}$$

In the last equation, we note that in the case $\rho_A = 0$, the shear decays as $\sigma \propto a^{-3}$, i.e., the anisotropy of the Universe is erased by the expansion. This resembles the well-known no-cosmic hair theorem valid for ΛCDM [284]. Instead, in our case, the density of the vector field sources the shear preventing this fast decay. However, for a phenomenologically viable scenario, the predicted values must conform to the current observational constraints [142, 143].

Since the vector field is not coupled to ϕ_2, the equation of motion of this scalar field is not modified [see Eq. (2.8.19)]. In turn, the equation of motion for ϕ_1 and A_μ are given by

$$\begin{aligned} \ddot{\phi}_1 + 3H\dot{\phi}_1 + V_{\phi_1} - ff_{\phi_1}\dot{\phi}_2^2 - 2\frac{h_{\phi_1}}{h}\rho_A &= 0, && (2.8.44)\\ \ddot{A} + (H + 4\dot{\sigma})\dot{A} + 2\frac{h_{\phi_1}}{h}\dot{\phi}_1\dot{A} &= 0. && (2.8.45) \end{aligned}$$

In the following section we perform the analysis of this enriched dynamics.

---

effectively reduced to an axially symmetrical system. The axial symmetry is determined by the perpendicular component of the vector field, while its parallel component defines the residual symmetry plane.

[33] An equation of motion for the shear can be derived from the difference between the "11" and "22" components of the Einstein equations, i.e., $m_\mathrm{P}^2({G^2}_2 - {G^1}_1) = {T^2}_2 - {T^1}_1$.

Dynamical Analysis

To investigate the asymptotic evolution of the fully-fledged model, we introduce two extra dimensionless variables to the set outlined in Eq. (2.8.26). Furthermore, we adopt an exponential functional form for the gauge kinetic function, a choice motivated by results from string compactifications, as elucidated later on. Thus we define

$$z^2 \equiv \frac{\rho_A}{3M_{\rm P}^2H^2}, \qquad \Sigma \equiv \frac{\dot{\sigma}}{H}, \qquad h(\phi_1) \equiv h_0 e^{-\mu\phi_1/M_{\rm P}}, \tag{2.8.46}$$

where h_0 and μ are constants. The first Friedman equation in Eq. (2.8.41) becomes the constraint

$$1 = x_1^2 + x_2^2 + y^2 + z^2 + \Omega_m + \Omega_r + \Sigma^2. \tag{2.8.47}$$

Concerning the autonomous system in Eqs. (2.8.28)-(2.8.31), we observe that only the equation for the variable x_1 undergoes a modification in its structure. Additionally, two more equations must be incorporated to account for the introduction of new variables, namely z and Σ. We have that the complete set is

$$x_1' = x_1(1+q) + \sqrt{\frac{3}{2}}\left(\lambda y^2 - 2\mu z^2 - 2\nu x_2^2 - \sqrt{6}x_1\right), \tag{2.8.48}$$

$$x_2' = x_2\left(1 + q + \sqrt{6}\nu x_1 - 3\right), \tag{2.8.49}$$

$$y' = y\left(1 + q - \frac{\sqrt{6}}{2}\lambda x_1\right), \tag{2.8.50}$$

$$z' = z\left\{(q-1) + \sqrt{6}\mu x_1 - 2\Sigma\right\}, \tag{2.8.51}$$

$$\Sigma' = \Sigma\,(q-2) + 2z^2, \tag{2.8.52}$$

$$\Omega_r' = 2\,(q-1)\,\Omega_r, \tag{2.8.53}$$

where we used the equation of motion for the vector field, which we have conveniently recast in terms of the density ρ_A as

$$\dot{\rho}_A + 4\,(H + \dot{\sigma})\,\rho_A + 2\frac{\dot{h}_{\phi_1}}{h}\dot{\phi}_1\rho_A = 0. \tag{2.8.54}$$

The deceleration parameter $1 + q \equiv -\dot{H}/H^2$ is given by

$$1 + q = \frac{1}{2}\left(3x_1^2 + 3x_2^2 - 3y^2 + \Omega_r + z^2 + 3\Sigma^2 + 3\right). \tag{2.8.55}$$

FP	x_1	x_2	y	z	Σ	Ω_r	$w_{\rm eff}$
(DE1)	$\frac{2\sqrt{6}\mathcal{A}}{8+\mathcal{A}\mathcal{C}}$	0	$\frac{\sqrt{6(8-\mathcal{A}\mathcal{B})(2+\mu\mathcal{A})}}{8+\mathcal{A}\mathcal{C}}$	$\frac{\sqrt{3(8-\mathcal{A}\mathcal{B})(\lambda\mathcal{A}-4)}}{8+\mathcal{A}\mathcal{C}}$	$\frac{2(\lambda\mathcal{A}-4)}{8+\mathcal{A}\mathcal{C}}$	0	$-1+\frac{4\lambda\mathcal{A}}{8+\mathcal{A}\mathcal{C}}$
(DE2)	$\frac{\sqrt{6}}{\lambda+2\nu}$	$\frac{\sqrt{3}\sqrt{\mathcal{A}(\mathcal{B}+4\nu)-8}}{2(\lambda+2\nu)}$	$\frac{\sqrt{\frac{3}{2}\nu(\lambda-2\mu+4\nu)}}{\lambda+2\nu}$	$\frac{\sqrt{\frac{3}{2}\nu(\mathcal{C}-4\nu)}}{\lambda+2\nu}$	$\frac{\mathcal{C}-4\nu}{2\lambda+4\nu}$	0	$-1+\frac{2\lambda}{\lambda+2\nu}$

Table 2.1: Values of the variables in the anisotropic accelerated solutions (DE1) and (DE2). We have defined $\mathcal{A}\equiv(\lambda+2\mu)$, $\mathcal{B}\equiv\lambda-6\mu$, $\mathcal{C}\equiv\lambda+6\mu$ to keep the presentation simple.

In this case, the effective equation of state undergoes corrections due to the presence of shear. It can be computed as

$$w_{\rm eff}=-1-\frac{2}{3}\frac{\dot{H}}{H^2}\frac{1}{1-\Sigma^2}-2\frac{\Sigma^2}{1-\Sigma^2}, \tag{2.8.56}$$

Together with the scalar and vector fields, it is convenient to include the shear in the definition of the dark energy fluid, as follows:

$$\rho_{\rm DE}\equiv\rho_\phi+\rho_A+3M_{\rm P}^2\dot{\sigma}^2, \qquad p_{\rm DE}\equiv p_\phi+p_A+3M_{\rm P}^2\dot{\sigma}^2, \tag{2.8.57}$$

such that the equation of state of dark energy is

$$w_{\rm DE}\equiv\frac{p_{\rm DE}}{\rho_{\rm DE}}=-1+\frac{2}{3}\frac{3(x_1^2+x_2^2+\Sigma^2)+2z^2}{x_1^2+x_2^2+y^2+z^2+\Sigma^2}. \tag{2.8.58}$$

The autonomous system exhibits the following symmetries:

$$\{x_1,\lambda,\nu,\mu\}\to\{-x_1,-\lambda,-\nu,-\mu\}, \quad x_2\to-x_2, \quad y\to-y, \quad z\to-z. \tag{2.8.59}$$

Hence, without loss of generality, we confine our exploration to solutions with positive values for x_2, y, and z, along with non-negative parameters λ and ν, while leaving x_1 and μ unrestricted. Under these conditions, we obtained the isotropic solutions ($\mathcal{G}$) and ($\mathcal{NG}$), as discussed in section 2.8.2. Additionally, we identified two potential anisotropic accelerated solutions, named (DE1) and (DE2). The variable values at these points are presented in Table 2.1. Notably, point (DE1) aligns precisely with the anisotropic accelerated solution discovered in Ref. [5] for the quintessence model. This correspondence is expected since $x_2=0$ is an automatic solution to (2.8.49), reducing the system to a case where ϕ_2 is absent. On the other hand, point (DE2) corresponds to a clear generalisation of point ($\mathcal{NG}$), considering anisotropies.

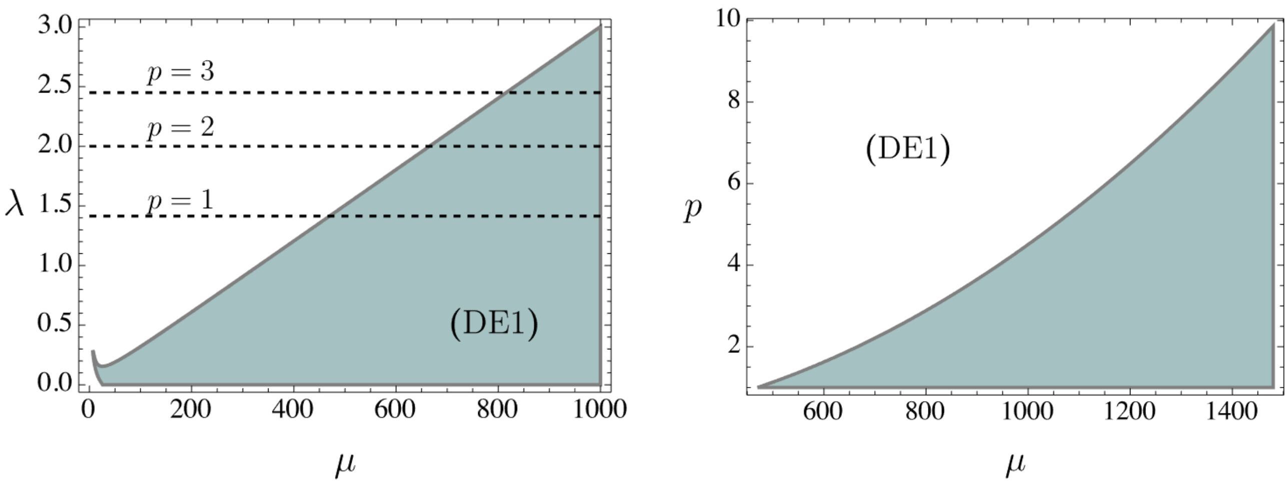

Figure 2.8.2: (Left) Existence region of the point (DE1). The dashed lines represent $\lambda = \sqrt{2p}$ for some values of p. Viable solutions [$w_{\rm DE} \sim -1$ and Σ small as in Eq. (2.8.60)] within the string theory requirements ($\lambda = \sqrt{2p}$) imply $\mu \gg \lambda$. Note that the value of ν is irrelevant for the existence of this fixed point since $x_2 = 0$ in (DE1). (Right) Stability region of (DE1) considering $\mu \gg \lambda$, $\lambda = \sqrt{2p}$ and $\nu = \sqrt{2/p}$ in the approximated expresions for the eigenvalues $\eta_{1,\ldots,6}$ in Eq. (2.8.62). We can see that this point can provide viable anisotropic accelerated solutions adjusting the values of μ to the given discrete value of p.

Fixed Point (DE1)

In left panel of figure 2.8.2, we plot the existence region for (DE1) considering that

$$-1 \leq w_{\rm DE} < -0.98, \qquad -0.001 \leq \Sigma \leq 0.001, \tag{2.8.60}$$

where the bounds for Σ are within the constraints given in Refs. [142, 143]. We also plot three lines denoting the values of λ for $p = 1$, 2, and 3. We see that in general, the existence of anisotropic accelerated solutions in agreement with observations require $\lambda \ll \mu$. Under this condition, we see that

$$w_{\rm eff} = w_{\rm DE} \approx -1 + \frac{2}{3}\frac{\lambda}{\mu}, \qquad \Sigma \approx \frac{\lambda}{3\mu} - \frac{2}{3\mu^2}. \tag{2.8.61}$$

Also, it is possible to estimate the eigenvalues of the Jacobian matrix in this point. We get

$$\eta_1 \approx -4 + \frac{2\lambda}{\mu}, \quad \eta_2 \approx -3 + \frac{\lambda + 2\nu}{\mu}, \quad \eta_{3,4} \approx -3 - \frac{7\lambda}{2\mu}, \quad \eta_{5,6} \approx -\frac{3}{2} - \frac{7\lambda}{2\mu}. \tag{2.8.62}$$

From the latter expressions, we can estimate the attraction region of (DE1), i.e., the region where $\eta_{1,\ldots,6} < 0$. We get two branches depending on the sign of μ:

$$\mu < 0: \ \{\lambda < -3\mu/7, \ \nu > 0\}, \qquad \mu > 0: \ \{\lambda < 2\mu, \ 2\nu < 3\mu - \lambda\}. \tag{2.8.63}$$

However, when we consider the parameter space for viable cosmological solutions [Eq. (2.8.60)], the positive branch is dynamically selected and $\mu \gg \lambda$ implies that the cosmological interesting attraction region is delimited by

$$\mu > 2\nu/3. \tag{2.8.64}$$

Notably, when $\lambda = \sqrt{2p}$ and $\nu = \sqrt{2/p}$, we observe in Fig. 2.8.2 that (DE1) serves as an accelerated attractor of the system, for some values of p within the range expected from string theory and large values of μ. For instance, for $p = 1$, the viable cosmological attractor require $\mu \gtrsim 496$. This can be physically interpreted as the vector field interaction, controlled by μ, playing a crucial role in inducing a slow-roll behavior in the multifield configuration evolution, despite the presence of a steep potential. Additionally, it becomes evident that the ϕ_2 field assumes a secondary role, not only due to its null contribution at the fixed point but also because an increase in its interaction, controlled by ν, tends to destabilise the fixed point. This destabilising effect is discernible from the behaviour of the η_2 eigenvalue of the Jacobian matrix.

Fixed Point (DE2)

From the expressions in Table 2.1, we see that for (DE2) to be a cosmologically viable point, i.e., $w_{\rm DE} \sim -1$ and Σ small [see Eq. (2.8.60)], we require $\nu \gg \lambda$. Under this condition, we get

$$w_{\rm eff} \approx -1 + \frac{\lambda}{\nu}, \qquad \Sigma \approx -1 + \frac{3}{2}\frac{\mu}{\nu} + \frac{3}{4}\frac{\lambda}{\nu}\left(\frac{\mu - \nu}{\nu}\right). \tag{2.8.65}$$

Hence, the admissible solutions for any μ dismiss the values $\lambda = \sqrt{2p}$ and $\nu = \sqrt{2/p}$ stemming from string theory. Nevertheless, in the subsequent analysis, we extensively survey the parameter space of this novel solution, allowing for arbitrary values of these parameters.

Concerning (DE2), the eigenvalues of the Jacobian matrix manifest as highly intricate expressions, rendering an analytical approach challenging to implement. Consequently, we opt for a numerical assessment of the real part of the eigenvalues of the Jacobian matrix at these points, employing a methodology akin to that proposed in Ref. [6].

The numerical methodology can be succinctly encapsulated in the following manner. A large number of random points is sampled within the parameter space $\{\lambda, \nu, \mu\}$, and the fixed points are assessed at these locations. Subsequently, only the parameter sets corresponding to real-valued fixed points are retained. The eigenvalues of the Jacobian matrix are then computed

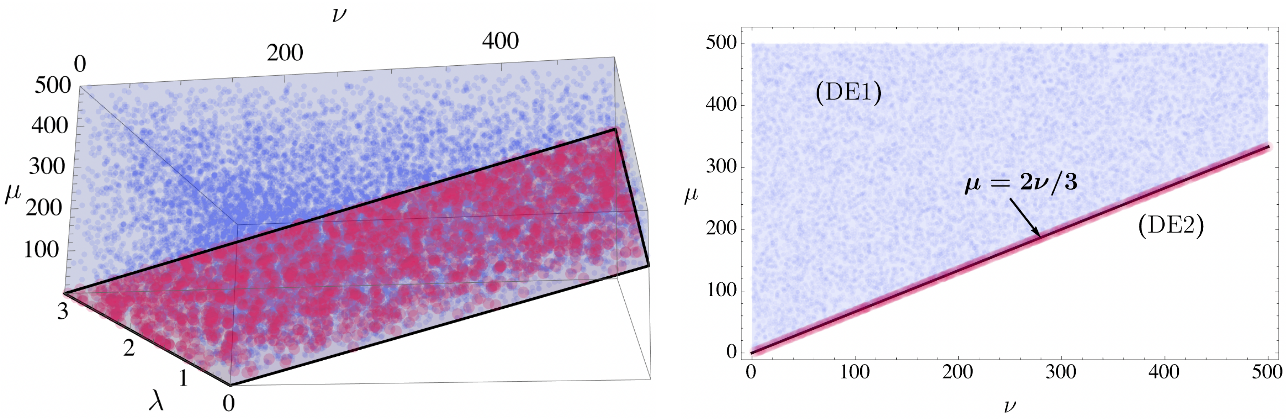

Figure 2.8.3: Attraction regions of the points (DE1) (blue) and (DE2) (red), for $\lambda \in [0, 3]$, and $\{\nu, \mu\} \in [0, 500]$. The solid lines correspond to the boundaries of the $\mu = 2\nu/3$ plane, ruling the (DE2) attractor points. This is further supported by projecting onto the $\{\nu, \mu\}$ plane in the right panel.

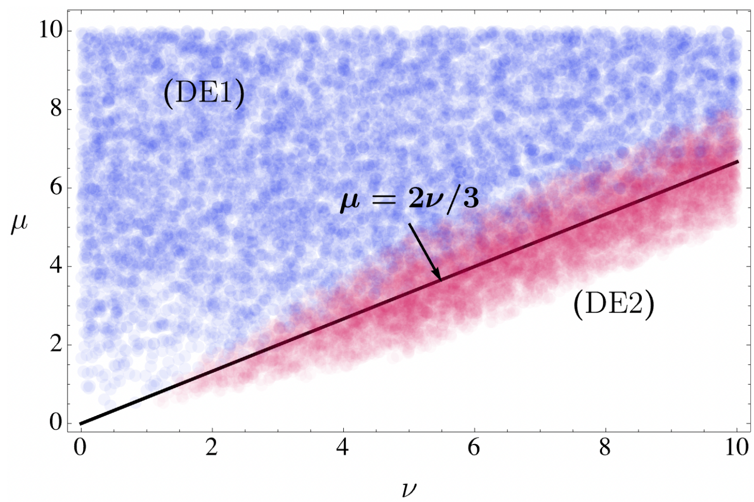

Figure 2.8.4: Similar to Figure 2.8.3 but considering a smaller parameter region to perform the random sampling, namely, $\{\lambda, \nu, \mu\} \in [0, 10]$. All the (DE2) attractors are near the plane $\mu = 2\nu/3$ but not necessarily into this plane as it seems in Figure 2.8.3. We corroborated that the overlap between blue and red points is merely due to the projection onto λ, and that a proper bifurcation manifold between (DE1) and (DE2) exists in the complete parameter space $\{\lambda, \nu, \mu\}$.

for these specific parameter sets, and those associated with attractor solutions are selected. In figures 2.8.3 and 2.8.4, we show the result of this procedure when applied to the points (DE1) and (DE2).

In Fig. 2.8.3, we explored the parameter space by varying λ from 0 to 3, and $\{\nu, \mu\}$ from 0 to 500. The left panel of the figure illustrates that all the blue points, corresponding to locations where all eigenvalues evaluated at (DE1) are negative above the plane $\mu = 2\nu/3$. Conversely, the red points, indicating positions where all eigenvalues at (DE2) are negative, align with the plane described by $\mu = 2\nu/3$. This observation is further supported by analysing the projection of the stability regions onto the $\{\nu, \mu\}$ plane, as depicted in the right panel of Fig. 2.8.3.

To assess scenarios where all parameters are of the same order, we conducted a more focused sampling within the parameter space, specifically $\{\lambda, \nu, \mu\} \in [0, 10]$. The outcomes are presented in Fig. 2.8.4. In this case, the projection onto the $\{\nu, \mu\}$ plane reveals a mixture of attractor locations between (DE1) and (DE2). However, this should be expected since we are considering a projection while there is a mild dependency on λ. We numerically corroborate that a proper bifurcation manifold exists in the complete parameter space $\{\lambda, \nu, \mu\}$. We also notice that (DE2) attractors (red points) are situated near the plane $\mu = 2\nu/3$, but not necessarily into this plane as it seems in Fig. 2.8.3.

Intriguingly, the attractor nature of (DE2) emerges at points where the anisotropy is naturally suppressed, i.e., $\mu \approx 2\nu/3$, while, simultaneously, exhibits a late-time accelerated phase, implying $\lambda \ll \nu$, as evident from equation (2.8.65). However, this observation also implies that the parameter μ, which governs the gauge dynamics, should be finely tuned in relation to scalar couplings controlled by ν, while also resulting in a subdominant contribution of the vector field to the dark energy budget.

This final observation leads us to the conclusion that, although both (DE1) and (DE2) can portray a scenario explaining the current observations, (DE2) is much less likely to occur compared to (DE1) when the complete model is taken into account. This is evident in figures 2.8.3 and 2.8.4, where the parameter space for (DE1) is significantly larger than that for (DE2).

Another way to understand the unlikely nature of (DE2) comes directly from the solution of the equations of motion which for ϕ_2 and A^μ read

$$\nabla_\mu \left(f^2(\phi_2) \nabla^\mu \phi_2 \right) = 0, \qquad \nabla_\mu \left(h^2(\phi_1) F^{\mu\nu} \right) = 0. \tag{2.8.66}$$

Indeed, for homogeneous fields in the context of the Bianchi I spacetime and a vector field as given in Eq. (2.8.39), yields the solutions:

$$\dot{\phi}_2 = \frac{c_{\phi_2}}{a^3 f^2(\phi_1)}, \qquad \dot{A} = \frac{c_A e^{-4\sigma}}{a h^2(\phi_1)}, \tag{2.8.67}$$

with c_{ϕ_2} and c_A integration constants. Consequently, the corresponding density contributions of these fields to the first Friedman equation are given by:

$$\rho_{\phi_2} \equiv \frac{1}{2} f^2(\phi_1) \dot{\phi}_2^2 \propto \frac{1}{a^6 f^2(\phi_1)}, \qquad \rho_A \equiv \frac{1}{2} h^2(\phi_1) \frac{\dot{A}^2 e^{4\sigma}}{a^2} \propto \frac{1}{a^4 h^2(\phi_1)}. \tag{2.8.68}$$

At late-time the systems approaches the fixed point and $\dot{\phi}_1 \approx 0$, thus the scalar field ϕ_1 reaches its asymptotic value and the coupling functions $f(\phi_1)$ and $h(\phi_1)$ also stabilise at constant values. Therefore, it can be concluded that $\rho_{\phi_2} \propto 1/a^6$ while $\rho_A \propto 1/a^4$. Considering the rapid decay of ρ_{ϕ_2}, two main observations can be made: *i*) scalar fields can exhibit stiff matter behaviour, dominating the Universe's energy budget at very early times before the radiation-dominated epoch, and *ii*) at late-times the contribution of the vector field to the total density consistently supersedes that of the scalar ϕ_2. Hence, (DE1) describes the most natural asymptotic evolution of the system, while (DE2) corresponds only to a marginal option needing some degree of fine-tuning for its viability.

2.8.4 Vector field from supergravity

We have already mentioned the possibility of including some dynamics from gauge symmetries when contemplating a potential contribution to the scalar dynamics from the D-term scalar potential. Indeed, it is expected to have such, and to be general enough, we might also include the dynamics of the vector fields themselves. As before, we consider only the simplest case of a $U(1)$ sector, different from the one already included for the D-term scalar potential, as a non-vanishing D-term contribution implies a gauge symmetry breaking for the corresponding sector.

The minimal setup will include a pure gauge $U(1)$, which can be justified by the absence of charged particles in the effective theory; that is, the charged sector turns out to be heavy compared with the energy scale involved in our studies. The general pure gauge sector in SUGRA is given by [266]

$$\mathcal{L}_{\rm gau} = \sqrt{-g}\left(-\frac{1}{4}\mathrm{Re}(f_{AB})F^A_{\mu\nu}F^{\mu\nu\ B} + \frac{i}{4}\mathrm{Im}(f_{AB})F^A_{\mu\nu}\tilde{F}^{\mu\nu\,B}\right) , \tag{2.8.69}$$

where the gauge kinetic function f_{AB} is a holomorphic function of the chiral superfields, and $F_{\mu\nu}$ and $\tilde{F}_{\mu\nu}$ are the usual field strength and its dual. The main outshot extracted from this structure is the possibility of having field-dependent gauge couplings, once the gauge kinetic function is not trivial, and a clear connection between the kinetics term and the *theta term*, i.e., the gauge coupling and the axion are superpartners. As before, we consider a diagonal metric in the gauge sector, $f_{AB} \propto \delta_{AB}$. Moreover, for homogenous field configurations, like the ones we are dealing with, the pseudoscalar term vanishes. Then we end up with a Lagrangian of the form

$$\mathcal{L}_{\rm gau} = -\sqrt{-g}\frac{1}{4}\mathrm{Re}\left(f\left(\Phi^I\right)\right)F_{\mu\nu}F^{\mu\nu}. \tag{2.8.70}$$

As advertised when dealing with the D-term scalar dynamics, gauge kinetic functions in superstring compactifications are naturally linear in the moduli fields, i.e., $f = \Psi/M_{\rm P}$. Thus, once the canonical normalization is done, $s = M_{\rm P} e^{\sqrt{2/p}\phi_1/M_{\rm P}}$.

$$\mathcal{L}_{\rm gau} = -\sqrt{-g}\frac{1}{4}e^{\sqrt{2/p}\phi_1/M_{\rm P}} F_{\mu\nu}F^{\mu\nu}. \tag{2.8.71}$$

Therefore, an exponential dependence on the scalar field ϕ_1 is inherent in an effective field theory originating from string theory, providing a rationale for its inclusion in the preceding analysis. However, aligning the parameter μ with the microscopic result yields $\mu = -\sqrt{2/p} = -\nu$. Unfortunately, this falls beyond the attractor region for both fixed points, (DE1) and (DE2): firstly, as this requires positive values for μ; additionally, all parameters are anticipated to be of the same order, whereas an accelerated expansion scenario necessitates substantially small values of λ compared to μ and ν in each case; finally, achieving the relation $\mu \approx 2\nu/3$ appears challenging given the precise expression from string compactifications.

Unfortunately, this non-isotropic backgrounds have not been the primary focus of investigations in superstring constructions. However, during the 1990s, several works emerged that delved into the direct solution of the equations of motion of the superstring sigma model with background fields [285, 286]. These endeavors sought to address the question of what types of solutions are consistent with non-zero background fields in the vacuum.

Probably the first exploration of such a possibility was the work by Kaloper [287], where anisotropic spaces with a constant dilaton were discovered, albeit exhibiting a recollapse cosmology. Subsequently, possible homogeneous solutions that included a non-trivial 3-form field (H field) have been classified. These identified a specific class representing spaces with 4 non-compact dimensions akin to Bianchi spaces. Similar studies and results can be found in [288, 289], and [290]. Notably, the latter work, in particular, incorporated a background with B field, $H = \mathrm{d}B$, and no H as a background. Interestingly, it found that under these circumstances, an expanding universe is only possible in the anisotropic case. The inclusion of non-trivial moduli also presents solutions with this characteristic, as found in [291, 292]. Non-isotropic solutions to the beta functions, now including 2-loop α' corrections and cases with central charge deficit, were also found recently in [293, 294], confirming the existence of non-isotropic solutions.

String 4D effective actions

The primary challenge in establishing a connection between superstring theory and reality lies in the complexity arising when transitioning from a ten-dimensional description to an effective four-dimensional theory. Although there exist only five consistent descriptions in ten dimen-

sions, obtaining an effective four-dimensional theory leads to an exceedingly diverse situation. For instance, in the context of type II flux compactifications, the estimated number of 4D vacua is on the order of 10^{500} [295]. In such circumstances, formulating general statements applicable to model building seems nearly impossible.
Nevertheless, the insights provided by four-dimensional $\mathcal{N}=1$ supersymmetry allow for the extraction of valuable information from the universal sector of the ten-dimensional effective theory. This approach was pioneered by Witten in the realm of Heterotic string compactifications [296] (see also [297]). Supersymmetry dictates that the low-energy spectrum must be invariant under translations and $SU(3)$ rotations of the six compact dimensions.

The starting point is the bosonic ten-dimensional action [298], working with dimensionless fields:

$$S_{10} = \frac{1}{2\kappa_{10}^2}\int \mathrm{d}^{10}x(-G)^{1/2}e^{-2\phi}\left(R - 2(\partial\phi)^2 - \frac{1}{2}|H_3|^2 - \frac{\alpha'}{4}\mathrm{tr}_v|F|^2\right), \tag{2.8.72}$$

where $\sqrt{\alpha'} = \ell_s$ denotes the fundamental string length controlling the world sheet perturbative expansion, and $\kappa_{10} = \frac{1}{2}(2\pi)^7\alpha'^4$ represents the reduced ten-dimensional Planck mass.
Following the described procedure and disregarding the gauge sector, the dimensional reduction yields:

$$\begin{aligned} S_4 = \frac{1}{2m_{\mathrm{P}}^2}\int \mathrm{d}^4x\sqrt{-g}\,\Bigg[&R - 2\partial_\mu\phi_4\partial^\mu\phi_4 - \frac{1}{2}e^{-4\phi_4}|H_3|^2 \\ &-\frac{1}{2}\tilde{g}^{i\bar{j}}g^{k\bar{\ell}}\left(\partial_\mu\tilde{g}_{i\bar{\ell}}\partial^\mu\tilde{g}_{\bar{j}k} + \partial_\mu\tilde{B}_{i\bar{\ell}}\partial^\mu\tilde{B}_{\bar{j}k}\right)\Bigg], \end{aligned} \tag{2.8.73}$$

where, $\kappa_4^2 \equiv \kappa_{10}^2 e^{2\phi}/V_6$ represents the 4D reduced Planck mass, $m_{\mathrm{P}}^2 = 1/\kappa_4$, and

$$\phi_4 = \phi - \frac{1}{2}\ln(V_6/\alpha'^3), \tag{2.8.74}$$

where V_6 is the compact manifold volume, $H_3 = dB_2$, and $\tilde{g}$ is the compact manifold metric, assumed to be a Calabi-Yau manifold, thus denoted as a 6D complex manifold with indices $i = 1, 2, 3$. In four dimensions, the dual description of the B_2 field is achieved by a real scalar field:

$$H^{\mu\nu\rho} = -\frac{1}{\sqrt{-g}}e^{4\phi_4}\epsilon^{\mu\nu\rho\tau}\partial_\tau\sigma. \tag{2.8.75}$$

Defining chiral superfields with lower components:

$$S \equiv e^{-2\phi_4} + i\sigma \tag{2.8.76}$$

and

$$T_{k\bar{j}} \equiv \tilde{g}_{k\bar{j}} + iB_{k\bar{j}}, \tag{2.8.77}$$

the non-gravitational part in (2.8.73) can be expressed as the kinetic component of a $\mathcal{N} = 1$ SUGRA theory. The Kähler potential is given by:

$$\kappa_4 K = -\ln(S + \bar{S}) - \ln\left[\det(T + \bar{T})\right] \tag{2.8.78}$$

The fields $T_{i\bar{j}}$ are the Kähler moduli, distinctly associated with the geometry of the internal dimensions. A specific scenario arises when these are diagonal, and all terms are equal, i.e., $T_{i\bar{j}} = T\delta_{i\bar{j}}$, leading to:

$$\kappa_4 K = -\ln(S + \bar{S}) - 3\ln(T + \bar{T}). \tag{2.8.79}$$

In the context of string theory, where the only free parameter is the string length, gauge coupling is expected to emerge as expectation values of functions of the fields. This is reflected in field-dependent kinetic functions for the gauge fields. In the context of heterotic string theory, the gauge group is fixed in ten dimensions, explicitly either as $SO(32)$ or $E_8 \times E_8$. The latter holds great appeal as it encompasses the typical grand unification groups, namely, $SO(10)$ and $SU(5)$. Generally, compactification to four dimensions involves the breaking of gauge symmetries, resulting, in general, in additional Abelian factors, in addition to any groups contained within the Standard Model. Explicit examples are presented in [299–301]. In this case, the coupling constant is universal and related to the dilaton, ϕ_4, as evident from the gauge term in the action:

$$\int d^4x\sqrt{-g}\left(-\frac{1}{2}e^{-2\phi_4}\delta_{AB}F^A_{\mu\nu}F^{\mu\nu\ B} - \frac{i}{2}a\delta_{AB}F^A_{\mu\nu}\tilde{F}^{\mu\nu\ B}\right), \tag{2.8.80}$$

such that the gauge kinetic function is given by

$$f_{AB} = S\delta_{AB}. \tag{2.8.81}$$

Trying to reproduce our setup in a heterotic scenario the pure $U(1)$ sector can be easily obtained from the hidden E_8 sector of the 10D theory after the compactifications. Let us now examine the Kähler sector in Calabi-Yau compactifications. As mentioned earlier, Kähler moduli are linked to the geometric properties of the compact manifold, specifically to the volumes of four-cycles denoted as τ^a. These volumes are defined through the Calabi-Yau manifold volume, $\mathcal{V}$, which is, in turn, a homogeneous function of degree 3 in the volumes of the two-cycles, t_a.

Thus, $\tau^a = \mathcal{V}_{t_a}$, and the relation is expressed as:

$$t_a \tau^a = 3\mathcal{V}\,. \tag{2.8.82}$$

Type IIB compactifications exhibit an approximate no-scale symmetry in the Kähler sector, albeit broken by α' corrections [302]. This implies that the associated Kähler potential becomes independent of those for other fields, leading to the relation:

$$K_I K^{I\bar{J}} K_{\bar{J}} = 3. \tag{2.8.83}$$

Consequently, this results in a Kähler potential given by:

$$\kappa_4 K = -2\ln\mathcal{V}. \tag{2.8.84}$$

Subsequently, we recover the Kähler moduli part in (2.8.79) with $\mathcal{V} = \tau^{3/2} = (T+\bar{T})^{3/2}$. While neglecting the α' corrections can be initially justified in a large volume approximation, mixings with the axio-dilaton are expected in other scenarios.
Moving on to gauge dynamics in type II superstrings, they are encoded either in D-branes or the Ramond-Ramond sector. For our focus, we consider the former case. The dimensional reduction of the Dp-brane action combines a Dirac-Born-Infield contribution:

$$S_{\text{Dp, DBI}} = -\mu_p \int_{\text{Dp}} e^{-\phi}\sqrt{\det(G+B-2\pi\alpha' F)}, \tag{2.8.85}$$

with the brane tension given by $\mu_P = (\alpha')^{-(p+1)/2}/(2\pi)^p$, and a Chern-Simons term:

$$S_{\text{Dp,SC}} = \mu_p \int_{\text{Dp}} \sum_q C_q \operatorname{tr} e^{2\pi\alpha' F - B}. \tag{2.8.86}$$

The involved fields are the pullbacks of the metric, G, and NSNS 2-form, B, on the Dp-brane worldvolume, the $C^{(n)}$ RR forms, and the worldvolume gauge field strengths, F. The expansion up to the second order in F of the DBI action leads to:

$$S_{\text{Dp,DBI}} = \int d^4x\, \frac{(\alpha')^{(3-p)/2}}{(2\pi)^{p-2}} V_\Sigma e^{-\phi} F_{4d}^2 + \cdots\,, \tag{2.8.87}$$

where $V_\Sigma = \text{Vol}(\Pi_{p-3})$ is the volume of the cycle Π_{p-3} in the compact dimensions, with dimensionality $p-3$, allowing the brane to wrap around it. Hence, apart from the dilaton dependence, also encountered in the heterotic string case, the gauge couplings additionally depend on geometrical quantities:

$$\mathrm{Re}(f) = \frac{(\alpha')^{(3-p)/2}}{(2\pi)^{p-2}} V_\Sigma e^{-\phi}. \tag{2.8.88}$$

The Chern-Simons action contributes to the imaginary part of the gauge kinetic function:

$$S_{\mathrm{Dp,SC}} = \int_{\Pi_{p-3}} C_{p-3} \int d^4x \, \mathrm{tr}\,(F\tilde{F}). \tag{2.8.89}$$

The specific dependencies are situation-dependent, and explicit expressions are generally not feasible. However, in specific situations like compactifications on tori, it is possible to demonstrate, for instance, that the gauge kinetic function for D7-branes, appearing in type IIB string compactifications, on 4-cycles is given by:

$$2\pi f_i = \mathcal{N}_i S + \mathcal{M}_i T_i, \tag{2.8.90}$$

with T_i representing the Kähler moduli associated with the volume of the 4-cycle, and $\mathcal{N}$ and $\mathcal{M}$ being products of a pair of magnetic fluxes and a pair of wrapping numbers, i.e., products of integers, respectively. Therefore, both the axio-dilaton and the Kähler moduli generally appear in the gauge kinetic function in type IIB string compactifications, exhibiting a dependency similar to the one employed in the work. For more detailed descriptions and involved constructions with analogous results see for instance [303–309].

Now, to ensure decoupling from the visible sector, it is imperative that the D-brane carrying our $U(1)$ field is positioned away from the branes supporting the standard model.

2.8.5 Conclusions

Our study delved into the cosmological implications of a simple yet versatile string-inspired model for dynamical dark energy. The model, rooted in a chiral modulus, exhibits common features in superstring compactifications, including a logarithmic Kähler potential, a modulus-independent superpotential, and a modulus-dependent gauge kinetic function in a pure gauge sector. This formulation results in a 4D model featuring two scalar fields and an abelian $U(1)$ vector field, coupled through non-trivial kinetic functions, and governed by a scalar potential — all displaying an exponential dependence on only one of the fields. These choices prompted a comprehensive three-parameter dynamical analysis. The study reviews previous results in which one of the fields plays a spectator role, and explore a novel situation where the interplay of all three fields is in the game.

In the scenario where the vector field assumes the role of a spectator, we observe a reduction to the case studied in Ref. [256]. Here, the interplay of two fields with non-geodesic trajectories in the scalar manifold gives rise to a quintessence attractor point, characterized by a steep potential. However, achieving correct values for cosmological parameters necessitates the coupling parameters to lie outside the preferred values derived from superstring string theory constructions.

The introduction of a non-trivial contribution from the vector field inherently results in a preferred spatial direction, prompting the consideration of a Bianchi-I background space-time. Although such a structural choice for non-compact dimensions is unconventional in string constructions, positive outcomes from direct examinations of string sigma models suggest not only its potential relevance but also its potential natural appearance in superstring compactifications. In this context, the model manifests a quintessence attractor fixed point, that we called (DE1), where the axionic scalar component assumes a trivial value—a scenario previously investigated by two of the authors in Ref. [5]. In this particular instance, achieving alignment with the observed values and bounds for the equation of state parameters and shear necessitates a coupling with the vector field significantly stronger than the dynamics originating from the scalar potential.

This intriguing result aligns seamlessly with the swampland condition, as the dynamics from the vector field facilitate a slow-roll dynamics along a geodesic trajectory for the scalar field, despite its steep potential. In a broader context, this outcome extends the well-known results from non-geodesic trajectories in the scalar manifold, as formally discussed in Refs. [247, 248], and has already found application in various multifield scenarios.

Under these circumstances we analyse the cosmic evolution, which can be summarized as follows. An initially isotropic radiation domination epoch is followed by a matter domination period. Then, late accelerated expansion is driven by dark energy which also source anisotropies within current observational bounds [142, 143]. Another key feature of our dark energy model is the ocillating behavior of its equation of state. This feature has been found in other models [122] and thoroughly explained in [5].

A second and novel fixed point (DE2) is also under consideration, where all three fields actively contribute to the dynamics. Remarkably, the system naturally accommodates this configuration, and the attractor quintessence point is realised for parameter values that are concurrently consistent with a small anisotropy. Intriguingly, the region hosting the attractor dynamics, marked also by accelerated behaviour, resides within a parameter space where the dynamics of the scalar fields are finely tuned to that of the vector field. However, this fine-tuning implies this attractor is significantly more constrained compared to the parameter space for the fixed point (DE1). In other words, it represents a much less probable scenario compared to the fixed point discussed above as can be seen in Fig. 2.8.3. We numerically corroborated that cosmological dynamics stay around (DE1), even in the case when the parameters λ, ν, and μ are choice in the attraction region of (DE2), which is all around the plane $\mu = 2\nu/3$.

Unfortunately, in all the scenarios presented by the system, the parameter space required, either from stability requirements or cosmological observations, falls outside the suggested range from superstring compactifications. Specifically, in all four cases (two isotropic and two anisotropic attractors), a mandatory hierarchy for the coupling parameters is essential to obtain the correct value for the effective equation of state parameter and demonstrate a late accelerated epoch. In contrast, string compactifications naturally yield values of the same order. Additionally, for (DE1) and (DE2), achieving an attractor nature is only possible if the exponentials related to the kinetic coupling have the same sign in their exponents, whereas string compactifications are likely to produce exponents with opposite signs. Therefore, our findings intensify concerns about a top-down approach to constructing cosmological models for dark energy [310, 311]. The simplest realisations struggle to replicate a viable expansion history, and even more complex models, though anticipated from a UV completion theory, might face similar challenges. However, it could be worth exploring configurations involving non-abelian gauge sectors, where input from the vector field dynamics might aid in realizing an accelerated late epoch.

To assess the generalizability of our findings, it is imperative to consider various corrections. These encompass quantum corrections to the Kähler potential (e.g., [302, 312]), non-perturbative deformations of the superpotential (e.g., [296, 313, 314]), quantum corrections to the effective Lagrangian following Supersymmetry breaking [315], and thermal corrections (e.g., [316–319]). These factors have the potential to significantly influence the dynamics of the system. Despite the prospect of these modifications, we maintain our anticipation that our primary concern regarding the improbable region in parameter space holds true on general grounds.

Chapter 3

Modified Gravity Theories

3.1 Introduction

In order to address the problem of the Universe late-time accelerating expansion two paths are usually followed in alternative models to ΛCDM. On the one hand, it is expected that new kinds of matter with the right properties (e.g., a negative equation of state $w < -1/3$) will be discovered in laboratories. These exotic matter fields are collectively known as dark energy (DE). On the other hand, General Relativity (GR) might require modifications despite its success [95, 96], making plausible to consider modified gravity (MG) theories (for a review on DE and MG models see, for instance, [320]).

A number of popular DE and MG models (e.g., $f(R)$, Brans-Dicke, kinetic gravity braiding, quintessence, k-essence, etc.) can be nicely encompassed in a unified framework put forward by G. W. Horndeski in 1974 [321]. The generalisation of covariant Galileons led to the rediscovery of Horndeski's theory which ever since got a lot of attention [322–324]. The theory constitutes the most general Lorentz-invariant extension of GR in four dimensions considering non-minimal couplings between the metric tensor and a scalar field, restricting the equations of motion to being second order in the derivatives of the field functions. Although recent measurements of the propagation speed for gravitational waves severely reduced the Horndeski Lagrangian [102, 103, 325–331], remaining degrees of freedom are well worth an investigation.

Vector fields are also present in nature and it is plausible that they might be related to a late-time accelerating universe [1–3, 100, 114–121, 125, 332–340]. After a successful construction of consistent theories for general scalar-tensor interactions, it was shown that a similar procedure can be worked out for vector-tensor interactions, known as generalised Proca theories [259–263]. It turns out that more general theories having second-order equations of motion and simultaneously including a scalar field and a vector field, namely Scalar-Vector-Tensor (SVT) theories, were also found [140, 264, 341].

Construction of cosmological models is as important as model testing because in this way we can decide about plausibility of different theories for describing nature. Testing cosmological models is not a trivial task and besides the huge effort dealing with astrophysical measurements (e.g., instruments design, data pipelines), it also requires development of software to compute theoretical predictions for a given model. Boltzmann solvers are codes widely used in cosmology nowadays and they have become fundamental for model testing. These codes allow to not only compute the background evolution of a cosmological model, they also solve the involved differential equations governing the evolution of perturbations. `CAMB` [342] and `CLASS` [343] are two popular Boltzmann codes which focus on linear order perturbations[1] and compute observables such as the CMB angular power spectrum and the matter power spectrum, and thus make possible testing cosmological models against data sets.

There are in the literature a number of works where `CLASS` and `CAMB` were modified to include cosmological models differing from ΛCDM. For instance, MG models have been implemented by using functions parameterizing deviations from GR (i.e., $\mu(a,k)$, $\gamma(a,k)$) in `MGCAMB` [345–347]; by solving the full system of differential equations for a given model as in `FRCAMB` [348]; by exploiting an Effective Field Theory approach as in `EFTCAMB` [349, 350]; by using to good advantage a gauge invariant formalism in the framework of an equation of state (EoS) approach for perturbations in `CLASS` [351, 352]. A remarkable step for the investigation of alternative cosmological models was the development of `Hi-CLASS` [353] which implements Horndeski theories and, without using neither sub-horizon nor quasi-static approximations, solves differential equations for linear order perturbations. This was indeed not a trivial task due to the high number of degrees of freedom in the theory.

It turns out that by using an Effective Fluid Approach[2] things can become easier when implementing $f(R)$ and Horndeski theories in Boltzmann solvers [356, 357]. Quasi-static and sub-horizon approximations can be applied to these kinds of theories so that a fluid description is achieved for the effective DE fluid. Fairly general analytical expressions for the equation of state $w_{\rm DE}(z)$, sound speed $c^2_{s,{\rm DE}}(z,k)$, and anisotropic stress $\pi_{\rm DE}(z,k)$ enable a relatively easy implementation of these kinds of theories in `CLASS`. Interestingly, this effective fluid approach leads to no significant loss of accuracy when compared to the exact computation of observables in `Hi-CLASS` and agrees pretty well with other approaches such as the EoS [357–359].

[1]Non-linear corrections are usually taken into consideration via fitting functions such as HALOFIT [344].
[2]For an effective fluid description of MG see, for instance, Refs. [354, 355].

3.2 Perturbations in a General Dark Energy Model

3.2.1 General Setup

In GR, gravitational interactions are characterized by the Einstein-Hilbert action

$$S_{\rm EH} = \int {\rm d}^4x\sqrt{-g}\left[\frac{1}{2\kappa}R + \mathcal{L}\right], \tag{3.2.1}$$

where $\kappa \equiv 8\pi G_{\rm N}$, $G_{\rm N}$ is the Newton's constant, g is the determinant of the metric $g_{\mu\nu}$, R is the Ricci scalar, and $\mathcal{L}$ is a Lagrangian for all matter fields. On cosmological scales, the Universe is approximately homogeneous and isotropic [39]. Hence, its geometry can be described by the flat perturbed FLRW metric that in the Newtonian gauge reads

$${\rm d}s^2 = -\{1+2\Psi\left(\boldsymbol{x},t\right)\}{\rm d}t^2 + a(t)^2\{1+2\Phi\left(\boldsymbol{x},t\right)\}\delta_{ij}{\rm d}x^i{\rm d}x^j, \tag{3.2.2}$$

where a is the scale factor, and Ψ and Φ are the gravitational potentials which depend on both the spatial coordinates $\boldsymbol{x}$ and the cosmic time t. The dynamics is encoded in the Einstein field equations

$$G^{\mu}{}_{\nu} = \kappa T^{\mu}{}_{\nu}, \qquad T^{\mu}{}_{\nu} = \left(\rho + P\right)u^{\mu}u_{\nu} + P\delta^{\mu}{}_{\nu} + \Sigma^{\mu}{}_{\nu}, \tag{3.2.3}$$

where $G^{\mu}{}_{\nu}$ is the Einstein tensor, $T^{\mu}{}_{\nu}$ is the energy-momentum tensor which is given in terms of the density ρ, the pressure P, and the velocity four-vector $u^{\mu} = (1-\Psi, \frac{v^i}{a})$, with $v^i = a(t)\dot{x}^i$, and a trace-less anisotropic stress tensor $\Sigma^{\mu}{}_{\nu}$. The components of the energy-momentum tensor are given by

$$T^0{}_0 = -\left(\bar\rho + \delta\rho\right), \quad T^0{}_i = a(t)\left(\bar\rho + \bar P\right)ik_iv, \quad T^i{}_j = \left(\bar P + \delta P\right)\delta^i{}_j + \Sigma^i{}_j, \tag{3.2.4}$$

where $\bar\rho$ and $\bar P$ are the background density and pressure, $\delta\rho$ and δP are their respective perturbations, v defined from $v_i \equiv ik_iv$ is the velocity perturbation, k_i is the wave-vector in Fourier space.

3.2.2 Background and Perturbations

Since we are interested in the late-time cosmological dynamics, we assume that the cosmic fluid is solely composed by pressure-less matter and a dark energy component with equation of state $\bar P_{\rm DE} \equiv w_{\rm DE}\bar\rho_{\rm DE}$, where $w_{\rm DE}$ depends on time in general. This model is known as wCDM, and ΛCDM can be viewed as the particular case when $w_{\rm DE} = -1$. For the background metric in Eq. (3.2.2), the unperturbed Einstein field equations (3.2.3) give rise to the Friedmann equations

$$H^2 = \frac{\kappa}{3}\left(\bar{\rho}_m + \bar{\rho}_{\rm DE}\right), \quad \dot{H} = -\frac{\kappa}{2}\left[\bar{\rho}_m + \bar{\rho}_{\rm DE}(1+w_{\rm DE})\right], \tag{3.2.5}$$

where $H \equiv \dot{a}/a$ is the Hubble parameter. The linearized Einstein equations read

$$\frac{k^2}{a^2}\Phi + 3H\left(\dot{\Phi} - H\Psi\right) = \frac{\kappa}{2}\left(\bar{\rho}_m\delta_m + \bar{\rho}_{\rm DE}\delta_{\rm DE}\right), \tag{3.2.6}$$

$$k^2\left(\dot{\Phi} - H\Psi\right) = -\frac{\kappa}{2}a\left[\bar{\rho}_m\theta_m + \bar{\rho}_{\rm DE}(1+w_{\rm DE})\theta_{\rm DE}\right], \tag{3.2.7}$$

$$\ddot{\Phi} + H\left(3\dot{\Phi} - \dot{\Psi}\right) - \left(2\dot{H} + 3H^2\right)\Psi + \frac{k^2}{3a^2}\left(\Phi + \Psi\right) = -\frac{\kappa}{2}\delta P_{\rm DE}, \tag{3.2.8}$$

$$-\frac{k^2}{a^2}\left(\Phi + \Psi\right) = \frac{3\kappa}{2}\bar{\rho}_{\rm DE}(1+w_{\rm DE})\sigma_{\rm DE}, \tag{3.2.9}$$

corresponding to the "time-time", longitudinal "time-space", trace "space-space", and longitudinal trace-less "space-space" parts of the gravitational field equations (3.2.3), respectively. In the later equations we have defined the following quantities: the perturbation over-density or density contrast $\delta \equiv \delta\rho/\bar{\rho}$, the velocity divergence $\theta \equiv ik^i v_i = -k^2 v$, and the scalar anisotropic stress $(\bar{\rho} + \bar{P})\sigma \equiv -(\hat{k}_i\hat{k}_j - \frac{1}{3}\delta_{ij})\Sigma^{ij}$, where $k^2 \equiv k_i k^i$ and $\hat{k}_i \equiv k_i/k$. We have assumed that matter is also pressure-less at first-order ($\delta P_m = 0$) and that it has no anisotropic stress ($\sigma_m = 0$).

The conservation of the energy-momentum tensor, namely $\nabla_\mu T^\mu_{\ \nu} = 0$, impose the following zero-order continuity equations for matter and DE

$$\dot{\bar{\rho}}_m + 3H\bar{\rho}_m = 0, \quad \dot{\bar{\rho}}_{\rm DE} + 3H(1+w_{\rm DE})\bar{\rho}_{\rm DE} = 0. \tag{3.2.10}$$

At linear order we have:

$$\delta_m' = -3\Phi' - \frac{V_m}{a^2 H}, \tag{3.2.11}$$

$$V_m' = -\frac{V_m}{a} + \frac{k^2}{a^2 H}\Psi, \tag{3.2.12}$$

$$\delta_{\rm DE}' = -3\left(1+w_{\rm DE}\right)\Phi' - \frac{V_{\rm DE}}{a^2 H} - \frac{3}{a}\left(c^2_{s,\rm DE} - w_{\rm DE}\right)\delta_{\rm DE}, \tag{3.2.13}$$

$$V_{\rm DE}' = -\left(1 - 3w_{\rm DE}\right)\frac{V_{\rm DE}}{a} + \frac{k^2}{a^2 H}c^2_{s,\rm DE}\delta_{\rm DE} + \left(1+w_{\rm DE}\right)\frac{k^2}{a^2 H}\Psi - \frac{2}{3}\frac{k^2}{a^2 H}\pi_{\rm DE}, \tag{3.2.14}$$

where we have defined the scalar velocity $V \equiv (1+w)\theta$, the sound speed $c_s^2 \equiv \frac{\delta P}{\delta\rho}$, and the anisotropic stress parameter $\pi \equiv \frac{3}{2}(1+w)\sigma$.[3]

In brief, to know the evolution of the large scale structure inhomogeneities of the Universe

[3] A quote denotes a derivative with respect to the scale factor.

requires to solve the coupled set of differential equations given by the Einstein equations and the continuity equations, both at background and at linear order.

Background and linear perturbations in Conformal Time

Typically, the perturbations equations are worked either in cosmic time, or in conformal time. Both time variables are related by $\mathrm{d}t \equiv a\mathrm{d}\eta$. In the following, we will provide the background and perturbation equations in conformal time for completeness.

Now, assume a flat, linearly perturbed FLRW metric that in the Newtonian gauge reads

$$\mathrm{d}s^2 = a(\eta)^2 \left[-\{1+2\Psi(\boldsymbol{x},\eta)\}\mathrm{d}\eta^2 + \{1+2\Phi(\boldsymbol{x},\eta)\}\delta_{ij}\mathrm{d}x^i\mathrm{d}x^j\right], \tag{3.2.15}$$

For the FLRW metric (3.2.15) the unperturbed Einstein field equations read

$$\mathcal{H}^2 = \frac{\kappa}{3}a^2\left(\bar{\rho}_m + \bar{\rho}_{\mathrm{DE}}\right), \qquad \mathcal{H}' = -\frac{\kappa}{6}a^2\left(\bar{\rho}_m + \bar{\rho}_{\mathrm{DE}} + 3\bar{P}_{\mathrm{DE}}\right), \tag{3.2.16}$$

and describe the background evolution. In Eqs. (3.2.16), $\mathcal{H} \equiv a'/a$ is the conformal Hubble parameter, and a prime denotes derivative with respect to conformal time.

Now, we regard linear perturbations to the Einstein field equations and work on the Newtonian gauge (3.2.15). We find

$$3\mathcal{H}\left(\mathcal{H}\Psi - \Phi'\right) - k^2\Phi = -\frac{\kappa}{2}a^2\left(\bar{\rho}_m\delta_m + \bar{\rho}_{\mathrm{DE}}\delta_{\mathrm{DE}}\right), \tag{3.2.17}$$

$$k^2\left(\mathcal{H}\Psi - \Phi'\right) = \frac{\kappa}{2}a^2\left[\bar{\rho}_m\theta_m + \left(\bar{\rho}_{\mathrm{DE}} + \bar{P}_{\mathrm{DE}}\right)\theta_{\mathrm{DE}}\right], \tag{3.2.18}$$

$$-\frac{k^2}{3a^2}(\Phi+\Psi) + \left(2\mathcal{H}' + \mathcal{H}^2\right)\Psi + \mathcal{H}\left(\Psi' - 2\Phi'\right) - \Phi'' = \frac{\kappa}{2}a^2\delta P_{\mathrm{DE}}, \tag{3.2.19}$$

$$-k^2(\Phi+\Psi) = \frac{3\kappa}{2}a^2(\bar{\rho}_{\mathrm{DE}} + \bar{P}_{\mathrm{DE}})\sigma_{\mathrm{DE}}. \tag{3.2.20}$$

Conservation laws for energy and momentum lead to a couple of differential equations governing the evolution of linear perturbations. If the energy-momentum tensor for our general fluid is conserved, it satisfies $\nabla_\mu T^\mu_{\ \nu} = 0$, specifically,

$$\delta' = -(1+w)\left(\theta + 3\Phi'\right) - 3\mathcal{H}\left(c_s^2 - w\right)\delta, \tag{3.2.21}$$

$$\theta' = -\mathcal{H}(1-3w)\theta - \frac{w'}{1+w}\theta + \frac{c_s^2}{1+w}k^2\delta - k^2\sigma + k^2\Psi, \tag{3.2.22}$$

where the equation of state parameter is defined as $w \equiv \bar{P}/\bar{\rho}$, and the sound speed as $c_s^2 \equiv \delta P/\delta\rho$. From Eqs. (3.2.21)-(3.2.22), it becomes clear that when the equation of state crosses -1, problems emerge because there is a singularity. The trouble can be solved by a variable transformation: we use the scalar velocity perturbation $V \equiv ik^j T^0_{\ j}/\rho = (1+w)\theta$ instead of the velocity divergence θ. In terms of this new variable the evolution equations (3.2.21)-(3.2.22) are

$$\delta' = -3(1+w)\Phi' - \frac{V}{a^2 H} - \frac{3}{a}\left(c_s^2 - w\right)\delta, \tag{3.2.23}$$

$$V' = -(1-3w)\frac{V}{a} + \frac{k^2}{a^2 H}c_s^2\delta + (1+w)\frac{k^2}{a^2 H}\Psi - \frac{2}{3}\frac{k^2}{a^2 H}\pi, \tag{3.2.24}$$

where we define the anisotropic stress parameter $\pi \equiv \frac{3}{2}(1+w)\sigma$ and a quote ' denotes a derivative with respect to the scale factor.

3.3 Scalar-Vector-Tensor theories

3.3.1 Introduction

Although SVT theories encompass both Horndeski and generalised Proca theories, and therefore might have an interesting, new, richer phenomenology, they have received little attention thus far in the literature. In fact, as far as we know, there is no public Boltzmann code where SVT theories be fully implemented so that their phenomenology can be investigated in detail [360]. This is a major disadvantage for model testing because we cannot compare theoretical predictions against astrophysical measurements, hence seriously decide about viability of alternative cosmological models. In this work we show that SVT theories can be mapped into an effective fluid so that their phenomenology can be investigated through Boltzmann solvers such as `CLASS`. We apply quasi-static and sub-horizon approximations to SVT theories and find fairly general analytical expressions for the quantities defining the effective fluid, that is, $w_{\rm DE}(z)$, $c^2_{s,\rm DE}(z,k)$, and $\pi_{\rm DE}(z,k)$.[4] Our approach can be useful to carry out further investigations, for instance, on general EDE and Relativistic Modified Newtonian Dynamics (RMOND) models [335, 362].

3.3.2 Scalar-Vector-Tensor Theories

In this section, we introduce the most general SVT Lagrangian. Let us consider

$$\mathcal{L} \equiv \sum_{i=2}^{6} \mathcal{L}_i^{\rm SVT} + \sum_{i=2}^{5} \mathcal{L}_i^{\rm ST} + \mathcal{L}_m, \tag{3.3.1}$$

[4] While in this work we focus on DE, SVT theories have also been studied in inflation (see, for instance, [361]).

where terms $\mathcal{L}_i^{\rm ST}$ represent the scalar-tensor interactions, and terms $\mathcal{L}_i^{\rm SVT}$ denote the scalar-vector-tensor interactions.

A scalar field φ, a vector field A_μ, and the gravitational field $g_{\mu\nu}$ interact with each other through the Lagrangians $\mathcal{L}_i^{\rm SVT}$ taking into account interactions with a broken U(1) gauge symmetry. The Lagrangians for SVT interactions read

$$
\begin{aligned}
\mathcal{L}_2^{\rm SVT} &= f_2(\varphi, X_1, X_2, X_3, F, Y_1, Y_2, Y_3), && (3.3.2)\\
\mathcal{L}_3^{\rm SVT} &= f_3(\varphi, X_3) g^{\mu\nu} S_{\mu\nu} + \tilde{f}_3(\phi, X_3) A^\mu A^\nu S_{\mu\nu}, && (3.3.3)\\
\mathcal{L}_4^{\rm SVT} &= f_4(\varphi, X_3) R + f_{4X_3}(\varphi, X_3)\left\{(\nabla_\mu A^\mu)^2 - \nabla_\mu A_\nu \nabla^\nu A^\mu\right\}, && (3.3.4)\\
\mathcal{L}_5^{\rm SVT} &= f_5(\varphi, X_3) G^{\mu\nu}\nabla_\mu A_\nu + \mathcal{M}_5^{\mu\nu}\nabla_\mu\nabla_\nu\varphi + \mathcal{N}_5^{\mu\nu} S_{\mu\nu} \\
&\quad - \frac{1}{6} f_{5X_3}(\varphi, X_3)\left\{(\nabla_\mu A^\mu)^3 - 3\left(\nabla_\mu A^\mu\right)\nabla_\rho A_\sigma \nabla^\sigma A^\rho + 2\nabla_\rho A_\sigma \nabla^\tau A^\rho \nabla^\sigma A_\tau\right\}, && (3.3.5)\\
\mathcal{L}_6^{\rm SVT} &= f_6(\varphi, X_1) L^{\mu\nu\alpha\beta} F_{\mu\nu} F_{\alpha\beta} + \tilde{f}_6(\varphi, X_3) L^{\mu\nu\alpha\beta} F_{\mu\nu} F_{\alpha\beta} \\
&\quad + \mathcal{M}_6^{\mu\nu\alpha\beta}\nabla_\mu\nabla_\alpha\varphi\nabla_\nu\nabla_\beta\varphi + \mathcal{N}_6^{\mu\nu\alpha\beta} S_{\mu\alpha} S_{\nu\beta}, && (3.3.6)
\end{aligned}
$$

where we have used the simplified notation $g_\xi = \frac{\partial g}{\partial \xi}$, for the derivative of any free function g with respect to a scalar ξ. Let us define the different terms involved in Eqs. (3.3.2)-(3.3.6). Firstly, note that the kinetic term of the scalar field φ, the coupling between φ and the vector field A_μ, and the quadratic term of A_μ are defined respectively by

$$
X_1 \equiv -\frac{1}{2}\nabla_\mu\varphi\nabla^\mu\varphi, \quad X_2 \equiv -\frac{1}{2}A_\mu\nabla^\mu\varphi, \quad X_3 \equiv -\frac{1}{2}A_\mu A^\mu. \qquad (3.3.7)
$$

Secondly, the antisymmetric strength tensor $F_{\mu\nu}$ and its dual $\tilde{F}^{\mu\nu}$ are constructed from A_μ as

$$
F_{\mu\nu} \equiv \nabla_\mu A_\nu - \nabla_\nu A_\mu, \quad \tilde{F}^{\mu\nu} \equiv \frac{1}{2}\varepsilon^{\mu\nu\alpha\beta} F_{\alpha\beta}, \qquad (3.3.8)
$$

where $\varepsilon^{\mu\nu\alpha\beta} \equiv \frac{\epsilon^{\mu\nu\alpha\beta}}{\sqrt{-g}}$, $\epsilon^{\mu\nu\alpha\beta}$ is the Levi-Civita symbol. Thirdly, using $F_{\mu\nu}$ we can construct the Lorentz invariant quantities

$$
\begin{gathered}
F \equiv -\frac{1}{4}F_{\mu\nu}F^{\mu\nu}, \\
Y_1 \equiv \nabla_\mu\varphi\nabla_\nu\varphi F^{\mu\alpha}F^\nu{}_\alpha, \qquad Y_2 \equiv \nabla_\mu\varphi A_\nu F^{\mu\alpha}F^\nu{}_\alpha, \qquad Y_3 \equiv A_\mu A_\nu F^{\mu\alpha}F^\nu{}_\alpha, \qquad (3.3.9)
\end{gathered}
$$

which vanish in the scalar limit when $A_\mu \to \nabla_\mu \pi$, π being a scalar field. Note that quantities in Eqs. (3.3.9) carry the intrinsic vector modes in the Lagrangian $\mathcal{L}_2^{\rm SVT}$. Fourthly, in $\mathcal{L}_3^{\rm SVT}$ we find a symmetric tensor constructed from A_μ as

$$S_{\mu\nu} \equiv \nabla_\mu A_\nu + \nabla_\nu A_\mu. \tag{3.3.10}$$

Fifthly, note that the intrinsic vector modes in Lagrangians $\mathcal{L}_5^{\rm SVT}$ and $\mathcal{L}_6^{\rm SVT}$ are carried by the tensors $\mathcal{M}$ and $\mathcal{N}$ given by

$$\mathcal{M}_5^{\mu\nu} \equiv \mathcal{G}^{h_5}_{\rho\sigma}\tilde{F}^{\mu\rho}\tilde{F}^{\nu\sigma}, \quad \mathcal{N}_5^{\mu\nu} \equiv \mathcal{G}^{\tilde{h}_5}_{\rho\sigma}\tilde{F}^{\mu\rho}\tilde{F}^{\nu\sigma}, \tag{3.3.11}$$

$$\mathcal{M}_6^{\mu\nu\alpha\beta} \equiv 2 f_{6X_1}(\varphi, X_1)\tilde{F}^{\mu\nu}\tilde{F}^{\alpha\beta}, \quad \mathcal{N}_6^{\mu\nu\alpha\beta} \equiv \frac{1}{2}\tilde{f}_{6X_3}(\varphi, X_1)\tilde{F}^{\mu\nu}\tilde{F}^{\alpha\beta}, \tag{3.3.12}$$

where

$$\mathcal{G}^{h_5}_{\rho\sigma} \equiv h_{51}(\varphi, X_i)g_{\rho\sigma} + h_{52}(\varphi, X_i)\nabla_\rho\varphi\nabla_\sigma\varphi + h_{53}(\varphi, X_i)A_\rho A_\sigma + h_{54}(\varphi, X_i)A_\rho\nabla_\sigma\varphi, \tag{3.3.13}$$

$$\mathcal{G}^{\tilde{h}_5}_{\rho\sigma} \equiv \tilde{h}_{51}(\varphi, X_i)g_{\rho\sigma} + \tilde{h}_{52}(\varphi, X_i)\nabla_\rho\varphi\nabla_\sigma\varphi + \tilde{h}_{53}(\varphi, X_i)A_\rho A_\sigma + \tilde{h}_{54}(\varphi, X_i)A_\rho\nabla_\sigma\varphi, \tag{3.3.14}$$

are effective metrics containing possible combinations of $g_{\rho\sigma}$, A_ρ, and $\nabla_\sigma\varphi$, and X_i is a shorthand notation for the set $\{X_1, X_2, X_3\}$. Finally, the double dual Riemann tensor is defined as

$$L^{\mu\nu\alpha\beta} \equiv \frac{1}{4}\varepsilon^{\mu\nu\rho\sigma}\varepsilon^{\alpha\beta\gamma\delta}R_{\rho\sigma\gamma\delta}. \tag{3.3.15}$$

Scalar-tensor interactions are taken into consideration in Eq. (3.3.1) through the Horndeski theory

$$\mathcal{L}_2^{\rm ST} = G_2(\varphi, X_1), \tag{3.3.16}$$

$$\mathcal{L}_3^{\rm ST} = -G_3(\varphi, X_1)\Box\varphi, \tag{3.3.17}$$

$$\mathcal{L}_4^{\rm ST} = G_4(\varphi, X_1)R + G_{4X_1}(\varphi, X_1)\left\{(\Box\varphi)^2 - \nabla_\mu\nabla_\nu\varphi\nabla^\nu\nabla^\mu\varphi\right\}, \tag{3.3.18}$$

$$\begin{aligned}\mathcal{L}_5^{\rm ST} &= G_5(\varphi, X_1)G^{\mu\nu}\nabla_\mu\nabla_\nu\varphi \\ &\quad - \frac{1}{6}G_{5X_1}(\varphi, X_1)\left\{(\Box\varphi)^3 - 3(\Box\varphi)\nabla_\mu\nabla_\nu\varphi\nabla^\nu\nabla^\mu\varphi + 2\nabla^\mu\nabla_\sigma\varphi\nabla^\sigma\nabla_\rho\varphi\nabla^\rho\nabla_\mu\varphi\right\}.\end{aligned} \tag{3.3.19}$$

In Eqs. (3.3.2)-(3.3.6), Eqs. (3.3.13)-(3.3.14), and Eqs. (3.3.16)-(3.3.19), all the f_i, $\tilde{f}_i$, h_{5i}, $\tilde{h}_{5i}$, and G_i denote free functions.

Although in its most general form the theory (3.3.1) has several free functions, it got significantly constrained by the discovery of gravitational waves [103, 325–331, 363–368]. In the next subsection we explain it with more details.

Remaining SVT theories

In this paper we restrict ourselves to the FLRW metric. Our matter fields will also respect constraints on homogeneity and isotropy, thus we will regard a scalar field and a vector field with the following configurations

$$\varphi \equiv \varphi(\eta) + \delta\varphi(\boldsymbol{x}, \eta), \qquad A_\mu \equiv (A_0(\eta) + \delta A_0(\boldsymbol{x}, \eta), \delta A_i(\boldsymbol{x}, \eta)). \tag{3.3.20}$$

By using definitions in Eqs. (3.3.7)-(3.3.15), it is relatively easy to show that up to first order in perturbation theory

$$F_{\mu\nu} = 0, \quad \tilde{F}^{\mu\nu} = 0, \tag{3.3.21}$$

which implies

$$F = Y_i = 0,\ \mathcal{M}_5^{\mu\nu} = \mathcal{N}_5^{\mu\nu} = 0,\ \mathcal{M}^{\mu\nu\alpha\beta} = \mathcal{N}^{\mu\nu\alpha\beta} = 0,\ L^{\mu\nu\alpha\beta}F_{\mu\nu}F_{\alpha\beta} = 0. \tag{3.3.22}$$

As a result, Lagrangians (3.3.2)-(3.3.6) get reduced. In particular, $\mathcal{L}_2^{\rm SVT}$ becomes $f_2(\varphi, X_1, X_2, X_3)$, in $\mathcal{L}_5^{\rm SVT}$ the terms involving the matrices $\mathcal{M}$ and $\mathcal{N}$ vanish, while the Lagrangian $\mathcal{L}_6^{\rm SVT}$ fully disappears.

Speed of gravitational waves

Taking into consideration the full Lagrangian of Horndeski theory [see Eqs. (3.3.16)-(3.3.19)] and the remaining parts of the Lagrangians (3.3.2)-(3.3.6), we can obtain the propagation speed of gravitational waves through the computation of the evolution equation for tensor modes. For this calculation, the perturbed metric reads

$$\mathrm{d}s^2 = a^2(\eta)\left[-\mathrm{d}\eta^2 + \{\delta_{ij} + h_{ij}(\boldsymbol{x}, \eta)\}\mathrm{d}x^i\mathrm{d}x^j\right], \tag{3.3.23}$$

where h_{ij} are the tensor modes. Using the metric (3.3.23), and the configuration for the fields in Eq. (3.3.20), we compute the gravitational field equations for the tensor modes up to first order. We get

$$\left(h^i_j\right)'' + (2\mathcal{H} + \gamma_T)\left(h^i_j\right)' + c_T^2 k^2 h^i_j = 0, \tag{3.3.24}$$

where γ_T is a drag term due to the expansionary dynamics and

$$c_T^2 \equiv \frac{f_4 - \frac{A_0^2 A_0' f_{5X_3}}{2a^4} + G_4 + \frac{A_0^3 f_{5X_3}\mathcal{H}}{2a^4} - \frac{A_0 f_{5\varphi}\varphi'}{2a^2} - \frac{G_{5\varphi}\varphi'^2}{2a^2} + \frac{G_{5X_1}\mathcal{H}\varphi'^3}{2a^4} - \frac{G_{5X_1}\varphi'^2\varphi''}{2a^4}}{f_4 - \frac{A_0^2 f_{4X_3}}{a^2} + G_4 - \frac{A_0^3 f_{5X_3}\mathcal{H}}{2a^4} + \frac{A_0 f_{5\varphi}\varphi'}{2a^2} - \frac{G_{4X_1}\varphi'^2}{a^2} + \frac{G_{5\varphi}\varphi'^2}{2a^2} - \frac{G_{5X_1}\mathcal{H}\varphi'^3}{2a^4}} \tag{3.3.25}$$

is the speed of gravitational waves, which agrees with the result presented in Ref. [264]. As previously mentioned, observations indicate that the propagation speed of gravitational waves is practically the speed of light. If we want general SVT theories to satisfy the constraint $c_T^2 = 1$ without fine-tuning,[5] the following free functions in the general Lagrangian have to fulfill[6]

$$f_4 = f_4(\varphi), \quad f_5 = \text{constant}, \quad G_4 = G_4(\varphi), \quad G_5 = \text{constant}. \tag{3.3.26}$$

Consequently, the remaining SVT theories are given by

$$\mathcal{L}_2^{\rm SVT} = f_2(\varphi, X_1, X_2, X_3), \tag{3.3.27}$$
$$\mathcal{L}_3^{\rm SVT} = f_3(\varphi, X_3) g^{\mu\nu} S_{\mu\nu} + \tilde{f}_3(\varphi, X_3) A^\mu A^\nu S_{\mu\nu}, \tag{3.3.28}$$
$$\mathcal{L}_3^{\rm ST} = -G_3(\varphi, X_1)\Box\varphi, \tag{3.3.29}$$
$$\mathcal{L}_4^{\rm ST} = G_4(\varphi) R, \tag{3.3.30}$$

and the complete Lagrangian reads

$$\mathcal{L} = \mathcal{L}_2^{\rm SVT} + \mathcal{L}_3^{\rm SVT} + \mathcal{L}_3^{\rm ST} + \mathcal{L}_4^{\rm ST}. \tag{3.3.31}$$

Note that the Lagrangian $\mathcal{L}_2^{\rm ST}$ is contained in $\mathcal{L}_2^{\rm SVT}$, while $\mathcal{L}_4^{\rm SVT}$ is taken into account in $\mathcal{L}_4^{\rm ST}$. Since G_5 and f_5 are constants, the Lagrangians $\mathcal{L}_5^{\rm SVT}$ and $\mathcal{L}_5^{\rm ST}$ are total derivatives. As a result $\mathcal{L}_5^{\rm SVT}$ and $\mathcal{L}_5^{\rm ST}$ are disregarded in (3.3.31); they do not contribute to the dynamics. In the next sections, we focus on the cosmological implications of the Lagrangian (3.3.31). In order to avoid very long expressions within the main text, we provide our results in terms of coefficients defined in the appendices of the corresponding accompanion reference [8].

Equations of motion

Varying the action for the Lagrangian in Eq. (3.3.31) with respect to the metric $g^{\mu\nu}$, we obtain the gravitational field equations

$$\sum_{i=2}^{3} \mathcal{G}_{\mu\nu}^{(i)} + \sum_{i=3}^{4} \mathscr{H}_{\mu\nu}^{(i)} = \frac{1}{2} T_{\mu\nu}^{(m)}, \tag{3.3.32}$$

[5] In Bayesian statistics models that have to be finely tuned to fit the data are penalised by the Occam factor [369].

[6] For the choice (3.3.26), the drag term γ_T vanishes, and we get the usual wave equation for a mass-less field h_{ij} propagating at the speed of light $c_T^2 = 1$.

while varying with respect to the scalar field φ, and the vector field A_μ we get

$$\sum_{i=2}^{3}\mathcal{J}_i+\sum_{i=3}^{4}\mathcal{K}_i=0,\quad \sum_{i=2}^{3}\mathcal{A}^{\mu}{}_{(i)}=0, \tag{3.3.33}$$

respectively. The terms $\mathcal{G}^{(i)}_{\mu\nu}$, $\mathcal{J}_i$, and $\mathcal{A}^{\mu}{}_{(i)}$, are associated with the SVT Lagrangians $\mathcal{L}_i^{\mathrm{SVT}}$ $(i=2,3)$, while $\mathscr{H}^{(i)}_{\mu\nu}$ and $\mathcal{K}_i$ are associated to $\mathcal{L}_i^{\mathrm{ST}}$ $(i=3,4)$. The expressions for these terms can be found in the appendices A.1, A.2, and A.3 in Ref. [8].

The background equations of motion are obtained after replacing the unperturbed FLRW metric, and the zeroth-order part of the scalar field and the vector field [see Eqs. (3.3.20)] in Eqs. (3.3.32) and (3.3.33). For the gravitational field equations, due to rotational invariance, only the "time-time" equation and one of the diagonal "space-space" equations are needed, i.e.

$$\sum_{i=2}^{3}\mathcal{G}^{(i)}_{00}+\sum_{i=3}^{4}\mathscr{H}^{(i)}_{00}=\frac{1}{2}T^{(m)}_{00}=\frac{1}{2}a^2\bar{\rho}_m,\qquad \sum_{i=2}^{3}\mathcal{G}^{(i)}_{11}+\sum_{i=3}^{4}\mathscr{H}^{(i)}_{11}=\frac{1}{2}T^{(m)}_{11}=0, \tag{3.3.34}$$

where $T^{(m)}_{11}=0$ since we have assumed that matter is a pressure-less fluid. For the scalar field and the vector field we obtain

$$\sum_{i=2}^{3}\bar{\mathcal{J}}_i+\sum_{i=3}^{4}\bar{\mathcal{K}}_i=0,\quad \sum_{i=2}^{3}\bar{\mathcal{A}}_i=0, \tag{3.3.35}$$

where $\mathcal{A}^{0}{}_{(i)}\equiv\bar{\mathcal{A}}_i$, since only the time component of the vector field has dynamics at the background level. The expressions for $\mathcal{G}^{(i)}_{00}$ and $\mathscr{H}^{(i)}_{00}$ are found in Appendix B.1, $\mathcal{G}^{(i)}_{11}$ and $\mathscr{H}^{(i)}_{11}$ in Appendix B.2, those for $\bar{\mathcal{J}}_i$, $\bar{\mathcal{K}}_i$ and $\bar{\mathcal{A}}_i$ in Appendix B.3 of Ref. [8].

Before discussing the linear perturbations of the model, we want to mention that our results differ from those in Ref. [264] due to the choice of the vector field profile. In Ref. [264], the homogeneous vector field is chosen as

$$A_\mu\equiv(N(t)A_0(t),0,0,0), \tag{3.3.36}$$

where $N(t)$ is the lapse function, which is defined in the background metric as

$$\mathrm{d}s^2=-N^2(t)\mathrm{d}t^2+a^2(t)\delta_{ij}\mathrm{d}x^i\mathrm{d}x^j. \tag{3.3.37}$$

The choice (3.3.37) implies that $X_3=A_0^2/2$, and thus the variation of $\mathcal{L}_2^{\mathrm{SVT}}$ with respect to N will yield no terms with f_{2X_3}. Furthermore, the Lagrangian $\mathcal{L}_3^{\mathrm{SVT}}$ will not contribute to the first Friedman equation. In our case, these terms do appear in the first Friedman equation, as can be seen in Appendix B.1 of Ref. [8], where f_{2X_3} can be found and $\mathcal{G}^{(3)}_{00}$ is not zero. Having clarified this aspect, let us discuss the first order perturbations of the theory.

Since we are only interested in scalar perturbations, we take just the scalar part of the perturbed spatial component of the vector field in Eq. (3.3.20), namely, $\delta A_i(\boldsymbol{x},\eta) \equiv \partial_i \psi(\boldsymbol{x},\eta)$, where $\psi(\boldsymbol{x},\eta)$ is a scalar field. Having this in mind, the linear perturbations of the gravitational equations are given by

$$0 = A_1\frac{\Phi'}{a} + A_2\frac{\delta\varphi'}{a} + A_3\frac{k^2}{a^2}\Phi + A_4\Psi + \left(A_5\frac{k^2}{a^2} - \mu_\varphi\right)\delta\varphi + A_6\frac{\delta A_0}{a} + A_7\frac{k^2}{a^2}\psi - \delta\rho_m, \quad (3.3.38)$$

$$0 = C_1\frac{\Phi'}{a} + C_2\frac{\delta\varphi'}{a} + C_3\Psi + C_4\delta\varphi + C_5\frac{\delta A_0}{a} + C_6\psi - \frac{a\bar{\rho}_m V_m}{k^2}, \quad (3.3.39)$$

$$0 = B_1\frac{\Phi''}{a^2} + B_2\frac{\delta\varphi''}{a^2} + B_3\frac{\Phi'}{a} + B_4\frac{\delta\varphi'}{a} + B_5\frac{\Psi'}{a} + B_6\frac{k^2}{a^2}\Phi + \left(B_7\frac{k^2}{a^2} + 3\nu_\varphi\right)\delta\varphi \quad (3.3.40)$$
$$+ \left(B_8\frac{k^2}{a^2} + B_9\right)\Psi + B_{10}\frac{\delta A_0'}{a^2} + B_{11}\frac{\delta A_0}{a},$$

$$0 = G_4\left(\Psi + \Phi\right) + G_{4\varphi}\delta\varphi, \quad (3.3.41)$$

corresponding to the “time-time”, longitudinal “time-space”, trace “space-space”, and longitudinal trace-less “space-space” parts of the gravitational field equations (3.3.32), respectively. Here, $\delta\rho_m$ and V_m are the density perturbation and the scalar velocity of matter, respectively.

The evolution of linear perturbations for the scalar field, for the temporal component, and for the spatial component of the vector field are obtained from (3.3.33), respectively giving

$$0 = D_1\frac{\Phi''}{a^2} + D_2\frac{\delta\varphi''}{a^2} + D_3\frac{\Phi'}{a} + D_4\frac{\delta\varphi'}{a} + D_5\frac{\Psi'}{a} + \left(D_7\frac{k^2}{a^2} + D_8\right)\Phi \quad (3.3.42)$$
$$+ \left(D_9\frac{k^2}{a^2} - m_\varphi^2\right)\delta\varphi + \left(D_{10}\frac{k^2}{a^2} + D_{11}\right)\Psi + D_{12}\frac{\delta A_0'}{a^2} + D_{13}\frac{\delta A_0}{a} + D_{14}\frac{k^2}{a^2}\psi,$$

$$0 = F_1\frac{\Phi'}{a^2} + F_2\frac{\delta\varphi'}{a^2} + F_3\frac{\Psi}{a} + F_4\frac{\delta\varphi}{a} + F_5\frac{\delta A_0}{a^2} + F_6\frac{k^2}{a^2}\frac{\psi}{a}, \quad (3.3.43)$$

$$0 = H_1\frac{\Psi}{a^2} + H_2\frac{\delta\varphi}{a^2} + H_3\frac{\delta A_0}{a^3} + H_4\frac{\psi}{a^2}. \quad (3.3.44)$$

All the coefficients in the first-order equations (3.3.38)-(3.3.44) can be found in Appendix C of

Ref. [8].

3.3.3 The effective fluid approach

In this section, we show that it is possible to rearrange the equations previously obtained, in order to define an effective dark energy fluid.[7] First, note that an equation similar to the gravitational field equations

$$G_{\mu\nu} = \kappa \left(T^{(m)}_{\mu\nu} + T^{(\mathrm{DE})}_{\mu\nu} \right) , \tag{3.3.45}$$

can be obtained in SVT theories if we define the energy-momentum tensor of dark energy as

$$T^{(\mathrm{DE})}_{\mu\nu} \equiv \frac{1}{\kappa} G_{\mu\nu} - 2 \left(\sum_{i=2}^{3} \mathcal{G}^{(i)}_{\mu\nu} + \sum_{i=3}^{4} \mathscr{H}^{(i)}_{\mu\nu} \right) . \tag{3.3.46}$$

Then, we can extract an effective dark energy density and pressure as

$$\bar{\rho}_{\mathrm{DE}} = \frac{T^{(\mathrm{DE})}_{00}}{a^2}, \qquad \bar{P}_{\mathrm{DE}} = \frac{1}{3a^2} \mathrm{tr}\, T^{(\mathrm{DE})}_{ij}, \tag{3.3.47}$$

yielding to

$$\begin{aligned} \bar{\rho}_{\mathrm{DE}} = &-f_2 + \frac{\varphi'^2 f_{2X_1}}{a^2} + \frac{A_0 \varphi' f_{2X_2}}{a^2} + \frac{A_0^2 f_{2X_3}}{a^2} + \frac{2A_0 \varphi' f_{3\varphi}}{a^2} - \frac{2A_0^3 \varphi' \tilde{f}_{3\varphi}}{a^4} - \frac{\varphi'^2 G_{3\varphi}}{a^2} \\ &- \frac{6A_0^3 f_{3X_3} \mathcal{H}}{a^4} - \frac{6A_0^3 \tilde{f}_3 \mathcal{H}}{a^4} + \frac{3\varphi'^3 G_{3X_1} \mathcal{H}}{a^4} - \frac{6\varphi' G_{4\varphi} \mathcal{H}}{a^2} - \frac{6G_4 \mathcal{H}^2}{a^2} + \frac{3\mathcal{H}^2}{\kappa a^2}, \end{aligned} \tag{3.3.48}$$

$$\begin{aligned} \bar{P}_{\mathrm{DE}} = &f_2 + \frac{2A_0^2 A_0' f_{3X_3}}{a^4} + \frac{2A_0 \varphi' f_{3\varphi}}{a^2} + \frac{2A_0^2 A_0' \tilde{f}_3}{a^4} - \frac{\varphi'' \varphi'^2 G_{3X_1}}{a^4} - \frac{\varphi'^2 G_{3\varphi}}{a^2} \\ &+ \frac{2\varphi'' G_{4\varphi}}{a^2} + \frac{2\varphi'^2 G_{4\varphi\varphi}}{a^2} - \frac{2A_0^3 f_{3X_3} \mathcal{H}}{a^4} - \frac{2A_0^3 \tilde{f}_3 \mathcal{H}}{a^4} + \frac{\varphi'^3 G_{3X_1} \mathcal{H}}{a^4} + \frac{2\varphi' G_{4\varphi} \mathcal{H}}{a^2} \\ &+ \frac{2G_4 \mathcal{H}^2}{a^2} - \frac{\mathcal{H}^2}{\kappa a^2} + \frac{4G_4 \mathcal{H}'}{a^2} - \frac{2\mathcal{H}'}{\kappa a^2}, \end{aligned} \tag{3.3.49}$$

which allows us to characterize the effective dark energy fluid by its equation of state parameter $w_{\mathrm{DE}} \equiv \bar{P}_{\mathrm{DE}}/\bar{\rho}_{\mathrm{DE}}$. The background evolution is governed by the usual Friedman equations in Eq. (3.2.5).

First-order variables may also be extracted from the energy-momentum tensor in Eq. (3.3.46).

[7]Effective quantities are also studied in Ref. [370].

In general, we obtain expressions with the following structure:

$$\delta\rho_{\rm DE} = (\cdots)\delta\varphi + (\cdots)\delta\varphi' + (\cdots)\Psi + (\cdots)\Phi + (\cdots)\Phi' + (\cdots)\delta A_0 + (\cdots)\psi, \tag{3.3.50}$$

$$\delta P_{\rm DE} = (\cdots)\delta\varphi + (\cdots)\delta\varphi' + (\cdots)\delta\varphi'' + (\cdots)\Psi + (\cdots)\Psi' + (\cdots)\Phi \\ + (\cdots)\Phi' + (\cdots)\Phi'' + (\cdots)\delta A_0 + (\cdots)\delta A_0', \tag{3.3.51}$$

$$V_{\rm DE} = (\cdots)\delta\varphi + (\cdots)\delta\varphi' + (\cdots)\Psi + (\cdots)\Phi' + (\cdots)\delta A_0 + (\cdots)\psi. \tag{3.3.52}$$

However, the expressions in $(\cdots)$ are cumbersome and it is worthwhile to look for ways to simplify them. Firstly, the quasi-static approximation (QSA) allows us to consider the gravitational potentials Φ and Ψ as nearly time-independent functions during the matter dominated epoch, in such a way that any time derivative of these potentials can be neglected. Secondly, we assume the so-called sub-horizon approximation (SHA) where only modes deep inside the Hubble horizon are physically interesting, i.e., $k^2 \gg \mathcal{H}^2$. Under these approximations time derivatives acting on perturbations variables and terms of order $\mathcal{H}\times$perturbation can also be neglected.[8] For example, applying the SHA in Eq. (3.3.42) we may simplify the coefficient D_9 as

$$\begin{aligned} D_9\delta\varphi &= \Big(- f_{2X_1} - \frac{2\varphi'' G_{3X_1}}{a^2} - \frac{\varphi''\varphi'^2 G_{3X_1X_1}}{a^4} + 2G_{3\varphi} - \frac{\varphi'^2 G_{3\varphi X_1}}{a^2} - \frac{2\varphi' G_{3X_1}\mathcal{H}}{a^2} \\ &\quad + \frac{\varphi'^3 G_{3X_1X_1}\mathcal{H}}{a^4}\Big)\delta\varphi \\ &\approx \left(-f_{2X_1} - \frac{2\varphi'' G_{3X_1}}{a^2} - \frac{\varphi''\varphi'^2 G_{3X_1X_1}}{a^4} + 2G_{3\varphi} - \frac{\varphi'^2 G_{3\varphi X_1}}{a^2} \right)\delta\varphi, \end{aligned} \tag{3.3.53}$$

where we neglected terms of order $\mathcal{H}\delta\varphi$. We apply the QSA and the SHA to the linear gravitational field and scalar field equations [Eqs. (3.3.38), (3.3.40), and (3.3.42)] to obtain

$$0 = A_3\frac{k^2}{a^2}\Phi + A_5\frac{k^2}{a^2}\delta\varphi + A_7\frac{k^2}{a^2}\psi - \delta\rho_m, \tag{3.3.54}$$

$$0 = B_6\frac{k^2}{a^2}\Phi + B_7\frac{k^2}{a^2}\delta\varphi + B_8\frac{k^2}{a^2}\Psi, \tag{3.3.55}$$

$$0 = D_7\frac{k^2}{a^2}\Phi + \left(D_9\frac{k^2}{a^2} - m_\varphi^2\right)\delta\varphi + D_{10}\frac{k^2}{a^2}\Psi + D_{14}\frac{k^2}{a^2}\psi, \tag{3.3.56}$$

where we had into account that in some models the mass m_φ of the scalar field may play a significant role in the past, given that $m_\varphi \gg H$ (e.g., quintessence). For the perturbed vector field equations of motion (3.3.43)-(3.3.44), we only apply the QSA and neglect derivatives of

[8] See the appendix in Ref. [100] for a detailed explanation of QSA and SHA approximations.

the fields obtaining

$$0 = F_3\frac{\Psi}{a} + F_4\frac{\delta\varphi}{a} + F_5\frac{\delta A_0}{a^2} + F_6\frac{k^2}{a^2}\frac{\psi}{a}, \tag{3.3.57}$$

$$0 = H_1\frac{\Psi}{a^2} + H_2\frac{\delta\varphi}{a^2} + H_3\frac{\delta A_0}{a^3} + H_4\frac{\psi}{a^2}. \tag{3.3.58}$$

If we also applied the SHA to Eq. (3.3.43), we would obtain that the only relevant term would be $\frac{k^2}{a^2}\psi$, yielding the trivial solution $\psi = 0$. In that case, the gravitational field equations and the scalar field equation will not be affected by the presence of the vector field; the system would be reduced to that of Horndeski theory which was already studied in Ref. [357]. Note however that our set of equations (3.3.54)-(3.3.56) agrees with results in Ref. [357] [see their Eqs. (91)-(93)] when the vector field vanishes.

Applying the approximations as explained above, we get five algebraic equations (3.3.54)-(3.3.58) that we solve for the five perturbation variables Ψ, Φ, $\delta\varphi$, δA_0, and ψ. We obtain

$$\delta\varphi = \frac{\frac{k^2}{a^2}W_1 + W_2}{\frac{k^4}{a^4}W_3 + \frac{k^2}{a^2}W_4 + W_5}\delta\rho_m,$$

$$\frac{\delta A_0}{a} = \frac{\frac{k^4}{a^4}W_6 + \frac{k^2}{a^2}W_7 + W_8}{\frac{k^6}{a^6}W_3 + \frac{k^4}{a^4}W_4 + \frac{k^2}{a^2}W_5}\delta\rho_m, \quad \psi = \frac{\frac{k^2}{a^2}W_9 + W_{10}}{\frac{k^6}{a^6}W_3 + \frac{k^4}{a^4}W_4 + \frac{k^2}{a^2}W_5}\delta\rho_m,$$

$$\frac{k^2}{a^2}\Phi = \frac{\frac{k^4}{a^4}W_{11} + \frac{k^2}{a^2}W_{12} + W_{13}}{\frac{k^4}{a^4}W_3 + \frac{k^2}{a^2}W_4 + W_5}\delta\rho_m, \quad \frac{k^2}{a^2}\Psi = -\frac{\frac{k^4}{a^4}W_{14} + \frac{k^2}{a^2}W_{15} + W_{13}}{\frac{k^4}{a^4}W_3 + \frac{k^2}{a^2}W_4 + W_5}\delta\rho_m, \tag{3.3.59}$$

where we took into account that some of the perturbations coefficients are related (see Appendix C of Ref. [8]),

$$A_3 = B_6 = B_8, \quad D_{10} = A_5, \quad D_7 = B_7, \quad D_{14} = H_2, \quad A_7 = H_1, \quad F_6 = H_3. \tag{3.3.60}$$

The coefficients W_i ($i = 1, \ldots, 15$) are given in Appendix D of Ref. [8]. Actually, we could have four dynamical degrees of freedom. From Eq. (3.3.58), we could retrieve δA_0 and insert it in the approximated linear equations, thus reducing one dynamical degree of freedom. Nonetheless, the procedure we follow might be clearer since the mentioned reduction yields results for Φ, Ψ, φ, and ψ much more complicated to handle.

From the expressions for the potentials in Eq. (3.3.59), we can characterize deviations from

GR by defining the gravitational slip parameters

$$\eta \equiv \frac{\Psi+\Phi}{\Phi} = \frac{\frac{k^4}{a^4}(W_{11}-W_{14})+\frac{k^2}{a^2}(W_{12}-W_{15})}{\frac{k^4}{a^4}W_{11}+\frac{k^2}{a^2}W_{12}+W_{13}}, \tag{3.3.61}$$

$$\gamma \equiv -\frac{\Phi}{\Psi} = \frac{\frac{k^4}{a^4}W_{11}+\frac{k^2}{a^2}W_{12}+W_{13}}{\frac{k^4}{a^4}W_{14}+\frac{k^2}{a^2}W_{15}+W_{13}}, \tag{3.3.62}$$

where the GR case corresponds to $\eta=0$ and $\gamma=1$. Note that the expressions of the gravitational potentials can be written as Poisson-like equations if we define parameters $G_{\rm eff}$ and $Q_{\rm eff}$ such that

$$\frac{k^2}{a^2}\Psi = -\frac{1}{2}\frac{G_{\rm eff}}{G_N}\delta\rho_m, \qquad \frac{k^2}{a^2}\Phi = \frac{1}{2}Q_{\rm eff}\delta\rho_m. \tag{3.3.63}$$

These parameters also characterize modifications to gravity. The GR case corresponds to $G_{\rm eff}/G_N = 1$, and $Q_{\rm eff} = G_N$, with $\Phi=-\Psi$. In the case of SVT theories, as shown in Eq. (3.3.41), the presence of the scalar field prevents both potential to be opposite. Hence, anisotropic stress in SVT theories is sourced solely by the scalar field whenever the function $G_4(\varphi)$ is not a constant. Note that, under this scheme, generalised Proca theories do not admit anisotropic stress.

As we will show below, the parameter $G_{\rm eff}$ largely determines the evolution of the growth of matter perturbations. Using the QSA and the SHA in the Eqs. (3.2.11) and (3.2.12) for matter we get

$$\delta'_m \sim -\frac{V_m}{a^2H}, \qquad V'_m \sim -\frac{V_m}{a}+\frac{k^2}{a^2H}\Psi. \tag{3.3.64}$$

Therefore, differentiating the equation for δ'_m, inserting V'_m in that derivative, and using the Poisson equation for Ψ in Eq. (3.3.63), the evolution equation for δ_m will be given by

$$\delta''_m(a) + \left(\frac{3}{a}+\frac{H'(a)}{H(a)}\right)\delta'_m(a) - \frac{3}{2}\frac{\Omega_{m0}G_{\rm eff}/G_N}{a^5H(a)^2/H_0^2}\delta_m(a) = 0. \tag{3.3.65}$$

Hence, by solving Eq. (3.3.65), we can determine the growth factor. We will work out a fully numerical solution of Eq. (3.3.65) for a specific $G_{\rm eff}$ obtained from our designer SVT model.

In what follows we will consider perturbations to the effective dark energy under QSA and SHA in two cases: i) non-vanishing anisotropic stress $\pi_{\rm DE}$; ii) $G_4=$ constant and hence vanishing anisotropic stress $\pi_{\rm DE}=0$.

SVT theories with non-vanishing anisotropic stress

Now, we apply the QSA and the SHA to the quantities in Eqs. (3.3.50)-(3.3.52). We proceed as follows. Since the QSA breaks down due to rapid oscillations of the scalar field [357], we use the trace-less "space-space" equation (3.3.41) in order to solve for $\delta\varphi$ in terms of the gravitational potentials. By differentiating (3.3.41), we can also solve for the derivatives of $\delta\varphi$, also applying the QSA and the SHA at the end of the differentiation. For instance, for the first derivative we get

$$\delta\varphi' = -\frac{G_{4\varphi\varphi}}{G_{4\varphi}}\varphi'\delta\varphi - \varphi'(\Psi+\Phi). \tag{3.3.66}$$

This is the reason why we discriminate models with and without anisotropic stress: since G_4 = constant when anisotropic stress vanishes, Eq. (3.3.66) would diverge. When we deal with models having a non-vanishing anisotropic stress we can then replace the potentials using the Poisson equations in Eq. (3.3.63), leaving all the expressions in terms of $\delta\rho_m$. We obtain

$$\delta\rho_{\rm DE} = \frac{\frac{k^6}{a^6}Z_1 + \frac{k^4}{a^4}Z_2 + \frac{k^2}{a^2}Z_3 + Z_4}{\frac{k^6}{a^6}Z_5 + \frac{k^4}{a^4}Z_6 + \frac{k^2}{a^2}Z_7}\delta\rho_m, \quad \delta P_{\rm DE} = \frac{1}{3Z_{12}}\frac{\frac{k^6}{a^6}Z_8 + \frac{k^4}{a^4}Z_9 + \frac{k^2}{a^2}Z_{10} + Z_{11}}{\frac{k^6}{a^6}Z_5 + \frac{k^4}{a^4}Z_6 + \frac{k^2}{a^2}Z_7}\delta\rho_m,$$

$$\frac{a\bar{\rho}_{\rm DE}}{k^2}V_{\rm DE} = \frac{\frac{k^4}{a^4}Z_{13} + \frac{k^2}{a^2}Z_{14} + Z_{15}}{\frac{k^6}{a^6}Z_5 + \frac{k^4}{a^4}Z_6 + \frac{k^2}{a^2}Z_7}\delta\rho_m, \quad \bar{\rho}_{\rm DE}\pi_{\rm DE} = \frac{k^2}{a^2}\frac{\frac{k^2}{a^2}(W_{14}-W_{11}) + (W_{15}-W_{12})}{\frac{k^4}{a^4}W_3 + \frac{k^2}{a^2}W_4 + W_5}\delta\rho_m,$$

$$c^2_{s,\rm DE} = \frac{1}{3Z_{12}}\frac{\frac{k^6}{a^6}Z_8 + \frac{k^4}{a^4}Z_9 + \frac{k^2}{a^2}Z_{10} + Z_{11}}{\frac{k^6}{a^6}Z_1 + \frac{k^4}{a^4}Z_2 + \frac{k^2}{a^2}Z_3 + Z_4}. \tag{3.3.67}$$

The coefficients Z_i ($i = 1, \ldots, 15$) are presented in Appendix E.1 of Ref. [8]. Due to the presence of the anisotropic stress, the sound speed in Eq. (3.3.67) does not fully determine the stability of sub-horizon perturbations. This can be seen by solving Eq. (3.2.21) for θ and substituting the result (and its derivative) into (3.2.22). Doing so, we obtain the following second-order equation for δ

$$\begin{aligned}
&\delta'' + (1-6w)\mathcal{H}\delta' + 3\mathcal{H}\left(\frac{\delta P}{\delta\rho}\right)' + 3\left[(1-3w)\mathcal{H}^2 + \mathcal{H}'\right]\left(\frac{\delta P}{\bar{\rho}} - w\delta\right) - 3\mathcal{H}w'\delta \\
&\quad = -3(1+w)\left[\Phi'' + \left(1 - 3w + \frac{w'/\mathcal{H}}{1+w}\right)\mathcal{H}\Phi'\right] - k^2\left[(1+w)\Psi + \frac{\delta P}{\bar{\rho}} - \frac{2}{3}\pi\right],
\end{aligned} \tag{3.3.68}$$

where we have used the relation $\pi = \frac{3}{2}(1+w)\sigma$. For sub-horizon modes, the last term factorized by k^2 in Eq. (3.3.68) is the relevant term which determines the stability of perturbations. Since the potential scales as $\Psi \sim 1/k^2$ for these modes, therefore, the stability of sub-horizon perturbations is driven mainly by an effective sound speed defined as [371]

$$c^2_{s,\rm eff} \equiv c^2_{s,\rm DE} - \frac{2}{3}\frac{\bar{\rho}_{\rm DE}\pi_{\rm DE}}{\delta\rho_{\rm DE}}. \tag{3.3.69}$$

Thus far the discussion has been quite general, providing analytical expressions for the field perturbations $\delta\varphi$, δA_0, ψ, and the potentials Φ and Ψ in Eqs. (3.3.59). Now we want to test our equations against known results in literature. Here, we only present the results for $f(R)$ theories. More examples can be found in Ref. [8].

- **$f(R)$ Theories**

Through a conformal transformation, $f(R)$ theories can be seen as a theory for a scalar field non-minimally coupled to R. This theory will be contained in SVT theories if we do the following identification

$$f_2 = -\frac{RF - f}{2}, \quad f_{2\varphi} = -\frac{R}{2}, \quad f_{2\varphi\varphi} = -\frac{1}{2F_R}, \quad G_4 = \frac{F}{2}, \quad G_{4\varphi} = \frac{1}{2}, \tag{3.3.70}$$

where $F \equiv f_R = \sqrt{\kappa}\varphi$, $F_R \equiv f_{RR}$; unspecified derivatives and free-functions are set to zero, and we have assumed $\kappa = 1$. Replacing (3.3.70) in Eqs. (3.3.48)-(3.3.49), we get the well-known expressions for the density and pressure of DE in $f(R)$ theories:

$$a^2\bar{\rho}_{\rm DE} = -\frac{a^2 f}{2} + 3\mathcal{H}^2 + 3F\mathcal{H}' - 3\mathcal{H}F', \tag{3.3.71}$$

$$a^2\bar{P}_{\rm DE} = \frac{a^2 f}{2} - (1+2F)\mathcal{H}^2 - (2+F)\mathcal{H}' + \mathcal{H}F' + F''. \tag{3.3.72}$$

Under the QSA and the SHA, replacing the above functions [Eq. (3.3.70)] in Eqs. (3.3.59) we get for the perturbation variables

$$\delta\varphi = \frac{F_R}{F + 3\frac{k^2}{a^2}F_R}\delta\rho_m, \quad \delta A_0 = 0, \quad \psi = 0,$$

$$\Psi = -\frac{F + 4\frac{k^2}{a^2}F_R}{2\frac{k^2}{a^2}F^2 + 6\frac{k^4}{a^4}FF_R}\delta\rho_m, \quad \Phi = \frac{F + 2\frac{k^2}{a^2}F_R}{2\frac{k^2}{a^2}F^2 + 6\frac{k^4}{a^4}FF_R}\delta\rho_m. \tag{3.3.73}$$

Since $\Phi \neq -\Psi$, the slip parameters are not constants and Eqs. (3.3.61) and (3.3.62) become

$$\eta = -\frac{2\frac{k^2}{a^2}F_R}{F + 2\frac{k^2}{a^2}F_R}, \quad \gamma = \frac{F+2\frac{k^2}{a^2}F_R}{F+4\frac{k^2}{a^2}F_R}. \tag{3.3.74}$$

The effective DE perturbed quantities in Eq. (3.3.67) take on

$$\delta\rho_{\rm DE} = \frac{(1-F)F + (2-3F)\frac{k^2}{a^2}F_R}{F(F + 3\frac{k^2}{a^2}F_R)}\delta\rho_m, \quad \delta P_{\rm DE} = \frac{1}{3F}\frac{2\frac{k^4}{a^4}F_R + 15\frac{k^2}{a^4}F_RF'' + \frac{3FF''}{a^2}}{3\frac{k^4}{a^4}F_R + \frac{k^2}{a^2}F}\delta\rho_m,$$
$$\bar{\rho}_{\rm DE}V_{\rm DE} = \frac{1}{2F}\frac{(F + 6\frac{k^2}{a^2}F_R)F'}{F + 3\frac{k^2}{a^2}F_R}\delta\rho_m, \quad \bar{\rho}_{\rm DE}\pi_{\rm DE} = \frac{\frac{k^2}{a^2}F_R}{F^2 + 3\frac{k^2}{a^2}FF_R}\delta\rho_m. \tag{3.3.75}$$

These results are in perfect agreement with those reported in Refs. [356, 357, 372].

SVT theories with vanishing anisotropic stress

If the DE anisotropic stress vanishes, then $\Phi = -\Psi$ and from Eq. (3.3.41) G_4 does not depend on the scalar field. For the sake of simplicity, we assume $G_4 = 1/2\kappa$ so that $\mathcal{L}_4^{\rm ST}$ in Eq. (3.3.30) equals the Einstein-Hilbert Lagrangian. Applying these assumptions in Eqs. (3.3.50)-(3.3.52) as well as the QSA and the SHA, we get

$$\delta\rho_{\rm DE} = \frac{\frac{k^6}{a^6}Y_1 + \frac{k^4}{a^4}Y_2 + \frac{k^2}{a^2}Y_3 + Y_4}{\frac{k^6}{a^6}Y_5 + \frac{k^4}{a^4}Y_6 + \frac{k^2}{a^2}Y_7}\delta\rho_m, \quad \delta P_{\rm DE} = \frac{1}{3}\frac{\frac{k^4}{a^4}Y_8 + \frac{k^2}{a^2}Y_9 + Y_{10}}{\frac{k^6}{a^6}Y_5 + \frac{k^4}{a^4}Y_6 + \frac{k^2}{a^2}Y_7}\delta\rho_m,$$

$$\frac{a\bar{\rho}_{\rm DE}}{k^2}V_{\rm DE} = \frac{\frac{k^4}{a^4}Y_{11} + \frac{k^2}{a^2}Y_{12} + Y_{13}}{\frac{k^6}{a^6}Y_5 + \frac{k^4}{a^4}Y_6 + \frac{k^2}{a^2}Y_7}\delta\rho_m, \quad c_{s,\rm DE}^2 = \frac{1}{3}\frac{\frac{k^4}{a^4}Y_8 + \frac{k^2}{a^2}Y_9 + Y_{10}}{\frac{k^6}{a^6}Y_1 + \frac{k^4}{a^4}Y_2 + \frac{k^2}{a^2}Y_3 + Y_4}. \tag{3.3.76}$$

The coefficients Y_i, $(i = 1, \ldots, 14)$ are presented in Appendix E.2 of Ref. [8]. Next we present the results for the quintessence model and encourage the interested reader to refer to [8] for other examples.

- **Quintessence**

The typical Lagrangian of a quintessence scalar field can be recovered by defining

$$f_2 = X_1 - V(\varphi), \quad f_{2\varphi} = -V_\varphi, \quad f_{2\varphi\varphi} = -V_{\varphi\varphi}, \quad G_4 = \frac{1}{2}, \tag{3.3.77}$$

while any other function vanishes, and $\kappa = 1$. Using the definitions (3.3.77) in Eqs. (3.3.48) and (3.3.49) we get the usual density and pressure

$$\bar{\rho}_{\rm DE} = X_1 + V, \quad \bar{P}_{\rm DE} = X_1 - V. \tag{3.3.78}$$

The full perturbations in Eqs. (3.3.50)-(3.3.52) are simply given by

$$\delta\rho_{\rm DE} = \frac{\varphi'\delta\varphi'}{a^2} + V_\varphi\delta\varphi - \frac{\varphi'^2}{a^2}\Psi, \quad \delta P_{\rm DE} = \frac{\varphi'\delta\varphi'}{a^2} - V_\varphi\delta\varphi - \frac{\varphi'^2}{a^2}\Psi, \tag{3.3.79}$$

$$\bar{\rho}_{\rm DE}V_{\rm DE} = k^2 a^{-1}\frac{\varphi'\delta\varphi}{a}, \quad c_{s,\rm DE}^2 = \frac{\delta P_{\rm DE}}{\delta\rho_{\rm DE}}. \tag{3.3.80}$$

Note however that, under the SHA and the QSA, Eqs. (3.3.76) provide simplified expressions

$$\delta\rho_{\rm DE} = \delta P_{\rm DE} = \frac{\varphi'^2}{2k^2}\delta\rho_m, \quad \bar{\rho}_{\rm DE}V_{\rm DE} = 0, \quad c_{s,\rm DE}^2 = 1. \tag{3.3.81}$$

These results agree with those reported in Refs. [357].

3.3.4 Designer SVT

For the SVT theories regarded in this work, Eqs. (3.3.67) and (3.3.76) represent analytical expressions for the effective DE perturbations under the QSA and the SHA. General SVT theories have several free functions (i.e., $f_2(\varphi, X_1, X_2, X_3)$, $f_3(\varphi, X_3)$, $\tilde{f}_3(\varphi, X_3)$, $G_3(\varphi, X_1)$, and $G_4(\varphi)$) which could be useful for unravelling conundrums in the standard cosmological model. In this section, we will show an example of how our effective fluid approach to SVT theories makes it possible to design a cosmological model matching the background evolution in the ΛCDM model while having non-vanishing DE perturbations. We will designate this model as SVTDES.

Designer procedure

To begin with, note that using the Leibniz rule, the general equation of motion for the scalar field in the left-hand side of Eq. (3.3.33) can be recast as

$$\nabla^\mu J_\mu = \mathcal{K}_\varphi, \tag{3.3.82}$$

where

$$\begin{aligned} J_\mu &= \left(-f_{2X_1} + G_{3X_1}\Box\varphi + 2G_{3\varphi}\right)\nabla_\mu\varphi + G_{3X_1}\nabla_\mu X_1 \\ &\quad + \left(-\frac{1}{2}f_{2X_2} - 2f_{3\varphi} + 4X_3\tilde{f}_{3\varphi}\right)A_\mu, \end{aligned} \tag{3.3.83}$$

$$\begin{aligned} \mathcal{K}_\varphi &= f_{2\varphi} - 2A_\mu\nabla^\mu f_{3\varphi} - 2\tilde{f}_{3\varphi}\left(A_\nu\nabla^\mu A^\nu + A^\nu\nabla^\mu A_\nu\right)A_\mu + 4X_3A_\mu\nabla^\mu\tilde{f}_{3\varphi} \\ &\quad + \nabla^\mu G_{3\varphi}\nabla_\mu\varphi + G_{4\varphi}R, \end{aligned} \tag{3.3.84}$$

where $\Box \equiv \nabla_\rho\nabla^\rho$ is the usual Laplacian operator. Substituting the background configuration for the fields [see Eq. (3.3.20)] in the Eq. (3.3.83), we find that only the temporal component of the current J_μ does not vanish

$$J_0 \equiv J(\eta) = \left(-f_{2X_1} - 3\frac{\mathcal{H}\varphi'}{a^2}G_{3X_1} + 2G_{3\varphi}\right)\varphi' + \left(-\frac{1}{2}f_{2X_2} - 2f_{3\varphi} + 2\frac{A_0^2}{a^2}\tilde{f}_{3\varphi}\right)A_0, \tag{3.3.85}$$

and satisfies the differential equation

$$J' + 2\mathcal{H}J + a^2\mathcal{K}_\varphi = 0. \tag{3.3.86}$$

When $\mathcal{K}_\varphi = 0$, the solution of Eq. (3.3.86) is simply

$$J(\eta) = -\frac{J_c}{a^2}, \tag{3.3.87}$$

where J_c is a constant. If $J_c = 0$, then the system is on the attractor solution. If $J_c \neq 0$, then the system is out of the attractor and interesting phenomenology might emerge. We will assume that J_c is small, and as we will see later, it will serve as a parameter tracking deviations from ΛCDM.

Avoiding fine-tuning of the functions, the term $\mathcal{K}_\varphi$ can be zero if we demand

$$f_{2\varphi} = 0, \quad f_{3\varphi} = 0, \quad \tilde{f}_{3\varphi} = 0, \quad G_{3\varphi} = 0, \quad G_{4\varphi} = 0, \tag{3.3.88}$$

which implies that the remaining SVT free-functions must be of the form

$$f_2 = f_2(X_1, X_2, X_3), \quad f_3 = f_3(X_3), \quad \tilde{f}_3 = \tilde{f}_3(X_3), \quad G_3 = G_3(X_1), \quad G_4 = \text{constant}. \tag{3.3.89}$$

From now on we will assume $G_4 = 1/2$ and $\kappa = 1$. Note that conditions (3.3.88)-(3.3.89) on the effective DE density (3.3.48) and pressure (3.3.49) yield an effective DE equation of state

$$w_{\rm DE} = \frac{f_2 + \frac{(f_{3X_3}+\tilde{f}_3)}{a^4}(2A_0^2A_0' - 2A_0^3\mathcal{H}) + (\varphi'^3\mathcal{H} - \varphi''\varphi'^2)\frac{G_{3X_1}}{a^4}}{-f_2 + \frac{\varphi'^2 f_{2X_1}}{a^2} + \frac{A_0\varphi' f_{2X_2}}{a^2} + \frac{A_0^2 f_{2X_3}}{a^2} - \frac{6A_0^3\mathcal{H}}{a^4}(f_{3X_3} + \tilde{f}_3) + \frac{3\varphi'^3 G_{3X_1}\mathcal{H}}{a^4}}. \tag{3.3.90}$$

Since G_4 is a constant, Eq. (3.3.41) implies $\Phi = -\Psi$, or in other words, we are designing a model with no anisotropic stress. Note that using the conditions (3.3.89), we can rewrite the Friedman equation [left-hand side of (3.3.34)], the equation of motion for the scalar field [Eqs. (3.3.85) and (3.3.87)], and the equation of motion for the vector field [right-hand side of (3.3.35)], respectively as

$$0 = -\frac{\mathcal{H}^2}{a^2} + H_0^2\frac{\Omega_{m0}}{a^3} - \frac{1}{3}f_2 + \frac{2}{3}X_1 f_{2X_1} + \frac{2}{3}X_2 f_{2X_2} + \frac{2}{3}X_3 f_{2X_3}$$
$$+ 2\sqrt{2}X_1^{3/2}\frac{\mathcal{H}}{a}G_{3X_1} - 4\sqrt{2}X_3^{3/2}\frac{\mathcal{H}}{a}\left(f_{3X_3} + \tilde{f}_3\right), \tag{3.3.91}$$

$$0 = \frac{J_c}{a^3} - 6X_1\frac{\mathcal{H}}{a}G_{3X_1} - \sqrt{2}X_1^{1/2}f_{2X_1} - \frac{\sqrt{2}}{2}X_3^{1/2}f_{2X_2}, \tag{3.3.92}$$

$$0 = -\sqrt{2}X_3^{1/2}f_{2X_3} + 12X_3\frac{\mathcal{H}}{a}\left(f_{3X_3} + \tilde{f}_3\right) - \frac{\sqrt{2}}{2}X_1^{1/2}f_{2X_2}, \tag{3.3.93}$$

where we have defined the density parameter of matter $\Omega_{m0} \equiv \rho_{m0}/3H_0^2$; ρ_{m0} is the density of matter today and H_0 is the Hubble constant. In Eqs. (3.3.91)-(3.3.93) we replaced the fields φ'

and A_0 by the variables

$$X_1 = \frac{\varphi'^2}{2a^2}, \quad X_2 = \frac{\varphi' A_0}{2a^2}, \quad X_3 = \frac{A_0^2}{2a^2}. \tag{3.3.94}$$

We are interested in a particular model in SVT theories whose background evolution matches identically that of ΛCDM, where the Hubble parameter is given by

$$\mathcal{H}^2 = a^2 H_0^2 (\Omega_{m0} a^{-3} + \Omega_{\Lambda 0}), \tag{3.3.95}$$

where $\Omega_{\Lambda 0}$ is the density parameter of dark energy today. From Eq. (3.3.90) we can see that $f_{3X_3} + \tilde{f}_3 = 0$, $G_{3X_1} = 0$, and $f_2 =$ constant imply $w_{\rm DE} = -1$ as in the standard cosmological model. In this case, the vector field equation of motion (3.3.93) is trivially satisfied while from Eq. (3.3.92) we see that the scalar field is on the attractor solution $J_c = 0$. Furthermore, the Friedman equation (3.3.91) and its solution for ΛCDM (3.3.95) allow us to determine $f_2 = -3H_0^2 \Omega_{\Lambda 0}$. Such a model has vanishing DE perturbations. Next we will show that there exists a SVT model matching ΛCDM background while having non-vanishing DE perturbations.

For SVT theories assuming Eq. (3.3.89), in general $\bar{\rho}_{\rm DE}$ depends on X_1, X_2, and X_3, and thus from the Friedman equation (3.3.91) we see that $\mathcal{H}$ might also be also a function of these terms, i.e., $\mathcal{H} = \mathcal{H}(X_1, X_2, X_3)$. We can consider a further simplification, by noting that $X_2^2 = X_1 X_3$ up to first order in perturbations, therefore we can assume $f_2 = f_2(X_1, X_3)$ and $\mathcal{H} = \mathcal{H}(X_1, X_3)$. These assumptions imply $f_{2X_2} = 0$ and using Eqs. (3.3.91)-(3.3.93) we find

$$f_2(X_1, X_3) = -3H_0^2 \Omega_{\Lambda 0} + \frac{J_c \sqrt{2} X_1^{1/2}}{\Omega_{m0}} \left[\frac{H^2}{H_0^2} - \Omega_{\Lambda 0} \right], \tag{3.3.96}$$

$$f_{2X_1} = \frac{J_c H^2}{\sqrt{2} H_0^2 X_1^{1/2} \Omega_{m0}} - \frac{J_c \Omega_{\Lambda 0}}{\sqrt{2} X_1^{1/2} \Omega_{m0}} + \frac{2\sqrt{2} H J_c X_1^{1/2} H_{X_1}}{H_0^2 \Omega_{m0}} \tag{3.3.97}$$

$$f_{2X_3} = \frac{2\sqrt{2} H J_c X_1^{1/2} H_{X_3}}{H_0^2 \Omega_{m0}} \tag{3.3.98}$$

$$G_{3X_1} = -\frac{2}{3} \frac{J_c H_{X_1}}{H_0^2 \Omega_{m0}}, \tag{3.3.99}$$

$$f_{3X_3} + \tilde{f}_3 = \frac{1}{3} \frac{J_c X_1^{1/2} H_{X_3}}{X_3^{1/2} H_0^2 \Omega_{m0}}, \tag{3.3.100}$$

where we have used the expression for the Hubble parameter in the standard model $H^2 = H_0^2 (\Omega_{m0} a^{-3} + \Omega_{\Lambda 0})$. We can now assume that the Hubble parameter can be written in terms of X_1 and X_3 as

$$H(X_1, X_3) = H_0 \left(\frac{X_1}{H_0^2} \right)^{-n} \left(\frac{X_3}{H_0^2} \right)^{-m}, \tag{3.3.101}$$

where n and m are constants. Note that the units in the previous expression are correct, given that $[X_1] = [X_3] = H_0^2$. For the sake of simplicity, we further assume $f_3 = 0$ which in turn defines $\tilde{f}_3$ from Eq. (3.3.100) and keeps alive the vector interactions in the model.[9] From Eqs. (3.3.96)-(3.3.101) it is possible to obtain expressions for $f_2, f_{2X_1}, f_{2X_3}, G_{3X_1}, \tilde{f}_3$ in terms of X_1 and X_3. In order to close the system, we assume that X_1 and X_3 depend on H as

$$X_1 = \frac{X_{10}}{H^p}, \;\; X_3 = \frac{X_{30}}{H^q}, \tag{3.3.102}$$

where $[X_{10}] = H_0^{p+2}$, $[X_{30}] = H_0^{2+q}$, p and q are constants. Thus, the problem of finding a model in SVT theories with the same background as ΛCDM is reduced to find an appropriate set of parameters $\{n, m, p, q\}$. From the effective DE density (3.3.48) and Eqs. (3.3.95)-(3.3.102) we obtain

$$\begin{aligned}\rho_{\rm DE} &= 3H_0^2\Omega_{\Lambda 0} \\ &+ \frac{4\sqrt{2}H_0^2(m+n)\tilde{J}}{\Omega_{m0}}\left[\frac{\Omega_{m0}}{a^{-3}} + \Omega_{\Lambda 0}\right]^{\frac{(2n-1)p+2mq+2}{4}}\left(1 - \left[\frac{\Omega_{m0}}{a^{-3}} + \Omega_{\Lambda 0}\right]^{\frac{np+mq-1}{2}}\right),\end{aligned} \tag{3.3.103}$$

so that for

$$np + mq = 1, \tag{3.3.104}$$

the model matches the ΛCDM background evolution, while having non-vanishing perturbations: $\bar{\rho}_{\rm DE} = 3H_0^2\Omega_{\Lambda 0}, \quad \bar{P}_{\rm DE} = -\bar{\rho}_{\rm DE}, \quad w_{\rm DE} = -1$. We choose

$$n = 1, \quad m = -2, \quad p = 2, \quad q = \frac{1}{2}, \tag{3.3.105}$$

as a suitable set of parameters yielding manageable expressions for the perturbations in Eq. (3.3.76). Then, the choice (3.3.105) defines our SVTDES model

$$f_2 = -3H_0^2\Omega_{\Lambda 0} + \frac{\sqrt{2}H_0\tilde{J}X_1^{1/2}}{\Omega_{m0}}\left[\left(\frac{X_1}{H_0^2}\right)^{-2}\left(\frac{X_3}{H_0^2}\right)^4 - \Omega_{\Lambda 0}\right], \quad f_3 = 0,$$

$$\tilde{f}_3 = \frac{2X_1^{1/2}\tilde{J}\left(\frac{X_1}{H_0^2}\right)^{-1}\left(\frac{X_3}{H_0^2}\right)^2}{3X_3^{3/2}\Omega_{m0}}, \quad G_{3X_1} = \frac{2\tilde{J}\left(\frac{X_1}{H_0^2}\right)^{-2}\left(\frac{X_3}{H_0^2}\right)^2}{3H_0^2\Omega_{m0}}, \quad G_4 = \frac{1}{2}. \tag{3.3.106}$$

where $\tilde{J} \equiv J_c/H_0$ is dimensionless. The equations of motion for the scalar field (3.3.92) and the vector field (3.3.93) are trivially satisfied for the SVTDES model. Having defined the

[9]Under the conditions (3.3.88), the cubic interactions of SVT theories are present at the first-order level only through the combination $f_{3X_3} + \tilde{f}_3$. See Appendix A of [8] where the perturbations coefficients in Eqs. (3.3.38)-(3.3.44) are shown.

background evolution for the SVTDES model, we will focus on the evolution of perturbations which are defined by the coefficients Y_i in the Appendix E.2 of [8]. The non-vanishing Y_i for the SVTDES model (3.3.106) are the coefficients $Y_1, Y_2, Y_3, Y_5, Y_6, Y_8, Y_9, Y_{11}, Y_{12}$, which yield

$$
\begin{aligned}
\delta\rho_{\rm DE} \approx\, & \frac{2\sqrt{2}\tilde{J}}{21\Omega_{m0}}\sqrt{a\left(\Omega_{m0}+a^3\Omega_{\Lambda 0}\right)} \\
& \times\left[\frac{28a}{29\Omega_{m0}+20a^3\Omega_{\Lambda 0}}+3H_0^2\left(\frac{5}{k^2}-\frac{96a}{8ak^2+273H_0^2\Omega_{m0}+336a^3H_0^2\Omega_{\Lambda 0}}\right)\right]\delta\rho_m, \quad (3.3.107)
\end{aligned}
$$

$$
\begin{aligned}
\delta P_{\rm DE} \approx\, & \frac{aH_0^2\tilde{J}\delta\rho_m}{3\sqrt{2}k^2\Omega_{m0}\sqrt{a\left(\Omega_{m0}+a^3\Omega_{\Lambda 0}\right)}(8ak^2+273H_0^2\Omega_{m0}+336a^3H_0^2\Omega_{\Lambda 0})} \quad (3.3.108) \\
& \times\left[13\Omega_{m0}\left(8ak^2+615H_0^2\Omega_{m0}\right)+4a^3(8ak^2+3669H_0^2\Omega_{m0})\Omega_{\Lambda 0}+5952a^6H_0^2\Omega_{\Lambda 0}^2\right],
\end{aligned}
$$

$$
\begin{aligned}
\bar{\rho}_{\rm DE}V_{\rm DE} \approx\, & -\frac{16\sqrt{2}aH_0\tilde{J}\delta\rho_m}{3\Omega_{m0}(29\Omega_{m0}+20a^3\Omega_{\Lambda 0})(8ak^2+273H_0^2\Omega_{m0}+336a^3H_0^2\Omega_{\Lambda 0})} \quad (3.3.109) \\
& \times\left(\Omega_{m0}\left(20ak^2+1161H_0^2\Omega_{m0}\right)+a^3\left(8ak^2+1791H_0^2\Omega_{m0}\right)\Omega_{\Lambda 0}+576a^6H_0^2\Omega_{\Lambda 0}^2\right),
\end{aligned}
$$

$$
\begin{aligned}
c_{s,\rm DE}^2 =\, & \frac{H_0^2(29\Omega_{m0}+20a^3\Omega_{\Lambda 0})}{4\left(\Omega_{m0}+a^3\Omega_{\Lambda 0}\right)} \\
& \times\left(13\Omega_{m0}\left(8ak^2+615H_0^2\Omega_{m0}\right)+4a^3\left(8ak^2+3669H_0^2\Omega_{m0}\right)\Omega_{\Lambda 0}+5952a^6H_0^2\Omega_{\Lambda 0}^2\right) \\
& \times[32a^2k^4+396aH_0^2k^2\Omega_{m0}+16965H_0^4\Omega_{m0}^2 \\
& +36a^3H_0^2(24ak^2+905H_0^2\Omega_{m0})\Omega_{\Lambda 0}+14400a^6H_0^4\Omega_{\Lambda 0}^2]^{-1}, \quad (3.3.110)
\end{aligned}
$$

where we have assumed $\tilde{J} \ll 1$. We have replaced X_1 and X_3 in terms of H using Eqs. (3.3.102) and (3.3.105), then H can be written in terms of a by using Eq. (3.3.95). It becomes clear that $\delta\rho_{\rm DE}$, $\delta P_{\rm DE}$, and $V_{\rm DE}$, vanish for $\tilde{J}=0$, therefore we recover ΛCDM. In the following subsections, we will explore the cosmological implications of the SVTDES model (3.3.106), always tracking deviations from ΛCDM through the parameter $\tilde{J}$.

Evolution of matter and dark energy perturbations

In this subsection, we numerically solve the differential equations in Eqs. (3.4.12) and (3.4.14) for matter perturbations, i.e., for δ_m and V_m.

To begin with, we check the stability of DE perturbations. Since G_4 is a constant for the SVTDES model, Eq. (3.3.41) implies that there is no anisotropic stress, and thus we do not have to consider an effective sound speed. The sound speed of DE perturbations in Eq. (3.3.76)

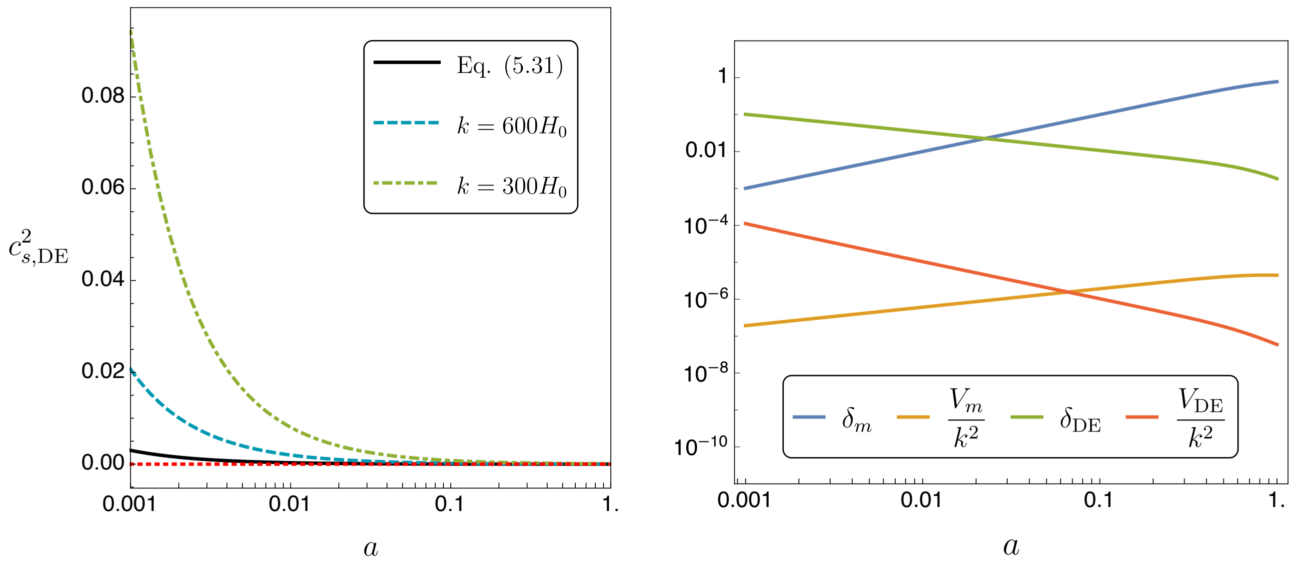

Figure 3.3.1: (Left) Evolution of the DE sound speed $c^2_{s,\mathrm{DE}}$ for the modes $k = 600H_0$ and $k = 300H_0$. For the two values considered, we can see $c^2_{s,\mathrm{DE}}$ is positive during the whole evolution, and it gets greater values than those in the black solid line, which marks a rough bound above which the SHA can be safely applied. (Right) Evolution of δ_m, δ_{DE}, V_m/k^2, and V_{DE}/k^2 (their absolute values) for $\tilde{J} = 0.01$. The other parameters used in this figure are $\Omega_{m0} = 0.3$, $\Omega_{\Lambda 0} = 0.7$, and $k = 300H_0$. The initial conditions are obtained from Eq. (3.3.116).

is the key quantity driving the stability of perturbations, and for the SVTDES model in the Newtonian gauge it is given by the Eq. (3.3.110) which interestingly does not depend on $\tilde{J}$. We show the evolution of $c^2_{s,\mathrm{DE}}$ as a function of a, for a few values of k, in the left panel of Fig. 3.3.1. We would like to make some comments about the behaviour of $c^2_{s,\mathrm{DE}}$. First, we can see that the squared sound speed is positive during the whole evolution, assuring that our SVTDES model avoids Laplacian instabilities. Second, the SHA indeed applies for modes well within the sound horizon, i.e., for modes such that [340]

$$c^2_{s,\mathrm{DE}} k^2 \gg \mathcal{H}^2. \tag{3.3.111}$$

Therefore, the SHA breaks down for $c^2_{s,\mathrm{DE}} \approx 0$. We can make a rough estimate of how small $c^2_{s,\mathrm{DE}}$ can be so that the SHA be justifiable. Since co-moving wavenumbers relevant to the observations of large-scale structures lay in the range $30H_0 \lesssim k \lesssim 600H_0$ [373], and it is reasonable to assume that during matter domination $H^2 \approx H_0^2 \Omega_{m0} a^{-3}$, from (3.3.111) and using $k \sim 300H_0$ we get

$$c^2_{s,\mathrm{DE}} \gtrsim 3 \times 10^{-6} a^{-1}, \tag{3.3.112}$$

which provides a rough bound for modes inside the sound horizon. In Fig. 3.3.1, the solid black line shows the relation $c^2_{s,\mathrm{DE}} = 3 \times 10^{-6} a^{-1}$. We see that the values taken by $c^2_{s,\mathrm{DE}}$ for the two values considered, namely, $k = 600H_0$ and $k = 300H_0$ (blue dashed line and green dot-dashed line, respectively), are higher than those taken in the black line, therefore, the SHA can be safely applied.

Now, we focus on the differential equations (3.2.11) and (3.2.12) for matter perturbations. For pressure-less matter we have $w_m = 0$, $\pi_m = 0$, and $c^2_{s,m} = 0$. Hence, matter perturbations equations read

$$\delta'_m = -\frac{V_m(a)}{a^2 H(a)} - 3\Phi'(a), \quad V'_m = -\frac{V_m(a)}{a} - \frac{k^2}{a^2}\frac{\Phi(a)}{H(a)}, \tag{3.3.113}$$

The evolution equations for matter perturbations in Eq. (3.3.113) couple to the DE perturbations through the gravitational potential Φ. From Eqs. (3.2.17)-(3.2.18), we can eliminate Φ' and obtain

$$\Phi(a) = \frac{a^2}{2k^2}\left\{3H_0^2\Omega_{m0}a^{-3}\left(\delta_m + \frac{3aH}{k^2}V_m\right) + \bar{\rho}_{\rm DE}\left(\delta_{\rm DE} + \frac{3aH}{k^2}V_{\rm DE}\right)\right\}. \tag{3.3.114}$$

Since the background of the SVTDES model is equivalent to that of ΛCDM, the Hubble parameter is given by Eq. (3.3.95), and the density of dark energy is $\bar{\rho}_{\rm DE} = 3H_0^2\Omega_{\Lambda 0}$, hence (3.3.114) is simplified to

$$\Phi(a) = \frac{3}{2}\frac{H_0^2}{ak^2}\left\{\Omega_{m0}\left(\delta_m + \frac{3aH}{k^2}V_m\right) + \Omega_{\Lambda 0}a^3\left(\delta_{\rm DE} + \frac{3aH}{k^2}V_{\rm DE}\right)\right\}. \tag{3.3.115}$$

In order to solve Eqs. (3.3.113), we need to determine $\delta_{\rm DE}$ and $V_{\rm DE}$. Our effective fluid approach allowed us to find analytical expressions for the perturbations $\delta\rho_{\rm DE}$ and $V_{\rm DE}$ which for our SVTDES model (3.3.106) are given by Eqs. (3.3.107)-(3.3.109), respectively.

The initial conditions required to solve Eqs. (3.3.113) are set by the following expressions

$$\delta_{m,i} = \delta_i\, a_i\left(1 + 3\frac{a_i^2 H^2(a_i)}{k^2}\right), \quad V_{m,i} = -\delta_i\, H_0\, \Omega_{m0}\, a_i^{1/2}, \tag{3.3.116}$$

corresponding to the standard solutions of Eqs. (3.3.113) for δ_m and V_m in matter dominance, i.e., assuming that $H^2 = H_0^2\Omega_{m0}a^{-3}$. The overall factor δ_i is set to unity, and we choose $a_i = 10^{-3}$, ensuring initial conditions well within the matter epoch, right after decoupling.

The evolution of δ_m, V_m/k^2, $\delta_{\rm DE}$, and $V_{\rm DE}/k^2$ (their absolute values) are depicted on the right panel of Fig. 3.3.1. Note that the velocity perturbation is u, which is defined through $u_i \equiv -\partial_i u$ for scalar perturbations. The relation of the velocity perturbation to the scalar velocity and the velocity divergence is $V \propto \theta = ik^j u_j = k^2 u$, and then $u \propto V/k^2$.

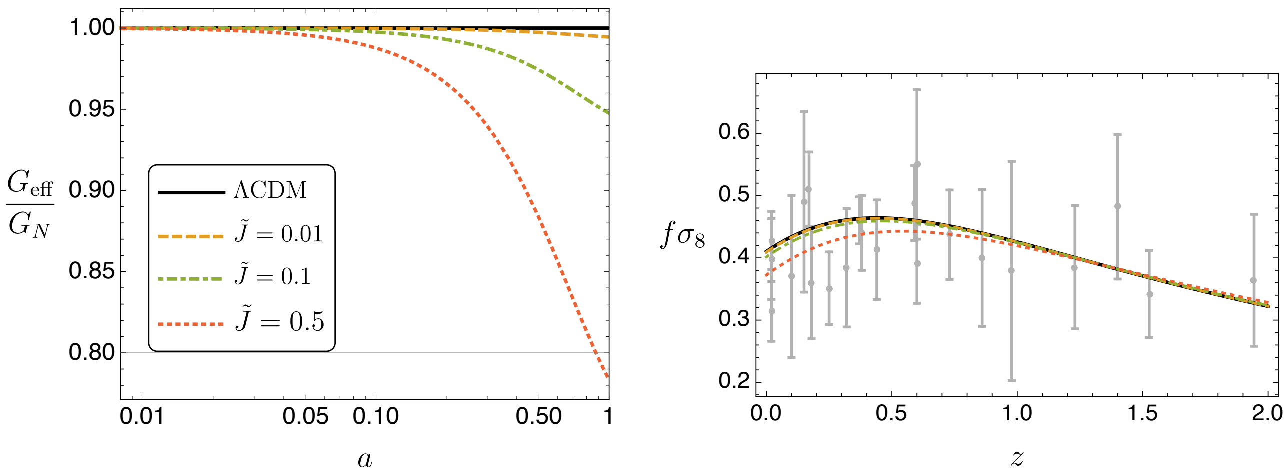

Figure 3.3.2: (Left) Deviations of $G_{\rm eff}$ from G_N from decoupling to today for different values of the parameter $\tilde{J}$. We can see that deviations from GR are only at late-times (occurring around the dark energy transition at $z \approx 0.3$), and smaller for $\tilde{J} \approx 0$ as expected. Observe that for $\tilde{J} = 0.5$, the difference between $G_{\rm eff}$ and G_N is around 20% at the present time. (Right) Evolution of $f\sigma_8(z)$ for the same values of $\tilde{J}$ shown in the left panel. In the case $\tilde{J} = 0.5$, deviations of SVTDES from ΛCDM are fairly noticeable. For the SVTDES model gravity is weaker than in the standard cosmological model leading to a less efficient late-time matter clustering. Other parameters used in the figures are $\Omega_{m0} = 0.3$, $\Omega_{\Lambda 0} = 0.7$, $\sigma_8 = 0.8$, and $k = 300H_0$.

Solution for the growth factor

As explained in Sec. 3.3.3, under the SHA and the QSA, the parameter $G_{\rm eff}$ plays an important role in the growth of structure, as can be seen in Eq. (3.3.65). In this subsection, we explore possible changes in the parameter $f\sigma_8$ within the SVTDES model due to variations in the strength of gravity which are encoded in the parameter $G_{\rm eff}$.

From Eqs. (3.3.59) and (3.3.63), we obtain the following analytical expression for $G_{\rm eff}$ under the QSA and the SHA

$$\frac{G_{\rm eff}}{G_N} = 2\frac{\frac{k^4}{a^4}W_{14} + \frac{k^2}{a^2}W_{15} + W_{13}}{\frac{k^4}{a^4}W_3 + \frac{k^2}{a^2}W_4 + W_5}, \tag{3.3.117}$$

where the coefficients W_i are given in the Appendix D of [8]. Replacing the SVTDES model [Eqs. (3.3.106)] in the parameter $G_{\rm eff}$ in Eq. (3.3.117), using the Hubble parameter of ΛCDM given in (3.3.95), and assuming some values for the parameter $\tilde{J}$, namely, $\tilde{J} = 0.01$, 0.1, 0.5, we can numerically solve the differential equation for δ_m in Eq. (3.3.65), where the initial conditions are set as $\delta_m(a_i) = a_i$ and $\delta'_m(a_i) = 1$ for a value of the scale factor a_i deep in the matter era ($a_i \sim 10^{-3}$). Other parameters used in the numerical solutions are $\Omega_{m0} = 0.3$, $\Omega_{\Lambda 0} = 0.7$, and $k = 300H_0$. In order to compare with observations, from this numerical solution we compute

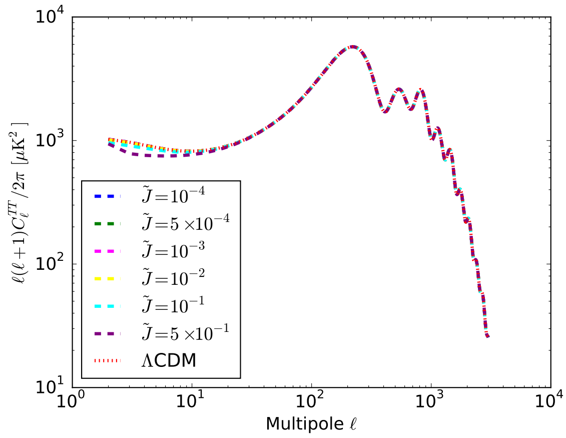

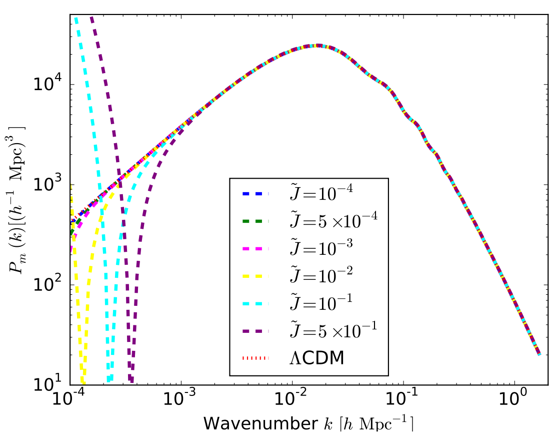

Figure 3.3.3: (Left) TT CMB angular power spectrum for the SVTDES model (dashed lines), and ΛCDM (dotted, red line). (Right) Linear matter power spectrum at $z = 0$ for the SVTDES model (dashed lines), and ΛCDM (dotted, red line). While the CMB angular power spectrum is almost identical in SVTDES and ΛCDM for small $\tilde{J}$, the matter power spectrum differs on very large scales where SHA cannot be applied: for late-times and modes as large as $k \sim 10^{-4}\, h$ Mpc^{-1} QSA and SHA cease to be valid. These plots were generated by slightly modifying `CLASS`, assuming $n_s = 0.9649$, $\ln 10^{10} A_s = 3.044$, $h = 0.6736$, $\omega_{\rm b} = 0.02237$, $\omega_{\rm cdm} = 0.1200$, $\tau = 0.0544$, $\sum m_\nu = 0.06$eV and $\tilde{J}$ as indicated in the legend.

the $f\sigma_8$ function, which is defined as

$$f\sigma_8(a) \equiv \sigma_8 \frac{a\, \delta'_m(a)}{\delta_m(a=1)}, \tag{3.3.118}$$

where $\sigma_8 \sim 0.8$ is the expected RMS over-density in a sphere of co-moving radius equal to $8h^{-1}$ Mpc, h being the normalized Hubble parameter. The results for the different values of $\tilde{J}$, aside the ΛCDM case $\tilde{J} = 0$, are shown in Fig. 3.3.2. In the left panel of Fig. 3.3.2 we can see that for $\tilde{J} = 0.5$, the modifications to GR, i.e., deviations of $G_{\rm eff}$ from G_N, are fairly noticeable at late-times. This difference translates to a weaker gravity when DE becomes relevant in the cosmic budget, which leads to a different evolution of the growth factor. In the right panel of Fig. 3.3.2, we plot $f\sigma_8(z)$ versus the data compilation from Ref. [374]. For $\tilde{J} = 0.5$, we can see that $f\sigma_8$ for SVTDES has a strong departure from ΛCDM (black solid curve) indicating a less efficient matter clustering in comparison with the standard model. Weaker gravity can be helpful in understanding the discrepancy in S_8 between low- and high-redshift probes. Gravity strength also decreases for smaller values of the parameter $\tilde{J} = 0.1$, 0.01, but differences with respect to ΛCDM are hardly significant.

CMB angular power spectrum and matter power spectrum

Having studied the evolution of matter perturbations in the previous subsections, here we present our results for the CMB power spectrum and the linear matter power spectrum. The advantage of the effective fluid approach is that it allows a relatively easy implementation of the SVTDES model in Boltzmann solvers. In its default version, Boltzmann codes usually have already a DE fluid implemented and parameterised by an equation of state w, sound speed in the fluid rest-frame $\hat{c}_s^2$, and vanishing anisotropic stress $\pi = 0$. In this work, we have computed the effective fluid quantities describing fairly general SVT theories.

We chose to carry out the implementation of the SVTDES model in the Boltzmann solver `CLASS`.[10] Since our model matches the ΛCDM background evolution ($w_{\rm DE} = -1$) and has vanishing anisotropic stress ($\pi_{\rm DE} = 0$), we decided to perform the smallest number of modifications in the code. It turns out that only one modification in the module `perturbations.c` is required: i) the scalar velocity $V_{\rm DE}$ (3.3.109) modifies the equation for Φ' in the function `perturbations_einstein`.

The CMB temperature power spectrum and the linear matter power spectrum are shown in Fig. 3.3.3. Perturbation equations were solved by using the cosmological parameters from the 2018 Planck baseline result [39]: scalar spectrum power-law index $n_s = 0.9649$, Log power of the primordial curvature perturbations $\ln 10^{10} A_s = 3.044$, reduced Hubble parameter $h = 0.6736$, baryon density today $\omega_{\rm b} = 0.02237$, cold dark matter density today $\omega_{\rm cdm} = 0.1200$, Thomson scattering optical depth due to reionization $\tau = 0.0544$, sum of neutrino masses in eV $\sum m_\nu = 0.06$, and some values of the SVTDES parameter $\tilde{J}$. We also plot the standard ΛCDM results for reference. As it can be seen in the left panel of Fig. 3.3.3, the match in the TT CMB angular power spectrum between SVTDES and ΛCDM is almost perfect. In the right panel of Fig. 3.3.3 we can see that the agreement in the linear matter power spectrum is also quite good for SVTDES and ΛCDM models. Nonetheless, for modes $k \sim 10^{-4} - 10^{-3}\, h$ Mpc^{-1} there is a departure from ΛCDM. Since we are working under the SHA and QSA, a big deviation is expected on large scales and late-times where the approximations are not valid.

Sound speed in the rest-frame

When implementing DE fluids in `CLASS`, it is important to bear in mind that the code uses the *co-moving sound speed* $\hat{c}_s^2$, i.e., the sound speed in the rest-frame of the fluid, which, in general, is given by

$$\hat{c}_s^2 = \frac{\delta P^C}{\delta \rho^C}, \tag{3.3.119}$$

[10] Version v3.2.0

where δP^C and $\delta\rho^C$ are the pressure and density perturbations computed in the co-moving gauge. These quantities are related to quantities in the Newtonian gauge (the gauge where our main results were derived) through the following transformation rules [375]

$$\delta\rho^C = \delta\rho^N + \bar{\rho}'\frac{\theta^N}{k^2}, \quad \delta P^C = \delta P^N + \bar{P}'\frac{\theta^N}{k^2}, \tag{3.3.120}$$

where the superscript N denotes a quantity computed in the Newtonian gauge. Therefore, the sound speed in the rest frame will be given by

$$\hat{c}_s^2 = \frac{\delta P^N + \bar{P}'\theta^N/k^2}{\delta\rho^N + \bar{\rho}'\theta^N/k^2}. \tag{3.3.121}$$

Since the background pressure and density of our SVTDES model are constants, we see from the last equations that the sound speed in Eq. (3.3.110) is actually equivalent to the sound speed in the rest frame. However, this is not the case in general. Let us take the quintessence field as an example. Replacing the full perturbations (3.3.79)-(3.3.80) in Eq. (3.3.121), computing the derivatives of $\bar{\rho}_{\rm DE}$ and $\bar{P}_{\rm DE}$ in Eqs. (3.3.78), and using the relation $\varphi'' = -2\mathcal{H}\varphi' - a^2 V_\varphi$, we find that

$$\hat{c}_s^2 = 1. \tag{3.3.122}$$

In this case, the result is equal to $c^2_{s,\rm DE}$ computed under the QSA and SHA [see Eq. (3.3.81)] since $V_{\rm DE} = 0$ for this particular model, but it is substantially different to $c^2_{s,\rm DE}$ given in Eq. (3.3.80) in the Newtonian gauge. Another interesting example concerns $f(R)$ theories where, in general, DE sound speed might depend on both time and scale. For instance, in Ref. [356] we can find expressions [see their Eqs. (61) $-$ (68)] under QSA and SHA for the Hu & Sawicki model that allow us to obtain $\hat{c}_s^2 \neq c^2_{s,\rm DE}$.

In summary, `CLASS` uses in their computations the sound speed in the co-moving gauge which is related to the Newtonian gauge by Eq. (3.3.121). Therefore, for a specific SVT model, we have to replace $\delta\rho_{\rm DE}$, $\delta P_{\rm DE}$, $V_{\rm DE} = (1+w_{\rm DE})\theta_{\rm DE}$ from Eq. (3.3.67) or Eq. (3.3.76) depending whether or not the model has a vanishing DE anisotropic stress, and compute the derivatives of the background density and pressure in Eqs. (3.3.48) and (3.3.49).

Numerical codes

Modified `CLASS` code reproducing results in this work can be found in the GitHub branch `svt` of the repository `EFCLASS`. A large part of the calculations in this paper were carried out using several `Mathematica` packages, like `xPand`. The notebooks showing these computations can be found in the GitHub repository `SVT`.

3.3.5 Conclusions

Both scalar and vector fields are present in nature and it is reasonable that they might provide explanations for shortcomings in the standard cosmological model ΛCDM. In this work we investigated fairly general scalar-vector-tensor theories having second order equations of motion: SVT theories encompass both Horndeski and generalised Proca Lagrangians. Although these kinds of theories might provide new, interesting phenomenology for cosmology, they have been overlooked in the literature. SVT theories have various free functions taking in all relevant interactions, hence possibly richer phenomenology than in the standard model. Nevertheless, more degrees of freedom come along with more complicate equations of motion. Even though complexity in SVT theories is reduced thanks to the constraint in the propagation speed of gravitational waves $c_T^2 = 1$, equations of motion remain intricate enough to find general analytical or numerical solutions.

Here, we applied an effective fluid approach to SVT theories satisfying $c_T^2 = 1$. In order to decrease the complexity in the equations of motion, we carefully performed both sub-horizon and quasi-static approximations. As a result, we obtained analytical expressions describing the effective dark energy fluid, namely, equation of state $w(a)$, squared sound speed $c_s^2(a,k)$, and anisotropic stress $\pi(a,k)$. Equations (3.3.67) and (3.3.76) summarise our main results for the behaviour of perturbations, while from Eqs. (3.3.48)-(3.3.49) the equation of state is obtained.

Our analytical expressions allowed us to retrieve well known results (e.g., quintessence and $f(R)$). Moreover, we also proposed extensions to these popular theories which exemplify possible, new phenomenology, for instance, changes in quantities driving the perturbations such as the sound speed and anisotropic stress.

An interesting aspect of our investigation is that it makes it possible to design cosmological models satisfying certain conditions. As an example, we found a SVT model (dubbed SVTDES in the main text) exactly matching the background behaviour in the standard cosmological model ΛCDM, while having non-vanishing dark energy perturbations. Our effective fluid approach and the analytical solutions for the effective dark energy perturbations made it possible a relatively easy implementation of SVTDES in the Boltzmann solver CLASS. Having a code computing numerical solutions for perturbation equations in SVT cosmological models is relevant because it allows testing against measurements, e.g., CMB angular power spectra, matter power spectrum. There is however no public Boltzmann solver including a fully numerical implementation of SVT models, that is, using neither QSA nor SHA. Therefore, our results might be helpful as a reference for future exact computations testing the limitations of QSA and SHA. Since our SVTDES model has one additional parameter with respect to ΛCDM, in a model comparison it would be penalised by the Bayesian evidence. However, our example also shows that exploring the construction of cosmological models satisfying additional conditions might be well worth an investigation. Given the current discrepancies in cosmological parameters such as H_0 and σ_8, theories providing non trivial behaviour for π and c_s^2 could alleviate the tensions while not being affected by the Occam's razor [362].

3.4 Tracking the Validity of the QSA and the SHA

3.4.1 Introduction

Generally, the main alternatives to the ΛCDM model imply either the existence of a fluid with negative pressure known as Dark Energy (DE) [60, 94], or covariant modifications to the geometric sector describing gravity, the so-called Modified Gravity (MG) theories [95, 376]. With respect to MG theories, a large portion in the plethora of candidate models are rule out by observations from, for example, gravitational waves [329, 377], and very precise extra-galactic tests [104, 378, 379]. However, there remains some alternatives. Among the still cosmologically viable MG theories, one of the most representative are the so-called $f(R)$ theories [380]. In principle, these theories could be distinguished from the standard cosmological model by their influence in the inhomogeneous Universe since, in general, they introduce modifications in several observables, e.g., the growth rate [381]. However, no $f(R)$ model is particularly favored by current growth data [382, 383].

It is fair to say that the distinction between DE and MG is rather academic in a sense, as both scenarios can be treated on equal footing under the Effective Fluid Approach (EFA) [384].[11] Within the EFA, all the modifications to gravity are encompassed in terms of the equation of state $w_{\rm DE}$, the sound speed $c^2_{s,\rm DE}$, and the anisotropic stress $\pi_{\rm DE}$ of an effective DE fluid. As shown in Refs. [8, 356, 357], the application of the Quasi-Static Approximation (QSA) and the Sub-Horizon Approximation (SHA) allows to get analytical expressions for the effective DE perturbations in very general MG theories. One of the advantage of this approach is that these expressions can be easily introduced in Boltzmann solvers, such as `CLASS` [343], facilitating the computation of cosmological observables, e.g., the linear matter power spectrum or the CMB angular power spectrum. These approximations also enable us to directly discriminate departures from General Relativity (GR), which could be encoded in, for instance, the effective Newton's constant $G_{\rm eff}$ and the effective lensing parameter $Q_{\rm eff}$. Albeit they have been extensively used in the literature [359, 372, 387–394], some works claim that the QSA, in particular, can be too aggressive and that relevant dynamical information could be omitted after their application [395, 396]. Therefore, the validity regime of these approximations

[11] The Effective Field Theory is another approach which allows to model dark energy and modified gravity in a common framework [349, 350, 385, 386].

is a highly relevant issue to be addressed in order to compare theoretical results with upcoming astrophysical observations.

Bearing in mind the above discussion, we propose to analyze the validity regime in time and scale of the QSA-SHA for modified gravity theories. We start our research program by revisiting well-known expressions obtained for the effective DE perturbations in $f(R)$ theories. In order to do so, we put forward a new parameterization scheme that allows us to track the relevance of each derivative term in the perturbation equations. In general, we find some correction terms which improve over the standard description of the effective DE perturbations by several orders of magnitude in some cases.

3.4.2 $f(R)$ Theories

In $f(R)$ models, covariant modifications of GR are performed by replacing R in the Einstein-Hilbert action by a general function $f(R)$ such that

$$S = \int \mathrm{d}^4x\sqrt{-g}\left[\frac{1}{2\kappa}f(R) + \mathcal{L}\right]. \tag{3.4.1}$$

Upon varying this action with respect to $g^{\mu\nu}$, the Einstein equations are replaced by

$$FG_{\mu\nu} - \frac{1}{2}\left(f - FR\right)g_{\mu\nu} + \left(g_{\mu\nu}\Box - \nabla_\mu\nabla_\nu\right)F = \kappa T_{\mu\nu}, \tag{3.4.2}$$

where[12] $F \equiv f_R$. Yet, it is possible to recast Eq. (3.4.2) to look as the usual Einstein field equations using the effective fluid approach. Under this framework, all the modifications to gravity are encoded in a generalized DE fluid which, in the case of $f(R)$ theories, is characterized by the following energy-momentum tensor

$$\kappa T^{(\mathrm{DE})}_{\mu\nu} = \left(1 - F\right)G_{\mu\nu} + \frac{1}{2}\left(f - FR\right)g_{\mu\nu} - \left(g_{\mu\nu}\Box - \nabla_\mu\nabla_\nu\right)F. \tag{3.4.3}$$

Hence, the Friedmann equations are obtained as the usual ones upon replacing the DE density and pressure by

$$\kappa\bar{\rho}_{\mathrm{DE}} = -\frac{f}{2} + 3H^2\left(1 + F\right) + 3F\dot{H} - 3H\dot{F}, \tag{3.4.4}$$

$$\kappa\bar{P}_{\mathrm{DE}} = \frac{f}{2} - 3H^2\left(1 + F\right) - \dot{H}\left(2 + F\right) + 2H\dot{F} + \ddot{F}. \tag{3.4.5}$$

[12] Derivatives with respect to R are denoted using a sub-index, e.g., $\frac{\mathrm{d}f}{\mathrm{d}R} \equiv f_R$.

On the other hand, Einstein linear perturbation equations are modified as

$$0 = -\kappa\bar{\rho}_m\delta_m + A_1\dot{\Phi} + A_2\dot{\Psi} + \left(A_3 + A_4\frac{k^2}{a^2}\right)\Phi + \left(A_5 + A_6\frac{k^2}{a^2}\right)\Psi, \tag{3.4.6}$$

$$0 = -\frac{a\kappa\bar{\rho}_m V_m}{k^2} + C_1\dot{\Phi} + C_2\dot{\Psi} + C_3\Phi + C_4\Psi, \tag{3.4.7}$$

$$0 = B_1\ddot{\Phi} + B_2\ddot{\Psi} + B_3\dot{\Phi} + B_4\dot{\Psi} + B_5\Phi + B_6\Psi, \tag{3.4.8}$$

$$0 = D_1\ddot{\Phi} + D_2\dot{\Phi} + D_3\dot{\Psi} + \left(D_4 + D_5\frac{k^2}{a^2}\right)\Phi + \left(D_6 + D_7\frac{k^2}{a^2}\right)\Psi. \tag{3.4.9}$$

The last equation is obtained from the relation

$$0 = F_R(\Phi + \Psi) + F\delta R, \tag{3.4.10}$$

where δR is the perturbation of the Ricci scalar which in the FLRW metric reads

$$\delta R = 6\ddot{\Phi} + 24H\dot{\Phi} - 6H\dot{\Psi} + 4\frac{k^2}{a^2}\Phi + \left(2\frac{k^2}{a^2} - 12\dot{H} + 24H^2\right)\Psi. \tag{3.4.11}$$

The coefficients A_i, C_i, B_i, and D_i can be found in Appendix A of [9]. In the EFA, we can assign to the $f(R)$ theory an effective DE perturbation variable for density, pressure, velocity, and anisotropic stress respectively. They are obtained from the energy tensor in Eq. (3.4.3) as

$$\kappa\delta\rho_{\rm DE} = W_1\dot{\Phi} + W_2\dot{\Psi} + \left(W_3 + W_4\frac{k^2}{a^2}\right)\Phi + \left(W_5 + W_6\frac{k^2}{a^2}\right)\Psi, \tag{3.4.12}$$

$$\kappa\delta P_{\rm DE} = Y_1\ddot{\Phi} + Y_2\ddot{\Psi} + Y_3\dot{\Phi} + Y_4\dot{\Psi} + \left(Y_5 + Y_6\frac{k^2}{a^2}\right)\Phi + \left(Y_7 + Y_8\frac{k^2}{a^2}\right)\Psi, \tag{3.4.13}$$

$$\frac{a\kappa\bar{\rho}_{\rm DE}}{k^2}V_{\rm DE} = Z_1\dot{\Phi} + Z_2\dot{\Psi} + Z_3\Phi + Z_4\Psi, \tag{3.4.14}$$

$$\kappa\bar{\rho}_{\rm DE}\pi_{\rm DE} = -\frac{k^2}{a^2}\left(\Phi + \Psi\right), \tag{3.4.15}$$

where the coefficients W_i, Y_i, and Z_i can be found in Appendix B of Ref. [9].

Quasi-Static and Sub-Horizon Approximations: Standard Approach

The dynamics of DE and matter inhomogeneities in $f(R)$ models can be unveiled if the evolution of the gravitational potentials is known. However, this implies to solve Eqs. (3.4.6)-(3.4.9) coupled to the matter perturbations equations in Eqs. (3.2.11) and (3.2.12), which in general is a difficult task. The application of the Quasi-Static Approximation (QSA) and the Sub-Horizon Approximation (SHA) can greatly simplify the related equations. In the following, we describe the standard steps to apply these approximations to the perturbation equations. We disregard time-derivatives of the potentials and consider that relevant modes for the cosmological dynamics are those well-inside the Hubble radius, i.e., $k \gg aH$. This allows us to neglect terms of the form $H\times$perturbation in favor of terms of the form $k^2\times$perturbation. As an example, applying these approximations to the perturbation of the Ricci scalar in Eq. (3.4.11) gives

$$
\begin{aligned}
\delta R &= 6\ddot{\Phi} + 24H\dot{\Phi} - 6H\dot{\Psi} + 4\frac{k^2}{a^2}\Phi + \left(2\frac{k^2}{a^2} - 12\dot{H} + 24H^2\right)\Psi \\
&\overset{\text{QSA}}{\approx} 4\frac{k^2}{a^2}\Phi + \left(2\frac{k^2}{a^2} - 12\dot{H} + 24H^2\right)\Psi \\
&\overset{\text{SHA}}{\approx} 4\frac{k^2}{a^2}\Phi + 2\frac{k^2}{a^2}\Psi.
\end{aligned}
$$

Using the QSA-SHA in the linear equations (3.4.6) and (3.4.9), we get two algebraic equations for the two potentials, namely

$$
0 = -\kappa\bar{\rho}_m\delta_m + A_4\frac{k^2}{a^2}\Phi + A_6\frac{k^2}{a^2}\Psi, \tag{3.4.16}
$$

$$
0 = \left(D_4 + D_5\frac{k^2}{a^2}\right)\Phi + \left(D_6 + D_7\frac{k^2}{a^2}\right)\Psi, \tag{3.4.17}
$$

from which we can solve directly for Φ and Ψ in terms of δ_m. The solution is

$$
\frac{k^2}{a^2}\Phi = -\frac{\left(D_6 + D_7\frac{k^2}{a^2}\right)\kappa\bar{\rho}_m\delta_m}{\left(A_6D_5 - A_4D_7\right)\frac{k^2}{a^2} + \left(A_6D_4 - A_4D_6\right)}, \tag{3.4.18}
$$

$$
\frac{k^2}{a^2}\Psi = \frac{\left(D_4 + D_5\frac{k^2}{a^2}\right)\kappa\bar{\rho}_m\delta_m}{\left(A_6D_5 - A_4D_7\right)\frac{k^2}{a^2} + \left(A_6D_4 - A_4D_6\right)}. \tag{3.4.19}
$$

Note that in Eq. (3.4.17), we do not neglect $D_4\Phi$ and $D_6\Psi$. The reason is that these terms are associated to the mass of the scalaron m_φ, which can be greater than H for some $f(R)$ models [372]. Replacing the coefficients (see Appendix A of [9]) in the last relations we get

$$
\frac{k^2}{a^2}\Phi = \frac{F - 12F_R(\dot{H} + 2H^2) + 2\frac{k^2}{a^2}F_R}{2F^2 - 12FF_R(\dot{H} + 2H^2) + 6\frac{k^2}{a^2}FF_R}\kappa\bar{\rho}_m\delta_m, \tag{3.4.20}
$$

$$
\frac{k^2}{a^2}\Psi = -\frac{F + 4\frac{k^2}{a^2}F_R}{2F^2 - 12FF_R(\dot{H} + 2H^2) + 6\frac{k^2}{a^2}FF_R}\kappa\bar{\rho}_m\delta_m. \tag{3.4.21}
$$

However, when neglecting H and its derivatives, we get the following well-known expressions

$$
\frac{k^2}{a^2}\Phi = \frac{F + 2\frac{k^2}{a^2}F_R}{2F^2 + 6\frac{k^2}{a^2}FF_R}\kappa\bar{\rho}_m\delta_m, \qquad \frac{k^2}{a^2}\Psi = -\frac{F + 4\frac{k^2}{a^2}F_R}{2F^2 + 6\frac{k^2}{a^2}FF_R}\kappa\bar{\rho}_m\delta_m. \tag{3.4.22}
$$

Applying the same procedure to the DE perturbations in Eqs. (3.4.12)-(3.4.15) we get

$$\delta_{\rm DE} = \frac{(1-F)F + (2-3F)\frac{k^2}{a^2}F_R}{F(F+3\frac{k^2}{a^2}F_R)}\frac{\bar{\rho}_m}{\bar{\rho}_{\rm DE}}\delta_m, \tag{3.4.23}$$

$$\frac{\delta P_{\rm DE}}{\bar{\rho}_{\rm DE}} = \frac{1}{3F}\frac{2\frac{k^4}{a^4}F_R + 15\frac{k^2}{a^2}F_R\ddot{F} + 3F\ddot{F}}{3\frac{k^2}{a^2}F_R + F}\frac{\bar{\rho}_m}{\bar{\rho}_{\rm DE}}\delta_m, \tag{3.4.24}$$

$$V_{\rm DE} = \frac{a\dot{F}}{2F}\frac{F + 6\frac{k^2}{a^2}F_R}{3\frac{k^2}{a^2}F_R + F}\frac{\bar{\rho}_m}{\bar{\rho}_{\rm DE}}\delta_m. \tag{3.4.25}$$

$$\pi_{\rm DE} = \frac{\frac{k^2}{a^2}F_R}{F^2 + 3\frac{k^2}{a^2}FF_R}\frac{\bar{\rho}_m}{\bar{\rho}_{\rm DE}}\delta_m, \tag{3.4.26}$$

which are the usual results found in the literature [8, 356, 357, 384]. We will refer to the steps performed to obtain the last expressions as the "standard QSA-SHA procedure", while the relations for the perturbations, namely Eqs. (3.4.22)-(3.4.26), will be called as the "standard QSA-SHA results".

We want to emphasize on one of the key steps in obtaining the above expressions. After replacing the coefficients in Appendices A and B of [9], we also neglected H and its derivatives by assuming that these terms are subdominant under the SHA. Nonetheless, noting that $\dot{F} = F_R\dot{R}$ and $R = 6(\dot{H}+2H^2)$, if we drop terms of the form $H\times$perturbation, we should naively conclude that $\dot{F}\delta_m \approx 0$, and thus the pressure perturbation and the scalar velocity would take the following form

$$\frac{\delta P_{\rm DE}}{\bar{\rho}_{\rm DE}} \approx \frac{1}{3F}\frac{2\frac{k^2}{a^2}F_R}{3\frac{k^2}{a^2}F_R + F}\frac{\bar{\rho}_m}{\bar{\rho}_{\rm DE}}\delta_m, \qquad V_{\rm DE} \approx 0. \tag{3.4.27}$$

As shown in several works (see Ref. [356] for example), $V_{\rm DE}$ is small at late times but certainly not zero. Indeed, as we will see in the following section, these last expressions correspond to the zero-order solution in our new parameterization of the QSA-SHA.

3.4.3 Tracking the Validity of the QSA and the SHA

Following the discussion in the last section, there are two main assumptions behind the QSA and the SHA: the potentials do not depend on time and $k \gg aH$. These allowed us to eliminate the time derivatives of the potentials and drop some terms of the form $H\times$perturbation in the effective DE perturbations. Then, in order to know the regime where these approximations can be safely applied, we need to track the relevance of each time-derivative term in the perturbation equations. We do so by introducing the dimension-less parameters:

$$\varepsilon \equiv \frac{aH}{k}, \qquad \delta \equiv \frac{\dot{\varepsilon}}{\varepsilon H}, \qquad \xi \equiv \frac{\ddot{\varepsilon}}{\varepsilon H^2}, \qquad \chi \equiv \frac{\dddot{\varepsilon}}{\varepsilon H^3}, \tag{3.4.28}$$

and

$$\varepsilon_\Phi \equiv \frac{\dot{\Phi}}{\Phi H}, \qquad \varepsilon_\Psi \equiv \frac{\dot{\Psi}}{\Psi H}, \qquad \chi_\Phi \equiv \frac{\dot{\varepsilon}_\Phi}{\varepsilon_\Phi H}, \qquad \chi_\Psi \equiv \frac{\dot{\varepsilon}_\Psi}{\varepsilon_\Psi H}. \tag{3.4.29}$$

Hence, $k \gg aH$ is translated to $\varepsilon \ll 1$, and $\dot{\Phi} \sim \dot{\Psi} \approx 0$ is translated to $\varepsilon_\Phi \sim \varepsilon_\Psi \ll 1$. We refer to the parameters in Eqs. (3.4.28) and (3.4.29) as "SHA parameters" and "QSA parameters", respectively.[13]

We want to comment on some previous considerations before implementing the parameterization into the equations in Sec. 3.4.2 describing $f(R)$ theories. First of all, in order to track all the terms proportional to H or its derivatives, we replace time derivatives of F in favor of H, i.e.,

$$\dot{F} = 6F_R(\ddot{H} + 4H\dot{H}), \quad \ddot{F} = 6F_R(\dddot{H} + 4H\ddot{H} + 4\dot{H}^2) + 36F_{RR}(\ddot{H} + 4H\dot{H})^2. \tag{3.4.30}$$

In addition, apart of the parameter ε, all the other SHA parameters are not necessarily small. For example, during matter domination we have $H = H_0\sqrt{\Omega_{m0}}a^{-3/2}$ and

$$\delta = -1/2, \quad \xi = 1, \quad \chi = -7/2, \qquad \text{(in matter domination)} \tag{3.4.31}$$

where Ω_{m0} is the matter density parameter today, and H_0 is the Hubble constant.

Re-writing Eqs. (3.4.6) and (3.4.9) using the new parameters, we obtain the following two "algebraic" equations to solve for Φ and Ψ

$$0 = -\kappa\bar{\rho}_m\delta_m + \mathcal{A}_1\frac{k^2}{a^2}\Phi + \mathcal{A}_2\frac{k^2\varepsilon^2}{a^2}\Phi + \mathcal{A}_3\frac{k^4\varepsilon^4}{a^4}\Phi + \mathcal{A}_4\frac{k^2}{a^2}\Psi + \mathcal{A}_5\frac{k^2\varepsilon^2}{a^2}\Psi + \mathcal{A}_6\frac{k^4\varepsilon^4}{a^4}\Psi, \tag{3.4.32}$$

$$0 = \left(\mathcal{D}_1 + \mathcal{D}_2\frac{k^2}{a^2}\right)\Phi + \mathcal{D}_3\frac{k^2\varepsilon^2}{a^2}\Phi + \left(\mathcal{D}_4 + \mathcal{D}_5\frac{k^2}{a^2}\right)\Psi + \mathcal{D}_6\frac{k^2\varepsilon^2}{a^2}\Psi, \tag{3.4.33}$$

where the coefficients $\mathcal{A}_i$ and $\mathcal{D}_i$ are found in Appendix C of [9]. Note that we wrote the above equations factorizing in terms of ε to facilitate the measurement of the relevance of each term. Now, solving for Φ and Ψ, expanding in powers of ε up to second-order, replacing the

[13] We would like to mention that the QSA parameters are inspired by the slow-roll approximation used in the background analysis of inflationary models.

coefficients $\mathcal{A}_i$ and $\mathcal{D}_i$, and considering only linear terms in the QSA parameters we get

$$\frac{k^2}{a^2}\Phi = \frac{F+2\frac{k^2}{a^2}F_R}{2F^2+6\frac{k^2}{a^2}FF_R}\kappa\bar{\rho}_m\delta_m + \frac{3\kappa\bar{\rho}_m\delta_m\varepsilon^2}{4F\left(F+3\frac{k^2}{a^2}F_R\right)^2}\Big\{F^2(2+\varepsilon_\Phi+\varepsilon_\Psi) \tag{3.4.34}$$
$$+2\frac{k^2}{a^2}FF_R[\delta(1+\varepsilon_\Phi)+4(2+\varepsilon_\Psi)+5\varepsilon_\Phi]+4\frac{k^4}{a^4}F_R^2[\delta(3+\varepsilon_\Phi)+4(2+\varepsilon_\Psi)+4\varepsilon_\Phi]\Big\},$$

$$\frac{k^2}{a^2}\Psi = -\frac{F+4\frac{k^2}{a^2}F_R}{2F^2+6\frac{k^2}{a^2}FF_R}\kappa\bar{\rho}_m\delta_m + \frac{3\kappa\bar{\rho}_m\delta_m\varepsilon^2}{4F\left(F+3\frac{k^2}{a^2}F_R\right)^2}\Big\{F^2(2+\varepsilon_\Phi+\varepsilon_\Psi) \tag{3.4.35}$$
$$-2\frac{k^2}{a^2}FF_R[\delta(3+\varepsilon_\Phi)-3(2+\varepsilon_\Psi)]-4\frac{k^4}{a^4}F_R^2[\delta(6+\varepsilon_\Phi)-2(2+\varepsilon_\Psi)+\varepsilon_\Phi]\Big\}.$$

We recognize the standard expressions for the potentials [see Eq. (3.4.22)] in the first term on the right-hand side of the last expressions. Hence, we can identify the standard results for the potentials as the solution for the *deepest* modes in the Hubble radius or, equivalently, the smallest scales where $\varepsilon \sim 0$.

Indeed, equations (3.4.32) and (3.4.33) are not "algebraic" equations for Φ and Ψ, since the QSA parameters ε_Φ and ε_Ψ depends on the dynamics of the potentials. Therefore, Eqs. (3.4.34) and (3.4.35) are coupled differential equations for Φ and Ψ. However, note that the QSA parameters are always coupled to SHA parameters, and thus terms of the form $\varepsilon_\Phi \times \varepsilon^2$ are third-order terms in the new QSA-SHA expansion. We will consider only second-order terms, and thus we neglect the QSA parameters, i.e., we will assume that $\varepsilon_\Phi = \varepsilon_\Psi = 0$. As we will see, these approximations, zero-order in QSA parameters and second-order in SHA parameters, are sufficiently accurate when compare against full numerical results for large modes. Under this assumptions, the expressions for the potentials are reduced to

$$\frac{k^2}{a^2}\Phi = \frac{F+2\frac{k^2}{a^2}F_R}{2F^2+6\frac{k^2}{a^2}FF_R}\kappa\bar{\rho}_m\delta_m \tag{3.4.36}$$
$$+\frac{3\kappa\bar{\rho}_m\delta_m\varepsilon^2}{2F\left(F+3\frac{k^2}{a^2}F_R\right)^2}\Big\{F^2+\frac{k^2}{a^2}(\delta+8)FF_R+2\frac{k^4}{a^4}(3\delta+8)F_R^2\Big\},$$

$$\frac{k^2}{a^2}\Psi = -\frac{F+4\frac{k^2}{a^2}F_R}{2F^2+6\frac{k^2}{a^2}FF_R}\kappa\bar{\rho}_m\delta_m \tag{3.4.37}$$
$$+\frac{3\kappa\bar{\rho}_m\delta_m\varepsilon^2}{2F\left(F+3\frac{k^2}{a^2}F_R\right)^2}\Big\{F^2-\frac{k^2}{a^2}(3\delta-6)FF_R-2\frac{k^4}{a^4}(6\delta-4)F_R^2\Big\}.$$

Now, applying the new parameterization to the DE perturbations quantities in Eqs. (3.4.12)-

(3.4.15), and then inserting these potentials we get:

$$
\begin{aligned}
\delta_{\rm DE} &= \frac{(1-F)F+\frac{k^2}{a^2}(2-3F)F_R}{F(F+3\frac{k^2}{a^2}F_R)}\frac{\bar\rho_m}{\bar\rho_{\rm DE}}\delta_m \\
&\quad -\frac{3\frac{k^2}{a^2}F_R\varepsilon^2}{F\left(F+3\frac{k^2}{a^2}F_R\right)^2}\left\{(\delta+1)F+2\frac{k^2}{a^2}(3\delta+2)F_R\right\}\frac{\bar\rho_m}{\bar\rho_{\rm DE}}\delta_m, \qquad (3.4.38)\\
\frac{\delta P_{\rm DE}}{\bar\rho_{\rm DE}} &= \frac{1}{3F}\frac{2\frac{k^2}{a^2}F_R}{3\frac{k^2}{a^2}F_R+F}\frac{\bar\rho_m}{\bar\rho_{\rm DE}}\delta_m+\frac{3\frac{\bar\rho_m}{\bar\rho_{\rm DE}}\delta_m\varepsilon^2}{F\left(F+3\frac{k^2}{a^2}F_R\right)^2}\Big\{F^2(F-1)(1+2\delta) \qquad (3.4.39)\\
&\quad +\frac{k^2}{a^2}(5F-10\delta+13F\delta-5)FF_R+\frac{k^4}{a^4}(6F-6\delta+21F\delta-4)F_R^2\Big\},\\
V_{\rm DE} &= \frac{a}{F\left(F+3\frac{k^2}{a^2}F_R\right)}\left\{F(F-1)+\frac{k^2}{a^2}(3F-4)F_R\right\}\frac{\bar\rho_m}{\bar\rho_{\rm DE}}\delta_m\frac{k}{a}\varepsilon, \qquad (3.4.40)\\
\pi_{\rm DE} &= \frac{\frac{k^2}{a^2}F_R}{F^2+3\frac{k^2}{a^2}FF_R}\frac{\bar\rho_m}{\bar\rho_{\rm DE}}\delta_m+\frac{3F_R\frac{\bar\rho_m}{\bar\rho_{\rm DE}}\delta_m\frac{k^2}{a^2}\varepsilon^2}{F\left(F+3\frac{k^2}{a^2}F_R\right)^2}\left\{F(1+2\delta)+\frac{k^2}{a^2}F_R(4+9\delta)\right\}. \qquad (3.4.41)
\end{aligned}
$$

From the last expressions, we can unravel similarities and differences between the standard QSA-SHA results in Eqs. (3.4.22)-(3.4.26) and our expressions in Eqs. (3.4.36)-(3.4.41). For instance, we see that the standard $\delta_{\rm DE}$ in Eq. (3.4.23) corresponds to the zero-order contribution in Eq. (3.4.38). In the new parameterization, $\delta P_{\rm DE}$ has contributions to second-order in ε, while $V_{\rm DE}$ is predominantly a first-order quantity in the ε-expansion. Now, bearing in mind that

$$\dot F = 6\frac{k^3}{a^3}(\delta+\xi-2)F_R\varepsilon^3, \qquad (3.4.42)$$

$$\ddot F = 6\frac{k^4}{a^4}(\delta^2-8\delta+\chi+6)F_R\varepsilon^4+36\frac{k^6}{a^6}(\delta+\xi-2)F_{RR}\varepsilon^6, \qquad (3.4.43)$$

we note that, in the new parameterization, the standard $\delta P_{\rm DE}$ in Eq. (3.4.24) corresponds to a zero-order quantity plus fourth and sixth-order corrections, while the standard $V_{\rm DE}$ in Eq. (3.4.25) is entirely a third-order quantity.

Equations (3.4.36)-(3.4.41) are the main results of our paper. They explicitly show that potentially relevant terms have been neglected in the effective DE perturbations when the QSA and the SHA are applied in the standard way. They also point out that similar expressions obtained for other MG theories, such as Horndeski theories, neglected terms which could potentially modify their predictions. Now, in order to determine the relevance of the correction terms uncovered by our new QSA-SHA procedure, we have to know the evolution of the SHA parameters which depend on H and its derivatives, i.e., they depend on the specific cosmological model. In the following section we will study the behavior of these parameters in the context of two well-known $f(R)$ models: the designer model [397, 398] and the Hu-Sawicki model [399].

3.4.4 Specific $f(R)$ Models

fDES Model

As shown in Refs. [400, 401], $f(R)$ models admit solutions which can be "designed" to reproduce any desirable expansion history. In particular, it is possible to find an $f(R)$ model matching the ΛCDM background but having deviations at the perturbative level. The Lagrangian of this designer model, fDES hereafter, reads [397]

$$f(R) = R - 2\Lambda + \alpha H_0^2 \left(\frac{\Lambda}{R-3\Lambda}\right)^{c_0} {}_2F_1\left(c_0, \frac{3}{2}+c_0, \frac{13}{6}+2c_0, \frac{\Lambda}{R-3\Lambda}\right), \tag{3.4.44}$$

where $c_0 \equiv (\sqrt{73}-7)/12$, α is a dimensionless constant, and ${}_2F_1$ denotes the hypergeometric function. Since the background is the same as in ΛCDM, from Eqs. (3.4.4) and (3.4.5) we have

$$H^2 = H_0^2\left(\Omega_{m0}a^{-3} + \Omega_{\Lambda 0}\right), \qquad \bar{\rho}_{\rm DE} = -\bar{P}_{\rm DE} = 3H_0^2\Omega_{\Lambda 0}, \tag{3.4.45}$$

where $\Omega_{\Lambda 0}$ is the DE density parameter today. The parameter α can be estimated following the prescription that viable $f(R)$ models require

$$f_{R0} \equiv F(a=1) - 1 \ll 1. \tag{3.4.46}$$

A typical value is $f_{R0} \sim -10^{-4}$ (see, for instance, Ref. [381]) which translates to $\alpha \approx 0.00107$.

Hu-Sawicki Model

The Hu-Sawicki (HS) model is a well-known model constructed in such a way that observational tests, such as solar system tests, can be surpassed. Its Lagrangian is given by [399]

$$f(R) = R - m^2\frac{c_1(R/m^2)^n}{1+c_2(R/m^2)^n}, \tag{3.4.47}$$

where m, c_1, c_2, and n are dimensionless constants. Through algebraic manipulation, it is possible to re-write the last function as [402]

$$f(R) = R - \frac{2\Lambda}{1+\left(\frac{b\Lambda}{R}\right)^n}, \quad \Lambda = \frac{m^2 c_1}{2c_2}, \quad b = \frac{2c_2^{1-1/n}}{c_1}. \tag{3.4.48}$$

Therefore, the background evolution in the HS model can be similar to ΛCDM depending on b and n. Usually n takes on positive integer values. Here, we choose $n=1$. Assuming $f_{R0} = -10^{-4}$, we estimate $b \approx 0.000989557$.

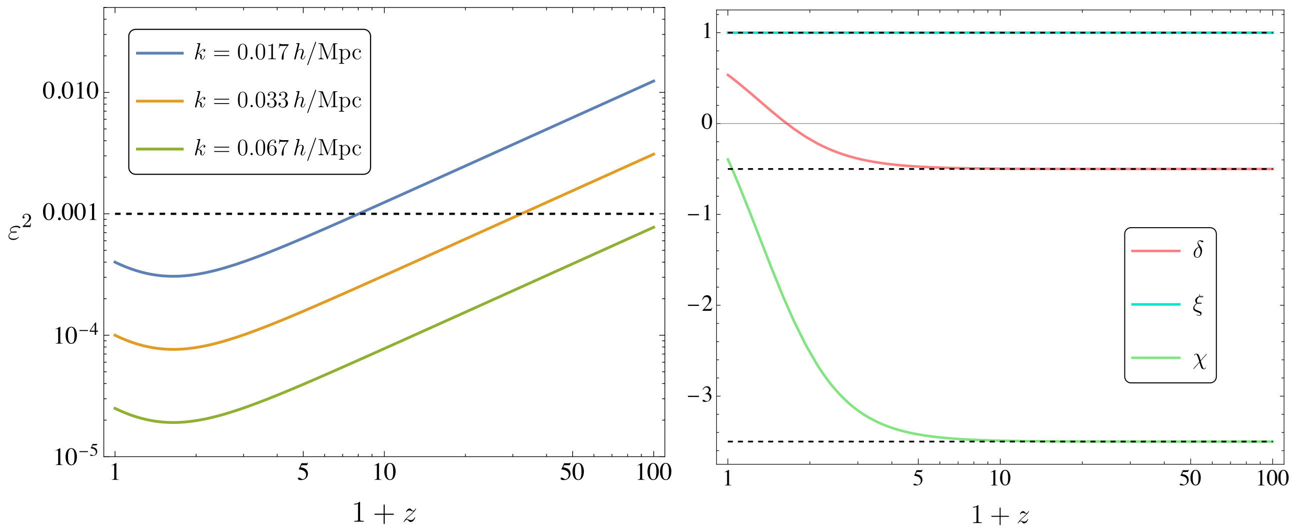

Figure 3.4.1: Left: Evolution of the ε parameter in the HS model for three values of k. We can see that $\varepsilon^2 \lesssim 10^{-3}$ during the whole matter dominated epoch until present days for scales $k \gtrsim 0.06\,h/\mathrm{Mpc}$. Right: Evolution of the SHA parameters δ, ξ, and χ in the HS model. Note that they behave as constants during the matter dominated epoch as expected from Eqs. (3.4.31) (see the dashed black lines), with a raising at late-times when the contribution of DE becomes more relevant.

In order to characterize the background evolution of the HS model, in general we would have to solve the Friedmann equations and the continuity equations. However, we can evade this issue by using the following analytical approximation to the Hubble parameter [402]

$$H_{\mathrm{HS}}(a)^2 = H_\Lambda(a)^2 + b\ \delta H_1(a)^2 + \mathcal{O}(b^2), \tag{3.4.49}$$

where the function $\delta H_1(a)$ is given in the Appendix of Ref. [402] and H_Λ is the Hubble parameter for the ΛCDM model. Overall, Eq. (3.4.49) is accurate to better than $\sim 10^{-5}\%$, for our choice of the parameter b.

Having the functional forms of H, Eqs. (3.4.45) and (3.4.49) for the fDES and HS models respectively, we can follow the evolution of the SHA parameters defined in Eq. (3.4.28). However, as noted in Eqs. (3.4.45) and (3.4.49), the HS can be regarded as a small deviation from the ΛCDM model for b small enough. We verified that indeed the evolution of the SHA parameters in both models are essentially indistinguishable for the values of α and b we chose. Then, to keep our presentation simple, in Fig. 3.4.1 we only plot the evolution of the SHA parameters for the HS model using as time variable the redshift z, which is related to the scale factor through the relation $a = 1/(1+z)$. In the left-panel of this figure, we see that ε^2 can be safely considered as "small" (i.e., $\varepsilon^2 \lesssim 10^{-3}$) for modes[14] $k \gtrsim 0.06\,h/\mathrm{Mpc}$. In the right panel

[14] In completely theoretical studies, k is typically given in units of H_0. Therefore, $k \approx 0.067\,h/\mathrm{Mpc}$ corresponds

we see that at earlier times the other SHA parameters behave as expected during the matter dominated epoch [see Eq. (3.4.31)] and grow when DE plays a more relevant role in the cosmic budget. Therefore, we say that the "safety region" where the SHA can be applied corresponds to the scales $0.067\, h/\mathrm{Mpc} \lesssim k \lesssim 0.2\, h/\mathrm{Mpc}$. The upper bound of this window scale comes from the fact that this is roughly the scale above which nonlinearities at present days cannot be ignored in the concordance model[15] [403]. This scale is also close to the maximum comoving wave number associated with the galaxy power spectrum measured by the Sloan Digital Sky Survey (SDSS) without entering the non-linear regime [373, 394].

We would like to point out that the fDES model and the HS model have a background evolution either identical or similar to that of ΛCDM, and that $f(R)$ models with different background evolution could yield to different results, in principle. Nonetheless, as clarified in Ref. [404], $f(R)$ models with expansion histories similar to that of ΛCDM are cosmologically viable, while more generic models have in general to meet a number of requirements, making the model-building process more contrived [352].

3.4.5 Numerical Solution of the Evolution Equations

In this section we numerically solve the equations for matter perturbations in Eqs. (3.2.11) and (3.2.12) assuming that Φ and Ψ are given by: *i*) the standard QSA and SHA expressions in Eqs. (3.4.22), and *ii*) the new parameterized expressions in Eqs. (3.4.36) and (3.4.37). Then, we use these solutions to find the evolution of the DE perturbations given by the standard procedure in Eqs. (3.4.23) and (3.4.25), and the second-order SHA expressions in Eqs. (3.4.38)-(3.4.40). We compare these results against full numerical solutions where no approximations are assumed. This will allow us to assess the relevance of the $O(\varepsilon^2)$ correction terms to the standard results.

Full Numerical Solution

It is desirable to solve the full set of linear equations in Eqs. (3.4.6)-(3.4.9) complemented with the continuity equations in Eqs. (3.2.11) and (3.2.12). However, this set of equations is highly unstable, and typical numerical methods do not yield to reliable results. In Ref. [381], this problem was solved by rendering the perturbation equations in a more treatable numerical way which we describe in the following.

Multiplying the "Time-Space" equation (3.4.7) by $-3H$ and using the "Time-Time" equation

to $k \approx 200 H_0$.

[15]The scale of nonlinearities k_{NL} is defined as the scale for which the "dimensionless" linear matter spectrum is equal to 1. In the case of ΛCDM, it is given by $k_{\mathrm{NL}} \approx 0.25\, h/\mathrm{Mpc}$ today [403].

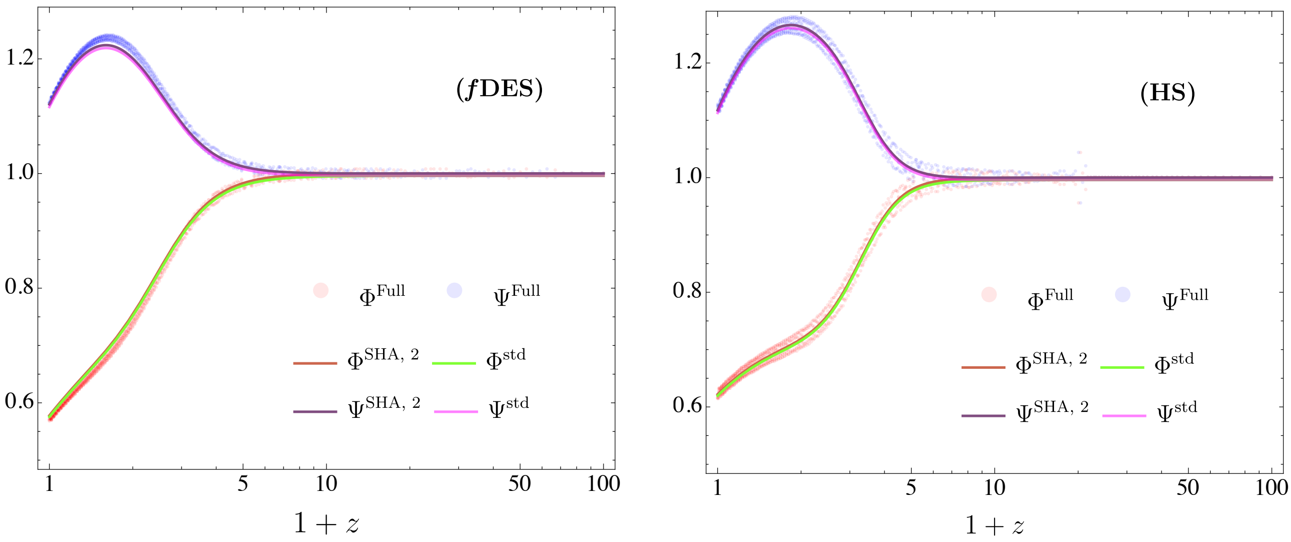

Figure 3.4.2: Comparison of the potentials Φ and Ψ obtained from the full numerical solution (Full), from the standard QSA-SHA procedure (std), and from our new approach (SHA, 2). Left panel corresponds to the results for the fDES model, while the right panel corresponds to the results for the HS model. For the plots we used $k = 0.1\,h/\mathrm{Mpc}$.

(3.4.6) we get the following Poisson-like equation

$$\frac{k^2}{a^2}(\Phi - \Psi)F = \kappa\bar{\rho}_m\Delta_m - 3\dot{F}\dot{\Phi} - 3F\dot{H}\Phi + (3H\dot{F} - 3F\dot{H})\Psi, \tag{3.4.50}$$

where we have defined the matter comoving density perturbation

$$\Delta_m = \delta_m + \frac{3aHV_m}{k^2}. \tag{3.4.51}$$

Now, we define the variables

$$\Phi_+ = \frac{1}{2}(\Phi - \Psi), \qquad \zeta = -F(\Phi + \Psi). \tag{3.4.52}$$

The evolution equations for these new variables can be obtained from the "Time-Space" equation (3.4.7) and the Poisson-like equation (3.4.50). We get

$$\Phi'_+ = -\frac{a\kappa\bar{\rho}_m V_m}{2FHk^2} - \left(1 + \frac{F'}{2F}\right)\Phi_+ - \frac{3F'}{4F^2}\zeta, \tag{3.4.53}$$

$$\zeta' = -\frac{2\kappa\bar{\rho}_m\Delta_m}{3H^2}\frac{F}{F'} + \left(1 + \frac{F'}{F} - 2\frac{F}{F'}\frac{H'}{H}\right)\zeta + 2F\Phi'_+ + 2F\left(1 + \frac{2}{3}\frac{k^2}{a^2H^2}\frac{F^2}{F'}\right)\Phi_+, \tag{3.4.54}$$

where a quote ' means derivative with respect to the number of e-folds, which is related to the time-derivative by $\mathrm{d}N \equiv H\mathrm{d}t$. These equations are complemented with the equations for V_m

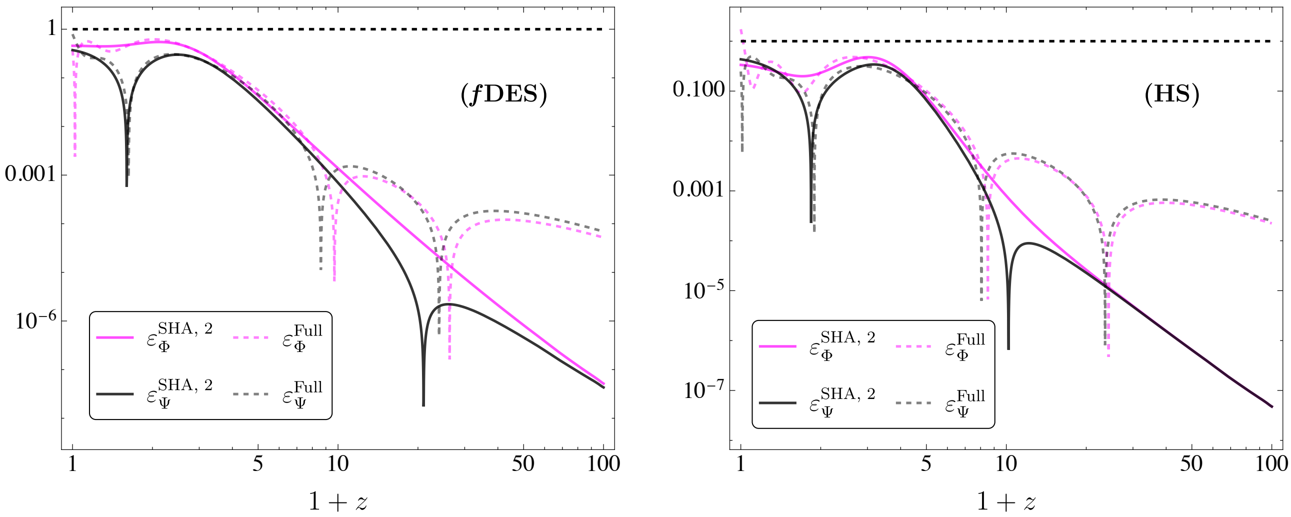

Figure 3.4.3: Evolution of the QSA parameters ε_Φ and ε_Ψ defined in Eqs. (3.4.29). For both models (fDES on the left panel and HS on the right panel), these parameters are small during the matter dominated epoch and significantly increase around the matter-DE transition. However, they are always suppressed by ε^2 and thus third-order terms, $(\varepsilon_\Phi \times \varepsilon^2)$ for example, are negligible.

and δ_m in Eqs. (3.2.12) and (3.2.11), having in mind that the relation between scale factor-derivatives and e-folds-derivatives is $\mathrm{d}a \equiv a\mathrm{d}N$. We assume that there are no deviations from GR at early times, then the initial conditions are

$$\Phi_{+,i} = 1, \qquad \zeta_i = 0, \qquad V_{m,i} = -\frac{2}{3}\frac{k^2}{a_i H_i}\Phi_{+,i}, \qquad \Delta_{m,i} = \frac{2k^2}{3a_i^2 H_i^2}\Phi_{+,i}, \tag{3.4.55}$$

where the expressions for $V_{m,i}$ and $\Delta_{m,i}$ correspond to the simplification of the "Time-Space" equation (3.4.7) and the Poisson equation (3.4.50) in matter dominance, i.e., taking $H^2 = H_0^2\Omega_{m0}a^{-3}$, and assuming that early modifications to GR are negligible. For H_i, we choose $a_i = 10^{-3}$ ($z \approx 1000$) ensuring initial conditions well within the matter epoch, right after decoupling.

3.4.6 Comparing Results

In this section, we compare the full numerical solutions, which are obtained using the approach described in the last section, the standard QSA-SHA results (see Sec. 3.4.2), and the results from our new parameterization described in Sec. 3.4.3, for the two models considered, namely, the fDES model and the HS model.

Gravitational Potentials

In order to solve the evolution equations for δ_m and V_m in Eqs. (3.2.11) and (3.2.12), we replace the analytic expressions for the potentials Φ and Ψ from either the standard procedure in Eqs. (3.4.22) or our new expressions in Eqs. (3.4.36) and (3.4.37), using the initial conditions [405]:

$$\delta_{m,i} = \delta_i \, a_i \left(1 + 3\frac{a_i^2 H^2(a_i)}{k^2}\right), \quad V_{m,i} = -\delta_i \, H_0 \, \Omega_{m0} \, a_i^{1/2}. \tag{3.4.56}$$

where the overall factor δ_i is set to unity. Then, knowing δ_m it is possible to track the evolution of the potentials and, consequently, of the DE perturbations.

As it can be seen in Fig. 3.4.2, the full solutions for the potentials for the two models undergo very rapid oscillations with small amplitudes, i.e., they remain well-behaved. This oscillatory behavior was also pointed out in Refs. [381, 406], where it was attributed to the evolution of δR, this being a generic feature of $f(R)$ models. In both plots, left-panel for the fDES model and right panel for the HS model, we can see that the standard QSA-SHA procedure and our new approach give accurate approximations to the full numerical solutions. On these scales, $k = 0.1\, h/\mathrm{Mpc}$, $\varepsilon^2 \ll 1$ and thus the second-order correction terms to the standard QSA-SHA are not compelling.

From the results for the potentials, it is possible to compute the QSA parameters ε_Φ and ε_Ψ in order to determine the time and scale validity regimes of the QSA; as we did for the SHA in Sec. 3.4.4. As depicted in Fig. 3.4.3, these parameters are very small ($\ll 10^{-3}$) during the whole matter dominated epoch, with a significant increasing at later times. However, as mentioned before, these parameters are always coupled to ε^2 in the expression for the potentials in Eqs. (3.4.34) and (3.4.35). Therefore, they are subdominant in comparison with purely ε^2 terms. We then conclude that in the case of $f(R)$ models under consideration, the assumption that the contributions of the time-derivatives of the potentials to the cosmological dynamics are negligible can be safely applied for the scales when the SHA is also applicable.

Dark Energy Perturbations

From the results for the potentials, it is possible to compute the full DE perturbations using Eqs. (3.4.12)-(3.4.15). As shown in Fig. 3.4.4, the contribution from correction terms to the standard QSA-SHA results are hardly noticeable in the evolution of δ_{DE}. Nonetheless, from the corresponding subplots, we can distinguish that some differences arise. In general, we define the percentage difference of an approximated quantity X_{Approx} (whether it is obtained from the standard approach or our new approach) with respect to the corresponding full numerical

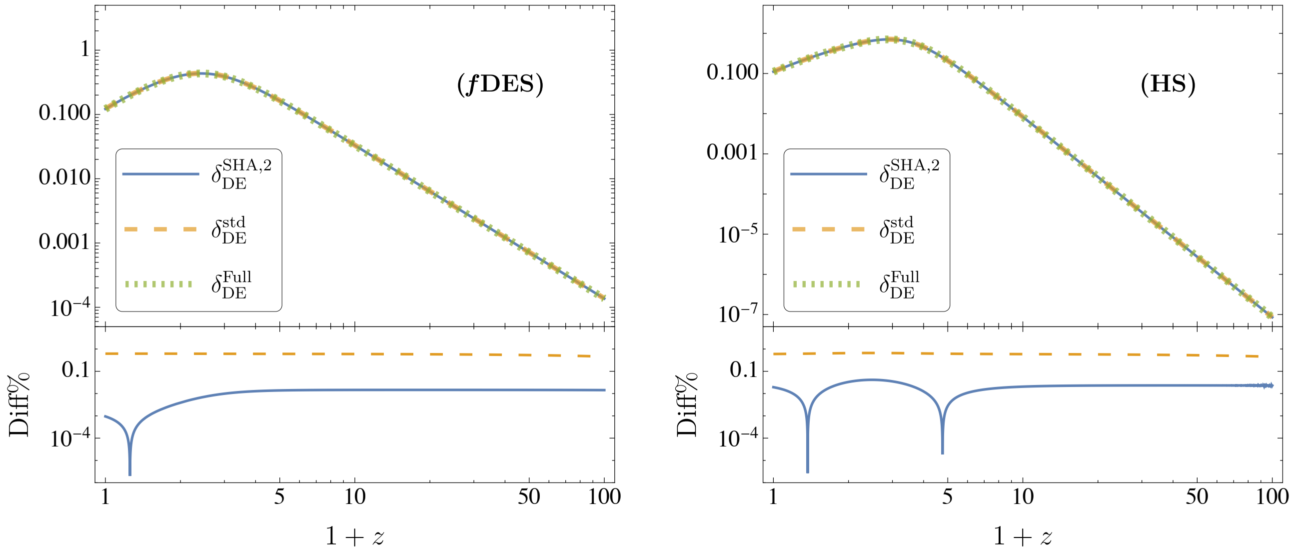

Figure 3.4.4: Comparison of the DE contrast $\delta_{\rm DE}$ obtained from full numerical solution, the standard QSA-SHA approach, and our new parameterization. For both models (fDES on the left panel and HS on the right panel), both descriptions are accurate at sub-percent level. However, it is noteworthy that our approach improve over the standard result by around two orders of magnitude.

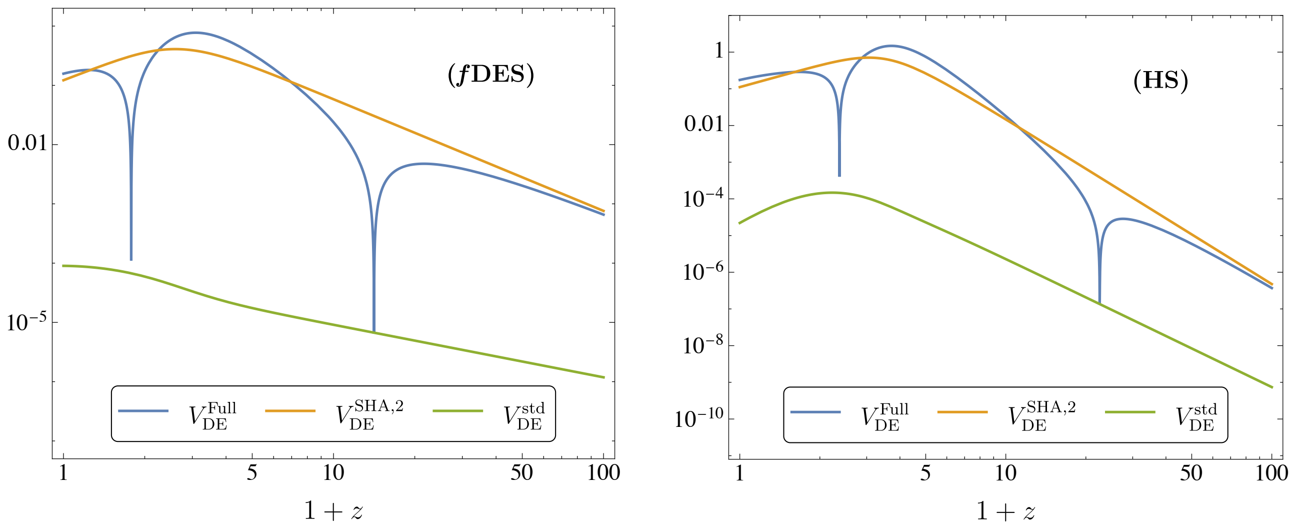

Figure 3.4.5: Comparison of the DE scalar velocity obtained from full numerical solution, the standard QSA-SHA procedure, and our new parameterization. For both models (fDES on the left panel and HS on the right panel), we see that our expressions show overall agreement with the full $V_{\rm DE}$, while the standard result is far smaller. This is due to $V_{\rm DE}^{\rm std}$ is a third-order expression in the new SHA parameterization.

solution $X_{\rm Full}$ as

$$\text{Diff\%} = \left| \frac{X_{\rm Full} - X_{\rm Approx}}{X_{\rm Full}} \right| \times 100. \tag{3.4.57}$$

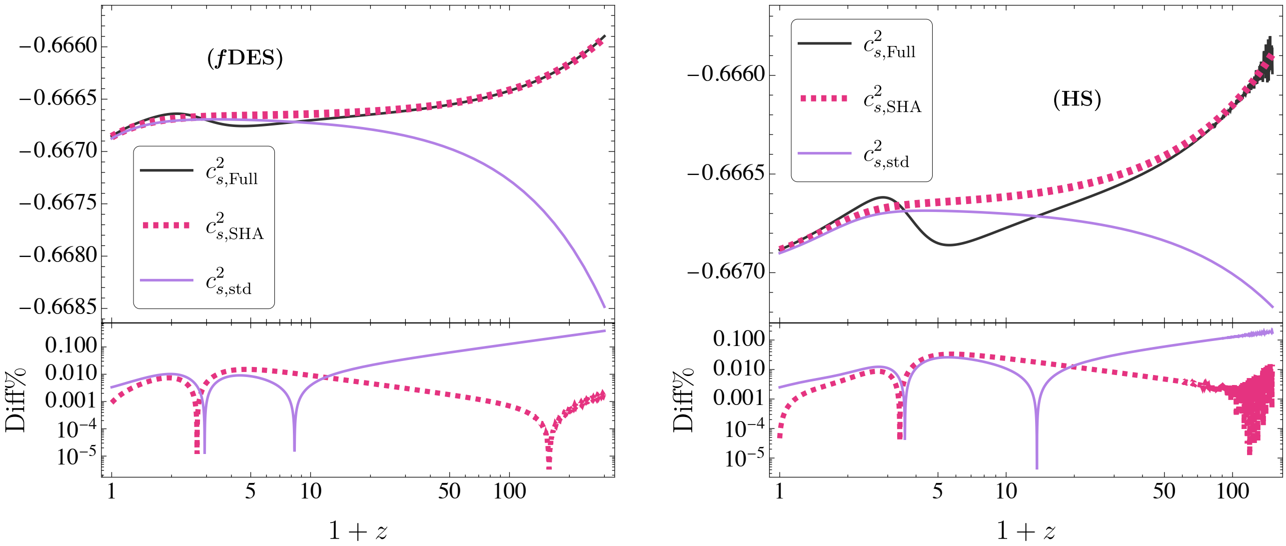

Figure 3.4.6: Comparison of the DE sound speed obtained from full numerical solution, the standard QSA-SHA approach, and our new parameterization. For both models (fDES on the left panel and HS on the right panel), we see that both approaches give accurate results, however, our new scheme performs better at earlier times since the standard approach fails in accounting the decaying behavior of $c^2_{s,\mathrm{DE}}$ from matter dominance. This difference is due to the existence of second-order terms neglected in $\delta P^{\mathrm{std}}_{\mathrm{DE}}$, which only considers fourth and sixth-order corrections in the new SHA parameterization.

It is noteworthy from the subplots in Fig. 3.4.4 that the simple extensions from our approach to the standard QSA-SHA results improve the accuracy in the description for δ_{DE} by around two orders of magnitude. On the other side, as expected from the discussion in Sec. 3.4.2, there are significant differences between the DE scalar velocity given by the standard approach in Eq. (3.4.25) and our result at first-order in SHA parameters in Eq. (3.4.40). In Fig. 3.4.5, we note that V_{DE} given by the standard QSA-SHA procedure is far smaller than the full V_{DE}, while our second-order expression shows overall agreement for both models. It is possible to track the origin of this disagreement. Note that our expression for V_{DE} is a first-order expression in the ε-expansion, however, if we use our parameterization in the standard V_{DE} given in Eq. (3.4.25) we get

$$V^{\mathrm{std}}_{\mathrm{DE}} = \frac{3aF_R}{F}\frac{F+6\frac{k^2}{a^2}F_R}{F+3\frac{k^2}{a^2}F_R}(\delta+\xi-2)\kappa\bar{\rho}_m\delta_m\frac{k^3}{a^3}\varepsilon^3, \tag{3.4.58}$$

which clearly is a third-order expression in the new SHA parameterization. We verified that a similar problem arises in the case of the pressure perturbation, since the standard results for δP_{DE} considers fourth and sixth-order corrections when $\ddot{F}$ is written in terms of ε [see Eqs. (3.4.24) and (3.4.43)], while our expression considers second-order corrections [see Eq. (3.4.39)]. The impact of this difference can be seen in the evolution of the sound speed $c^2_{s,\mathrm{DE}} \equiv \delta P_{\mathrm{DE}}/\delta\rho_{\mathrm{DE}}$.

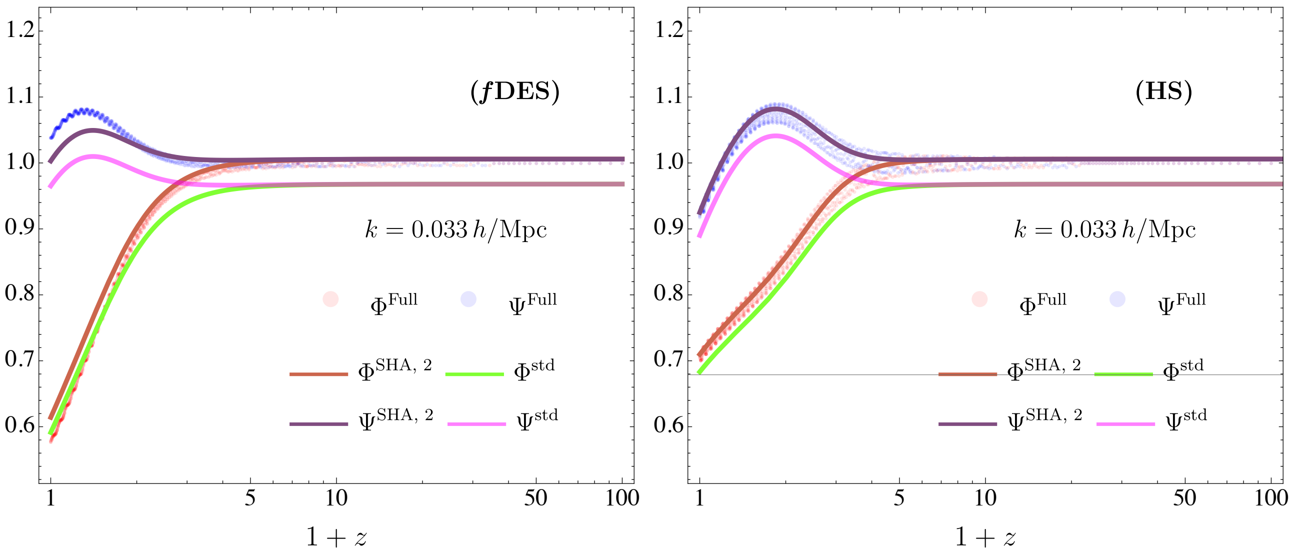

Figure 3.4.7: Comparison of the potentials for the fDES model (left panel) and the HS model (right panel) considering a value for k which is out of the "safety region", i.e., $k < 0.06\,h/\mathrm{Mpc}$. We see that the standard procedure provides less accurate results in contrast with the results from our approach, which is fairly acceptable for the HS model. However, in the case of the fDES model, results are not as accurate as in Fig. 3.4.2.

In Fig. 3.4.6, we can see that both methodologies provide accurate results for $c^2_{s,\mathrm{DE}}$. However, note that the standard approach fails in accounting the general trend of the DE sound speed to decay from matter domination to present days. Instead, our new scheme shows perfect agreement with this behavior, and thus performs better at early times, as it can be seen in the subplots of Fig. 3.4.6. To end this subsection, we would like to mention that in $f(R)$ theories, usually the sound speed is negative but the effective sound speed that also takes into account the DE anisotropic stress is always positive [371].

Other Scales

In order to test the "safety region" where the QSA and the SHA are applicable, namely $k \gtrsim 0.06\,h/\mathrm{Mpc}$, we compare the potentials obtained from the full solution considering $k = 0.033\,h/\mathrm{Mpc}$, and their corresponding results from the standard QSA-SHA procedure and our new approach. In the right panel Fig. 3.4.7, we see that in the case of the HS model, our zero-order expansion in QSA parameters and second-order expansion in SHA parameters expressions still provides fairly accurate descriptions of the potentials, while the potentials obtained from the standard procedure have an offset diminishing the accuracy of these expressions. This offset in the standard QSA-SHA expressions is also present in the fDES model, as it can be seen in the left panel of Fig. 3.4.7. Nonetheless, our new expressions also show deviations from the full solutions in this case. This indicates that both methods are not as accurate for $k = 0.033\,h/\mathrm{Mpc}$

(which is out of the safety region) as they are for $k = 0.1\,h/\mathrm{Mpc}$ (which is in the safety region), as can be seen in Fig. 3.4.2, and that the QSA parameters cannot be neglected anymore. As a final remark, we would like to mention that the "safety region" for the applicability of the QSA and the SHA, namely $0.06\,h/\mathrm{Mpc} \lesssim k \lesssim 0.2\,h/\mathrm{Mpc}$, is rather an estimation and not a general statement. The effectiveness of these approximations depends on the specific cosmological model and in this work we only studied models whose background are similar or equal to ΛCDM. However, we recall that $f(R)$ models with a very different background evolution in comparison to ΛCDM are tightly constrained by several tests [352, 381, 404].

3.4.7 Impact on Cosmological Observables

As we saw in the last section, some relevant terms are neglected in the DE perturbations when the standard QSA-SHA procedure is applied. So that, drastic modifications are taken into account for some quantities in our approach, e.g., the scalar velocity V_{DE} is raised by roughly three orders of magnitude (see Fig. 3.4.5), while some other quantities get minor corrections, such as the sound speed (see Fig. 3.4.6). Therefore, it is of great interest to assess the influence of these changes on cosmological observables or parameters used in forecasts. In particular, we will analyze the impact of DE perturbations on: *i*) the viscosity parameter which can be important in weak lensing experiments [407], and *ii*) the matter power spectrum and the CMB angular power spectrum using the `EFCLASS` branch [356] of the Boltzmann solver `CLASS` [343].

The Viscosity parameter

In the ΛCDM model, it is well known that the potentials are related by $\Phi = -\Psi$. As it can be seen in Eq. (3.4.10), this is not the case in $f(R)$, since this difference can be related to the anisotropic stress as shown in Eq. (3.4.15). Therefore, a detection of a non-zero anisotropic stress could favored MG theories over single-scalar field models which in general predicts a vanished π_{DE} [371, 408, 409]. The effect of the anisotropic stress can be modelled by introducing a viscosity parameter that appears in the right hand-side of an effective DE anisotropic stress Boltzmann equation of the form [410]:

$$\dot{\sigma} + 3H\frac{c_a^2}{w}\sigma = \frac{8}{3}\frac{c_{\mathrm{vis}}^2}{(1+w)^2}\frac{V_{\mathrm{DE}}}{a}, \tag{3.4.59}$$

where $c_a^2 = w - \frac{\dot{w}}{3H(1+w)} = w - \frac{aw'}{3(1+w)}$ is the adiabatic sound speed. This can be inverted to solve for the viscosity parameter

$$c_{\mathrm{vis}}^2 = \frac{aH(1+w_{\mathrm{DE}})}{4wV_{\mathrm{DE}}}\left[3c_{a,\mathrm{DE}}^2(1+w_{\mathrm{DE}})\pi_{\mathrm{DE}} + w\left(a\pi_{\mathrm{DE}}' - 3w\pi_{\mathrm{DE}}\right)\right], \tag{3.4.60}$$

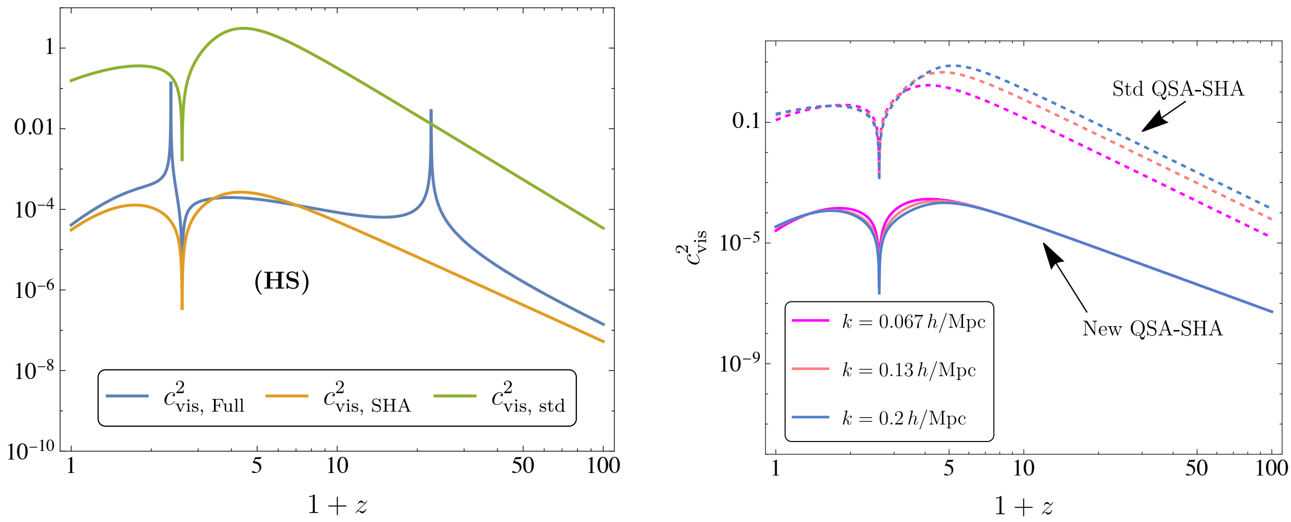

Figure 3.4.8: $c^2_{\rm vis}$ for the HS model. Left: Comparison between $c^2_{\rm vis}$ computed from the standard approach and our new approach for three values of k. We see that the standard approach predicts a large viscosity parameter, while our method predicts a small one. Right: Comparison of $c^2_{\rm vis}$ obtained from the standard approach, our new approach, and the full solution considering $k = 0.1\,h/\text{Mpc}$. We see that the evolution obtained using our new SHA parameterization (mustard line) agrees in overall with the full numerical solution (blue line), while the result obtained from the standard QSA-SHA procedure (green line) gives a large over-estimation of this parameter.

which is a function of the scale factor [356, 407, 410]. From the last equation, it is clear that a large modification to $V_{\rm DE}$ could strongly impact the evolution of the viscosity parameter. In the left panel of Fig. 3.4.8, we compute $c^2_{\rm vis}$ in the HS model considering three values of k in the safety region, namely $0.067\,h/\text{Mpc}$, $0.13\,h/\text{Mpc}$, and $0.2\,h/\text{Mpc}$. We can see that the viscosity parameter computed using the standard procedure reaches values greater than 1 for $z \sim 10$, in contrast, this parameter computed using our new approach remains small. In the right panel, we verify that, for $k = 0.1\,h/\text{Mpc}$, the parameter $c^2_{\rm vis}$ computed using our new parameterization is in overall agreement with respect to the full solution, while the computation using the standard approach over-estimates this parameter by several orders of magnitude. In Ref. [407], it was found that a small viscosity, around $c^2_{\rm vis} \sim 10^{-4}$ for the wCDM model, could be detected by Euclid when weak lensing and galaxy clustering data are combined. Although in Ref. [407], the viscosity parameter was taken as a constant, which is not realistic in a general dark energy scenario as was pointed out in Ref. [356], if we take this constant value as a representative value of the smallness of $c^2_{\rm vis}$, we see that our new parameterization indeed agrees with it.

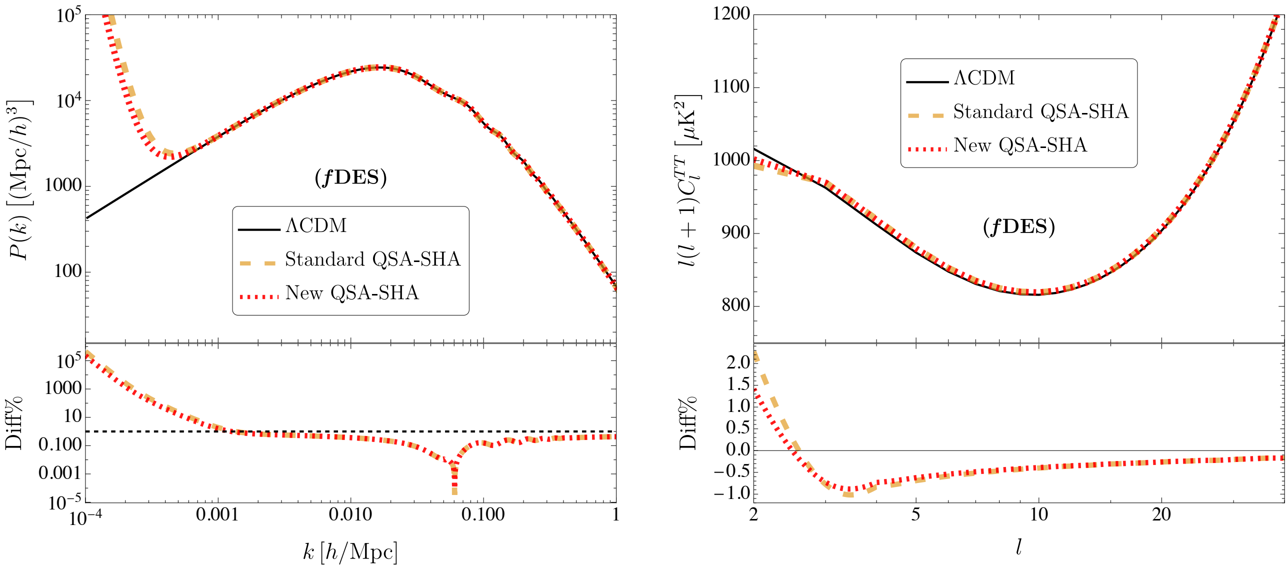

Figure 3.4.9: TT CMB power spectrum for low-l multipoles (left) and matter power spectrum (right) in the fDES and ΛCDM models. We see that the results from both approximation schemes are practically indistinguishable for $l \gtrsim 5$ in the case of the CMB spectrum and for $k \gtrsim 0.001\, h/\text{Mpc}$ in the case of $P(k)$. For lower multipoles, we see some minor differences, while for smaller values of k both methods give divergent results, mainly due to that the SHA is not applicable.

Linear Power Spectra

In Fig. 3.4.9 we plot the low-l multipoles of the CMB angular power spectrum (left), and the linear matter power spectrum (right) for the fDES model using the standard QSA-SHA procedure and our new approach. We plot the ΛCDM Planck best-fit 2018 standard result in both cases for comparison. In the case of the CMB power spectrum, we see that the fDES model do not apart significantly from the ΛCDM prediction, and only at the lowest multipoles ($l < 5$) both approximation scheme differ. However, this difference is not representative (less than 1%). For the matter power spectrum, we note that the standard approach and the new approach predictions for $P(k)$ are completely degenerate for modes $k \gtrsim 0.001\, h/\text{Mpc}$. For smaller modes, or equivalently for larger scales, both schemes yield to divergent results. This divergent behavior is common in theories where the QSA-SHA are assumed (see e.g. Ref. [8] where a similar divergency was found in the context of Scalar-Vector-Tensor theories [140, 341]). As mentioned in previous sections, we do not expect the QSA and the SHA hold for modes smaller than $k < 0.067\, h/\text{Mpc}$. Moreover, note that in the region $k \lesssim k_{\text{eq}}$, where k_{eq} is the mode entering the horizon at the radiation-matter equilibrium, radiation is not negligible anymore. Therefore, the expansion history cannot be described using the Hubble parameter and the perturbations do not follow equations similar to Eqs. (3.2.6)-(3.2.9).

Notice that although our new QSA-SHA scheme provide more accurate descriptions of the DE perturbations than the standard approach, this improvement is not reflected in the linear spectra in Fig. 3.4.9. We realized that $V_{\rm DE}$ is a dimensionful quantity, and thus it has to be compared with quantities with the same dimensions. In the case of the linear observables, they are mainly affected by the comoving density perturbation defined as

$$\Delta_{\rm DE} \equiv \delta_{\rm DE} + \frac{3aH}{k^2} V_{\rm DE}, \tag{3.4.61}$$

which is a gauge invariant quantity. For sub-horizon modes, the term $HV_{\rm DE}/k^2$ is completely negligible and $\Delta_{\rm DE} \approx \delta_{\rm DE}$. Since the standard approach indeed provides fairly accurate results for the potentials Φ and Ψ, and for the density contrast $\delta_{\rm DE}$, it is no a surprise that the improvement on these quantities do not represent a major modification on the linear observables in the scales where these approximations are valid.

Codes

Several codes with the main results presented here can be found in the GitHub repository https://github.com/BayronO/QSA-SHA-for-Modified-Gravity of BOQ.

3.4.8 Conclusions

In this work, we have revisited the quasi-static and sub-horizon approximations when applied to $f(R)$ theories. We do so by proposing a parameterization using slow-rolling functions (like in inflation) which allowed us to track the relevance of time-derivatives of the gravitational potentials and the scale k in contrast to the expansion rate H [see Eqs. (3.4.28) and (3.4.29)]. In the effective fluid approach to $f(R)$, we showed that the standard QSA-SHA results found in the literature [Eqs. (3.4.22)-(3.4.26)] correspond to the 0 order expansion in our new scheme. In particular, we showed that second-order corrections can improve the description of the dark energy perturbations by several orders of magnitude in most cases, e.g., $\delta_{\rm DE}$ (see Fig. 3.4.4), and turned out to be significant for some DE effective fluid quantities. In particular, we found large differences in the DE scalar velocity $V_{\rm DE}$ (see Fig. 3.4.5) and a minor correction in the sound speed $c^2_{s,{\rm DE}}$ which increases the accuracy of the approximations during the matter dominated epoch (see Fig. 3.4.6). The accuracy of our expressions [Eqs. (3.4.36)-(3.4.41)], and the standard QSA-SHA results, were assessed by comparing with results obtained from a full numerical solution of the linear perturbation equations. We found general agreement between the results from our new expressions and the full numerical solution where no approximations are assumed.

We estimated a "safety region" where the QSA and the SHA can be applied. We found that the QSA and the second-order expansion in the SHA yield very accurate results from matter domination ($z \lesssim 100$) to the present ($z = 0$) whenever $k \gtrsim 0.067\,h/\mathrm{Mpc}$. We also showed for a particular value out of this region the loss of accuracy of these approximations (see Fig. 3.4.7). This can also be seen in the matter power spectrum depicted in the right panel of Fig. 3.4.9, where we can see that the curves diverge for k small. We would like to stress that a similar divergent behavior was found in Ref. [8]. However, note that previous works on Horndeski theories [357], and Scalar-Vector-Tensor theories [8], where these approximations were used, all of them agree, in their corresponding limits, with the standard expressions in $f(R)$. In the case of the lowest multipoles of the CMB power spectrum, and in general for the matter power spectrum, the improvement in the accuracy from our expressions do not imply a corresponding improvement in these linear observables. This was expected since the QSA-SHA indeed provide accurate descriptions of the potentials Φ and Ψ, and the density contrast δ_{DE}. In the particular case of the scalar velocity V_{DE}, the large difference between the standard prediction and our new prediction is not relevant for these observables, since the term V_{DE}/k^2 is completely sub-dominant for sub-horizon scales.

We want to stress that the main goal of this work was to provide a transparent framework to track the relevance of each term in the perturbation equations, in order to clarify the application of the QSA-SHA when applied to modified gravity theories. To conclude, clearly our results warrant performing a more in-depth analysis of the validity of the QSA and the SHA approximations in more generalized MG theories, e.g., of the Horndeski type, however we leave this for future work.

Chapter 4

Inflation

4.1 Introduction

Inflation, an early accelerated expansion of the Universe, is arguably the most compelling theory to overcome the classical problems of the hot big bang cosmology while providing the seeds for large scale structure formation [411]. The simplest inflationary models are based in the dynamics of a scalar field, the inflaton. Although the inflaton is generally favored by data [218], some particular characteristics observed in the cosmic microwave background (CMB), known as CMB anomalies, suggest that modifications to this paradigm might be needed. For instance, careful analysis of the CMB indicates an asymmetry in the dipolar power spectrum on large angular scales [412–414]. This particular problem, which has the largest statistical significance among the different anomalies involving a preferred direction in the CMB sky[1] [415], motivates the study of alternative models based on other types of fields.

In this chapter, we analyze some of the implications, related to the inflationary era, when a vector field plays a primary role in the cosmological dynamics. In particular, we revisit the inflationary dynamics of a massive non-abelian gauge vector field, and the interplay between an abelian vector field and a geometric invariant in the curvaton mechanism.

4.2 Non-Abelian Gauge Vector Fields

4.2.1 Introduction

As mentioned above, the most popular models to account for the inflationary period and the current accelerated expansion of the Universe are based on single scalar fields. Despite the successes of these theories, other interesting alternatives, built with different types of fields, have been also explored. In this direction, models that include vector fields (see Refs. [160, 166–168] for reviews on the subject), higher spin fields [169–174], p-forms [124, 175–179], among others,

[1] For a review of the cosmic anomalies see Refs. [112, 113].

have called the attention within the past years because of their richer phenomenology and since many of their cosmological consequences have not been fully explored so far. Between these proposals, non-Abelian gauge fields have recently attracted a lot of attention since they could link cosmology with the phenomenology of particle physics [167]. The cosmological dynamics of these fields have been extensively discussed in the literature [151, 182–190, 193–195]. For instance, the early and the late-time accelerated expansions can be uniquely explained by non-Abelian gauge vector fields. These models are known as "gaugeflation" [151, 184] and "gaugessence" [125], respectively. Regarding the early accelerated expansion, gaugeflation was ruled out as a valid inflationary model, since the relation between the scalar spectral tilt and the tensor-to-scalar ratio does not get in the region allowed by Planck 2013 [416, 417]. Nevertheless, the introduction of a mass term in the theory can alleviate the problem [193, 195]. Some of the background inflationary trajectories of this proposal were studied in Refs. [193, 195], where it was concluded that, in particular, the addition of the mass term does not affect the existence of an inflationary period but it does reduce its length. Here, by using a dynamical system approach, we find the full available parameter space of this model and show that the inclusion of the mass term actually increases the length of inflation, instead of reducing it. We also remark that this particular result could yield to modifications at the linear perturbation level as worked out in Ref. [195].

4.2.2 Inflation from gauge fields

Let us consider the following action for a massive SU(2) gauge vector field

$$S = \int \mathrm{d}^4x\sqrt{-\tilde{g}}\Big[\frac{m_{\mathrm{P}}^2}{2}R - \frac{1}{4}F^a{}_{\mu\nu}F_a{}^{\mu\nu} + \frac{\kappa}{96}\left(\tilde{F}_a{}^{\mu\nu}F^a{}_{\mu\nu}\right)^2 - \frac{1}{2}m_a^2 A^a{}_\mu A_a{}^\mu\Big], \tag{4.2.1}$$

where $\tilde{g}$ is the determinant of the metric, κ is a positive-definite constant with dimensions $[m_{\mathrm{P}}^{-4}]$, $F^a{}_{\mu\nu}$ is the field strength tensor

$$F^a{}_{\mu\nu} \equiv \partial_\mu A^a{}_\nu - \partial_\nu A^a{}_\mu + g\,\varepsilon^a{}_{bc}A^b{}_\mu A^c{}_\nu, \tag{4.2.2}$$

of a non-Abelian gauge vector field $A^a{}_\mu$ with mass m_a, g is the SU(2) coupling constant and $\varepsilon^a{}_{bc}$ being the Levi-Civita symbol. The dual of the strength tensor is defined as usual by

$$\tilde{F}_a{}^{\mu\nu} \equiv \frac{1}{2}\varepsilon^{\mu\nu\rho\sigma}F^a{}_{\rho\sigma}, \tag{4.2.3}$$

with $\varepsilon^{\mu\nu\rho\sigma}$ denoting the completely antisymmetric tensor. This action was first studied in Ref. [193], in the context of inflation, as a modification of the original model in Ref. [184] where massless fields were considered.

In a FLRW spacetime, an ansatz for the massive gauge vector field consistent with the symmetries of this spacetime is [149]

$$A^a{}_0 \equiv 0, \quad A^a{}_i \equiv a(t)\psi(t)\delta^a{}_i, \tag{4.2.4}$$

where $\psi(t)$ is a scalar field. As a shorthand notation, we define $\phi(t) \equiv a(t)\psi(t)$. Isotropy also requires that the gauge fields have identical masses, i.e. $m_1 = m_2 = m_3 = m$.

The dynamics of this model, neglecting matter and radiation, was computed in chapter 2.5. We recall the energy tensor of the model

$$T_{\mu\nu} = F^a{}_{\mu\rho}F^a{}_{\nu\sigma}g^{\sigma\rho} + m^2 A^a{}_\mu A^a{}_\nu - g_{\mu\nu}\left[\frac{1}{4}F_a{}^{\rho\sigma}F^a{}_{\rho\sigma} + \frac{\kappa}{96}\left(\tilde{F}_a{}^{\rho\sigma}F^a{}_{\rho\sigma}\right)^2 + \frac{1}{2}m^2 A_a{}^\lambda A^a{}_\lambda\right]. \tag{4.2.5}$$

and the density and pressure

$$\rho = \rho_{\rm YM} + \rho_\kappa + \rho_A, \quad p = \frac{1}{3}\rho_{\rm YM} - \rho_\kappa - \frac{1}{3}\rho_A, \tag{4.2.6}$$

where

$$\rho_{\rm YM} \equiv \frac{3}{2}\left(\frac{\dot{\phi}^2}{a^2} + \frac{g^2\phi^4}{a^4}\right), \quad \rho_\kappa \equiv \frac{3}{2}\kappa g^2\frac{\phi^4\dot{\phi}^2}{a^6}, \quad \rho_A \equiv \frac{3}{2}\frac{m^2\phi^2}{a^2}. \tag{4.2.7}$$

In this case, the Friedmann equations do note consider the existence of matter and radiation, hence

$$3m_{\rm P}^2 H^2 = \frac{3}{2}\left[\frac{\dot{\phi}^2}{a^2} + \frac{g^2\phi^4}{a^4} + \kappa g^2\frac{\phi^4\dot{\phi}^2}{a^6} + \frac{m^2\phi^2}{a^2}\right], \quad 2m_{\rm P}^2\dot{H} = -2\left[\frac{\dot{\phi}^2}{a^2} + \frac{g^2\phi^4}{a^4} + \frac{1}{2}\frac{m^2\phi^2}{a^2}\right], \tag{4.2.8}$$

The variation with respect to $A^a{}_\nu$ read

$$0 = \nabla_\mu\left[F_a{}^{\mu\nu} - \frac{\kappa}{12}\left(\tilde{F}_d{}^{\rho\sigma}F^d{}_{\rho\sigma}\right)\tilde{F}_a{}^{\mu\nu}\right] - m^2 A_a{}^\nu - g\varepsilon_c{}^{ab}A^c{}_\mu\left[F_b{}^{\mu\nu} - \frac{\kappa}{12}\left(\tilde{F}_d{}^{\rho\sigma}F^d{}_{\rho\sigma}\right)\tilde{F}_b{}^{\mu\nu}\right]. \tag{4.2.9}$$

and yields the equation of motion for the gauge field

$$0 = \frac{\ddot{\phi}}{a}\left(1 + \kappa g^2\frac{\phi^4}{a^4}\right) + \frac{H\dot{\phi}}{a}\left(1 - 3\kappa g^2\frac{\phi^4}{a^4}\right) + \frac{2g^2\phi^3}{a^3}\left(1 + \kappa\frac{\dot{\phi}^2}{a^2}\right) + m^2\frac{\phi}{a}. \tag{4.2.10}$$

Equations (4.2.8), and (4.2.10) give the dynamics of the inflationary phase. It is more convenient to recast a set of nonlinear equations in terms of dimensionless expansion variables [97]. In our case we choose

$$x \equiv \frac{1}{\sqrt{2}m_{\rm P}}\frac{\dot{\phi}}{aH}, \quad y \equiv \frac{1}{\sqrt{2}m_{\rm P}}\frac{g\,\phi^2}{a^2 H}, \quad w \equiv \frac{1}{\sqrt{2}m_{\rm P}}\frac{m\phi}{aH}, \quad z \equiv \frac{1}{\sqrt{2}m_{\rm P}}\frac{\phi}{a}. \tag{4.2.11}$$

The Friedmann equation in Eq. (4.2.8) becomes the constraint

$$1 = x^2 + y^2 + w^2 + 4\alpha x^2 z^4, \tag{4.2.12}$$

from which we can write the variable y as a function of the other variables and a dimensionless parameter defined as $\alpha \equiv m_{\rm P}^4\,\kappa g^2$. By changing the cosmic time t with the number of e-folds N defined by $\mathrm{d}N \equiv H\mathrm{d}t$, and taking into account Eqs. (4.2.8), (4.2.10) and the constraint in Eq. (4.2.12), we can write the evolution equation for each independent variable as follows:

$$\begin{aligned} x' &= x(\epsilon - 1) \\ &\quad - \left(1 + 4\alpha z^4\right)^{-1}\left[\frac{2}{z}(1 - x^2) + x\left(1 - 12\alpha z^4\right) - \frac{w^2}{z}\right], && (4.2.13) \\ w' &= w\left(\frac{x}{z} + \epsilon - 1\right), && (4.2.14) \\ z' &= x - z && (4.2.15) \end{aligned}$$

where a prime denotes derivative with respect to N, and

$$\epsilon \equiv -\frac{\dot{H}}{H^2} = 2 - 8\alpha x^2 z^4 - w^2, \tag{4.2.16}$$

is the slow-roll parameter.

It is possible to calculate the expected number of e-folds of inflation at first order in the slow-roll approximation. Here we show the result for later use [193]

$$N \approx \frac{1 + \gamma_i + \omega_i/2}{2\epsilon_i}\ \ln\left(\frac{1 + \gamma_i + \omega_i/2}{\gamma_i + \omega_i/2}\right), \tag{4.2.17}$$

where

$$\gamma \equiv \frac{g^2\psi^2}{H^2} = \frac{y^2}{z^2}, \quad \omega \equiv \frac{m^2}{H^2} = \frac{w^2}{z^2}, \tag{4.2.18}$$

and the subindex i indicates some initial time before the end of inflation.

For completeness, in the following subsection we first study the case where the gauge fields are massless.

Massless case

This model was first introduced in Ref. [184] as "gaugeflation". Although several inflationary trajectories were analyzed in Ref. [184], an exploration of the full available parameter space of the theory has not been performed yet and thus only a few particular valid trajectories are known. In the following, we find the parameter window where slow-roll dynamics take place.

The massless case is characterized by $m = 0$ or equivalently $w = 0$. Equation (4.2.14) is trivially satisfied and the dynamical system is reduced to Eqs. (4.2.13) and (4.2.15). The autonomous set has just one physically acceptable fixed point given by[2]

$$x = z = \sqrt{\frac{\sqrt[3]{\alpha} f_\alpha^2 - \sqrt[3]{3}}{2 f_\alpha \sqrt[3]{9\alpha^2}}}, \quad f_\alpha \equiv \left(9 + \sqrt{81 + \frac{3}{\alpha}}\right)^{1/3}. \tag{4.2.19}$$

This point exists for all positive α.

The slow-roll parameter in the fixed point is given by

$$\epsilon = 2 - 8\alpha z^6 = 2 - \frac{\left(f_\alpha^2 - \sqrt[3]{3/\alpha^3}\right)^3}{9 f_\alpha^3}. \tag{4.2.20}$$

Now, assuming the reasonably upper bound for enough slow-roll phase [283]

$$\epsilon < 10^{-2}, \tag{4.2.21}$$

we find that

$$\alpha > 1.99 \times 10^6, \tag{4.2.22}$$

hence, in the massless case, the only relevant parameter of the system has to be very large in order to inflation has a correct length.

The linear stability analysis shows that the fixed point is hyperbolic, i.e. the Jacobian matrix obtained from the dynamical system does not have any vanishing eigenvalue upon evaluation in the fixed point. We verified the behavior of the two eigenvalues as functions of the parameter α in the region where slow-roll solutions exist. We could see that one eigenvalue is positive, $\lambda_1 > 0$, and the other one is negative, $\lambda_2 < 0$, therefore the fixed point is a saddle in the space $\{x, z\}$. Moreover, we have corroborated that $\lambda_1 \to 0$ and $\lambda_2 \to -3$ when $\alpha \to \infty$. This means that gaugeflation naturally agrees with the fact that inflation is a transient phase of the Universe. Inflation as a saddle fixed point has been addressed in other works (e.g. see Refs. [418, 419]). Therefore, the dynamical analysis shows that the only fixed point of the system

[2]The fixed point is found upon regularization due to possible singularities in $z = 0$, and it is physically acceptable because the variables take real values and the Friedmann constraint (4.2.12) is satisfied.

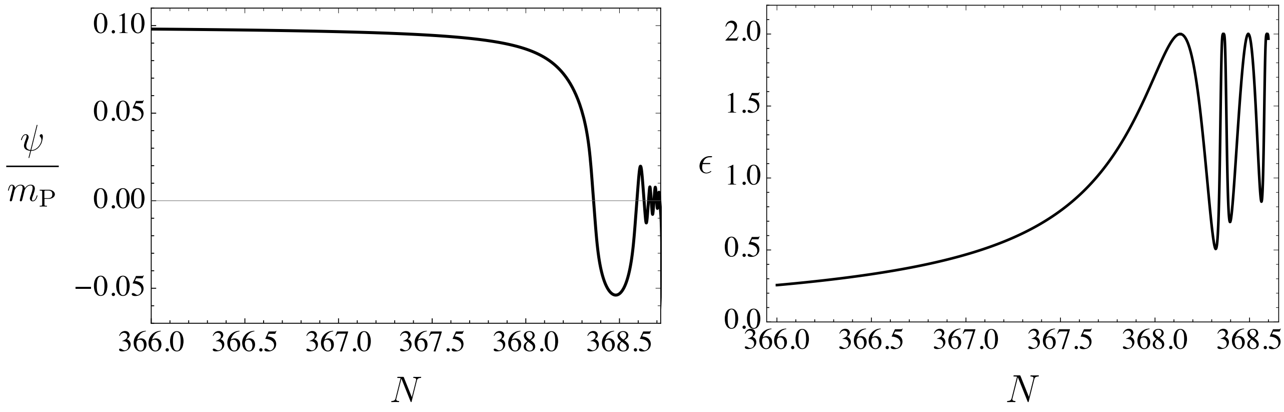

Figure 4.2.1: Evolution of the gauge field (Left) and the slow-roll parameter (Right). The field $\psi = \phi/a$ and the slow-roll parameter ϵ are nearly constant during inflation. The field suddenly decays while ϵ reaches its upper bound near to $N = 368$ around the value predicted in Eq. (4.2.26). The disagreement between these values is due to numerical approximation.

corresponds to a slow-roll inflationary solution for large α.

Now, we will proceed to present a numerical solution to see the behaviour of the system under specific initial conditions. In Ref. [184], each inflationary trajectory is specified by a set of four values[3] $\{\psi_i, \dot{\psi}_i; \kappa, g\}$. However, our dynamical analysis reveals that there is a particular point in the physical phase space $\{x, z\}$ which can be fully specified only by the parameter α, being very useful for fixing the initial conditions. As an example of this particular slow-roll trajectory in the massless case ($\omega = 0$), we choose

$$\alpha = 2 \times 10^6, \tag{4.2.23}$$

such that the variables in the fixed point in Eq. (4.2.19) are approximately

$$x_i = z_i \approx 0.0706517. \tag{4.2.24}$$

The function γ in Eq. (4.2.18) and the slow-roll parameter in Eq. (4.2.20) take the values

$$\gamma_i \approx 4.8 \times 10^{-4}, \quad \epsilon_i \approx 9.9 \times 10^{-3}, \tag{4.2.25}$$

which in Eq.(4.2.17) translates into

$$N \approx 383. \tag{4.2.26}$$

As it can be seen in the left part of Fig. 4.2.1, for the chosen initial conditions, the gauge

[3]Here, the subscript i means that the corresponding quantity is evaluated some time before the end of inflation.

field is nearly constant during inflation, then it suddenly falls off around $N = 368$ and starts to oscillate, showing good matching with the analytical results. As explained in Ref. [184], these oscillations are presented because $\rho_{\rm YM}$ becomes the dominant term at the end of inflation, and thus the system behaves as a quartic chaotic-like inflation theory. Support for this interpretation is given in the right part of Fig. 4.2.1 where we see that the slow-roll parameter is small during inflation and it grows around $N = 368$, oscillating and reaching its upper limit equal to 2, which represents a "dark radiation" domination epoch[4]. This is due to ϵ can be written as

$$\epsilon = 2\,\frac{\rho_{\rm YM}}{\rho_{\rm YM} + \rho_\kappa}. \tag{4.2.27}$$

Since the inflationary solution corresponds to a saddle fixed point, it is possible to find initial conditions that do not yield to slow-roll dynamics, i.e. inflation does not last enough time. For example, we can regard $x_i \neq z_i$, i.e. we choose a nonzero speed for the field as an initial condition. As expected, the main effect is a drastic reduction in the number of e-folds while generating bigger values for γ_i. For the same value of $\alpha = 2 \times 10^6$ and being careful about $y_i^2 > 0$ [remember the constraint in Eq. (4.2.12)], we consider the following initial values:

$$x_i = 0.070651, \quad z_i = 0.0706, \tag{4.2.28}$$

yielding to

$$\gamma_i = 0.58811, \quad \epsilon_i = 0.0158458, \tag{4.2.29}$$

and corresponding to

$$N \approx 49, \tag{4.2.30}$$

showing the great impact that a slight change in the speed of the field ($\dot{\psi}_i \approx 7.2 \times 10^{-5} H_i$) has on the evolution of the system. This feature is important since, at perturbative level, there are bounds on the possible values of γ (see Ref. [184]), and as shown in Ref. [417], the scalar perturbations present a strong tachyonic instability for $\gamma < 2$. Nonetheless, we do not care about these cumbersome features since we are only interested in the dynamical behaviour of the system at the background level.

From these numerical results, we also can give a rough estimation of the values of the parameters κ and g noticing that

$$\frac{H}{g} = \frac{\sqrt{2}z^2}{y}\, m_{\rm P}. \tag{4.2.31}$$

Although the energy scale of inflation is not known yet, the preferred scale is $H \lesssim 10^{-5} m_{\rm P}$.

[4]By dark radiation we mean the "radiation" associated to the Yang-Mills term.

Then, supposing $H_i = 3.5 \times 10^{-5} m_{\rm P}$ and using the first set of initial conditions we get

$$g \approx 7.6 \times 10^{-6}, \quad \kappa \approx 3.4 \times 10^{16}\ m_{\rm P}^{-4}. \tag{4.2.32}$$

These parameters were estimated in Ref. [184] after a linear perturbation treatment of the theory in order to agree with the observational data available at that time [420]. However, here we have shown that it is possible to estimate the order of magnitude of them through a classical dynamical system approach in a much simpler way.

Massive case

At the background level, the gaugeflation scenario can solve the classical cosmological problems by producing an inflationary phase which lasts enough number of e-folds. Nonetheless, the main test of any inflationary model relies in its observational signatures, which are imprinted on the CMB data. In Ref. [417], it was shown that some difficulties arise at the linear perturbative level: for $\gamma < 2$, the scalar perturbations show a strong tachyonic instability, and, in the stable region $\gamma > 2$, any set of initial conditions does not exist that preserves the relation between the tensor-to-scalar ratio r and the spectral index n_s in the confidence region allowed by the results of Planck 2013 [416]. Then, it is clear that the theory requires some modifications in order to not be discarded by observations.

In Ref. [193] was proposed "massive gaugeflation", where an explicit gauge-symmetry breaking mass term was considered. In that work, some of the classical inflationary trajectories of the model were studied, showing that the introduction of the mass term does not harm the good features of the original gaugeflation model while having the potential to modify the n_s vs r relation. The linear perturbation theory was carried out in Ref. [195], where it was shown that the dynamics remain unstable for $\gamma < 2$, nonetheless the model can produce observationally viable spectra in the stable region, according to Planck 2013 [416].

In this case $m \neq 0$, implying $\omega \neq 0$, and so the dynamical system is given by the full set of Eqs. (4.2.13)-(4.2.15). The system has again only one physically acceptable point, where x and z take the same values in Eq. (4.2.19) and $w = 0$. Since $w = 0$, this point has the same properties as in the massless case: it exists for all α, the slow-roll parameter is the same in Eq. (4.2.20), and slow-roll solutions require a large α. This is not a surprise since the mass term does not contribute to the existence of an accelerated expansion. Note that in this case, we cannot fully specify the initial conditions for inflation only by fixing α since ω is not given in terms of α.

The linear stability analysis shows that this point is hyperbolic as well since there are no vanishing eigenvalues. We verified the behavior of these eigenvalues as functions of the parameter α in the region where slow-roll solutions exist. We noted that two eigenvalues are positive, $\lambda_1 > 0$ and $\lambda_2 > 0$, while the other one is negative, $\lambda_3 < 0$, therefore the fixed point is a saddle in the phase space $\{x, w, z\}$, as expected. We verified that $\lambda_1 \to 0$, $\lambda_2 \to 0$ and $\lambda_3 \to -3$ when $\alpha \to \infty$.

The eigenvalues λ_2 and λ_3 are the same λ_1 and λ_2 from the massless case, respectively. The new eigenvalue is λ_1. The eigenvector associated with λ_1 is $(0, 1, 0)$ in the space $\{x, w, z\}$, meaning that the variable w runs away from 0 to a greater value during inflation. This is expected since at the end of inflation the κ-term decays to zero and the Yang-Mills term or the mass term becomes dominant.

As mentioned before, the parameter α does not fully specify the initial conditions (unless $m = 0$), then we have to investigate the impact that the mass term, encoded in the function ω in Eq. (4.2.18), has on the inflationary phase.

Using Eq. (4.2.18), we can write the constraint in Eq. (4.2.12) as

$$y^2 = 1 - x^2(1 + 4\alpha z^4) - \omega^2 z^2. \tag{4.2.33}$$

From the last equation, it is clear that once α, x, and z are fixed, ω cannot take arbitrary values since it could push the variable y to complex values, which is physically unacceptable. Now, using the first set of initial conditions of the massless case:

$$\alpha = 2 \times 10^6, \quad x_i = z_i = 0.0706517, \tag{4.2.34}$$

we get

$$\omega_i < 0.00047539, \tag{4.2.35}$$

for $y_i^2 > 0$. Since y_i depends on the choice of ω_i, we note that γ_i will depend on this function through Eq. (4.2.18). Therefore the number of e-folds can be given only in terms of ω_i. As it can be seen in the right part of Fig. 4.2.2, the case $\omega_i = 0$ corresponds to $N \approx 382$ agreeing perfectly with the result given in Eq. (4.2.26). From this figure, it is clear the effect that the mass term has on the model: it increases the length of the inflationary phase. Furthermore, by using Eq. (4.2.18), Eq. (4.2.31) and the Friedmann constraint in Eq. (4.2.33) we can write N in terms of the mass m which yields to the same conclusion (see Appendix A of [3] for a detailed derivation). It is worth mentioning here the results given in Ref. [193]. In that work, the authors claim that the mass "reduces" the length of inflation, which they show in their Fig. 3. However, this opposite conclusion to ours is because the authors of Ref. [193] plot the number of e-folds as a function of $\sqrt{\omega_i}$ (fixing H_i) ignoring the relation between this function and γ_i through Friedmann equations, i.e. γ_i cannot be fixed if ω_i is varying.

As a complement to our qualitative and analytical results, we numerically integrate the full

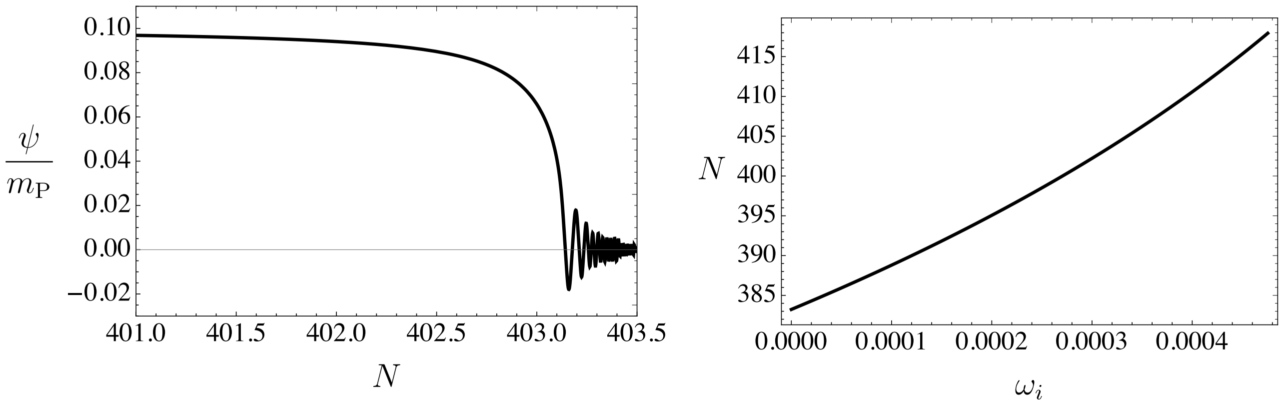

Figure 4.2.2: (Left) Evolution of the gauge field. The field suddenly decays around $N = 403$ as stated in Eq. (4.2.38). (Right) Number of e-folds in the function of ω_i. The mass term increases the length of the inflationary phase.

dynamical system in Eqs. (4.2.13)-(4.2.15). Choosing

$$\omega_i = 3 \times 10^{-4}, \tag{4.2.36}$$

we get

$$\gamma_i \approx 1.8 \times 10^{-4}, \quad \epsilon_i = 9.9 \times 10^{-3}, \tag{4.2.37}$$

and the expected number of e-folds

$$N \approx 402. \tag{4.2.38}$$

As can be seen in the left part of Fig. 4.2.2, for the chosen initial conditions, the gauge field is nearly constant during inflation, then it suddenly falls off around $N = 403$ and starts to oscillate, showing perfect matching with the analytical results.

It is also possible to consider greater values for ω_i, by regarding $x_i \neq z_i$. As in the massless gaugeflation model, this implies a nonzero speed for the field and it has the same effect here: it reduces the length of inflation. However, this does not cancel the effect of the mass term increasing this length as shown in the following. Taking the second set of initial conditions used in the massless case,

$$\alpha = 2 \times 10^6, \quad x_i = 0.070651, \quad z_i = 0.0706, \tag{4.2.39}$$

we get

$$\omega_i < 0.584146, \tag{4.2.40}$$

for $y_i^2 > 0$ from Eq. (4.2.33). So, choosing $\omega_i = 0.5$ we get $N \approx 69$ as the expected length of inflation although $\epsilon_i \approx 1.3 \times 10^{-2}$. Remember that with these initial conditions, the massless

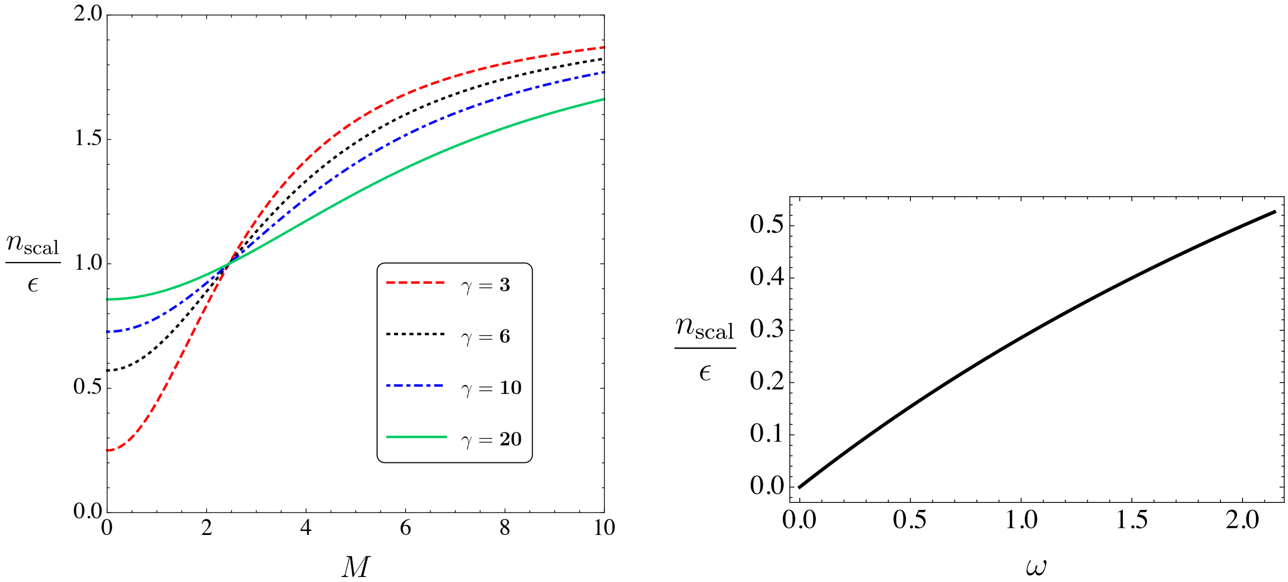

Figure 4.2.3: lot of the late-time decay of the scalar power spectrum $n_{\rm scal}/\epsilon$ as a function of the mass parameters given by Eq. (3.58) of [195]. Upper: result obtained when γ is fixed while $M = m/H$ can vary (see Fig. 5 of Ref. [195]). Lower: result obtained when the relation between γ and $\omega = M^2$ is considered.

model predicts $N \approx 49$ ruling it out as a viable inflationary solution.

From this analysis we can also estimate the values of the parameters κ and g, through Eq. (4.2.31). Using the energy scale $H_i = 3.5 \times 10^{-5} m_{\rm P}$ and using the second set of initial conditions we get

$$g \approx 10^{-4}, \quad \kappa \approx 1.9 \times 10^{14}\, m_{\rm P}^{-4}, \tag{4.2.41}$$

which are roughly of the order to the values estimated in Eq. (4.2.32) for the massless model.

Possible consequences at the perturbative level

From the analysis above we learn that once the constant α, the magnitude of the field ψ, and its speed $\psi' = \dot{\psi}/H$ are fixed, the parameters γ and ω are related by the Friedmann constraint in Eq. (4.2.12), in such a way that one cannot fix one of them while varying the other one. To elucidate the possible impact of the relation between γ and ω, we take a minimal example coming from the results obtained in Ref. [195] where the linear perturbation of the massive gaugeflation model was worked out. Assuming $\alpha = 10^9$, $x = 0.02509638$, $z = 0.02508$ and taking into account that y has to be real and $\gamma > 2$ in order to avoid tachyonic instabilities, we get the bound

$$\omega < 2.14366. \tag{4.2.42}$$

The late time decay rate of the scalar power spectrum is given by (see Eq. (3.58) of Ref. [195])

$$n_{\mathrm{scal}} = \epsilon \left[1 + \frac{M^2 - 6}{2\gamma + M^2 + 2} \right] . \tag{4.2.43}$$

In Figs. 4.2.3 we plot n_{scal} normalized to ϵ with respect to the mass parameter. The left part of Fig. 4.2.3 is the plot shown in Ref. [195], where γ is fixed and $M = m/H$ varies. The right part of Fig. 4.2.3 shows the result obtained when taking into account the relation between γ and ω, which of course corresponds to only one curve. We also found some differences between the plots of the chirality parameter [Eq. (3.114) of Ref. [195]] and those made by us, considering the relation between γ and ω. We want to stress that the perturbative analysis of the model is out of the scope of this work, and although the dependence between the parameters γ and ω has the potential to modify the scalar spectral index or the tensor-to-scalar ratio (as we see from the expression for n_{scal}), a full treatment of perturbations for the massive case is needed. We leave this complete examination for a future work, where we also plan to compare with the results given in Ref. [195], and also to see if the massive gaugeflation proposal can be (or not be) in agreement with the observational bounds.

4.2.3 Conclusions

In this work, we studied non-Abelian gauge vector fields endowed with SU(2) group representation as the unique source of inflation. In the inflationary scenario, it was shown that this primordial accelerated expansion can be driven solely by this kind of fields [184]. Since this model, known as gaugeflation, was ruled out by observations [417], several modifications to the original model have been proposed. In particular, the introduction of a mass term could ameliorate the tension [193, 195]. However, in these previous works, only some particular inflationary trajectories were analyzed. Here, by using a dynamical system approach, we have extended their results, finding the full available parameter space yielding to slow-roll inflationary solutions. We realized that slow-roll inflation is a saddle point in the phase space and thus this model provides a natural mechanism to end the inflationary period. We also found that the inclusion of the mass term increases the length of the slow-roll phase, instead of reducing it as claimed in Ref. [193]. This reduction is because the authors of Ref. [193] ignored the relation between the parameters γ_i and ω_i given by the Friedmann constraint, once the other initial conditions have been set. Hence an increase in ω_i implied an increase in the speed of the gauge field $\dot{\psi}_i$ yielding to a drastic reduction in the number of e-folds. Thereafter, we remark that our conclusion could modify the results obtained in Ref. [195] where the linear treatment of the model was worked out. For example, the relation between γ_i and ω_i changes the results of $n_{\mathrm{scal}}/\epsilon$ (see Fig. 4.2.3). To respond to this query, we plan to make a full treatment of perturbations for the massive case in a future work.

4.3 Vector Curvaton

4.3.1 Introduction

Single-field models, in which the inflationary expansion is driven by a scalar field minimally coupled to gravity, are clearly favored by data. Despite their excellent agreement with the available data, indications exist suggesting that single-field models might need to be extended. The most notorious among these indications are the possible presence of the so-called CMB anomalies (see for instance [59, 108, 112, 113] for an overview of some of them).

Although scalar fields have played a dominant role in inflationary cosmology, over the last decade it has been realized that vector fields may also have an important function provided their conformal symmetry is broken (see for instance [100, 140, 160, 166–168, 421] and references therein). This breaking, which can be brought about by the introduction of a mass term, for example, allows the vector field to obtain a superhorizon spectrum of perturbations during inflation. In turn, this opens up the possibility that the vector field becomes a curvaton and contributes to the curvature perturbation [422–431], for which the vector field must come to dominate (or nearly dominate) the energy density at a later epoch. However, the risk when considering the influence of vector fields in the cosmological dynamics is that, since they signal a preferred direction in space, they may result in an anisotropic expansion in excess of the current observational bounds. To quantify the level of statistical anisotropy[5] it is usual to parametrize the spectrum of the curvature perturbation as [432]

$$\mathcal{P}_\zeta(\boldsymbol{k}) = \mathcal{P}_\zeta^{\rm iso}(k)[1 + g(k)(\boldsymbol{d}\cdot\hat{\boldsymbol{k}})^2]\,, \tag{4.3.1}$$

where $\mathcal{P}_\zeta^{\rm iso}(k)$ denotes the isotropic part of the power spectrum, $g(k)$ is the so-called anisotropy parameter, which quantifies the statistical anisotropy in the spectrum $\mathcal{P}_\zeta$, $\boldsymbol{d}$ is the unit vector signaling the preferred direction, and $\hat{\boldsymbol{k}} \equiv \boldsymbol{k}/k$ is the unit vector along the wavevector $\boldsymbol{k}$ with modulus k. Observations from the Planck satellite suggests that g can be at most 0.97 [433], which represents a very tight constraint on the contribution of vector fields to the power spectrum of the CMB. Nevertheless, if the isotropy of the expansion is approximately preserved, vector fields could even be responsible for inflation [434–438]. The requirement in this case is to have either a large number (typically in the hundredths) of randomly oriented vector fields so that they collectively generate a nearly isotropic expansion, or consider three mutually orthogonal vector fields with equal vev [434]. It is also possible to retain an isotropic inflationary expansion by considering the dynamics of gauge vector fields. This is the case of gaugeflation

[5] We distinguish between background anisotropy from statistical anisotropy, given that the latter is perturbative in origin.

[193, 195, 196, 439–441], in which a nonabelian gauge field minimally coupled to gravity plays the role of the inflaton. In this proposal, an SU(2) gauge field is considered to form a triad of mutually orthogonal vectors, which in turn allows the gauge field to drive inflation without giving rise to an anisotropic expansion.

An interesting manner to break the conformal invariance is by considering a non-minimally coupled vector field, thus resulting in a modification of gravity [424, 434–436]. Unfortunately, the non-minimal coupling to gravity is known to be problematic due to the emergence of instabilities [442–444]. Although the existence of these problems represents a serious drawback for the consistency of the theory, the very nature of the instabilities has been called into question, and a number of scenarios have been envisaged to evade them [430]. In this paper, we examine a cosmological vector field non-minimally coupled to gravity through the Gauss-Bonnet invariant. Although couplings between the Gauss-Bonnet invariant and scalar fields have been explored in the context of inflationary cosmology [445–468], the coupling with a massive vector field has not been sufficiently explored in the literature[6] [470]. Arguably, this is due to the very presence of instabilities in relatively simple settings, as in the case of a non-minimal coupling to the Ricci scalar, which then invites to exercise caution when considering more complicated non-minimal couplings. Nevertheless, the reason for us to invoke such a coupling owes to the peculiar behavior of the Gauss-Bonnet invariant. Indeed, a very crucial feature is that it changes its sign when passing from inflation to a matter or radiation dominated phase. Consequently, a mass term for the vector field, coming from this coupling, features the same change of sign towards the end of inflation. In the vector curvaton scenario [471], a negative mass-squared is required for the vector field to generate a nearly flat power spectrum, while a positive mass-squared is required for the vector field engages into quick oscillations after inflation, in order to avoid the generation of large background anisotropies if the vector field dominates the Universe. However, a clear mechanism producing this change of sign is not provided, and thus it has to be assumed [471]. In this regard, the goal of this work is to investigate whether a vector field coupled to this topological term can contribute significantly to the total energy density after inflation, thus being able to play the role of a curvaton. Two key assumptions are made in order to keep the isotropy in the expansion: *i*) the vector field is subdominant during inflation [471] and *ii*) after inflation the vector field conduct itself as a pressureless mater [471]. These assumptions allow us to safely use an isotropic and homogeneous spacetime, i.e. the Friedmann-Lemaître-Robertson-Walker (FLRW) metric.

[6] Non-minimal couplings of the electromagnetic field to gravity, in particular to the Gauss-Bonnet invariant, have been considered as a mechanism to generate large-scale magnetic fields during inflation [449, 469].

4.3.2 Vector field coupled to the Gauss-Bonnet invariant

On the instability of non-minimally coupled vector fields

An issue of fundamental importance concerning theories of massive vector fields non-minimally coupled to gravity is their instability [430, 442–444], which originates from the longitudinal mode of the vector field. One of the known instabilities is perturbative in origin and arises when the effective mass squared of the vector field changes its sign from negative to positive [442–444]. In the scenario studied in Refs. [425, 430], it was shown in Ref. [425] that the instability is under control during inflation. However, the instability arises at some later epoch, when the field's effective mass squared crosses zero. In spite of this difficulty, the authors in [430] go on to argue that even if such instability exists, it still might be possible to avoid it if the bare mass of the vector field stems from the coupling to another field, which then would allow either a curvaton or an inhomogeneous reheating mechanism. To the best of our knowledge, the debate on this issue is not yet settled, and hence our attitude towards it will be the same as in Ref. [430], thus simply ignoring the instability or assuming that, if present, it can be circumvented by some mechanism. Although this attitude conveniently dispenses with the problem, it is also fair to say that such instability arises when the longitudinal mode becomes unphysical, and hence it is reasonable to suspect that the associated singularity might share the same unphysical nature.

Apart from the above, yet another problem plagues this kind of vector field models, the so-called *ghost instability*. It originates because, during inflation, the kinetic energy density for the longitudinal modes of the vector field have the *wrong* sign, which might entail the copious production of vector field quanta up to the point of ruining inflation. Regarding this instability, the authors in Ref. [430] argue that as long as the negative energy contributed by ghost states does not exceed the energy density driving inflation, these are in principle not problematic for the stability of the theory. In the following, we implicitly assume that this is indeed the case.

Theoretical Framework

We consider a massive vector field coupled to the Gauss-Bonnet invariant and evolving in an inflationary background, which we take to be quasi-de Sitter and driven by an unspecified matter source. The action of the system is

$$\mathcal{L} \equiv \mathcal{L}_{\rm EH} + \mathcal{L}_{\rm inf} + \mathcal{L}_A + \mathcal{L}_{\mathcal{G}}, \tag{4.3.2}$$

with

$$\mathcal{L}_{\rm EH} \equiv -\frac{m_{\rm P}^2}{2} R, \;\; \mathcal{L}_A \equiv -\frac{1}{4} F_{\mu\nu} F^{\mu\nu} + \frac{1}{2} \tilde{m}^2 \, A_\mu A^\mu,$$

$$\mathcal{L}_{\mathcal{G}} \equiv \frac{1}{2}\alpha\,\mathcal{G}\,A_\mu A^\mu, \tag{4.3.3}$$

where, $m_{\rm P}$ is the reduced Planck mass, R is the Ricci scalar, $F_{\mu\nu} \equiv \nabla_\mu A_\nu - \nabla_\nu A_\mu$ is the strength tensor associated to the vector field A_μ with bare mass $\tilde{m}$, $\mathcal{G} \equiv R^2 - 4R_{\alpha\beta}R^{\alpha\beta} + R_{\alpha\beta\gamma\delta}R^{\alpha\beta\gamma\delta}$ is the Gauss-Bonnet topological invariant with coupling strength[7] α, and $R_{\mu\nu}$, $R_{\mu\nu\rho\sigma}$ are the Ricci tensor and the Riemann tensor, respectively. $\mathcal{L}_{\rm inf}$ is the Lagrangian density for the energy content responsible for the inflationary period. The effective mass squared of the vector field is defined as

$$m^2 \equiv \tilde{m}^2 + \alpha\,\mathcal{G}. \tag{4.3.4}$$

In the case of the FLRW metric $\mathrm{d}s^2 = \mathrm{d}t^2 - a^2(t)\mathrm{d}\boldsymbol{x}^2$, where $a(t)$ is the scale factor and $\boldsymbol{x}$ are the Cartesian spatial coordinates, the Gauss-Bonnet invariant reads

$$\mathcal{G} = 24H^2(\dot{H} + H^2), \tag{4.3.5}$$

where $H = \dot{a}/a$ is the Hubble parameter.

Perturbation spectrum

Having clarified our position with respect to the instability of the theory, we investigate the conditions for which the vector field obtains a nearly scale-invariant spectrum of superhorizon perturbations. The equation of motion for the vector field, which is obtained by varying the action of the Lagrangian in Eq. (4.3.2) with respect to A_ν, is

$$\nabla_\mu F^{\mu\nu} + m^2 A^\nu = 0. \tag{4.3.6}$$

Assuming that inflation homogenizes the vector field; i.e. $\partial_i A_\mu = 0$, it is easy to show that its temporal component, A_t, must be zero, while the spatial components A^i obey[8]

$$\ddot{A}^i + H\dot{A}^i + m^2 A^i = 0. \tag{4.3.7}$$

Now, we perturb the vector field in the following way:

$$A_i(t,\boldsymbol{x}) \equiv A_i(t) + \delta A_i(t,\boldsymbol{x}),\; A_t(t,\boldsymbol{x}) = \delta A_t(t,\boldsymbol{x}), \tag{4.3.8}$$

[7] The dimensions of this coupling are $[\alpha] = m_{\rm P}^{-2}$.

[8] See Appendix A of [10] for the details of the calculations.

and write the equations of motion for transverse ($\delta\mathcal{A}^i{}_\perp$) and longitudinal ($\delta\mathcal{A}^i{}_\parallel$) modes as follows (see Appendix A of [10]),

$$\left[\partial_t^2 + H\partial_t + m^2 + \left(\frac{k}{a}\right)^2\right]\delta\mathcal{A}^i_\perp = 0, \tag{4.3.9}$$

$$\left[\partial_t^2 + \left(1 + \frac{2k^2}{k^2 + (am)^2}\right)H\partial_t + m^2 + \left(\frac{k}{a}\right)^2\right]\delta\mathcal{A}^i_\parallel = 0, \tag{4.3.10}$$

where $\delta\mathcal{A}^i$ are the Fourier modes of δA^i. In the above equations, we used the fact that m^2 is a constant during inflation since $\dot{H} \simeq 0$ and therefore $\mathcal{G} \approx 24H^4$.

In order to quantize the field, we introduce creation/annihilation $\hat{a}^\dagger/\hat{a}$ operators for each polarization mode

$$\begin{aligned}\delta\mathcal{A}^j(t,\boldsymbol{x}) \;\; &\equiv \;\; \int \frac{\mathrm{d}^3k}{(2\pi)^3}\sum_\lambda \Big[e^j{}_\lambda(\hat{\boldsymbol{k}})\hat{a}_\lambda(\boldsymbol{k})z_\lambda(t,k)e^{-i\boldsymbol{k}\cdot\boldsymbol{x}} \\ &\qquad + e^{j\,*}_{\lambda}(\hat{\boldsymbol{k}})\hat{a}^\dagger_\lambda(\boldsymbol{k})z^*_\lambda(t,k)e^{i\boldsymbol{k}\cdot\boldsymbol{x}}\Big] \,, \end{aligned} \tag{4.3.11}$$

where $\lambda = \mathrm{L},\mathrm{R}$ labels the left and right transverse polarizations and $\lambda = ||$ the longitudinal polarization. Choosing the $\boldsymbol{k}$-direction along the z-axis, the polarization vectors $\boldsymbol{e}_\lambda$ can be written as

$$\boldsymbol{e}_\mathrm{L} = \frac{1}{\sqrt{2}}(1,i,0),\;\; \boldsymbol{e}_\mathrm{R} = \frac{1}{\sqrt{2}}(1,-i,0),\;\; \boldsymbol{e}_{||} = (0,0,1), \tag{4.3.12}$$

while the commutation rules are

$$\left[\hat{a}_\lambda(\boldsymbol{k})\,,\,\hat{a}^\dagger_{\lambda'}(\boldsymbol{k}')\right] = (2\pi)^3\delta(\boldsymbol{k}-\boldsymbol{k}')\delta_{\lambda\lambda'}. \tag{4.3.13}$$

With all the above, the power spectrum for the λ-polarized modes z_λ is defined by

$$\mathcal{P}^z_\lambda(k) = \lim_{k/aH\to 0}\frac{k^3||z_\lambda||^2}{2\pi^2}\,. \tag{4.3.14}$$

In the following subsections we study each polarization individually.

Transverse modes

Defining the physical transverse modes as $b_{\,\mathrm{L,\,R}} \equiv z_{\,\mathrm{L,\,R}}/a$ and using the conformal time $\mathrm{d}\eta \equiv \mathrm{d}t/a$, the evolution equation (4.3.9) is rewritten as

$$\left[\partial_\eta^2 + 2\mathcal{H}\partial_\eta + 2\mathcal{H}^2 + (am)^2 + k^2\right]b_{\,\mathrm{L,\,R}} = 0, \tag{4.3.15}$$

with $\mathcal{H} \equiv aH$ being the Hubble parameter in conformal time. This equation can be recast in the form of a Bessel equation whose solution is given in terms of the Hankel functions H_ν as

$$b_{\,\mathrm{L,\,R}}(\eta,k) = C_k\, a^{-1}\sqrt{-\eta}\, H_\nu(-k\eta), \tag{4.3.16}$$

where

$$\nu^2 \equiv \frac{1}{4} - \frac{\tilde{m}^2 + \alpha\mathcal{G}}{H^2} = \frac{1}{4} - \frac{m^2}{H^2}\,. \tag{4.3.17}$$

The constant C_k can be found by matching Eq. (4.3.16) with the Bunch-Davies vacuum at early times (when $-k\eta \to \infty$), obtaining

$$C_k = \frac{\sqrt{\pi}}{2} \;\;\Rightarrow\;\; b_{\,\mathrm{L,\,R}}(\eta,k) \approx \frac{1}{a\sqrt{2k}} e^{-ik\eta}. \tag{4.3.18}$$

As expected, the modes behave as those for an oscillator. Now, we are interested in the late time behaviour (when $-k\eta \to 0$) of the physical modes. In this regime, the dominant contribution of the solution in Eq. (4.3.16) is

$$b_{\,\mathrm{L\,,R}}(k) \propto k^{-\nu}\,. \tag{4.3.19}$$

Replacing the later expression in the power spectrum defined in Eq. (4.3.14), we obtain

$$\mathcal{P}_{\,\mathrm{L,\,R}} \equiv \frac{\mathcal{P}^z_{\,\mathrm{L,\,R}}}{a^2} \propto k^{3-2\nu}, \tag{4.3.20}$$

which corresponds to the scale dependance of the power spectrum of the physical vector field perturbations. The spectral index is written as

$$n_{\,\mathrm{L,\,R}} - 1 \equiv \frac{d\,\ln\mathcal{P}_{\,\mathrm{L,\,R}}}{d\,\ln k} = 3 - 2\nu. \tag{4.3.21}$$

From Eqs. (4.3.17) and (4.3.21) it is clear that the physical vector field can attain a nearly flat power spectrum if and only if $m^2 \approx -2H^2$. Consequently, the coupling α must satisfy $\tilde{m}^2 + 24\alpha H^4 \approx -2H^2$. Moreover, if $\tilde{m} \ll H$, the condition for scale-invariance becomes

$$\alpha H^2 \approx -\frac{1}{12}. \tag{4.3.22}$$

This result must be compared to the one in Refs. [424, 444] where, instead of coupling the vector field to the Gauss-Bonnet invariant, the authors couple the vector field to the Ricci scalar, i.e. $\alpha R A_\mu A^\mu$. In Refs. [424, 444], it was shown that if the coupling constant is exactly 1/6 the power spectrum is perfectly flat, besides, the spectrum of each transverse mode is precisely the same as that for a scalar field. Finally, it is important to mention that the requirement

$m^2 \approx -2H^2$ is precisely one of the possibilities discussed in [430] to avoid the instabilities mentioned in Sec. 4.3.2.

Longitudinal modes

Equation (4.3.10) gives the evolution for the longitudinal modes $z_\parallel$, which, in terms of the conformal time, can be written as

$$\left[\partial_\eta^2 + \frac{2\mathcal{H}k^2}{k^2+(am)^2}\partial_\eta + (am)^2 + k^2\right] z_\parallel = 0. \tag{4.3.23}$$

Using the conditions $\tilde{m} = 0$ and $m^2 = -2H^2$ for a scale-invariant transverse power spectrum, and taking into account that the vacuum boundary condition is modified by

$$\lim_{-k\eta\to\infty} z_\parallel = \gamma\frac{1}{\sqrt{2k}}e^{-ik\eta}, \tag{4.3.24}$$

with $\gamma = \sqrt{(k/am)^2+1}$ the Lorentz boost factor which takes us from the frame with $\boldsymbol{k} = 0$ to the frame of momentum $\boldsymbol{k} \neq 0$, the solution of the above equation is [425–428]

$$z_\parallel = \frac{\sqrt{-\eta}}{2}\left[-k\eta + \frac{2}{k\eta} + 2i\right]\frac{e^{-ik\eta}}{\sqrt{-k\eta}}, \tag{4.3.25}$$

which at late times ($-k\eta \to 0$) behaves as $\sqrt{-\eta}(-k\eta)^{-3/2}$. Replacing the latter in the power spectrum in Eq. (4.3.14) we get

$$\mathcal{P}_\parallel^z \approx 2a^2\left(\frac{H}{2\pi}\right)^2, \tag{4.3.26}$$

where we used the approximation $H^2 \approx (a\eta)^{-2}$ which is valid during inflation for a quasi-de Sitter background. As in the transverse case, the physical longitudinal power spectrum $\mathcal{P}_\parallel$ can be obtained by defining the physical longitudinal modes as $b_\parallel \equiv z_\parallel/a$.

Statistical anisotropy

It is known that vector fields introduce inherently a preferred direction and therefore they can introduce large statistical anisotropies in the perturbation spectrum. If this is the case, the model will be ruled out because it is in disagreement with the observational results. For this reason, by using the δN formalism [472–475], in this section we compute the amount of statistical anisotropy in the spectrum, which is quantified in the parameter g defined in Eq. (4.3.1). We will show that g can be small enough to satisfy the observational bounds [415].

According to the δN formalism, the curvature perturbation ζ is the difference of the number of e-folds N between uniform density and spatially flat slices of spacetime: $\zeta \equiv \delta N$. We will assume that N is function of the scalar field ϕ and the vector field: $N = N(\phi, A^\mu)$. Then, the curvature perturbation can be written as [428]

$$\begin{aligned}\zeta &= N_\phi \delta\phi + N_A^i \delta A_i + \frac{1}{2} N_{\phi\phi} (\delta\phi)^2 \\ &+ \frac{1}{2} N_{\phi A}^i \delta\phi \delta A_i + \frac{1}{2} N_{AA}^{ij} \delta A_i \delta A_j + \cdots ,\end{aligned} \tag{4.3.27}$$

where $N_\phi \equiv \frac{\partial N}{\partial \phi}$, $N_A^i \equiv \frac{\partial N}{\partial A_i}$, $N_{\phi\phi} \equiv \frac{\partial^2 N}{\partial \phi^2}$, $N_{\phi A}^i \equiv \frac{\partial^2 N}{\partial \phi A_i}$, $N_{AA}^{ij} \equiv \frac{\partial^2 N}{\partial A_i A_j}$, $\delta\phi$ and δA_i are the perturbations of the scalar and vector field, respectively. From this result, the power spectrum of the curvature perturbation reads

$$\mathcal{P}_\zeta(\boldsymbol{k}) = N_\phi^2 \mathcal{P}_\phi + N_A^2 \left[\mathcal{P}_+ + \left(\mathcal{P}_\parallel - \mathcal{P}_+ \right) (\hat{\boldsymbol{d}} \cdot \boldsymbol{k})^2 \right], \tag{4.3.28}$$

where $\mathcal{P}_\phi$ denotes the power spectrum of the scalar field, we have defined the even and odd polarizations for the transverse spectra as $2\mathcal{P}_\pm \equiv \mathcal{P}_{\rm L} \pm \mathcal{P}_{\rm R}$, respectively. We have taken into account that our theory is parity conserving, i.e. $\mathcal{P}_{\rm R} = \mathcal{P}_{\rm L}$, and thus $\mathcal{P}_+ = \mathcal{P}_{\rm R}$ and $\mathcal{P}_- = 0$. In the latter equation, we have also defined $N_A^2 \equiv ||\boldsymbol{N}_A||^2 \equiv N_A^i N_{Ai}$ and $\hat{\boldsymbol{d}} \equiv \boldsymbol{N}_A / N_A$, which defines the preferred direction signaled by the vector field. By comparing the above equation with Eq. (4.3.1), we identify the isotropic part of the spectrum as

$$\mathcal{P}_k^{\rm iso}(k) = N_\phi^2 \mathcal{P}_\phi(k) + N_A^2 \mathcal{P}_+(k), \tag{4.3.29}$$

and hence the anisotropy parameter g can be written as

$$g = \beta \frac{\mathcal{P}_\parallel - \mathcal{P}_+}{\mathcal{P}_\phi + \beta \mathcal{P}_+}, \quad \beta \equiv \frac{N_A^2}{N_\phi^2}, \tag{4.3.30}$$

where β quantifies the relative contribution of the vector field over the scalar field to the modulation of N. Now, since the power spectra of the transverse solutions are nearly flat, they are given by $\mathcal{P}_{\rm L,\,R} \approx (H/2\pi)^2$, and assuming that the potential of the scalar field is sufficiently flat during inflation, such that the power spectrum of the scalar field is also nearly flat at horizon exit [422], i.e. $\mathcal{P}_\phi \approx (H/2\pi)^2$, we get

$$g \approx \frac{\beta}{1+\beta} \approx \beta, \tag{4.3.31}$$

where we took into account that N is primarily modulated by the scalar field, since the vector field is subdominant during inflation, implying $\beta \ll 1$, then $g \approx \beta \ll 1$. This result agrees with the bounds given by Planck which suggest that g can be at most 0.97 [415].

4.3.3 Evolution of the vector field

In this section, we follow the evolution of the homogeneous vector field during and after inflation in order to determine if the vector field is able to play the role of a curvaton [422, 471].

Defining the physical components of the vector A^i as $B^i \equiv A^i/a$ and supposing, by simplicity, that $B_\mu = (0, 0, 0, B)$, the equation of motion (4.3.7) is rewritten as

$$\ddot{B} + 3H\dot{B} + \left(\dot{H} + 2H^2 + m^2\right) B = 0. \tag{4.3.32}$$

In the following, we solve this equation during and after inflation.

Evolution during inflation

As shown in section 4.3.2, the nearly scale-invariant spectrum of vector perturbations is obtained if the effective mass of the vector field is $m^2 \approx -2H^2$, which remains constant during inflation because $H \simeq$ constant. Therefore, the solution of Eq. (4.3.32) during inflation is

$$B(t) = B_0 + B_1 a^{-3}, \tag{4.3.33}$$

where B_0 and B_1 are integration constants. The decaying mode in the solution in Eq. (4.3.33) is quickly diluted by inflation, thus the field is nearly constant given that $B \approx B_0$. This means that the vector field remains frozen and therefore it is not "erased" in the inflationary phase.

Evolution after inflation

The post-inflationary evolution of the vector field is also described by Eq. (4.3.32), but now H is time depending. Assuming that H evolves as

$$H(t) = \frac{2\,t^{-1}}{3(1+w)}, \tag{4.3.34}$$

where w is the equation of state parameter of the dominant fluid after inflation and that $\alpha H^2 = \gamma$, where γ is a constant (not necessarily the same required for a flat power spectrum),[9] Eq. (4.3.32) can be recast in the following form

$$t^2\ddot{B} + \frac{2\,t}{1+w}\dot{B} + \left[(\tilde{m}t)^2 - \tau^2\right] B = 0, \tag{4.3.35}$$

[9] We assume this condition for simplicity, and having in mind the condition in Eq. (4.3.22) which is valid during inflation.

where

$$\tau^2 \equiv \frac{2(1+3w)}{3(1+w)^2}\left(8\gamma - \frac{1-3w}{3(1+3w)}\right). \tag{4.3.36}$$

The general solution of the above equation is

$$B(t) = t^u \left[c_1 J_v(\tilde{m}\, t) + c_2 Y_v(\tilde{m}\, t)\right], \tag{4.3.37}$$

where

$$u \equiv \frac{w-1}{2(w+1)}\,, \quad v \equiv \frac{\sqrt{1+3w}}{6(1+w)}\sqrt{1+3w+192\gamma}, \tag{4.3.38}$$

c_1 and c_2 being constants of integration and J_v and Y_v being the Bessel functions of first and second kind, respectively. This solution should be contrasted with the solution for the equation of motion of a vector field non-minimally coupled to the Ricci scalar. In Ref. [424], it was shown that, since this coupling is negligible after inflation[10], the vector field behaves as a massive minimally-coupled abelian vector. In contrast, in our model, the Gauss-Bonnet coupling contributes to the effective mass after inflation as well. This dependence is very important because, since the Gauss-Bonnet invariant changes its sign when passing from inflation to a matter or radiation dominated phase, naturally entails the change of sign of the vector mass. In Refs. [424, 426, 471], it was shown that a vector field with positive mass after inflation can engage into quick oscillations, avoiding the generation of large-scale anisotropies. However, this sign change has to be assumed since a mechanism provoking this feature is not presented.

Now, we consider two possible approximations of the solution (4.3.37) regarding the dependence of the Bessel functions with respect to the bare mass $\tilde{m}$ of the vector field. Firstly, we assume that the vector field is "light", i.e. $\tilde{m}t \to 0$. Hence the solution (4.3.37) is approximated by

$$B(t) \approx \tilde{c}_1 a^{3(1+w)(u+v)/2} + \tilde{c}_2 a^{3(1+w)(u-v)/2}, \tag{4.3.39}$$

where $\tilde{c}_1$ and $\tilde{c}_2$ are constants. The latter solution means that the evolution of the light vector field is described by a power law for the scale factor. On the other hand, for a "heavy" vector field we take the limit of Eq. (4.3.37) when $\tilde{m}t \to \infty$ obtaining

$$B(t) \approx a^{-3/2}\left[b_1 \cos(\tilde{m}t - \varphi) + b_2 \sin(\tilde{m}t - \varphi)\right], \tag{4.3.40}$$

where b_1 and b_2 are constants. This solution shows that a heavy vector field oscillates with phase φ (which is a function of v) and envelope decreasing as

$$\bar{B(t)} \propto a^{-3/2}. \tag{4.3.41}$$

[10] This is true if a radiation dominated period follows after the inflationary phase, since $R \approx 0$ for an equation of state $w \approx 1/3$.

This shows that the vector field performs rapid oscillations, hence its dynamical behavior is effectively characterized by the envelope.

Evolution of the energy density

In the last section, we showed that the vector field has a constant magnitude during inflation. After inflation, it follows either a power law or an oscillatory motion depending whether it is light or heavy, respectively. However, if the vector field is to have a chance to imprint its perturbation spectrum at late times, it must nearly dominate the universe after inflation, according to the curvaton scenario [422]. Therefore, it is necessary to follow the evolution of its energy density.

Varying the corresponding action for the Lagrangian in Eq. (2) with respect to the metric $g_{\mu\nu}$, it follows that [446, 476]:

$$\frac{\delta\mathcal{L}_{\rm EH}}{\delta g_{\mu\nu}}+\frac{\delta\mathcal{L}_{\rm inf}}{\delta g_{\mu\nu}}+\frac{\delta\mathcal{L}_{A}}{\delta g_{\mu\nu}}+\frac{\delta\mathcal{L}_{\mathcal{G}}}{\delta g_{\mu\nu}}=0, \tag{4.3.42}$$

where

$$\frac{\delta\mathcal{L}_{\rm EH}}{\delta g_{\mu\nu}}=-\frac{m_{\rm P}^2}{2}\left(-R^{\mu\nu}+\frac{1}{2}g^{\mu\nu}R\right), \tag{4.3.43}$$

$$\frac{\delta\mathcal{L}_{A}}{\delta g_{\mu\nu}}=-\frac{1}{8}g^{\mu\nu}F_{\alpha\beta}F^{\alpha\beta}+\frac{1}{2}F^{\mu\rho}F^{\nu}{}_{\rho}-\frac{1}{2}\,\tilde{m}^2\left(A^\mu A^\nu-\frac{1}{2}\,g^{\mu\nu}A^\sigma A_\sigma\right), \tag{4.3.44}$$

$$\begin{aligned}\frac{\delta\mathcal{L}_{\mathcal{G}}}{\delta g_{\mu\nu}}=&-\frac{1}{2}\alpha\mathcal{G}A^\mu A^\nu+\frac{1}{2}g^{\mu\nu}f\mathcal{G}-2fRR^{\mu\nu}+2\nabla^\mu\nabla^\nu(fR)-2g^{\mu\nu}\Box(fR)+8fR^{\mu}{}_{\rho}R^{\nu\rho}\\&-4\nabla_\rho\nabla^\mu(fR^{\nu\rho})-4\nabla_\rho\nabla^\nu(fR^{\mu\rho})+4\Box(fR^{\mu\nu})+4g^{\mu\nu}\nabla_\rho\nabla_\sigma(fR^{\rho\sigma})\\&-2fR^{\mu\rho\sigma\tau}R^{\nu}{}_{\rho\sigma\tau}+4\nabla_\rho\nabla_\sigma(fR^{\mu\rho\sigma\nu}),\end{aligned} \tag{4.3.45}$$

and $f\equiv\frac{1}{2}\alpha A_\mu A^\mu$. Using the FLRW metric, the "00″ component of Eq. (4.3.42) can be written as $3\,m_{\rm P}^2\,H^2=\rho_{\rm inf}+\rho_B$, where $\rho_{\rm inf}$ is the energy density of the source driving inflation and

$$\rho_B=\frac{1}{2}\dot{B}^2+\frac{1}{2}\left[\tilde{m}^2+H^2\left(1+2\frac{\dot{B}}{BH}\right)\right]B^2+24\alpha H^4B^2\left(\frac{\dot{B}}{HB}+\frac{\dot{\alpha}}{2\alpha H}\right), \tag{4.3.46}$$

is the energy density of the physical vector field $B_\mu=(0,0,0,B)$. This is to be compared with the energy density $\rho_B=\frac{1}{2}\dot{B}^2+\frac{1}{2}\,\tilde{m}^2B^2$ of a vector field non-minimally coupled to gravity through the Ricci scalar [424, 430, 434–436]. In our case, the energy density of the vector field has an extra term coming from the coupling with the Gauss-Bonnet invariant.

During inflation, Eq. (4.3.46) gives

$$\rho_B \simeq \frac{1}{2} H^2 B^2 \simeq \text{const.}\,, \tag{4.3.47}$$

where we used the fact that $\tilde{m} \ll H$ and B, H and α are nearly constants. We can see that the energy density of the vector field is not diluted by inflation since it remains almost constant.

In order to avoid anisotropic expansion after inflation, the contribution to the energy tensor coming from the vector field must not introduce anisotropic pressures. This can be achieved if the vector field condensate behaves as a pressureless matter, i.e. $\rho_B \propto a^{-3}$ [471]. In this section we investigate the available parameter space for the constant γ that allows this behavior in a radiation dominated universe characterized by $w \approx 1/3$. Before to continue our discussion, we want to point out the following. During inflation, the Gauss-Bonnet term is positive and it can be approximated by $\mathcal{G} \approx 24H^4$. On the other hand, in order to get a nearly flat power spectrum for the transverse modes we have $\alpha H^2 \approx -1/12$, and therefore $\alpha < 0$. After inflation, when the Hubble parameter $H(t)$ is given by Eq. (4.3.34), the Gauss-Bonnet invariant is given by

$$\mathcal{G} = -\frac{64}{27} \frac{1+3w}{t^4(1+w)}. \tag{4.3.48}$$

So, the Gauss-Bonnet invariant is negative if $w > -1/3$ (eg. a matter ($w = 0$) or a radiation ($w = 1/3$) fluid). This implies $\gamma < 0$ and a change in the sign of the effective mass, $m^2 = \tilde{m}^2 + \alpha\mathcal{G}$, from negative, during inflation, to positive, after inflation. As explained in [471], a minimally-coupled vector plays the role of a curvaton if it has a negative mass-squared (explicitly $m^2 \approx -2H^2$) during inflation. After inflation, the mass-squared has to become positive so that the vector field engages into oscillations and thus avoiding the production of large background anisotropy. As we show, in our model, this change of sign is tacitly provided by the "evolution" of the Gauss-Bonnet invariant.

Regarding a light field, we showed in Sec. 4.3.3 that the dynamics of the vector field is described as a power law in the scale factor (see Eq. (4.3.39)). The power is given in terms of the equation of state parameter w and the constant γ. Then, replacing Eqs. (4.3.34) and (4.3.39) in Eq. (4.3.46), and considering that the dominant fluid after inflation can be either a stiff fluid ($w = 1$) or a radiation fluid ($w = 1/3$), one can realize that is impossible to satisfy the condition that $\gamma < 0$ and the condition that the density of the vector field scales as pressureless matter, so we discard the light field solution.

For a heavy field, we showed that it is oscillating with decreasing envelope as $a^{-3/2}$. Following Ref. [471], the period of oscillations is much smaller than the Hubble time, which means that the effective behaviour of the vector field is given by its envelope. Therefore, replacing Eq.

(4.3.41) in the density in Eq. (4.3.46) we get the average density over many oscillations as

$$\bar{\rho_B} = B_0^2\left(\frac{1}{32}+3\gamma\right)a^{-7}+\frac{1}{2}\tilde{m}^2B_0^2a^{-3}, \tag{4.3.49}$$

where B_0 is the constant of proportionality implicit in Eq. (4.3.41). The first term in Eq. (4.3.49) goes as a^{-7}, so it decays faster than the radiation dominant fluid (which decays as a^{-4}) and even faster than the second term. This means that $\bar{\rho_B} \propto a^{-3}$. The fact that the average energy density decays as a^{-3} implies two important things: *i*) the vector field may eventually dominate the Universe and imprint its perturbation spectrum, and *ii*) the average energy density of the vector field scales as pressureless matter, so the average pressure is zero and therefore there is no generation of large background anisotropy.

4.3.4 Conclusions

In this paper, we have examined the evolution of a cosmological vector field coupled to the Gauss-Bonnet invariant. Assuming that $\tilde{m} \ll H$, we found that, in order to get a nearly flat power spectrum for the transverse modes during inflation, the coupling α must satisfy the condition $\alpha H^2 \approx -1/12$. This implies that the power spectrum for the longitudinal modes is $\mathcal{P}_\parallel = 2\mathcal{P}_{\text{L, R}}$. Consequently, we showed that the amount of statistical anisotropy in our model, quantified by the parameter g, is within the observational bounds, given that the vector field is subdominant during inflation. We also found that the vector field remains constant during the inflationary phase, but it performs rapid oscillations after that whenever $\tilde{m} \gg H$. Averaging over many oscillations, the vector field effectively decays as $a^{-3/2}$, which means that the average energy density, $\bar{\rho_B}$, decays as a^{-3}, so, after inflation, the vector field behaves like a pressureless fluid. This indicates that the vector field has a chance to nearly dominate the universe after inflation, without introducing large background anisotropy, and thus be able to imprint its curvature perturbation.

According to the vector curvaton scenario, the mass of the vector must be negative during inflation and positive after that. In our model, this feature is provided by the particular behavior of the Gauss-Bonnet invariant because it changes its sign when passing from inflation to a matter or radiation dominated epoch. Therefore, we conclude that this non-minimal coupling between a vector field and the Gauss-Bonnet invariant can be a reliable and realistic vector curvaton model.

Chapter 5

Machine Learning in Cosmology

5.1 General Introduction

One of the most important cosmological probes we have in favor of the concordance model is the distribution of galaxies at large scales [373, 477]. In order to contrast our theoretical predictions against these observational data, it is necessary to extract the statistical information in the distribution of the large scale structure by computing the matter power spectrum, $P(k, z)$, which depends on the scale k and the redshift z. It can be shown that at first order in cosmological perturbations, and neglecting neutrinos, the dependence of $P(k, z)$ on k is encoded in the so-called matter transfer function $T(k)$, while the dependence on z is encoded in the growth factor $D_+(z)$ [478]. Therefore, for a fixed redshift, the matter power spectrum is a function only of the scale and its form is mostly described by the matter transfer function.

The calculation of $P(k, z)$ generally requires to solve the multi-species Boltzmann equations, which can be done numerically in a matter of seconds using Boltzmann solvers, like the codes `CLASS` [479] and `CAMB` [342]. However, to have an accurate analytical description for specific quantities is always desirable. Following this line of thought, Bardeen, Bond, Kaiser, and Szalay found a fitting function for the transfer function considering radiation, baryons, and cold dark matter [480]. This BBKS formula is accurate up to 10% which is well-below the precision of current data [481]. A better alternative is the fitting formula given by Eisenstein and Hu (EH) in Ref. [482]. The EH formula achieves a precision of around 1-2%, however it is given in terms of around 30 different, complicated expressions. These fitting formulae have been extensively used in the literature [483–485].

Machine learning has long been exploited in physics (see Ref. [486] for a review). In particular, machine learning has been used to address symbolic regression problems, i.e., finding an analytical expression that accurately describe a given data set [487–490]. In this work, we use a specific machine learning technique known as Genetic Algorithms (GAs). GAs are loosely based on biological evolution concepts. In a nutshell, they attempt to improve the goodness of fit of the candidate expressions by randomly combining them and/or modifying some parts of them [491]. This approach seems to be suitable for finding analytical formulae for quantities of interest in cosmology [492–498].

Here, we use GAs to find analytical functions for the matter transfer function with sub-percent accuracy while being significantly shorter and thus easier to handle than other available formulae.

5.2 Preliminaries

5.2.1 Genetic Algorithms

Here we briefly review the GA, which can be used as a stochastic symbolic regression approach. Basically, the symbolic regression problem consists in finding a fitting function for a given dataset, and thus defining a non-parametric approach to describe data. There are several free and commercial codes to perform symbolic regression [487–490]. The GAs have been widely used in several branches of physics, like particle physics [499, 500], astrophysics [501, 502], and cosmology [503–508].

In the GA, which is a machine learning technique inspired by concepts in evolutionary biology [491], a population composed by several individuals (mathematical expressions in this case) evolves expecting to optimize the goodness of fit of next generations to a given dataset, which can be measured by a goodness of fit function, usually taken to be a χ^2. Each individual is in turn composed by a selected set of basic operations, i.e., the grammar, which are randomly selected depending on the “nucleotides”. These nucleotides are random numbers which in group form the genes setting the mathematical expression of an individual. Once the initial population is created, i.e., the progenitors, the goodness of fit of each individual is measured and, using a tournament scheme, a set containing the best prospects is selected for reproduction and survival to contribute to the next generation.

The reproduction is carried out by the so-called genetic operators, namely, crossover and mutation. In the crossover stage, two individuals are randomly combined to produce new individuals sharing characteristics of both parents. In the mutation stage, one nucleotide of an individual is randomly selected and modified. This process is repeated for a given number of generations.

Now, we describe the way reproduction works in GA with an example. In the upper part of Fig. 5.2.1, there are two expressions in tree representation, i.e., two individuals xe^x and $2x^2$. Let us assume that these individuals were selected for reproduction. Left panel of Figure 5.2.1 shows possible combinations of the two individuals, while the right panel of Fig. 5.2.1 shows their possible mutations. For instance, the new individual in the left-hand side of Fig. 5.2.1 is born

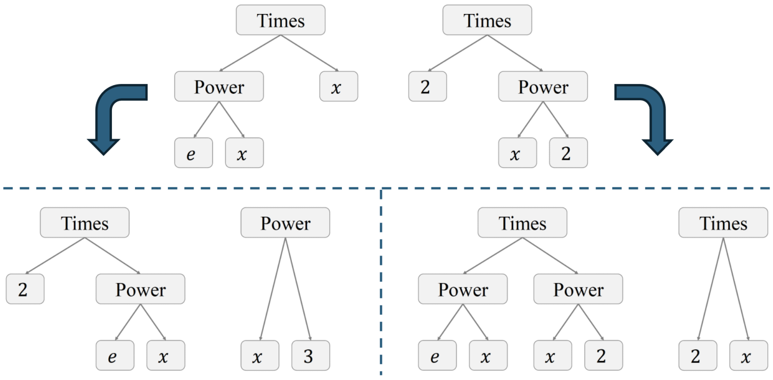

Figure 5.2.1: In the upper part we see two exemplifying grammatical expressions corresponding to the individuals xe^x and $2x^2$. (Left) The two selected individuals have been combined to produce two new individuals: $2e^x$ and x^3. (Right) The two selected individuals have suffered a mutation to become two new individuals: x^2e^x and $2x$.

from the combination of the expressions e^x and 2 from its parents, while the other individual is made from the remaining parts, x and x^2, using the proper basic operation "Times" or product. During the mutation stage, a selected individual is altered randomly. As shown in the right panel of Fig. 5.2.1, for instance, the individual xe^x mutated to x^2e^x, and the individual $2x^2$ mutated to $2x$.

5.2.2 The Matter Transfer Function

On large scales where non-linearities are negligible, the linear matter power spectrum can be compared against observations of galaxy clustering, and gravitational lensing, among others [509–511].

In the concordance model, the primordial curvature perturbations generated during inflation are related to the gravitational potential at late times by means of two functions: *i*) the matter transfer function $T(k)$ which encodes its scale dependence and describes the evolution of perturbations during horizon crossing and transition from radiation to matter domination, *ii*) the growth factor $D_+(a)$ which describes the time-dependent growth of matter density perturbations at late times. Thus, the gravitational potential can be written as

$$\Phi(k,a) \propto \mathcal{R}(k)T(k)D_+(a), \tag{5.2.1}$$

where $\mathcal{R}$ is the primordial curvature perturbation, and a is the scale factor. At late times, for sub-horizon modes, and neglecting massive neutrinos, this gravitational potential can be related to the matter contrast δ_m by means of the Poisson equation:

$$k^2\Phi(k,a) \propto \rho_m a^2 \delta_m(k,a), \tag{5.2.2}$$

where ρ_m is the background density of pressure-less matter. Taking into account that the primordial perturbations are nearly Gaussian with zero mean [218], the linear matter power spectrum can be written as [478]

$$P(k,a) \propto \frac{k^{n_s}}{\Omega_m^2} D_+^2(a) T^2(k), \tag{5.2.3}$$

where n_s is the scalar spectral index of primordial fluctuations, and Ω_m is the density parameter of pressure-less matter. Therefore, for a fixed redshift, the power spectrum is given by

$$P(k) \propto k^{n_s} T^2(k), \tag{5.2.4}$$

namely, it is fully determined by the transfer function. In this work, we present a very accurate fitting formula for $T(k)$ as a function of the density of baryons and matter, such that it is straightforward to compute the linear matter power spectrum.

As it is well-known from experiments, neutrinos are massive [512, 513]. At sufficiently small scales, free streaming massive neutrinos imprint their effects on the cosmological evolution, which translates to a further suppression of the matter power spectrum. In this case, the growth factor acquires a scale dependency, making non-trivial a similar separation as in Eq. (5.2.3). However, for a fixed redshift, it is possible to absorb all the scale dependent effects in an effective matter transfer function, as shown in Ref. [514].

5.2.3 Previous Fitting Formulae

BBKS Formula

Before the advent of fast and accurate Boltzmann solvers, several attempts were made to describe analytically the matter transfer function. One of the most remarkable results of this pursuit is the BBKS formula which is based on previous fitting formulae by Bardeen, Bond, Efstathiou, and Szalay [515–517]. In the case that $\Omega_b \ll \Omega_m$, that is, the main contribution to the matter content is in the form of Cold Dark Matter (CDM), the BBKS formula reads

$$T_{c,\mathrm{BBKS}}(k) \equiv \frac{\ln(1+2.34q)}{2.34q}\left[1+3.89q+(16.1q)^2+(5.46q)^3+(6.71q)^4\right]^{-1/4}, \tag{5.2.5}$$

where

$$q(k) \equiv \frac{k\theta^{1/2}}{(\omega_m - \omega_b)\mathrm{Mpc}^{-1}}, \qquad \theta \equiv \frac{\rho_r}{1.68\rho_\gamma}, \tag{5.2.6}$$

and $\omega_X \equiv \Omega_X h^2$ the reduced density parameter (Ω_X being the density parameter of species X), h the reduced Hubble constant, ρ_X the background density, and $X = b$, c, m, r, ν, γ denotes baryons, CDM, pressure-less matter, radiation, neutrinos, photons, respectively. When ω_b is not negligible, the transfer function is modified as

$$T_{\mathrm{BBKS}}(k;\omega_b,\omega_m) \equiv T_{c,\mathrm{BBKS}}(k)\left[1 + \frac{(kR_{\mathrm{Jr}})^2}{2}\right]^{-1}, \tag{5.2.7}$$

where $R_{\mathrm{Jr}} \equiv 1.6(\omega_m - \omega_b)^{-1/2}\,\mathrm{kpc}$.

EH Formula

A more accurate formula was presented by Eisenstein and Hu in Ref. [482]. This formula is constructed from several physically motivated terms, such as acoustic oscillations, Compton drag, velocity overshoot, baryon in-fall, adiabatic damping, Silk damping, CDM suppression. These terms accurately describe, for instance, the suppression in the transfer function on small scales due to the presence of baryons, and the amplitude and location of baryonic oscillations [482]. All the mentioned effects are taken into account in the EH formula by around 30 expressions, which we present in the following.

The transfer function given by Eisenstein and Hu [482] has the following form:

$$T(k) = \frac{\Omega_b}{\Omega_0}T_b(k) + \frac{\Omega_c}{\Omega_0}T_c(k), \tag{5.2.8}$$

where $\Omega_0 = \Omega_b + \Omega_c$. The terms involved in this formula are the following:

$$T_b = \left[\frac{\tilde{T}_0(k;1,1)}{1+(ks/5.2)^2} + \frac{\alpha_b}{1+(\beta_b/ks)^3}e^{-\left(\frac{k}{k_{\mathrm{Silk}}}\right)^{1.4}}\right]j_0(k\tilde{s}), \tag{5.2.9}$$

$$T_c = f\tilde{T}_0(k,1,\beta_c) + (1-f)\tilde{T}_0(k,\alpha_c,\beta_c), \tag{5.2.10}$$

$$\tilde{T}_0(k,\alpha_c,\beta_c) = \frac{\ln(e+1.8\beta_c q)}{\ln(e+1.8\beta_c q) + Cq^2}, \tag{5.2.11}$$

$$f = \frac{1}{1 + (ks/5.4)^4}, \tag{5.2.12}$$

$$C = \frac{14.2}{\alpha_c} + \frac{386}{1 + 69.9q^{1.08}}, \tag{5.2.13}$$

$$q = \frac{k}{13.41k_{\rm eq}}, \tag{5.2.14}$$

$$R \equiv 3\rho_b/4\rho_\gamma = 31.5\omega_b\Theta_{2.7}^{-4}(z/10^3)^{-1}, \tag{5.2.15}$$

$$k_{\rm Silk} = 1.6\omega_b^{0.52}\omega_0^{0.73}\left[1 + (10.4\,\omega_0)^{-0.95}\right]\ {\rm Mpc}^{-1}, \tag{5.2.16}$$

$$k_{\rm eq} = 7.46 \times 10^{-2}\omega_0\Theta_{2.7}^{-2}\,{\rm Mpc}^{-1}, \tag{5.2.17}$$

$$\alpha_b = 2.07k_{\rm eq}s(1 + R_d)^{-3/4}G\left(\frac{1 + z_{\rm eq}}{1 + z_d}\right), \tag{5.2.18}$$

$$\beta_b = 0.5 + \frac{\Omega_b}{\Omega_0} + \left(3 - 2\frac{\Omega_b}{\Omega_0}\right)\sqrt{(17.2\,\omega_0)^2 + 1}, \tag{5.2.19}$$

$$\beta_{\rm node} = 8.41\omega_0^{0.435}, \tag{5.2.20}$$

$$s = \frac{2}{3k_{\rm eq}}\sqrt{\frac{6}{R_{\rm eq}}}\ln\frac{\sqrt{1 + R_d} + \sqrt{R_d + R_{\rm eq}}}{1 + \sqrt{R_{\rm eq}}}, \tag{5.2.21}$$

$$\tilde{s} = s\left[1 + \left(\frac{\beta_{\rm node}}{ks}\right)^3\right]^{-1/3}, \tag{5.2.22}$$

$$G(y) = -6y\sqrt{1 + y} + y(2 + 3y)\ln\left(\frac{\sqrt{1 + y} + 1}{\sqrt{1 + y} - 1}\right), \quad y \equiv \frac{1 + z_{\rm eq}}{1 + z}, \tag{5.2.23}$$

$$\alpha_c = a_1^{-\Omega_b/\Omega_0}a_2^{-(\Omega_b/\Omega_0)^3}, \tag{5.2.24}$$

$$a_1 = (46.9\omega_0)^{0.670}[1 + (32.1\omega_0)^{-0.532}], \tag{5.2.25}$$

$$a_2 = (12.0\omega_0)^{0.424}[1 + (45.0\omega_0)^{-0.582}], \tag{5.2.26}$$

$$\beta_c^{-1} = 1 + b_1[(\Omega_c/\Omega_0)^{b_2} - 1], \tag{5.2.27}$$

$$b_1 = 0.944[1 + (458\omega_0)^{-0.708}]^{-1}, \tag{5.2.28}$$

$$b_2 = (0.395\omega_0)^{-0.0266}. \tag{5.2.29}$$

$$z_{\rm eq} = 2.50 \times 10^4 \omega_0 \Theta_{2.7}^{-4}, \tag{5.2.30}$$

$$z_d = 1291 \frac{\omega_0^{0.251}}{1 + 0.659\omega_0^{0.828}} \left[1 + b_{1,z}\omega_b^{b_{2,z}}\right], \tag{5.2.31}$$

$$b_{1,z} = 0.313\omega_0^{-0.419}\left[1 + 0.607\omega_0^{0.674}\right], \tag{5.2.32}$$

$$b_{2,z} = 0.238\omega_0^{0.223}, \tag{5.2.33}$$

where we have defined $\omega_0 = (\Omega_c + \Omega_b)h^2$, and $T_{\rm CMB} \equiv 2.7\Theta_{2.7}\,{\rm K}$, $R_d \equiv R(z_d)$ and $R_{\rm eq} \equiv R(z_{\rm eq})$

EH Formula with Massive Neutrinos

The free-streaming scale of massive neutrinos is imprinted in the transfer function, which translates to a further suppression on the smallest scales. In Ref. [514], Eisenstein and Hu provided a fitting formula when baryons, CDM and massive neutrinos are considered. The latter formulation also requires around 30 expressions, which we write in the following.

The transfer function given by Eisenstein and Hu considering massive neutrinos has the following form [514]:

$$T_{cb\nu}(k, z) = T_{\rm master}(k)\frac{D_{cb\nu}(k, z)}{D_1(z)}, \tag{5.2.34}$$

The terms involved in this formula are the following:

$$T_{\rm master}(k) = T_{\rm sup}(k)B(k), \tag{5.2.35}$$

$$D_{cb\nu}(z, q) = \left[f_{cb}^{0.7/p_{cb}} + \left(\frac{D_1(z)}{1 + y_{\rm fs}(q; f_\nu)}\right)^{0.7}\right]^{p_{cb}/0.7} D_1(z)^{1-p_{cb}}, \tag{5.2.36}$$

$$D_1(z) = \left(\frac{1+z_{eq}}{1+z}\right)\frac{5\Omega(z)}{2}\left\{\Omega(z)^{4/7} - \Omega_\Lambda(z) + \left[1 + \frac{\Omega(z)}{2}\right]\left[1 + \frac{\Omega_\Lambda(z)}{70}\right]\right\}^{-1}, \tag{5.2.37}$$

$$\Omega(z) = \Omega_0(1+z)^3 g^{-2}(z), \tag{5.2.38}$$

$$\Omega_\Lambda(z) = \Omega_\Lambda g^{-2}(z), \tag{5.2.39}$$

$$g^2(z) = (1 - \Omega_0 - \Omega_\Lambda)(1+z)^2 + \Omega_0(1+z)^3 + \Omega_\Lambda, \tag{5.2.40}$$

$$T_{\rm sup}(k) = \frac{L}{L + Cq_{\rm eff}^2},$$

$$L = \ln(e + 1.84\beta_c\sqrt{\alpha_\nu}q_{\rm eff}), \quad C = 14.4 + \frac{325}{1 + 60.5q_{\rm eff}^{1.08}}, \quad \beta_c = (1 - 0.949f_{\nu b})^{-1},$$

$$y_{\rm fs}(q) = 17.2 f_\nu (1+0.488 f_\nu^{-7/6})(qN_\nu/f_\nu)^2, \quad q = \frac{k}{\rm Mpc^{-1}}\Theta_{2.7}^2\omega_0^{-1}, \tag{5.2.41}$$

$$B(k) = 1 + \frac{1.24 f_\nu^{0.64} N_\nu^{0.3+0.6f_\nu}}{q_\nu^{-1.6}+q_\nu^{0.8}}, \quad q_\nu = 3.92q\sqrt{\frac{N_\nu}{f_\nu}} \tag{5.2.42}$$

$$f_c = \frac{\Omega_b}{\Omega_m+\Omega_\nu}, \quad f_\nu = \frac{\Omega_\nu}{\Omega_m+\Omega_\nu}, \quad f_{cb} = \frac{\Omega_m}{\Omega_m+\Omega_\nu}, \quad f_{\nu b} = \frac{\Omega_b+\Omega_\nu}{\Omega_m+\Omega_\nu}, \tag{5.2.43}$$

$$q_{\rm eff} = \frac{k\Theta_{2.7}^2}{\Gamma_{\rm eff}\,{\rm Mpc^{-1}}}, \quad \Gamma_{\rm eff} = \omega_0\left[\sqrt{\alpha_\nu} + \frac{1-\sqrt{\alpha_\nu}}{1+(0.43ks)^4}\right], \tag{5.2.44}$$

$$\begin{aligned}\alpha_\nu =& \frac{f_c}{f_{cb}}\frac{5-2(p_c+p_{cb})}{5-4p_{cb}} \times \frac{1-0.553f_{\nu b}+0.126f_{\nu b}^3}{1-0.193\sqrt{f_\nu N_\nu}+0.169f_\nu N_\nu^{0.2}}(1+y_d)^{p_{cb}-p_c} \\ &\times\left[1+\frac{p_c-p_{cb}}{2}\left(1+\frac{1}{(3-4p_c)(7-4p_{cb})}\right)(1+y_d)^{-1}\right],\end{aligned} \tag{5.2.45}$$

$$p_c \equiv \frac{1}{4}\left[5-\sqrt{1+24f_c}\right], \quad p_{cb} \equiv \frac{1}{4}\left[5-\sqrt{1+24f_{cb}}\right], \tag{5.2.46}$$

$$s = \frac{44.5\ln(9.83\omega_0)}{\sqrt{1+10\omega_b^{3/4}}}\,{\rm Mpc}, \tag{5.2.47}$$

where N_ν is the number of massive neutrinos, Ω_Λ is the density parameter of cosmological constant, and we have redefine some terms like $\Omega_0 = \Omega_c + \Omega_b + \Omega_\nu$, and $\omega_0 = \Omega_0 h^2$.

Although accurate and based on known physics, the EH expressions are, at the end, fitting formulae and not a fundamental result. As we will show, our GA fitting formulae are notably shorter, as accurate as the EH expression when only baryons and CDM are considered, and slightly more accurate when the effects of massive neutrinos are non-negligible. Therefore, our GA provides compelling alternatives to other available fitting formulae.

5.3 De-Wiggled $T(k)$ from Genetic Algorithms

In this section, we present our fitting formulae for the matter transfer function. We firstly consider the case when $T(k)$ depends only on the amount of baryons and matter, and then we add the effects of massive neutrinos. For both cases, we start describing how the data for the fitting process was gathered using `CLASS`, and later we proceed to introduce the simple fitting function we found using the GA.

	Expression	% Accuracy
BBKS	Eq. (5.2.7)	8.70957
EH	Eq. (5.2.8)	0.777504
GA	Eq. (5.3.4)	0.815012

Table 5.1: Expression and accuracy of the fitting formulae for the matter transfer function as a function of k, ω_b, and ω_m. Although the GA does not provide a more accurate formula than the full EH formula, the simplicity of the former [Eq. (5.3.4)] is a major improvement over the EH formula.

5.3.1 Baryons and Matter

Data

We use the Boltzmann solver `CLASS` to compute the linear matter transfer function[1] $T(k)$. In this code, each pair of parameters $\{\omega_b, \omega_m\}$ defines a cosmology for which we can compute the gravitational potential Φ as a function of the scale k at a fixed redshift. Hence, to see the dependence of the transfer function on these parameters, we make a grid of 4×4 pairs of $\{\omega_b, \omega_m\}$ and compute the gravitational potential for each pair. We consider that $\omega_b \in [0.0214, 0.0234]$, and $\omega_m \in [0.13, 0.15]$, which are around 10σ from the best-fit values found by the Planck Collaboration [39]. For each considered cosmology (16 in total), `CLASS` retrieves 114 points $\{k, \Phi\}$. Therefore, our preliminary dataset is composed by 1824 points whose rows are given as $\{k, \omega_b, \omega_m, \Phi\}$. Now, since the transfer function is basically the normalized potential, we normalize each of the 16 sub-datasets to get $T(k; \omega_b, \omega_m)$. At the end, our final dataset is a table of dimensions 1824×4 with data points given as $\{k, \omega_b, \omega_m, T\}$.

We quantify the goodness of fit of a given analytical expression by the following function

$$\%\text{Acc} = \frac{100}{N} \sum_{i=1}^{N} \left| \frac{T_{i,\text{CLASS}} - T_{i,\text{analytical}}}{T_{i,\text{CLASS}}} \right|, \tag{5.3.1}$$

where $N = 1824$ is the number of data points in our dataset, and T_i is a simplified notation for the transfer function evaluated at k_i, ω_{b_i}, and ω_{m_i}.

Fitting Formula from the GA

Here, we give a few details concerning the specific GA configuration we used and present our fitting formula.

[1]Note that `CLASS` can take into account non-linear effects via fitting functions such as HALOFIT [344]. Here however we focus on the linear regime and neglect non-linear contributions when generating the data.

As explained before, the GA looks for a fitting formula to a dataset by evolving the population, which is composed by expressions combining specific operations (grammar) and coefficients. Schematically, our GA is searching for a function of the form

$$T_{\rm GA}(x) \equiv \left[1 + f_{\rm GA}(x)\right]^{-1/4}, \tag{5.3.2}$$

where

$$x \equiv \frac{k\,{\rm Mpc}/h}{\omega_m - \omega_b}, \quad f_{\rm GA} \equiv \sum_{i=1}^{4} a_i g_i\left((b_i x)^{c_i}\right). \tag{5.3.3}$$

We see that x is a dimensionless quantity since k is given in units $[h\,{\rm Mpc}^{-1}]$, h the reduced Hubble parameter. The constants a_i, b_i, c_i are non-negative random numbers, and g_i is an operation in the grammar set, which we consider to be simply of the form $\{x\}$. The quantities a_i, g_i, b_i, and c_i are the 4 nucleotides. The sum goes from 1 to 4 because we are considering that the genome of the individuals is formed by 4 genes, each one composed by the 4 nucleotides, such that the chromosomes are 4×4 matrices.

It should be noted that the number of genes has to be fixed before the code starts running and we have chosen the number four for two reasons: i) first, from experience we have found that a number of four genes is a compromise (found by trial and error) on the length of the function, as less than is not enough to fit the data, while a much larger number slows down the code considerably, ii) second, if the number of genes is too high, then this could obviously lead to overfitting or instabilities in the fitting. Furthermore, even though at first sight it seems so, the parameters a_i and b_i, in general are not degenerate as b_i appears inside the grammar function, however there may be some degeneracies only when the grammar is linear.

Overall, this configuration, although restrictive, fixes the length of the expressions, thus avoiding over-fitting problems. A couple of reasons motivate the specific forms of Eqs. (5.3.2) and (5.3.3): *i*) the transfer function has specific limits: $T \to 0$ when $k \to \infty$, and $T \to 1$ when $k \to 0$, *ii*) the transfer function only takes on non-negative values, and *iii*) $T(k)$ is smooth.

Now, we present our fitting formula when only baryons and matter are considered. Using the configuration of the GA as explained, the stochastic search ended up with the function

$$T_{\rm GA}(k;\omega_b,\omega_m) = \left[1 + 59.0998\,x^{1.49177} + 4658.01\,x^{4.02755} + 3170.79\,x^{6.06} + 150.089\,x^{7.28478}\right]^{-1/4}, \tag{5.3.4}$$

whose goodness of fit, as measured by Eq. (5.3.1), is $\%{\rm Acc}_{\rm GA} = 0.815012$. The accuracy of the BBKS formula in Eq. (5.2.7) is $\%{\rm Acc}_{\rm BBKS} = 8.70957$, and for the EH formula is $\%{\rm Acc}_{\rm EH} = 0.777504$. We compile these results in Table 5.1. In Fig. 5.3.1, we compare the performance of the fitting formulae. As it can be seen in the left panel of this figure, the three formulae are very

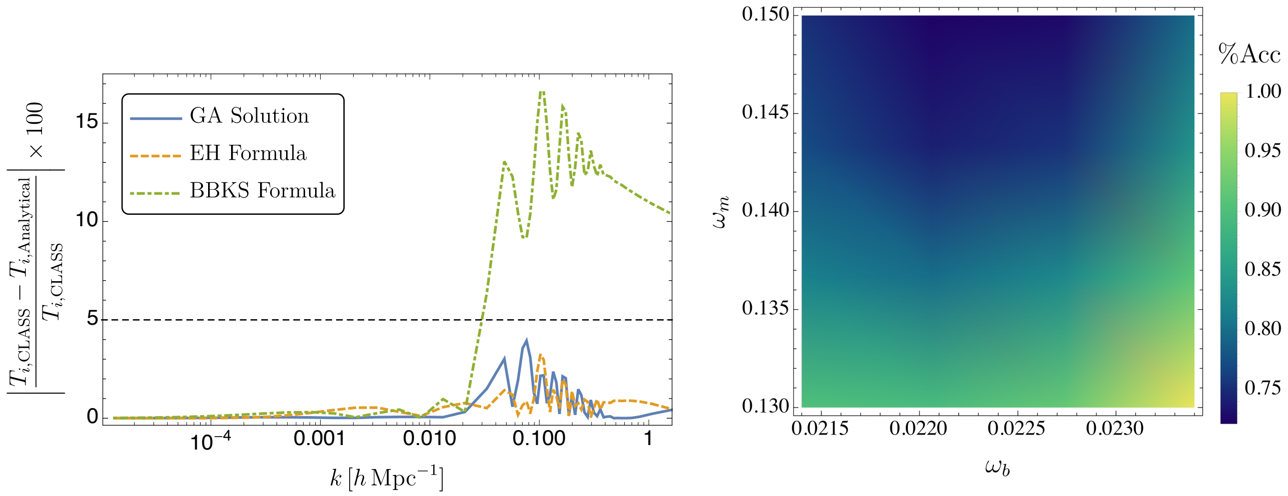

Figure 5.3.1: (Left) Accuracy of the BBKS (green dot-dashed line), EH (mustard dashed line), and the GA (blue solid line) fitting formulae as a function of the scale k and fixed $\{\omega_m, \omega_b\}$. The parameters for these plots are: $\omega_b = 0.02273$, and $\omega_m = 0.1366$. Note that the accuracy of the three formulae notably decrease on the scales where the effects of baryons are most prominent on the cosmological evolution. However, the accuracy of the EH and GA formulae are below 5% in this scale. (Right) Average accuracy of the GA fitting formula for all k as a function of $\{\omega_m, \omega_b\}$. As it can be seen, the formula is up to 1% accurate in overall.

accurate on the large scales ($k < 0.01h\,\text{Mpc}^{-1}$), while for smaller scales ($k > 0.01h\,\text{Mpc}^{-1}$), where the effects of baryons are most prominent on the cosmological evolution, the accuracy of the three formulae decrease. However, we note that our GA formula and the EH formula can be accurate up to 5%, while the BBKS formula is accurate up to 18% in these scales. We would like to emphasize that our GA formula in Eq. (5.3.4) is remarkably simpler than the EH formula which is described by around 30 expressions which occupy around two pages, while their difference in accumulative accuracy is just about 0.04. We also want to stress that, in principle, the GA could get even better results if some modifications are introduced. For instance, a larger grammar set and a more complex f_{GA} function [instead of Eq. (5.3.3)]. Nonetheless, our choices avoid over-fitting while yielding a smooth transfer function with the correct limits in k.

5.3.2 Baryons, Matter and Massive Neutrinos

Data

Apart of baryons and cold dark matter, massive neutrinos can contribute to the matter content once they are freely streaming. We can take into account the effects of massive neutrinos in the matter transfer function using `CLASS`. We compute $T(k)$ at redshift zero as a function of ω_b, ω_m in the same ranges as in Sec. 5.3.1, and $\omega_\nu \equiv 0.0107(\sum_\nu m_\nu/1.0\,\text{eV})$, assuming just one massive

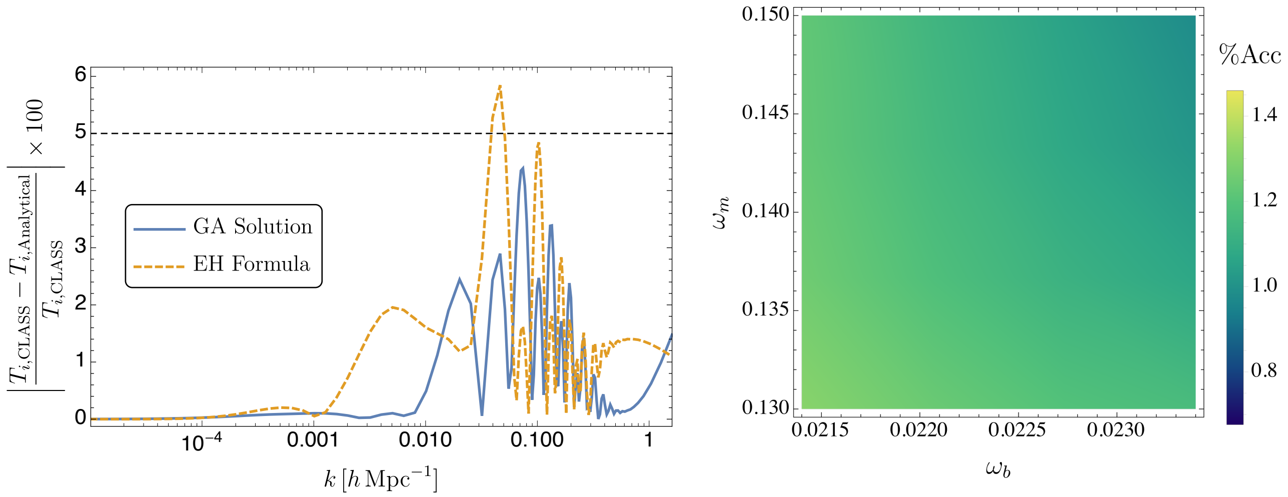

Figure 5.3.2: (Left) Accuracy of the EH (mustard dashed line), and the GA (blue solid line) fitting formulae as a function of the scale k for fixed $\{\omega_m, \omega_b\, \omega_\nu\}$. The parameters for these plots are: $\omega_b = 0.02206$, $\omega_m = 0.1499$, and $\omega_\nu = 0.0008599$ which corresponds to a mass of $\sum_\nu m_\nu = 0.08\,\mathrm{eV}$. As can be seen, the accuracy of the GA formula is below 5% on the whole range of k considered here. (Right) Average accuracy of the GA fitting formula for all k and ω_ν as a function of $\{\omega_m, \omega_b\}$. As it can be seen, the formula is around 1% accurate in overall.

neutrino, and that the total mass of massive neutrinos is in the range $0.06\,\mathrm{eV} \leq \sum m_\nu \leq 0.12\,\mathrm{eV}$. The lower bound of the later constraint corresponds to the minimum mass allowed from neutrino flavour oscillation experiments [512], and the upper bound is the maximum mass value allowed by Planck [39]. In this case, we get a grid of $4 \times 4 \times 4$ data points for $\{\omega_b, \omega_m, \omega_\nu\}$ and compute the gravitational potential for each triad. Again, for each considered cosmology (64 in total), `CLASS` retrieves 114 points $\{k, \Phi\}$. Normalizing the potential to get the transfer function, our final data set is a table of dimensions 7296×5 with data points given as $\{k, \omega_b, \omega_m, \omega_\nu, T\}$. We use Eq. (5.3.1) to quantify the goodness of fit of the analytical expressions, but now $N = 7296$ is the number of data points in our dataset, and T_i is the transfer function evaluated at k_i, ω_{b_i}, ω_{m_i}, and ω_{ν_i}.

Fitting Formula from the GA

Based on the success of the GA in finding an accurate formula for $T(k)$ when neutrinos are massless, this time our GA is looking for a function of the form

$$T_{\mathrm{GA}}(y) \equiv \left[1 + f_{\mathrm{GA}}(y)\right]^{-1/4}, \tag{5.3.5}$$

	Expression	% Accuracy
EH	Eq. (5.2.34)	1.23449
GA	Eq. (5.3.7)	0.993916

Table 5.2: Expression and accuracy of the fitting formulae for the matter transfer function as a function of k, ω_b, ω_m, and ω_ν. Although the accuracy of both formulations are similar, the simplicity of the GA function in Eq. (5.3.7) is a major improvement over the EH formula, which is fully displayed in Appendix 5.2.3.

where

$$y \equiv \frac{k\,\mathrm{Mpc}/h}{\omega_m - \omega_b + \omega_\nu}, \quad f_{\mathrm{GA}} \equiv \sum_{i=1}^{4} a_i g_i\left((b_i y)^{c_i}\right). \tag{5.3.6}$$

Now, we present our fitting formula which considers baryons, matter, and one massive neutrino:

$$T_{\mathrm{GA}}(k;\omega_b,\omega_m) = \left[1 + 56.4933\,y^{1.48261} + 3559.23\,y^{3.76407} + 4982.44\,y^{5.68246} + 374.167\,y^{7.14558}\right]^{-1/4}, \tag{5.3.7}$$

whose goodness of fit, as measured by Eq. (5.3.1), is $\%\mathrm{Acc}_{\mathrm{GA}} = 0.993916$. The accuracy of the extended EH formula considering massive neutrinos is $\%\mathrm{Acc}_{\mathrm{EH}} = 1.23449$. We compile these results in Table 5.2. In Fig. 5.3.2, we compare the performance of the fitting formulae. Similar to the last section, the formulae are more accurate on large scales ($k < 0.01h\,\mathrm{Mpc}^{-1}$) than on the smaller scales ($k > 0.01h\,\mathrm{Mpc}^{-1}$). Note in the left panel of this figure that the accuracy of the GA formula is below the 5% in the whole range of k. Furthermore, the GA formula (5.3.7) is significantly simpler than the EH formula, whose description requires around 30 expression which we give in full in Appendix 5.2.3. Our result is a compelling analytical alternative to compute the matter transfer function.

Numerical Codes

The genetic algorithm code used here can be found in the GitHub repository:

https://github.com/BayronO/Transfer-Function-GA

5.3.3 Conclusions

Genetic Algorithms (GAs), a machine learning technique, have been previously used to obtain improved formulation of cosmological quantities of interest such as the redshift at recombination and the sound horizon at drag epoch [496], and also to perform consistency tests to probe for deviations from ΛCDM [493, 494, 497, 498, 518–520]. Here we used the GA to find analytical alternatives to existing fitting functions for the matter transfer function, such as the BBKS and the EH formulae.

When the transfer function depends only on ω_b and ω_m, the GA finds a very simple fitting formula for $T(k)$ [see Eq. (5.3.4)], which is as accurate as the EH formula, while being significantly shorter (see Sec. 5.2.3). In a more realistic scenario, at least one neutrino should be massive. In this case, our GA finds a fitting function which is both more accurate and notably simpler [see Eq. (5.3.7)] than the EH formula in Sec. 5.2.3. The simplicity of the GA fitting formulae and their accuracy represent a major improvement over other existing analytical formulations of the matter transfer function which are extensively used in the literature [483–485]. Therefore, the GA formulae in Eqs. (5.3.4) and (5.3.7) are compelling semi-analytic alternatives to easily and accurately compute the matter power spectrum.

5.4 The Matter Power Spectrum of Modified Gravity

5.4.1 Introduction

The clustering of matter, due to gravitational instabilities, forming the structure of our Universe constitutes a key physical process in the expansion history. This process offers one of the main links between observations and theoretical models through the so-called matter power spectrum $P(k, z)$, which in general is a function of the wavenumber k and the redshift z [373, 403, 477]. For a given redshift, $P(k)$ can be numerically computed using Boltzmann solvers, like the codes `CAMB` [342] or `CLASS` [479]. Nonetheless, it is desirable to have an analytical formulation of $P(k)$ in some cases; for instance, when computing costs are demanding and high accuracy is not required. When ΛCDM is the assumed cosmological model, there are two well-known fitting formulae to determine the transfer function involved in the computation of $P(k)$. These are the Bardeen-Bond-Kaiser-Szalay (BBKS) formula [480] and the Eisenstein-Hu (EH) formulae [482, 514], which are widely used in the literature [484, 521–527]. However, up to the best of our knowledge, there are no similar formulations considering alternative models.

In Ref. [11] two of the authors here used a machine learning technique known as the Genetic Algorithms (GAs) to find an analytical expression for the matter power spectrum under the ΛCDM framework and neglecting the representative wiggles of $P(k)$ due to the BAOs (Baryon Acoustic Oscillations). This new formula shows to be as accurate as its predecessors while being considerably simpler; and thus, easier to implement in other numerical computations where the knowledge of the de-wiggled $P(k)$ is required. Here, we want to extend that work by considering some possible effects on $P(k)$ introduced by modifications of gravity. Briefly, using the GAs, we find a parametric function for the de-wiggled $P_{\rm MG}(k)$ whose performance is tested by comparing against numerical data obtained from the popular Boltzmann solver `CLASS`. In particular, we use the branches `hi_class` [353, 528] and `mgclass` [347, 529]. Both allow to numerically compute $P(k)$ for MG theories. The former considers the whole Horndeski theories, while the later uses the slip parameters framework.

5.4.2 The Matter Power Spectrum of Modified Gravity

As mentioned in the Introduction, the existence of structure in our Universe follows from the agglomeration of matter due to gravitational instabilities. One of the key statistical correlation functions of this process is the matter power spectrum $P(k, z)$. It can be shown that, when non-linear effects are neglected, the matter power spectrum for a given redshift can be written as [403]

$$P(k) \equiv P_0(k)T^2(k) \tag{5.4.1}$$

where $P_0(k)$ is an initial matter power spectrum and $T(k)$ is the matter transfer function. Now, we firstly comment on the form of $P(k)$ for ΛCDM, and then we discuss some of the possible alterations to this observable when modifications of gravity are considered.

In the standard case, the initial matter power spectrum is approximately given by

$$P_0(k) \equiv A_0 k^{n_s}, \quad A_0 \equiv \frac{8\pi^2}{25} \frac{\mathcal{A}_s}{\Omega_{m0}^2 H_0^4} k_p^{1-n_s} \tag{5.4.2}$$

where Ω_{m0} is the matter density parameter today, H_0 is the Hubble constant, n_s and $\mathcal{A}_s$ are the spectral tilt and amplitude of primordial scalar perturbations, respectively, and k_p is an arbitrary pivot scale [403].[2] On the other hand, the matter transfer function takes into account the effects of all the interacting species, e.g. acoustic oscillations due to baryonic pressure, amplitude suppression due to the free streaming of massive neutrinos, transition from a radiation dominated epoch to a matter dominated epoch, and more. All these physical details are encompassed by the fitting functions presented in Ref. [482, 514], which achieve an accuracy of 1-2% while needing around 30 different expressions in their full formulations. However, in Ref. [11], two of the authors here shows that the GAs are able to find much more economical expressions while achieving the same accuracy range.

To the best of our knowledge, there are currently no similar analytical formulations available when considering alternative models. To find derive such a formula, our first step is to characterize the potential effects that MG theories introduce in the matter power spectrum compared to the concordance model. In the following, we undertake this characterization process. Firstly, a background history different to that of ΛCDM can change the growth factor, which in turn

[2]Note that $P_0(k)$ is not the primordial power spectrum which is given by $P_{\mathcal{R}}(k) \equiv \mathcal{A}_s(k/k_p)^{1-n_s}$ [218].

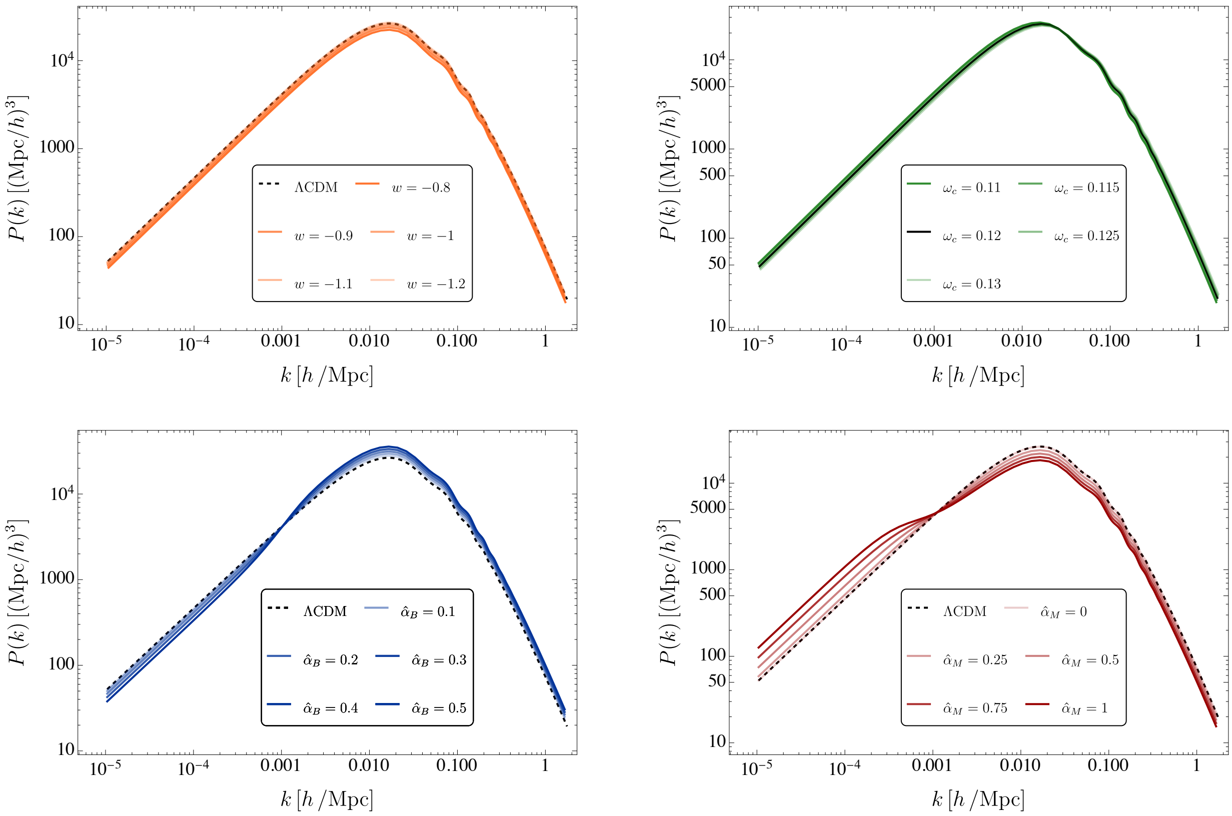

Figure 5.4.3: Typical effects of modified gravity on the theoretical matter power spectrum. In the upper panels, we consider a wCDM model varying the dark energy equation of state w (left), and the reduced CDM density parameter ω_c (right). In the lower panels, we consider the `proto_scale` models in `hi_class`, varying the braiding $\hat{\alpha}_B$ (left) and the mass running $\hat{\alpha}_M$ (right) parameters. In the former case, the matter power spectrum is suppressed at very large scales while in the later it is enhanced. Then, we see a transition between the large scale spectrum to an enhanced (left) or suppressed (right) spectrum at smaller scales.

modifies the overall amplitude of $P(k)$. Secondly, a variation in the reduced matter density parameter ω_m implies a variation in the redshift and scale at the radiation-matter transition, denoted respectively as $z_{\rm eq}$ and $k_{\rm eq}$. This causes a shift in the position of the maximum of the matter power spectrum. Before continuing, we want to mention that it is possible to estimate $z_{\rm eq}$ and $k_{\rm eq}$ using the approximated expressions given in Ref. [482]. Nevertheless, as shown in the Appendix A of [12], the GAs are able to find expressions with an accuracy improved by two orders of magnitude while keeping simplicity. As a third effect, modified gravity can induce a clustering effective dark energy component when the structure formation process is occurring. This of course modifies the amplitude of $P(k)$, [405, 407, 530]. Modifications at the largest scales due to ISW or normalization. Finally, there could be a variation in the amplitude and location of the acoustic peaks. However, these effects are principally controlled by the reduced baryon density parameter ω_b which is tightly constrained by observations [39]. Here, we fix it to its default value in the popular Boltzmann solver `CLASS`; i.e. $\omega_b = 0.0223828$, and neglect the small oscillations in our formulation.

In Fig. 5.4.3 we have plotted the matter power spectra for four different models varying some of their parameters in order to exemplify the physical effects introduced by modifications of gravity, as explained above. These plots were obtained using the branch `hi_class` of `CLASS`. In the upper-left panel, we consider a wCDM model, with a constant speed of sound c_s^2, no anisotropic stress, and the equation of state of dark energy w varying in the interval $[-1.2, -0.8]$. We can see that the overall amplitude of $P(k)$ is modified when w varies. In the upper-right panel, we consider a ΛCDM model, varying the reduced CDM density parameter ω_c in the range $[0.11, 0.13]$. We note small shifts in scale of the maximum of $P(k)$. For the lower panels, we used one of the implemented models by default in `hi_class`; namely, the `propto_scale` model. In this model, the effective field theory (EFT) parameters characterizing the cosmological dynamics of the whole Horndeski theory are taken as proportional to the scale factor. For more details about the EFT of Horndeski theories see Refs. [390, 531], and for the code `hi_class` see Refs. [353, 528]. In particular, for these plots we fixed the EFT parameters and vary only the proportionality constant of the braiding parameter $\hat{\alpha}_B$ (lower-left panel), and of the mass running parameter $\hat{\alpha}_M$ (lower-right), while the background evolution matches that of ΛCDM. As it can be seen, there is a clear distinction between the behavior of $P(k)$ at large scales and at small scales, with a marked transition occurring before the scale at equality. The matter power spectrum at the largest scales holds the form of the initial matter power spectrum proportional to k^{n_s} while differences can be attributed to variations in the amplitude A. Then, at smaller scales, the spectrum can be enhanced (as in the lower-left panel) or suppressed (as in the lower-right panel) by modified gravity. In all the cases, we have depicted the matter power spectrum of ΛCDM to make notable the differences introduced by MG models.

In the next section, we propose a parameterized function for the matter power spectrum $P(k)$ that incorporates the aforementioned effects.

5.4.3 Parameterization of $P(k)$

Summarizing our discussion in the last section, we consider the following modified gravity effects on the $P(k)$:

1. Variations in the amplitude A of the initial matter power spectrum $P_0(k)$ at large scales.

2. Overall enhancement or suppression of the amplitude.

3. Shift of the equality scale $k_{\rm eq}$.

In order to encompass these three effects in one single expression, we assume that the total matter power spectrum considers the contribution of two different spectra. At large scales, the most relevant contribution to $P(k)$ comes from the following expression

$$P_{\text{large}}(k; s, n_s) \equiv A(s) \left(\frac{k}{h/\text{Mpc}} \right)^{n_s} \left[(\text{Mpc}/h)^3 \right], \tag{5.4.3}$$

where

$$A(s) \equiv (1+s) \frac{P_{\Lambda\text{CDM}}(k_i)}{k_i^{n_s} T^2_{\Lambda\text{CDM}}(k_i)}, \tag{5.4.4}$$

is a dimensional constant. The matter power spectrum $P_{\Lambda\text{CDM}}$ and the matter transfer function $T_{\Lambda\text{CDM}}$ for ΛCDM can be retrieved from e.g. `CLASS`, and thus k_i corresponds to the smallest value of k considered by the Boltzmann solver. Notice that this parameter is basically a modification of A_0 defined in Eq. (5.4.2). However, we do not use A_0 directly in the definition of $A(s)$, i.e., we do not define this parameter as $A(s) \equiv A_0(1+s)$, since the expression for A_0 is an approximation only valid for sub-horizon modes [403]. The parameter s takes on negatives values when the matter power spectrum is suppressed (as shown in the lower-left panel of Fig. 5.4.3), and positive values when the primordial matter power spectrum is enhanced (as depicted in the lower-right panel of Fig. 5.4.3) at large scales. The additional effects, such as an overall modification of the amplitude and the shift of the maximum, are incorporated into the matter power spectrum (referred to as P_{small}), which primarily manifest at smaller scales. In the upper-right panel of Fig. 5.4.3, it is evident that a change in the parameter w in the wCDM model can result in an overall enhancement or suppression of the amplitude of the matter power spectrum. Hence, we adopt this model as a reference to develop a formula for P_{small} utilizing the GAs. The accuracy of such a formula is measured by the following fitness function

$$\text{Acc}\% \equiv \left\langle \frac{|P_{\text{CLASS}} - P_{\text{analytical}}|}{P_{\text{CLASS}}} \right\rangle \times 100, \tag{5.4.5}$$

where P_{CLASS} is the matter power spectrum numerically computed using `CLASS`, and $P_{\text{analytical}}$ is the expression obtained from the GAs. In particular, we consider a constant sound speed given by $c_s^2 = 0.001$, fix the spectral tilt n_s to the default value in `CLASS`, and vary w in the range $[-1.2, -0.8]$. The GAs runs give the following expression[3] in units $[(\mathrm{Mpc}/h)^3]$

$$P_{\mathrm{small}}(k) = \frac{2.52395 \times 10^6 \left(\frac{k}{h/\mathrm{Mpc}}\right)^{0.96452} (1 + 0.710636\alpha^3 + 1.88019\alpha^4 + 0.939217\alpha^5)}{(1 + 59.0998\, x^{1.49177} + 4658.01\, x^{4.02755} + 3170.79\, x^{6.06} + 150.089\, x^{7.28478})^{1/2}}, \tag{5.4.6}$$

whose accuracy is 1.72%. In the last equation, we have defined the dimensionless variable $x \equiv k/(\omega_m - \omega_b)\,\mathrm{Mpc}/h$, since k is given in units $[h/\mathrm{Mpc}]$, and we promoted w to a general parameter α in order to avoid possible confusions with the notation. The parameter α, in general, measures the overall modifications in the amplitude of $P(k)$ and it is not restricted to assume values in the range $[-1.2, -0.8]$. However, this parameter has the lower bound $\alpha > -1.68492$ since P_{small} is positive for all k. It is important to emphasize that the wCDM model is used purely as a template in our study, as the variation of w specifically generates the effect we aim to capture, which is an overall modification of the amplitude of the matter power spectrum.

Finally, we assume that the spectra in Eqs. (5.4.3) and (5.4.6) are smoothly connected by a transition function given by

$$\sigma(k; k_0, \beta) = \left[1 + e^{-(\ln k - \ln k_0)/\beta}\right]^{-1}. \tag{5.4.7}$$

where the transition is centered at k_0 and β determines its width.[4] It is noteworthy that the limits of this function are $\sigma \to 0$ when $k \ll k_0$, and $\sigma \to 1$ when $k \gg k_0$, and that we have defined σ using logarithms since usually $P(k)$ is depicted in log-space. The transition between these limits occurs around $k \sim k_0$ with a smoothing level determined by β. Consequently, a small β corresponds to a rapid transition, while a large β results in a slower transition. Combining these considerations, the parameterized expression for $P(k)$ in the context of modified gravity is given by:

$$P_{\mathrm{MG}}(k; \alpha, \beta, k_0, s, \omega_m, n_s) \equiv [1 - \sigma(k; k_0, \beta)] P_{\mathrm{large}}(k; s, n_s) + \sigma(k; k_0, \beta) P_{\mathrm{small}}(k; \alpha, \omega_m). \tag{5.4.8}$$

The new expression requires 6 parameters as input: the spectral tilt n_s, the shift s at large scales, the overall enhancement (or suppression) parameter α, the reduced matter density parameter ω_m, the transition center k_0, and the transition width β switching between P_{large} and P_{small}. With the exception of n_s and ω_m, which are determined through observations, the remaining four parameters are free. We want to emphasize that the expression obtained through GAs was

[3]For details about the specific structure of the GAs, e.g., the genome arrangement and avoidance of overfitting problems, please refer to Ref. [11].

[4]This transition function is not unique. Another common option for a "smooth step function" which would be valid is $\sigma(k; k_0, \beta) \equiv (1 + \tanh[(\ln k - \ln k_0)/\beta])/2$.

Model	Parameter	α	$k_0 \times 10^{-3}$	β	s	Acc%
`propto_scale`	$\hat{\alpha}_B = 0.5$	0.68153	1.16918	0.42243	-0.21975	1.53%
`propto_scale`	$\hat{\alpha}_M = 0.5$	0.36380	0.73084	0.45974	0.53958	1.62%
`propto_scale`	$\hat{\alpha}_T = -1$	0.53444	0.40205	0.39972	-0.47066	1.52%
`propto_omega`	$\tilde{\alpha}_B = 0.625$	0.54866	0.76693	0.45681	-0.07756	1.46%
`propto_omega`	$\tilde{\alpha}_M = 3.0$	0.59006	0.39858	0.46187	1.57924	1.48%
`propto_omega`	$\tilde{\alpha}_T = -0.25$	0.53215	1.16323	0.42635	0.02292	1.47%
`plk_late`	$E_{11} = E_{22} = 0.5$	0.54762	0.76681	0.49599	-0.62532	1.43%
	$E_{11} = E_{22} = -0.5$	0.42644	0.28607	0.51071	2.99343	1.51%
HDES	$\tilde{J}_c = 0.005$	0.56331	2.24347	0.443931	0.05417	1.39%

Table 5.3: Best-fit parameters α, k_0, β, and s for several models in the codes `hi_class` and `mgclass`. Just one value of the parameters of each model is shown to keep our presentation simple. We can see that the mean accuracy in each example is around 1-2%.

$P_{\rm small}$ in Eq. (5.4.6), while $P_{\rm large}$ in Eq. (5.4.3) and σ in Eq. (5.4.7) are assumed and motivated by physical intuitions.

In the following section, we will evaluate the effectiveness of Eq. (5.4.8) by estimating the best-fit values of parameters to accurately reproduce the numerical matter power spectra obtained from various MG theories using the `hi_class` and `mgclass` codes.

5.4.4 Performance

Here, we numerically compute matter power spectra using the codes `hi_class` and `mgclass` considering several models. Subsequently, we find the best-fit values of the parameters α, k_0, β, and s by minimizing the fitness function in Eq. (5.4.5). This procedure will yield to the best match of $P_{\rm MG}(k)$ in Eq. (5.4.8) with respect to the data from `CLASS`.

There are several models already implemented in `hi_class`, and we make use of two specific ones: `proto_scale` and `propto_omega`. In the `propto_scale` model, the EFT parameters of the Horndeski theory are proportional to the scale factor a, i.e. to $\alpha_i \equiv \hat{\alpha}_i a$, where $i = K, B, M, T$ denotes the kineticity, braiding, mass running and tensor speed excess parameters, respectively. On the other hand, in the `propto_omega` model, the EFT parameters are proportional to the dark energy density parameter $\Omega_{\rm DE}$, i.e. $\alpha_i \equiv \tilde{\alpha}_i \Omega_{\rm DE}$. We also add to `hi_class` the designer Horndeski model (HDES) introduced in Ref. [357]. The HDES model has two parameters; namely, $\tilde{J}_c$ and n. We fix $n = 1$, and consider a small value for $\tilde{J}_c$. In all these models, it is assumed that the background evolution exactly matches that of ΛCDM. In `mgclass`, we also use an already implemented model called `plk_late`, in which the slip parameters are parameterized in terms of $\Omega_{\rm DE}$ (see Ref. [347]). This model in particular has been used by observational collaborations such as Planck [378] and DES [532].

In Table 5.3, we show the best-fit values of the parameter set $\{\alpha, k_0, \beta, s\}$ along with the associated mean accuracy, achieved by selecting a specific parameter value from each model. It is important to mention that we have explored multiple parameter values for each model. However, for the sake of simplicity in the presentation, we report only one value. The details of the analysis and the parameter exploration for each model can be found in the provided codes (see the Numerical Codes statement). Table 5.3 shows that the mean accuracy for the considered models is approximately 1-2%.[5] In Fig. 5.4.4, we plot three examples of the matter power spectra from MG theories to visually show the excellent fit provided by our formula with respect to numerical data. In this plot, we use the models `propto_scale` of `hi_class` varying the braiding constant $\hat{\alpha}_B$ and the mass running constant $\hat{\alpha}_M$. From `mgclass`, we used the `plk_late` model assuming the parameters $E_{11} = E_{22} = -1.0$. We also plot the ΛCDM matter power spectrum to highlight the modifications introduced by these alternative theories. In the subplot, we depict the accuracy as a function of k, which can be measure as

$$\text{Acc}\%(k) \equiv \left(\frac{P_{\rm CLASS} - P_{\rm analytical}}{P_{\rm CLASS}} \right) \times 100, \tag{5.4.9}$$

where no mean value is taken, as in Eq. (5.4.5). This shows that most of values are in the 2% region defined by the black dotted lines. Remarkably, our formula is able to capture the substantial deviation at large scales observed in the spectrum of the `plk_late` model (depicted in blue) and the significant enhancement around $k_{\rm eq}$ in the `propto_scale` braiding model (depicted in pink). It is also noteworthy that although the expression of $P_{\rm small}$ in Eq. (5.4.6) does not consider the wiggles introduced by BAOs in the matter power spectrum, the error of neglecting this oscillatory behavior is around 5% in the most inaccurate cases. The amplitude of the acoustic peaks depends mainly on the amount of baryonic matter, which translate to the parameter ω_b. However, observations indicate that $\omega_b \approx 0.022$ implying small peaks. Therefore, a line passing through these oscillations seems to be a good approximation.[6]

[5] We want to mention that since we fix n_s to find $P_{\rm small}$ using the GAs, this could yield to errors when different values of n_s are considered. Although, the effect of n_s on $P(k)$ is small, we verified that the mean accuracy of our formula $P_{\rm MG}$ is still around 1% when n_s is varied in the interval $[0.96, 0.97]$ which is 1σ away from the value measured by Planck [39].

[6] However, the formula for $P_{\rm MG}(k)$ should not be used when an accurate description of these wiggles is required. The introduction of these oscillations in $P_{\rm MG}(k)$ is a further improvement which we leave for a future work.

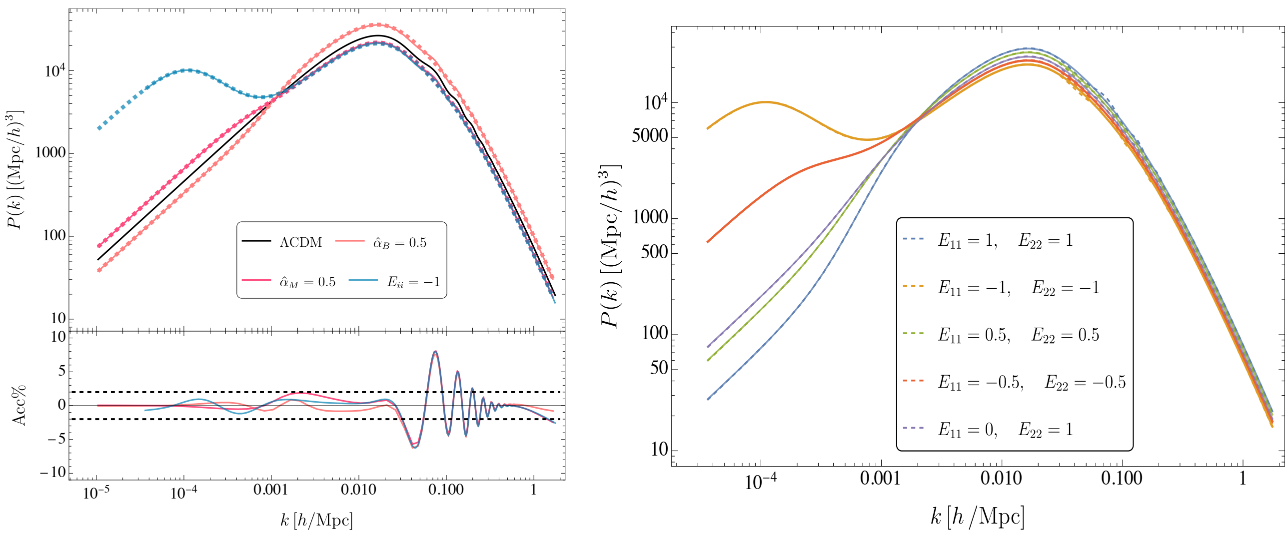

Figure 5.4.4: (Left) Three examples showing the fitting of our formula in Eq. (5.4.8) (dots) with respect to numerical results (solid lines). The matter power spectrum of ΛCDM (black line) is plotted to highlight the effects introduced by MG theories. The subplot shows the accuracy of the formulae as a function of k. We can see that most of points are in the 5% region defined by the black dotted lines. (Right) Fit for the `plk_late` model showing the fitting of our formula in Eq. (5.4.8) (dots) with respect to `hi_class` results (solid lines). It can be seen an excellent qualitative agreement between our formula and this model for several variations of its parameters.

Numerical Codes

The genetic algorithm code used here can be found in the GitHub repository:

https://github.com/BayronO/Pk-in-Modified-Gravity

5.4.5 Conclusions

Accurate fitting formulations for the matter transfer function allow to compute the matter power spectrum within the context of the ΛCDM model [11, 480, 482, 514]. However, there is no any formulation available when modifications of gravity are considered. In this work, we have put forward a parametric function for $P(k)$ considering several effects introduced by modified gravity theories. The new formula for $P_{\rm MG}(k)$ was presented in Eq. (5.4.8) and it is composed by two main parts. A matter power spectrum $P_{\rm large}$ encompassing modifications at large scales, and the spectrum $P_{\rm small}$ which manifest at smaller scales. The former is proportional to k^{n_s} with amplitude $A(s) \approx A_0(1+s)$, where s is a parameter measuring the shift of the initial amplitude A_0 which in the case of ΛCDM is approximately given in Eq. (5.4.2). The other spectrum; namely $P_{\rm small}$, was obtained through the machine learning technique of the genetic algorithms using a wCDM model as template. The expression for $P_{\rm small}$ in Eq. (5.4.6) involves two parameters: a parameter α measuring overall modifications (enhancement or suppression) in the amplitude of the spectrum, and ω_m which controls the value of the scale at equality $k_{\rm eq}$. These two spectra; $P_{\rm large}$ and $P_{\rm small}$, are smoothly connected by the transition function σ defined in Eq. (5.4.7). This function marks the transition center at the scale k_0 with a smoothness measured by the parameter β. Therefore, our formulation requires 6 input parameters: the spectral tilt n_s, the shift s of A_0 at large scales, the enhancement (suppression) factor α measuring modifications in the amplitude of $P_{\rm small}(k)$, the reduced matter density parameter ω_m, and two parameters, k_0 and β, that determine the center and width of the transition region between the matter power spectra $P_{\rm large}$ and $P_{\rm small}$ [see Eq. (5.4.8)].

The performance of our formulation was compared against numerical results obtained from the codes `hi_class` and `mgclass` for several models. The relatively simple expression in Eq. (5.4.8) showed a mean accuracy of about 1-2% (see Table 5.3). In Fig. 5.4.4, we showed three examples of the fitting of our formula with respect to some MG models. In the subplot, the accuracy of the formulae as a function of k using Eq. (5.4.9) was measured. This showed that most of values predicted by our formula lies in the 2% region. Furthermore, although our expression does not consider baryonic acoustic oscillations, neglecting these wiggles introduces an error not greater than 5%. Given that ongoing surveys, like Euclid, expect to reach an observational accuracy of around 1% for some cosmological parameters which are obtained using the matter power spectrum, and that they already use the Eisenstein-Hu formula in their analysis [533], our formula could extend these analysis to model beyond ΛCDM without loosing accuracy. Therefore, the function $P_{\rm MG}(k)$ in Eq. (5.4.8) represents a compelling fitting formula for the matter power spectrum of alternative models to ΛCDM.

While this solution does not possess the baryonic wiggles necessary for inferring cosmological parameters from the BAO signal, it can still be used for parameter inference. To illustrate this, let us consider the approach used to forecast cosmological parameters for the Euclid survey [533]. The observed galaxy power spectrum relies on the de-wiggled matter power spectrum, which is the sum of two components: the linear matter power spectrum obtained from a Boltzmann code and the linear matter power spectrum without wiggles but exhibiting the same broad band as the linear matter power spectrum. Both components are modulated by a function that controls the non-linear damping of the BAO signal in all directions. The no-wiggles power spectrum is often computed using the a fitting formula (for instance, for the ΛCDM models, the EH). It is clear that, when exploring cosmological models beyond the standard framework, it becomes crucial to appropriately parameterize the no-wiggles matter power spectrum in order to accurately capture the amplitude and shape of the observed galaxy power spectrum.

Chapter 6

Concluding Remarks and Outlooks

In the vast expanse of cosmological inquiry, the tapestry of our understanding has expanded exponentially in recent decades. As graduate students, we often find ourselves at the crossroads of myriad possibilities, and often, the gravitational pull of convention or the inertia of established pathways can dictate our trajectories. However, within this cosmos of possibilities, I fervently believe in the power of individual agency and the pursuit of diverse interests. It was with this conviction that I embarked on my doctoral journey, driven by a desire to explore the breadth of cosmological inquiry. While the path to contributing across multiple subfields proved to be full with challenges, it was a journey marked by invaluable learning and growth. As I reflect on my contributions, I am reminded of the intrinsic interconnectedness of cosmological phenomena and the potential for interdisciplinary approaches to yield profound insights. Now, I will provide a concise overview of the research presented in this thesis, reflecting on the exploration that has unfolded across its chapters.

In chapter 2, I delved into the investigation of various dark energy models, encompassing unconventional cosmological fields such as non-abelian gauge fields and inhomogeneous scalar fields. Many of these models were situated within a framework of homogeneous but anisotropic spacetime. By exploring diverse metrics, we aimed to illuminate prevailing cosmological puzzles, including anomalies observed in the cosmic microwave background (CMB). Moving forward, our efforts will extend towards further elucidating the implications of these models through observational avenues.

In Chapter 3, I explored an alternative avenue to dark energy, focusing on the realm of modified gravity. Specifically, my attention was drawn to highly general models, such as the Scalar-Vector-Tensor theories. The vast array of available models in contemporary theoretical cosmology presents a formidable challenge, making it impractical to exhaustively study the cosmological ramifications of each individual model. In light of this, I advocate for the study of overarching, comprehensive models as a means to systematically analyze entire sectors of cosmological dynamics. However, this endeavor is not without its complexities, as such general theories necessitate numerous underlying assumptions. Of particular interest to me was the examination of the validity of commonly used approximations, such as the quasi-static and sub-horizon approximations. Through our investigations, we discovered discrepancies in the application of these approximations within the context of $f(R)$ theories, despite the absence of observable modifications. This observation suggests a potential misapplication of this approximation scheme in other theoretical frameworks. Advancing on this, I aspire to expand upon this research by exploring more general theories, such as Horndeski or Scalar-Vector-Tensor theories, in pursuit of a deeper understanding of their implications within the cosmological landscape.

In Chapter 4, I embarked on an exploration of the flip side of accelerated expansion: the inflationary epoch. Specifically, our focus shifted to analyzing the inflationary dynamics of non-abelian gauge fields, uncovering intriguing disparities in comparison to existing literature. This serves as an explicit reminder that errors can manifest in even the most meticulous of research endeavors—a humbling realization that extends to my own work. Additionally, we delved into the investigation of a primordial mechanism known as the vector curvaton, which holds a relevant role in shaping the dynamics of the isocurvature modes and possible primordial anisotropy.

I was captivated by the rapid advancement of artificial intelligence and its burgeoning application in the field of cosmology. Driven by a desire to leverage these innovative techniques for scientific inquiry, I decided to explore their potential contributions. Specifically, I immersed myself in the realm of symbolic regression using genetic algorithms.

Our endeavors yielded fascinating results. We unveiled novel expressions for the de-wiggled matter transfer function of ΛCDM, and its simple extension considering massive neutrinos, offering simpler yet slightly more accurate alternatives to the long-standing Eisenstein-Hu formulae that have dominated the field for nearly three decades. Our hope is that these new formulae will garner increased attention in the years to come, enriching the toolkit available to researchers in their quest to unravel the mysteries of the cosmos. Furthermore, our exploration extended to the examination of the broader effects of gravitational modifications on the matter power spectrum. Through meticulous analysis, we identified overarching patterns and subsequently proposed a parametric formula capable of faithfully reproducing the de-wiggled matter power spectrum across a multitude of modified gravity models with remarkable precision, typically within the range of 1% to 2%. To the best of our knowledge, the formulae we have developed represent a pioneering effort aimed at encompassing a vast array of cosmological models. Building upon these foundations, we aspire to expand our investigations to encompass the intricate phenomena of baryon acoustic oscillations, with the aim of developing fitting formulae that capture this phenomenon with similar fidelity.

Reflecting on the question posed in the preface of this work—"How can I honor the tireless efforts of my predecessors and current colleagues while contributing to the advancement of cosmology?"—I must acknowledge that despite years of inquiry, a definitive answer eludes me. However, this realization only fuels my determination to continue expanding my horizons, exploring new avenues of research, and engaging with the global scientific community.

As I journey forward, I am committed to sharing my insights, experiences, and discoveries with others, fostering collaboration and dialogue across borders and disciplines. It is through this collective effort that we may unearth the transformative ideas capable of reshaping our understanding of the cosmos.

With each conversation, presentation, and publication, I aspire to catalyze the emergence of groundbreaking concepts. Though the path ahead may be uncertain, I remain steadfast in my conviction that through perseverance, passion, and collaboration, we can chart a course towards profound discovery and lasting impact. I carry with me the unwavering belief that the next big idea may be just over the horizon, waiting to be seized and celebrated by the global scientific community.

Bibliography

[1] M. Álvarez, J.B. Orjuela-Quintana, Y. Rodriguez and C.A. Valenzuela-Toledo, *Einstein Yang–Mills Higgs dark energy revisited*, Class. Quant. Grav. **36** (2019) 195004 [1901.04624].

[2] J.B. Orjuela-Quintana, M. Alvarez, C.A. Valenzuela-Toledo and Y. Rodriguez, *Anisotropic Einstein Yang-Mills Higgs Dark Energy*, JCAP **10** (2020) 019 [2006.14016].

[3] A. Guarnizo, J.B. Orjuela-Quintana and C.A. Valenzuela-Toledo, *Dynamical analysis of cosmological models with non-Abelian gauge vector fields*, Phys. Rev. D **102** (2020) 083507 [2007.12964].

[4] J. Motoa-Manzano, J. Bayron Orjuela-Quintana, T.S. Pereira and C.A. Valenzuela-Toledo, *Anisotropic solid dark energy*, Phys. Dark Univ. **32** (2021) 100806 [2012.09946].

[5] J.B. Orjuela-Quintana and C.A. Valenzuela-Toledo, *Anisotropic k-essence*, Phys. Dark Univ. **33** (2021) 100857 [2106.06432].

[6] S. García-Serna, J.B. Orjuela-Quintana, C.A. Valenzuela-Toledo and H. Ocampo-Durán, *Reconstructing the parameter space of nonanalytical cosmological fixed points*, Int. J. Mod. Phys. D **32** (2023) 2350073 [2302.09181].

[7] D. Gallego, J.B. Orjuela-Quintana and C.A. Valenzuela-Toledo, *Anisotropic dark energy from string compactifications*, JHEP **04** (2024) 131 [2402.09570].

[8] W. Cardona, J.B. Orjuela-Quintana and C.A. Valenzuela-Toledo, *An effective fluid description of scalar-vector-tensor theories under the sub-horizon and quasi-static approximations*, JCAP **08** (2022) 059 [2206.02895].

[9] J.B. Orjuela-Quintana and S. Nesseris, *Tracking the validity of the quasi-static and sub-horizon approximations in modified gravity*, JCAP **08** (2023) 019 [2303.14251].

[10] J.C. Bueno Sanchez, J.B. Orjuela-Quintana and C.A. Valenzuela-Toledo, *On the coupling of vector fields to the Gauss-Bonnet invariant*, *Rev. Acad. Colomb. Cienc. Ex. Fis. Nat.* **45** (2021) 67 [1504.07983].

[11] J.B. Orjuela-Quintana, S. Nesseris and W. Cardona, *Using machine learning to compress the matter transfer function T(k)*, *Phys. Rev. D* **107** (2023) 083520 [2211.06393].

[12] J.B. Orjuela-Quintana, S. Nesseris and D. Sapone, *Machine learning unveils the linear matter power spectrum of modified gravity*, *Phys. Rev. D* **109** (2024) 063511 [2307.03643].

[13] E. Hubble, *A Relation between Distance and Radial Velocity among Extra-Galactic Nebulae*, *Proceedings of the National Academy of Science* **15** (1929) 168.

[14] A. Einstein, *Cosmological Considerations in the General Theory of Relativity*, *Sitzungsber. Preuss. Akad. Wiss. Berlin (Math. Phys.)* **1917** (1917) 142.

[15] W. de Sitter, *On Einstein's Theory of Gravitation and its Astronomical Consequences. First Paper*, *Monthly Notices of the Royal Astronomical Society* **76** (1916) 699.

[16] W. de Sitter, *On Einstein's Theory of Gravitation and its Astronomical Consequences. Second Paper.*, *Monthly Notices of the Royal Astronomical Society* **77** (1916) 155.

[17] W. de Sitter, *On Einstein's Theory of Gravitation and its Astronomical Consequences. Third Paper.*, *Monthly Notices of the Royal Astronomical Society* **78** (1917) 3.

[18] A. Friedman, *On the Curvature of space*, *Z. Phys.* **10** (1922) 377.

[19] A. Friedmann, *On the Possibility of a world with constant negative curvature of space*, *Z. Phys.* **21** (1924) 326.

[20] G. Lemaitre, *A Homogeneous Universe of Constant Mass and Growing Radius Accounting for the Radial Velocity of Extragalactic Nebulae*, *Annales Soc. Sci. Bruxelles A* **47** (1927) 49.

[21] H.P. Robertson, *Kinematics and World-Structure*, *Astrophys. J.* **82** (1935) 284.

[22] H.P. Robertson, *Kinematics and World-Structure. 2*, *Astrophys. J.* **83** (1935) 187.

[23] H.P. Robertson, *Kinematics and World-Structure. 3*, *Astrophys. J.* **83** (1936) 257.

[24] A.G. Walker, *On Milne's Theory of World-Structure*, Proc. Lond. Math. Soc. s **2-42** (1937) 90.

[25] G. Gamow, *Expanding universe and the origin of elements*, Phys. Rev. **70** (1946) 572.

[26] R.A. Alpher, H. Bethe and G. Gamow, *The origin of chemical elements*, Phys. Rev. **73** (1948) 803.

[27] R.A. Alpher and R. Herman, *Evolution of the Universe*, Nature **162** (1948) 774.

[28] R.A. Alpher and R.C. Herman, *Theory of the Origin and Relative Abundance Distribution of the Elements*, Rev. Mod. Phys. **22** (1950) 153.

[29] R.A. Alpher, J.W. Follin and R.C. Herman, *Physical Conditions in the Initial Stages of the Expanding Universe*, Phys. Rev. **92** (1953) 1347.

[30] A.A. Penzias and R.W. Wilson, *A Measurement of Excess Antenna Temperature at 4080 Mc/s.*, Amer. Phys. J. **142** (1965) 419.

[31] R.H. Dicke, P.J.E. Peebles, P.G. Roll and D.T. Wilkinson, *Cosmic Black-Body Radiation*, Astrophys. J. **142** (1965) 414.

[32] COBE collaboration, *Structure in the COBE differential microwave radiometer first year maps*, Astrophys. J. Lett. **396** (1992) L1.

[33] J.C. Mather et al., *Measurement of the Cosmic Microwave Background spectrum by the COBE FIRAS instrument*, Astrophys. J. **420** (1994) 439.

[34] "Nobel press release:." `https://www.nobelprize.org/prizes/physics/2006/press-release/`.

[35] F. Zwicky, *Die Rotverschiebung von extragalaktischen Nebeln*, Helv. Phys. Acta **6** (1933) 110.

[36] F. Zwicky, *Republication of: The redshift of extragalactic nebulae*, General Relativity and Gravitation **41** (2009) 207.

[37] V.C. Rubin and W.K. Ford, Jr., *Rotation of the Andromeda Nebula from a Spectroscopic Survey of Emission Regions*, Astrophys. J. **159** (1970) 379.

[38] SDSS collaboration, *Detection of the Baryon Acoustic Peak in the Large-Scale Correlation Function of SDSS Luminous Red Galaxies*, Astrophys. J. **633** (2005) 560 [`astro-ph/0501171`].

[39] PLANCK collaboration, *Planck 2018 results. VI. Cosmological parameters*, Astron. Astrophys. **641** (2020) A6 [1807.06209].

[40] BOOMERANG collaboration, *A Flat universe from high resolution maps of the cosmic microwave background radiation*, Nature **404** (2000) 955 [astro-ph/0004404].

[41] SDSS collaboration, *The Sloan Digital Sky Survey: Technical Summary*, Astron. J. **120** (2000) 1579 [astro-ph/0006396].

[42] SUPERNOVA SEARCH TEAM collaboration, *Observational evidence from supernovae for an accelerating universe and a cosmological constant*, Astron. J. **116** (1998) 1009 [astro-ph/9805201].

[43] SUPERNOVA COSMOLOGY PROJECT collaboration, *Measurements of Ω and Λ from 42 High Redshift Supernovae*, Astrophys. J. **517** (1999) 565 [astro-ph/9812133].

[44] CORE collaboration, *Exploring cosmic origins with CORE: Survey requirements and mission design*, JCAP **04** (2018) 014 [1706.04516].

[45] A. Kogut and D.J. Fixsen, *Calibration method and uncertainty for the primordial inflation explorer (PIXIE)*, JCAP **2020** (2020) 041 [2002.00976].

[46] A. Suzuki et al., *The LiteBIRD Satellite Mission: Sub-Kelvin Instrument*, Journal of Low Temperature Physics **193** (2018) 1048 [1801.06987].

[47] L. Amendola et al., *Cosmology and fundamental physics with the Euclid satellite*, Living Rev. Rel. **21** (2018) 2 [1606.00180].

[48] DESI collaboration, *Overview of the Instrumentation for the Dark Energy Spectroscopic Instrument*, Astron. J. **164** (2022) 207 [2205.10939].

[49] SUPERNOVA SEARCH TEAM collaboration, *Observational evidence from supernovae for an accelerating universe and a cosmological constant*, Astron. J. **116** (1998) 1009 [astro-ph/9805201].

[50] SUPERNOVA SEARCH TEAM collaboration, *The High Z supernova search: Measuring cosmic deceleration and global curvature of the universe using type Ia supernovae*, Astrophys. J. **507** (1998) 46 [astro-ph/9805200].

[51] SUPERNOVA COSMOLOGY PROJECT collaboration, *Measurements of Ω and Λ from 42 high redshift supernovae*, Astrophys. J. **517** (1999) 565 [astro-ph/9812133].

[52] SDSS collaboration, *Cosmological parameters from SDSS and WMAP*, Phys. Rev. D **69** (2004) 103501 [astro-ph/0310723].

[53] SDSS collaboration, *Cosmological Constraints from the SDSS Luminous Red Galaxies*, Phys. Rev. D **74** (2006) 123507 [astro-ph/0608632].

[54] WMAP collaboration, *First year Wilkinson Microwave Anisotropy Probe (WMAP) observations: Determination of cosmological parameters*, Astrophys. J. Suppl. **148** (2003) 175 [astro-ph/0302209].

[55] W.J. Percival, S. Cole, D.J. Eisenstein, R.C. Nichol, J.A. Peacock, A.C. Pope et al., *Measuring the Baryon Acoustic Oscillation scale using the SDSS and 2dFGRS*, Mon. Not. Roy. Astron. Soc. **381** (2007) 1053 [0705.3323].

[56] E. Aubourg et al., *Cosmological implications of baryon acoustic oscillation measurements*, Phys. Rev. D **92** (2015) 123516 [1411.1074].

[57] Boomerang collaboration, *A Flat universe from high resolution maps of the cosmic microwave background radiation*, Nature **404** (2000) 955 [astro-ph/0004404].

[58] A.H. Jaffe et al., *Recent results from the maxima experiment*, New Astron. Rev. **47** (2003) 727 [astro-ph/0306504].

[59] Planck collaboration, *Planck 2018 results. VII. Isotropy and Statistics of the CMB*, Astron. Astrophys. **641** (2020) A7 [1906.02552].

[60] L. Amendola and S. Tsujikawa, *Dark Energy*, Cambridge University Press (2015).

[61] S. Weinberg, *The Cosmological Constant Problem*, Rev. Mod. Phys. **61** (1989) 1.

[62] J. Martin, *Everything You Always Wanted To Know About The Cosmological Constant Problem (But Were Afraid To Ask)*, Comptes Rendus Physique **13** (2012) 566 [1205.3365].

[63] E. Abdalla et al., *Cosmology intertwined: A review of the particle physics, astrophysics, and cosmology associated with the cosmological tensions and anomalies*, JHEAp **34** (2022) 49 [2203.06142].

[64] A.G. Riess, S. Casertano, W. Yuan, L.M. Macri and D. Scolnic, *Large Magellanic Cloud Cepheid Standards Provide a 1% Foundation for the Determination of the Hubble Constant and Stronger Evidence for Physics beyond ΛCDM*, Astrophys. J. **876** (2019) 85 [1903.07603].

[65] W.L. Freedman, *Measurements of the Hubble Constant: Tensions in Perspective*, *Astrophys. J.* **919** (2021) 16 [2106.15656].

[66] A.G. Riess et al., *A Comprehensive Measurement of the Local Value of the Hubble Constant with 1 km/s/Mpc Uncertainty from the Hubble Space Telescope and the SH0ES Team*, *Astrophys. J. Lett.* **934** (2022) L7 [2112.04510].

[67] DES, SPT collaboration, *Joint analysis of Dark Energy Survey Year 3 data and CMB lensing from SPT and Planck. II. Cross-correlation measurements and cosmological constraints*, *Phys. Rev. D* **107** (2023) 023530 [2203.12440].

[68] DES collaboration, *Dark Energy Survey Year 3 results: Cosmology with moments of weak lensing mass maps*, *Phys. Rev. D* **106** (2022) 083509 [2110.10141].

[69] DES collaboration, *Dark energy survey year 3 results: Cosmology with peaks using an emulator approach*, *Mon. Not. Roy. Astron. Soc.* **511** (2022) 2075 [2110.10135].

[70] L. Huang, Z. Huang, H. Zhou and Z. Li, *The S_8 tension in light of updated redshift-space distortion data and PAge approximation*, *Sci. China Phys. Mech. Astron.* **65** (2022) 239512 [2110.08498].

[71] Y. Kobayashi, T. Nishimichi, M. Takada and H. Miyatake, *Full-shape cosmology analysis of the SDSS-III BOSS galaxy power spectrum using an emulator-based halo model: A 5% determination of $\sigma 8$*, *Phys. Rev. D* **105** (2022) 083517 [2110.06969].

[72] KiDS, Euclid collaboration, *KiDS and Euclid: Cosmological implications of a pseudo angular power spectrum analysis of KiDS-1000 cosmic shear tomography*, *Astron. Astrophys.* **665** (2022) A56 [2110.06947].

[73] E. Macaulay, I.K. Wehus and H.K. Eriksen, *Lower Growth Rate from Recent Redshift Space Distortion Measurements than Expected from Planck*, *Phys. Rev. Lett.* **111** (2013) 161301 [1303.6583].

[74] R.A. Battye, T. Charnock and A. Moss, *Tension between the power spectrum of density perturbations measured on large and small scales*, *Phys. Rev. D* **91** (2015) 103508 [1409.2769].

[75] DES collaboration, *Dark Energy Survey Year 1 Results: Measurement of the Baryon Acoustic Oscillation scale in the distribution of galaxies to redshift 1*, *Mon. Not. Roy. Astron. Soc.* **483** (2019) 4866 [1712.06209].

[76] DES collaboration, *Dark Energy Survey Year 3 results: Cosmological constraints from galaxy clustering and weak lensing*, Phys. Rev. D **105** (2022) 023520 [2105.13549].

[77] A. Blanchard and S. Ilić, *Closing up the cluster tension?*, Astron. Astrophys. **656** (2021) A75 [2104.00756].

[78] C. Heymans et al., *KiDS-1000 Cosmology: Multi-probe weak gravitational lensing and spectroscopic galaxy clustering constraints*, Astron. Astrophys. **646** (2021) A140 [2007.15632].

[79] O.H.E. Philcox and M.M. Ivanov, *BOSS DR12 full-shape cosmology: ΛCDM constraints from the large-scale galaxy power spectrum and bispectrum monopole*, Phys. Rev. D **105** (2022) 043517 [2112.04515].

[80] S. Joudaki et al., *CFHTLenS revisited: assessing concordance with Planck including astrophysical systematics*, Mon. Not. Roy. Astron. Soc. **465** (2017) 2033 [1601.05786].

[81] B.D. Fields, *The primordial lithium problem*, Ann. Rev. Nucl. Part. Sci. **61** (2011) 47 [1203.3551].

[82] R.H. Cyburt, B.D. Fields, K.A. Olive and T.-H. Yeh, *Big Bang Nucleosynthesis: 2015*, Rev. Mod. Phys. **88** (2016) 015004 [1505.01076].

[83] G.J. Mathews, A. Kedia, N. Sasankan, M. Kusakabe, Y. Luo, T. Kajino et al., *Cosmological Solutions to the Lithium Problem*, JPS Conf. Proc. **31** (2020) 011033 [1909.01245].

[84] L. Sbordone et al., *The metal-poor end of the Spite plateau. 1: Stellar parameters, metallicities and lithium abundances*, Astron. Astrophys. **522** (2010) A26 [1003.4510].

[85] C. Pitrou, A. Coc, J.-P. Uzan and E. Vangioni, *A new tension in the cosmological model from primordial deuterium?*, Mon. Not. Roy. Astron. Soc. **502** (2021) 2474 [2011.11320].

[86] F. Iocco, G. Mangano, G. Miele, O. Pisanti and P.D. Serpico, *Primordial Nucleosynthesis: from precision cosmology to fundamental physics*, Phys. Rept. **472** (2009) 1 [0809.0631].

[87] J.D. Bowman, A.E.E. Rogers, R.A. Monsalve, T.J. Mozdzen and N. Mahesh, *An absorption profile centred at 78 megahertz in the sky-averaged spectrum*, Nature **555** (2018) 67 [1810.05912].

[88] V. Poulin, T.L. Smith, D. Grin, T. Karwal and M. Kamionkowski, *Cosmological implications of ultralight axionlike fields*, *Phys. Rev. D* **98** (2018) 083525 [1806.10608].

[89] S. Singh, J. Nambissan T., R. Subrahmanyan, N. Udaya Shankar, B.S. Girish, A. Raghunathan et al., *On the detection of a cosmic dawn signal in the radio background*, *Nature Astron.* **6** (2022) 607.

[90] J. Sakstein and M. Trodden, *Early Dark Energy from Massive Neutrinos as a Natural Resolution of the Hubble Tension*, *Phys. Rev. Lett.* **124** (2020) 161301 [1911.11760].

[91] V. Poulin, T.L. Smith and A. Bartlett, *Dark energy at early times and ACT data: A larger Hubble constant without late-time priors*, *Phys. Rev. D* **104** (2021) 123550 [2109.06229].

[92] B. Ratra and P.J.E. Peebles, *Cosmological Consequences of a Rolling Homogeneous Scalar Field*, *Phys. Rev.* **D37** (1988) 3406.

[93] C. Armendariz-Picon, V.F. Mukhanov and P.J. Steinhardt, *A Dynamical solution to the problem of a small cosmological constant and late time cosmic acceleration*, *Phys. Rev. Lett.* **85** (2000) 4438 [astro-ph/0004134].

[94] E.J. Copeland, M. Sami and S. Tsujikawa, *Dynamics of dark energy*, *Int. J. Mod. Phys.* **D15** (2006) 1753 [hep-th/0603057].

[95] T. Clifton, P.G. Ferreira, A. Padilla and C. Skordis, *Modified Gravity and Cosmology*, *Phys. Rept.* **513** (2012) 1 [1106.2476].

[96] J. Li and G.-B. Zhao, *Cosmological Tests of Gravity with the Latest Observations*, *Astrophys. J.* **871** (2019) 196 [1806.05022].

[97] J. Wainwright and G.F.R. Ellis, *Dynamical Systems in Cosmology*, Cambridge University Press, New York (2009).

[98] R. García-Salcedo, T. Gonzalez, F.A. Horta-Rangel, I. Quiros and D. Sanchez-Guzmán, *Introduction to the application of dynamical systems theory in the study of the dynamics of cosmological models of dark energy*, *Eur. J. Phys.* **36** (2015) 025008 [1501.04851].

[99] S. Bahamonde et al., *Dynamical systems applied to cosmology: dark energy and modified gravity*, *Phys. Rept.* **775-777** (2018) 1 [1712.03107].

[100] A. De Felice et al., *Cosmology in generalized Proca theories*, *JCAP* **06** (2016) 048 [1603.05806].

[101] S. Basilakos, G. Leon, G. Papagiannopoulos and E.N. Saridakis, *Dynamical system analysis at background and perturbation levels: Quintessence in severe disadvantage comparing to ΛCDM*, *Phys. Rev. D* **100** (2019) 043524 [1904.01563].

[102] VIRGO, LIGO SCIENTIFIC collaboration, *GW170817: Observation of Gravitational Waves from a Binary Neutron Star Inspiral*, *Phys. Rev. Lett.* **119** (2017) 161101 [1710.05832].

[103] P. Creminelli and F. Vernizzi, *Dark Energy after GW170817 and GRB170817A*, *Phys. Rev. Lett.* **119** (2017) 251302 [1710.05877].

[104] T.E. Collett, L.J. Oldham, R.J. Smith, M.W. Auger, K.B. Westfall, D. Bacon et al., *A precise extragalactic test of General Relativity*, *Science* **360** (2018) 1342 [1806.08300].

[105] J.M. Ezquiaga and M. Zumalacárregui, *Dark Energy in light of Multi-Messenger Gravitational-Wave astronomy*, *Front. Astron. Space Sci.* **5** (2018) 44 [1807.09241].

[106] J.-h. He, L. Guzzo, B. Li and C.M. Baugh, *No evidence for modifications of gravity from galaxy motions on cosmological scales*, *Nature Astron.* **2** (2018) 967 [1809.09019].

[107] LIGO SCIENTIFIC, VIRGO collaboration, *Tests of General Relativity with GW170817*, *Phys. Rev. Lett.* **123** (2019) 011102 [1811.00364].

[108] C.L. Bennett et al., *Seven-Year Wilkinson Microwave Anisotropy Probe (WMAP) Observations: Are There Cosmic Microwave Background Anomalies?*, *Astrophys. J. Suppl.* **192** (2011) 17 [1001.4758].

[109] PLANCK collaboration, *Planck 2018 results. IX. Constraints on primordial non-Gaussianity*, *Astron. Astrophys.* **641** (2020) A9 [1905.05697].

[110] PLANCK collaboration, *Planck 2018 results. VII. Isotropy and Statistics of the CMB*, *Astron. Astrophys.* **641** (2020) A7 [1906.02552].

[111] R. Battye and A. Moss, *Anisotropic dark energy and CMB anomalies*, *Phys. Rev. D* **80** (2009) 023531 [0905.3403].

[112] L. Perivolaropoulos, *Large Scale Cosmological Anomalies and Inhomogeneous Dark Energy*, *Galaxies* **2** (2014) 22 [1401.5044].

[113] D.J. Schwarz, C.J. Copi, D. Huterer and G.D. Starkman, *CMB Anomalies after Planck*, *Class. Quant. Grav.* **33** (2016) 184001 [1510.07929].

[114] C. Armendariz-Picon, *Could dark energy be vector-like?*, JCAP **0407** (2004) 007 [astro-ph/0405267].

[115] T. Koivisto and D.F. Mota, *Anisotropic Dark Energy: Dynamics of Background and Perturbations*, JCAP **0806** (2008) 018 [0801.3676].

[116] T. Koivisto and D.F. Mota, *Vector Field Models of Inflation and Dark Energy*, JCAP **08** (2008) 021 [0805.4229].

[117] M. Thorsrud, D.F. Mota and S. Hervik, *Cosmology of a Scalar Field Coupled to Matter and an Isotropy-Violating Maxwell Field*, JHEP **10** (2012) 066 [1205.6261].

[118] R.C.G. Landim, *Dynamical analysis for a vector-like dark energy*, Eur. Phys. J. C **76** (2016) 480 [1605.03550].

[119] S. Nakamura, R. Kase and S. Tsujikawa, *Coupled vector dark energy*, JCAP **12** (2019) 032 [1907.12216].

[120] L.G. Gomez and Y. Rodriguez, *Coupled multi-Proca vector dark energy*, Phys. Dark Univ. **31** (2021) 100759 [2004.06466].

[121] L.G. Gomez, Y. Rodriguez and J.P.B. Almeida, *Anisotropic Scalar Field Dark Energy with a Disformally Coupled Yang-Mills Field*, Int. J. Mod. Phys. D **31** (2022) 2250060 [2103.11826].

[122] J.P. Beltrán Almeida, A. Guarnizo, R. Kase, S. Tsujikawa and C.A. Valenzuela-Toledo, *Anisotropic 2-form dark energy*, Phys. Lett. B **793** (2019) 396 [1902.05846].

[123] A. Guarnizo, J.P.B. Almeida and C.A. Valenzuela-Toledo, *p-form quintessence: exploring dark energy of $p-$forms coupled to a scalar field*, in *15th Marcel Grossmann Meeting on Recent Developments in Theoretical and Experimental General Relativity, Astrophysics, and Relativistic Field Theories*, 10, 2019 [1910.10499].

[124] J.P. Beltrán Almeida, A. Guarnizo and C.A. Valenzuela-Toledo, *Arbitrarily coupled $p-$forms in cosmological backgrounds*, Class. Quant. Grav. **37** (2020) 035001 [1810.05301].

[125] A. Mehrabi, A. Maleknejad and V. Kamali, *Gaugessence: a dark energy model with early time radiation-like equation of state*, Astrophys. Space Sci. **362** (2017) 53 [1510.00838].

[126] J.C. Bueno Sanchez and L. Perivolaropoulos, *Topological Quintessence*, Phys. Rev. D **84** (2011) 123516 [1110.2587].

[127] R.R. Caldwell, R. Dave and P.J. Steinhardt, *Cosmological imprint of an energy component with general equation of state*, Phys. Rev. Lett. **80** (1998) 1582 [astro-ph/9708069].

[128] J. Yoo and Y. Watanabe, *Theoretical Models of Dark Energy*, Int. J. Mod. Phys. D **21** (2012) 1230002 [1212.4726].

[129] J. Ohashi, J. Soda and S. Tsujikawa, *Anisotropic power-law k-inflation*, Phys. Rev. D **88** (2013) 103517 [1310.3053].

[130] T. Chiba, T. Okabe and M. Yamaguchi, *Kinetically driven quintessence*, Phys. Rev. D **62** (2000) 023511 [astro-ph/9912463].

[131] M.R. Garousi, *Tachyon couplings on nonBPS D-branes and Dirac-Born-Infeld action*, Nucl. Phys. B **584** (2000) 284 [hep-th/0003122].

[132] C. Armendariz-Picon, V.F. Mukhanov and P.J. Steinhardt, *Essentials of k essence*, Phys. Rev. D **63** (2001) 103510 [astro-ph/0006373].

[133] M. Malquarti, E.J. Copeland and A.R. Liddle, *K-essence and the coincidence problem*, Phys. Rev. D **68** (2003) 023512 [astro-ph/0304277].

[134] N. Arkani-Hamed, H.-C. Cheng, M.A. Luty and S. Mukohyama, *Ghost condensation and a consistent infrared modification of gravity*, JHEP **05** (2004) 074 [hep-th/0312099].

[135] F. Piazza and S. Tsujikawa, *Dilatonic ghost condensate as dark energy*, JCAP **07** (2004) 004 [hep-th/0405054].

[136] C. Bonvin, C. Caprini and R. Durrer, *A no-go theorem for k-essence dark energy*, Phys. Rev. Lett. **97** (2006) 081303 [astro-ph/0606584].

[137] E. Babichev, V. Mukhanov and A. Vikman, *k-Essence, superluminal propagation, causality and emergent geometry*, JHEP **02** (2008) 101 [0708.0561].

[138] J. Martin and M. Yamaguchi, *DBI-essence*, Phys. Rev. D **77** (2008) 123508 [0801.3375].

[139] Z.-K. Guo and N. Ohta, *Cosmological Evolution of Dirac-Born-Infeld Field*, JCAP **04** (2008) 035 [0803.1013].

[140] L. Heisenberg, R. Kase and S. Tsujikawa, *Cosmology in scalar-vector-tensor theories*, Phys. Rev. D **98** (2018) 024038 [1805.01066].

[141] C.G. Boehmer, G. Caldera-Cabral, R. Lazkoz and R. Maartens, *Dynamics of dark energy with a coupling to dark matter*, *Phys. Rev. D* **78** (2008) 023505 [0801.1565].

[142] L. Campanelli, P. Cea, G.L. Fogli and A. Marrone, *Testing the Isotropy of the Universe with Type Ia Supernovae*, *Phys. Rev. D* **83** (2011) 103503 [1012.5596].

[143] H. Amirhashchi and S. Amirhashchi, *Constraining Bianchi Type I Universe With Type Ia Supernova and H(z) Data*, *Phys. Dark Univ.* **29** (2020) 100557 [1802.04251].

[144] L. Ribes and P. Zalesskii, *Free profinite groups*, in *Profinite Groups*, pp. 75–118, Springer (2010).

[145] Y. Rongjia and Q. Jingzhao, *Dynamics of generalized tachyon field*, *Eur. Phys. J. C* **72** (2012) 2095 [1205.5968].

[146] K. Nozari and N. Rashidi, *Some Aspects of Tachyon Field Cosmology*, *Phys. Rev. D* **88** (2013) 023519 [1306.5853].

[147] C. Armendariz-Picon, *Creating Statistically Anisotropic and Inhomogeneous Perturbations*, *JCAP* **09** (2007) 014 [0705.1167].

[148] S. Endlich, A. Nicolis and J. Wang, *Solid Inflation*, *JCAP* **1310** (2013) 011 [1210.0569].

[149] M. Bento, O. Bertolami, P. Moniz, J. Mourao and P. Sa, *On the cosmology of massive vector fields with SO(3) global symmetry*, *Class. Quant. Grav.* **10** (1993) 285 [gr-qc/9302034].

[150] A. Golovnev, V. Mukhanov and V. Vanchurin, *Vector Inflation*, *JCAP* **0806** (2008) 009 [0802.2068].

[151] A. Maleknejad and M.M. Sheikh-Jabbari, *Gauge-flation: Inflation From Non-Abelian Gauge Fields*, *Phys. Lett. B* **723** (2013) 224 [1102.1513].

[152] H. Firouzjahi et al., *Charged Vector Inflation*, *Phys. Rev. D* **100** (2019) 043530 [1812.07464].

[153] N. Bartolo, S. Matarrese, M. Peloso and A. Ricciardone, *Anisotropy in solid inflation*, *JCAP* **1308** (2013) 022 [1306.4160].

[154] N. Bartolo, M. Peloso, A. Ricciardone and C. Unal, *The expected anisotropy in solid inflation*, *JCAP* **11** (2014) 009 [1407.8053].

[155] S. Kanno, M. Kimura, J. Soda and S. Yokoyama, *Anisotropic Inflation from Vector Impurity*, *JCAP* **08** (2008) 034 [0806.2422].

[156] S. Yokoyama and J. Soda, *Primordial statistical anisotropy generated at the end of inflation*, *JCAP* **08** (2008) 005 [0805.4265].

[157] M.-a. Watanabe, S. Kanno and J. Soda, *Inflationary Universe with Anisotropic Hair*, *Phys. Rev. Lett.* **102** (2009) 191302 [0902.2833].

[158] M.-a. Watanabe, S. Kanno and J. Soda, *The Nature of Primordial Fluctuations from Anisotropic Inflation*, *Prog. Theor. Phys.* **123** (2010) 1041 [1003.0056].

[159] K. Yamamoto, M.-a. Watanabe and J. Soda, *Inflation with Multi-Vector-Hair: The Fate of Anisotropy*, *Class. Quant. Grav.* **29** (2012) 145008 [1201.5309].

[160] J. Soda, *Statistical Anisotropy from Anisotropic Inflation*, *Class. Quant. Grav.* **29** (2012) 083001 [1201.6434].

[161] J. Ohashi, J. Soda and S. Tsujikawa, *Anisotropic Non-Gaussianity from a Two-Form Field*, *Phys. Rev. D* **87** (2013) 083520 [1303.7340].

[162] M. Celoria, D. Comelli and L. Pilo, *Fluids, Superfluids and Supersolids: Dynamics and Cosmology of Self Gravitating Media*, *JCAP* **09** (2017) 036 [1704.00322].

[163] A.A. Coley, *Dynamical systems and cosmology*, vol. 291, Kluwer, Dordrecht, Netherlands (2003), 10.1007/978-94-017-0327-7.

[164] T.S. Pereira, C. Pitrou and J.-P. Uzan, *Weak-lensing B-modes as a probe of the isotropy of the universe*, *Astron. Astrophys.* **585** (2016) L3 [1503.01127].

[165] S. Appleby, R. Battye and A. Moss, *Constraints on the anisotropy of dark energy*, *Phys. Rev. D* **81** (2010) 081301 [0912.0397].

[166] E. Dimastrogiovanni, N. Bartolo, S. Matarrese and A. Riotto, *Non-Gaussianity and Statistical Anisotropy from Vector Field Populated Inflationary Models*, *Adv. Astron.* **2010** (2010) 752670 [1001.4049].

[167] A. Maleknejad, M.M. Sheikh-Jabbari and J. Soda, *Gauge Fields and Inflation*, *Phys. Rept.* **528** (2013) 161 [1212.2921].

[168] L. Heisenberg, *A systematic approach to generalisations of General Relativity and their cosmological implications*, *Phys. Rept.* **796** (2019) 1 [1807.01725].

[169] M. Shiraishi, E. Komatsu, M. Peloso and N. Barnaby, *Signatures of anisotropic sources in the squeezed-limit bispectrum of the cosmic microwave background*, JCAP **05** (2013) 002 [1302.3056].

[170] N. Bartolo, A. Kehagias, M. Liguori, A. Riotto, M. Shiraishi and V. Tansella, *Detecting higher spin fields through statistical anisotropy in the CMB and galaxy power spectra*, Phys. Rev. D **97** (2018) 023503 [1709.05695].

[171] A. Moradinezhad Dizgah, H. Lee, J.B. Muñoz and C. Dvorkin, *Galaxy Bispectrum from Massive Spinning Particles*, JCAP **05** (2018) 013 [1801.07265].

[172] G. Franciolini, A. Kehagias, A. Riotto and M. Shiraishi, *Detecting higher spin fields through statistical anisotropy in the CMB bispectrum*, Phys. Rev. D **98** (2018) 043533 [1803.03814].

[173] A. Moradinezhad Dizgah, G. Franciolini, A. Kehagias and A. Riotto, *Constraints on long-lived, higher-spin particles from galaxy bispectrum*, Phys. Rev. D **98** (2018) 063520 [1805.10247].

[174] L. Bordin and G. Cabass, *Probing higher-spin fields from inflation with higher-order statistics of the CMB*, JCAP **06** (2019) 050 [1902.09519].

[175] T.S. Koivisto, D.F. Mota and C. Pitrou, *Inflation from N-Forms and its stability*, JHEP **09** (2009) 092 [0903.4158].

[176] T.S. Koivisto and N.J. Nunes, *Inflation and dark energy from three-forms*, Phys. Rev. **D80** (2009) 103509 [0908.0920].

[177] T.S. Koivisto and N.J. Nunes, *Coupled three-form dark energy*, Phys. Rev. **D88** (2013) 123512 [1212.2541].

[178] D.J. Mulryne, J. Noller and N.J. Nunes, *Three-form inflation and non-Gaussianity*, JCAP **1212** (2012) 016 [1209.2156].

[179] K. Sravan Kumar, D.J. Mulryne, N.J. Nunes, J. Marto and P. Vargas Moniz, *Non-Gaussianity in multiple three-form field inflation*, Phys. Rev. **D94** (2016) 103504 [1606.07114].

[180] J.P.B. Almeida, A. Guarnizo, R. Kase, S. Tsujikawa and C.A. Valenzuela-Toledo, *Anisotropic inflation with coupled $p-$forms*, JCAP **03** (2019) 025 [1901.06097].

[181] J.P.B. Almeida, A. Guarnizo, L. Heisenberg, C.A. Valenzuela-Toledo and J. Zosso, *Topological mass generation and 2−forms*, Phys. Rev. D **102** (2020) 063521 [2003.11736].

[182] H. Emoto, Y. Hosotani and T. Kubota, *Cosmology in the Einstein electroweak theory and magnetic fields*, Prog. Theor. Phys. **108** (2002) 157 [hep-th/0201141].

[183] Y. Hosotani, H. Emoto and T. Kubota, *Cosmic solutions in the Einstein-Weinberg-Salam theory and the generation of large electric and magnetic fields*, Nucl. Phys. B Proc. Suppl. **117** (2003) 139 [hep-ph/0209112].

[184] A. Maleknejad and M.M. Sheikh-Jabbari, *Non-Abelian Gauge Field Inflation*, Phys. Rev. D **84** (2011) 043515 [1102.1932].

[185] A. Maleknejad, M. Sheikh-Jabbari and J. Soda, *Gauge-flation and Cosmic No-Hair Conjecture*, JCAP **01** (2012) 016 [1109.5573].

[186] K. Murata and J. Soda, *Anisotropic Inflation with Non-Abelian Gauge Kinetic Function*, JCAP **06** (2011) 037 [1103.6164].

[187] A. Maleknejad, M. Noorbala and M. Sheikh-Jabbari, *Leptogenesis in inflationary models with non-Abelian gauge fields*, Gen. Rel. Grav. **50** (2018) 110 [1208.2807].

[188] A. Maleknejad and M. Zarei, *Slow-roll trajectories in Chromo-Natural and Gauge-flation Models, an exhaustive analysis*, Phys. Rev. D **88** (2013) 043509 [1212.6760].

[189] P. Adshead and M. Wyman, *Chromo-Natural Inflation: Natural inflation on a steep potential with classical non-Abelian gauge fields*, Phys. Rev. Lett. **108** (2012) 261302 [1202.2366].

[190] A. Maleknejad and E. Erfani, *Chromo-Natural Model in Anisotropic Background*, JCAP **03** (2014) 016 [1311.3361].

[191] M. Rinaldi, *Higgs Dark Energy*, Class. Quant. Grav. **32** (2015) 045002 [1404.0532].

[192] M. Rinaldi, *Dark energy as a fixed point of the Einstein Yang-Mills Higgs Equations*, JCAP **1510** (2015) 023 [1508.04576].

[193] C.M. Nieto and Y. Rodriguez, *Massive Gauge-flation*, Mod. Phys. Lett. **A31** (2016) 1640005 [1602.07197].

[194] P. Adshead, E. Martinec, E.I. Sfakianakis and M. Wyman, *Higgsed Chromo-Natural Inflation*, JHEP **12** (2016) 137 [1609.04025].

[195] P. Adshead and E.I. Sfakianakis, *Higgsed Gauge-flation*, *JHEP* **08** (2017) 130 [1705.03024].

[196] Y. Rodríguez and A.A. Navarro, *Non-Abelian S-term dark energy and inflation*, *Phys. Dark Univ.* **19** (2018) 129 [1711.01935].

[197] L.G. Gómez and Y. Rodríguez, *Stability Conditions in the Generalized SU(2) Proca Theory*, *Phys. Rev.* **D100** (2019) 084048 [1907.07961].

[198] I. Wolfson, A. Maleknejad and E. Komatsu, *How attractive is the isotropic attractor solution of axion-SU(2) inflation?*, *JCAP* **09** (2020) 047 [2003.01617].

[199] M. Sheikh-Jabbari, *Gauge-flation Vs Chromo-Natural Inflation*, *Phys. Lett. B* **717** (2012) 6 [1203.2265].

[200] I. Antoniou and L. Perivolaropoulos, *Searching for a Cosmological Preferred Axis: Union2 Data Analysis and Comparison with Other Probes*, *JCAP* **12** (2010) 012 [1007.4347].

[201] A. Salehi and M.R. Setare, *Searching for Cosmological Preferred Axis using cosmographic approach*, *Gen. Rel. Grav.* **49** (2017) 147 [1603.02659].

[202] L. Visinelli, *(Non-)thermal production of WIMPs during kination*, *Symmetry* **10** (2018) 546 [1710.11006].

[203] D. Bettoni and J. Rubio, *Quintessential Affleck-Dine baryogenesis with non-minimal couplings*, *Phys. Lett. B* **784** (2018) 122 [1805.02669].

[204] D. Bettoni, G. Domènech and J. Rubio, *Gravitational waves from global cosmic strings in quintessential inflation*, *JCAP* **02** (2019) 034 [1810.11117].

[205] K. Dimopoulos and T. Markkanen, *Non-minimal gravitational reheating during kination*, *JCAP* **1806** (2018) 021 [1803.07399].

[206] D. Bettoni and J. Rubio, *Hubble-induced phase transitions: Walls are not forever*, *JCAP* **01** (2020) 002 [1911.03484].

[207] T. Opferkuch, P. Schwaller and B.A. Stefanek, *Ricci Reheating*, *JCAP* **1907** (2019) 016 [1905.06823].

[208] S. Weinberg, *The quantum theory of fields. Vol. 2: Modern applications*, Cambridge University Press (1996).

[209] G.L. Kane, *Modern Elementary Particle Physics*, Cambridge University Press (2017).

[210] P.V. Moniz, J.M. Mourao and P.M. Sa, *The Dynamics of a flat Friedmann-Robertson-Walker inflationary model in the presence of gauge fields*, Class. Quantum Grav. **10** (1993) 517.

[211] U. Ochs and M. Sorg, *Cosmological solutions for the coupled Einstein-Yang-Mills-Higgs equations*, Gen. Rel. Grav. **28** (1996) 1177.

[212] ATLAS collaboration, *Observation of a new particle in the search for the Standard Model Higgs boson with the ATLAS detector at the LHC*, Phys. Lett. B **716** (2012) 1 [1207.7214].

[213] CMS collaboration, *Observation of a new boson at a mass of 125 GeV with the CMS experiment at the LHC*, Phys. Lett. B **716** (2012) 30 [1207.7235].

[214] L.A. Boyle and M. Caldwell, R. R. an Kamionkowski, *Spintessence! New models for dark matter and dark energy*, Phys. Lett. B **545** (2002) 17 [astro-ph/0105318].

[215] Y. Rodríguez, L.G. Gómez and C.M. Nieto, *Towards a proof of the equivalence between FRW background expansion and statistical isotropy*, in *Proceedings, 2nd Argentinian-Brazilian Meeting on Gravitation, Relativistic Astrophysics and Cosmology (GRACo II): Buenos Aires, Argentina, April 22-25, 2014*, pp. 139–144, 2015 [1502.07292].

[216] J.M. Wagstaff and K. Dimopoulos, *Particle Production of Vector Fields: Scale Invariance is Attractive*, Phys. Rev. **D83** (2011) 023523 [1011.2517].

[217] D.H. Lyth, *Cosmology for physicists*, CRC Press, Boca Raton (2017).

[218] Planck collaboration, *Planck 2018 results. X. Constraints on inflation*, Astron. Astrophys. **641** (2020) A10 [1807.06211].

[219] P. Adshead and A. Liu, *Anisotropic Massive Gauge-flation*, JCAP **1807** (2018) 052 [1803.07168].

[220] A. Paliathanasis and G. Leon, *Dynamics and exact Bianchi I spacetimes in Einstein–æther scalar field theory*, Eur. Phys. J. C **80** (2020) 589 [2004.08663].

[221] H. Cendra, J. Marsden and T. Ratiu, *Geometric Mechanics, Lagrangian Reduction, and Nonholonomic Systems*, Springer, Berlin, Heidelberg (01, 2001).

[222] S. Weinberg, *Gravitation and Cosmology: Principles and Applications of the General Theory of Relativity*, John Wiley and Sons, New York (1972).

[223] A. Alho, V. Bessa and F.C. Mena, *Global dynamics of Yang–Mills field and perfect-fluid Robertson–Walker cosmologies*, J. Math. Phys. **61** (2020) 032502 [1910.04678].

[224] Y.B. Zeldovich, *A Hypothesis, unifying the structure and the entropy of the universe*, *Mon. Not. Roy. Astron. Soc.* **160** (1972) 1P.

[225] D. Huterer et al., *Growth of Cosmic Structure: Probing Dark Energy Beyond Expansion*, *Astropart. Phys.* **63** (2015) 23 [1309.5385].

[226] S. Hellerman, N. Kaloper and L. Susskind, *String theory and quintessence*, *JHEP* **06** (2001) 003 [hep-th/0104180].

[227] W. Fischler, A. Kashani-Poor, R. McNees and S. Paban, *The Acceleration of the universe, a challenge for string theory*, *JHEP* **07** (2001) 003 [hep-th/0104181].

[228] H. Ooguri and C. Vafa, *On the Geometry of the String Landscape and the Swampland*, *Nucl. Phys. B* **766** (2007) 21 [hep-th/0605264].

[229] H. Ooguri and C. Vafa, *Non-supersymmetric AdS and the Swampland*, *Adv. Theor. Math. Phys.* **21** (2017) 1787 [1610.01533].

[230] T.D. Brennan, F. Carta and C. Vafa, *The String Landscape, the Swampland, and the Missing Corner*, *PoS* **TASI2017** (2017) 015 [1711.00864].

[231] E. Palti, *The Swampland: Introduction and Review*, *Fortsch. Phys.* **67** (2019) 1900037 [1903.06239].

[232] T. Van Riet and G. Zoccarato, *Beginners lectures on flux compactifications and related Swampland topics*, *Phys. Rept.* **1049** (2024) 1 [2305.01722].

[233] R. Brandenberger, *Perspectives on the Dark Sector*, in *33rd Rencontres de Blois: Exploring the Dark Universe*, 11, 2022 [2211.11273].

[234] Y. Bergner and R. Jackiw, *Integrable supersymmetric fluid mechanics from superstrings*, *Phys. Lett. A* **284** (2001) 146 [physics/0103092].

[235] M. Hassaine, *Supersymmetric Chaplygin gas*, *Phys. Lett. A* **290** (2001) 157 [hep-th/0106252].

[236] M.C. Bento, O. Bertolami and A.A. Sen, *Generalized Chaplygin gas, accelerated expansion and dark energy matter unification*, Phys. Rev. D **66** (2002) 043507 [gr-qc/0202064].

[237] S. Panda, Y. Sumitomo and S.P. Trivedi, *Axions as Quintessence in String Theory*, Phys. Rev. D **83** (2011) 083506 [1011.5877].

[238] M. Cicoli, F.G. Pedro and G. Tasinato, *Natural Quintessence in String Theory*, JCAP **07** (2012) 044 [1203.6655].

[239] G. D'Amico, N. Kaloper and A. Lawrence, *Strongly Coupled Quintessence*, Phys. Rev. D **100** (2019) 103504 [1809.05109].

[240] M. Cicoli, M. Licheri, R. Mahanta, E. McDonough, F.G. Pedro and M. Scalisi, *Early Dark Energy in Type IIB String Theory*, JHEP **06** (2023) 052 [2303.03414].

[241] N. Kaloper and L. Sorbo, *Of pngb quintessence*, JCAP **04** (2006) 007 [astro-ph/0511543].

[242] N. Kaloper and L. Sorbo, *Where in the String Landscape is Quintessence*, Phys. Rev. D **79** (2009) 043528 [0810.5346].

[243] J. Blåbäck, U. Danielsson and G. Dibitetto, *Accelerated Universes from type IIA Compactifications*, JCAP **03** (2014) 003 [1310.8300].

[244] M. Kamionkowski, J. Pradler and D.G.E. Walker, *Dark energy from the string axiverse*, Phys. Rev. Lett. **113** (2014) 251302 [1409.0549].

[245] S. Alexander and E. McDonough, *Axion-Dilaton Destabilization and the Hubble Tension*, Phys. Lett. B **797** (2019) 134830 [1904.08912].

[246] E. McDonough and M. Scalisi, *Towards Early Dark Energy in string theory*, JHEP **10** (2023) 118 [2209.00011].

[247] A. Achúcarro and G.A. Palma, *The string swampland constraints require multi-field inflation*, JCAP **02** (2019) 041 [1807.04390].

[248] Y. Akrami, M. Sasaki, A.R. Solomon and V. Vardanyan, *Multi-field dark energy: Cosmic acceleration on a steep potential*, Phys. Lett. B **819** (2021) 136427 [2008.13660].

[249] A.R. Brown, *Hyperbolic Inflation*, Phys. Rev. Lett. **121** (2018) 251601 [1705.03023].

[250] P. Christodoulidis, D. Roest and E.I. Sfakianakis, *Scaling attractors in multi-field inflation*, *JCAP* **12** (2019) 059 [1903.06116].

[251] H. Bernardo, R. Brandenberger and J. Fröhlich, *Towards a dark sector model from string theory*, *JCAP* **09** (2022) 040 [2201.04668].

[252] M. Gasperini, F. Piazza and G. Veneziano, *Quintessence as a runaway dilaton*, *Phys. Rev. D* **65** (2002) 023508 [gr-qc/0108016].

[253] C. van de Bruck and C.C. Thomas, *Dark Energy, the Swampland and the Equivalence Principle*, *Phys. Rev. D* **100** (2019) 023515 [1904.07082].

[254] J. Sonner and P.K. Townsend, *Recurrent acceleration in dilaton-axion cosmology*, *Phys. Rev. D* **74** (2006) 103508 [hep-th/0608068].

[255] C. van de Bruck and J.M. Weller, *Quintessence dynamics with two scalar fields and mixed kinetic terms*, *Phys. Rev. D* **80** (2009) 123014 [0910.1934].

[256] M. Cicoli, G. Dibitetto and F.G. Pedro, *New accelerating solutions in late-time cosmology*, *Phys. Rev. D* **101** (2020) 103524 [2002.02695].

[257] M. Cicoli, G. Dibitetto and F.G. Pedro, *Out of the Swampland with Multifield Quintessence?*, *JHEP* **10** (2020) 035 [2007.11011].

[258] R. Catena and J. Moller, *Axion-dilaton cosmology and dark energy*, *JCAP* **03** (2008) 012 [0709.1931].

[259] L. Heisenberg, *Generalization of the Proca Action*, *JCAP* **05** (2014) 015 [1402.7026].

[260] G. Tasinato, *Cosmic Acceleration from Abelian Symmetry Breaking*, *JHEP* **04** (2014) 067 [1402.6450].

[261] J. Beltran Jimenez and L. Heisenberg, *Derivative self-interactions for a massive vector field*, *Phys. Lett. B* **757** (2016) 405 [1602.03410].

[262] E. Allys, P. Peter and Y. Rodriguez, *Generalized Proca action for an Abelian vector field*, *JCAP* **02** (2016) 004 [1511.03101].

[263] E. Allys, J.P. Beltran Almeida, P. Peter and Y. Rodríguez, *On the 4D generalized Proca action for an Abelian vector field*, *JCAP* **09** (2016) 026 [1605.08355].

[264] R. Kase and S. Tsujikawa, *Dark energy in scalar-vector-tensor theories*, *JCAP* **11** (2018) 024 [1805.11919].

[265] B. Ratra and P.J.E. Peebles, *Cosmological consequences of a rolling homogeneous scalar field*, *Phys. Rev. D* **37** (1988) 3406.

[266] D.Z. Freedman and A. Van Proeyen, *Supergravity*, Cambridge Univ. Press, Cambridge, UK (5, 2012), 10.1017/CBO9781139026833.

[267] M. Cicoli, J.P. Conlon, A. Maharana, S. Parameswaran, F. Quevedo and I. Zavala, *String cosmology: From the early universe to today*, *Phys. Rept.* **1059** (2024) 1 [2303.04819].

[268] A. Font, L.E. Ibanez, D. Lust and F. Quevedo, *Supersymmetry Breaking From Duality Invariant Gaugino Condensation*, *Phys. Lett. B* **245** (1990) 401.

[269] S. Ferrara, N. Magnoli, T.R. Taylor and G. Veneziano, *Duality and supersymmetry breaking in string theory*, *Phys. Lett. B* **245** (1990) 409.

[270] S. Kachru, R. Kallosh, A.D. Linde and S.P. Trivedi, *De Sitter vacua in string theory*, *Phys. Rev. D* **68** (2003) 046005 [hep-th/0301240].

[271] V. Balasubramanian, P. Berglund, J.P. Conlon and F. Quevedo, *Systematics of moduli stabilisation in Calabi-Yau flux compactifications*, *JHEP* **03** (2005) 007 [hep-th/0502058].

[272] O. DeWolfe, A. Giryavets, S. Kachru and W. Taylor, *Type IIA moduli stabilization*, *JHEP* **07** (2005) 066 [hep-th/0505160].

[273] P.G. Camara, A. Font and L.E. Ibanez, *Fluxes, moduli fixing and MSSM-like vacua in a simple IIA orientifold*, *JHEP* **09** (2005) 013 [hep-th/0506066].

[274] D. Gallego, M.C.D. Marsh, B. Vercnocke and T. Wrase, *A New Class of de Sitter Vacua in Type IIB Large Volume Compactifications*, *JHEP* **10** (2017) 193 [1707.01095].

[275] M. Dine, N. Seiberg and E. Witten, *Fayet-Iliopoulos terms in string theory*, *Nuclear Physics B* **289** (1987) 589.

[276] M. Dine, I. Ichinose and N. Seiberg, *F terms and D terms in string theory*, *Nuclear Physics B* **293** (1987) 253.

[277] J.J. Atick, L.J. Dixon and A. Sen, *String calculation of fayet-iliopoulos D-terms in arbitrary supersymmetric compactifications*, *Nuclear Physics B* **292** (1987) 109.

[278] D. Gallego and M. Serone, *An Effective Description of the Landscape - II*, *JHEP* **06** (2009) 057 [0904.2537].

[279] N.J. Secrest, S. von Hausegger, M. Rameez, R. Mohayaee, S. Sarkar and J. Colin, *A Test of the Cosmological Principle with Quasars*, *Astrophys. J. Lett.* **908** (2021) L51 [2009.14826].

[280] N.J. Secrest, S. von Hausegger, M. Rameez, R. Mohayaee and S. Sarkar, *A Challenge to the Standard Cosmological Model*, *Astrophys. J. Lett.* **937** (2022) L31 [2206.05624].

[281] L. Dam, G.F. Lewis and B.J. Brewer, *Testing the cosmological principle with CatWISE quasars: a bayesian analysis of the number-count dipole*, *Mon. Not. Roy. Astron. Soc.* **525** (2023) 231 [2212.07733].

[282] L. Perivolaropoulos and F. Skara, *Challenges for ΛCDM: An update*, *New Astron. Rev.* **95** (2022) 101659 [2105.05208].

[283] M. Karčiauskas, *Dynamical Analysis of Anisotropic Inflation*, *Mod. Phys. Lett. A* **31** (2016) 1640002 [1604.00269].

[284] R.M. Wald, *Asymptotic behavior of homogeneous cosmological models in the presence of a positive cosmological constant*, *Phys. Rev. D* **28** (1983) 2118.

[285] C.G. Callan, D. Friedan, E.J. Martinec and M.J. Perry, *Strings in background fields*, *Nuclear Physics B* **262** (1985) 593.

[286] J. Polchinski, *String Theory: Volume 1: An Introduction to the Bosonic String*, vol. 1 of *Cambridge Monographs on Mathematical Physics*, Cambridge University Press, Cambridge (1998), 10.1017/CBO9780511816079.

[287] N. Kaloper, *The Closed Bianchi I universe in string theory*, *Mod. Phys. Lett. A* **8** (1993) 421 [hep-th/9208025].

[288] M. Gasperini and R. Ricci, *Homogeneous conformal string backgrounds*, *Class. Quant. Grav.* **12** (1995) 677 [hep-th/9501055].

[289] J.D. Barrow and K.E. Kunze, *Spatially homogeneous string cosmologies*, *Phys. Rev. D* **55** (1997) 623 [hep-th/9608045].

[290] E.J. Copeland, A. Lahiri and D. Wands, *String cosmology with a time dependent antisymmetric tensor potential*, *Phys. Rev. D* **51** (1995) 1569 [hep-th/9410136].

[291] J.D. Barrow and M.P. Dabrowski, *Kantowski-Sachs string cosmologies*, *Phys. Rev. D* **55** (1997) 630 [hep-th/9608136].

[292] S. Kawai and J. Soda, *Nonsingular Bianchi type 1 cosmological solutions from 1 loop superstring effective action*, Phys. Rev. D **59** (1999) 063506 [gr-qc/9807060].

[293] F. Naderi and A. Rezaei-Aghdam, *Anisotropic homogeneous string cosmology with two-loop corrections*, Nuclear Physics B **923** (2017) 416.

[294] F. Naderi, A. Rezaei-Aghdam and F. Darabi, *Non-critical anisotropic Bianchi type \$I\$ string cosmology with \$\alpha'\$-corrections*, Phys. Rev. D **98** (2018) 026009.

[295] R. Blumenhagen, F. Gmeiner, G. Honecker, D. Lust and T. Weigand, *The Statistics of supersymmetric D-brane models*, Nucl. Phys. B **713** (2005) 83 [hep-th/0411173].

[296] E. Witten, *Dimensional reduction of superstring models*, Physics Letters B **155** (1985) 151.

[297] A. Font, L.E. Ibáñez, D. Lüst and F. Quevedo, *Supersymmetry breaking from duality invariant gaugino condensation*, Physics Letters B **245** (1990) 401.

[298] L.E. Ibanez and A.M. Uranga, *String theory and particle physics: An introduction to string phenomenology*, Cambridge University Press (2, 2012).

[299] W. Buchmuller, K. Hamaguchi, O. Lebedev and M. Ratz, *Supersymmetric standard model from the heterotic string*, Phys. Rev. Lett. **96** (2006) 121602 [hep-ph/0511035].

[300] O. Lebedev, H.P. Nilles, S. Ramos-Sanchez, M. Ratz and P.K.S. Vaudrevange, *Heterotic mini-landscape. (II). Completing the search for MSSM vacua in a Z(6) orbifold*, Phys. Lett. B **668** (2008) 331 [0807.4384].

[301] O. Lebedev, H.P. Nilles, S. Raby, S. Ramos-Sanchez, M. Ratz, P.K.S. Vaudrevange et al., *The Heterotic Road to the MSSM with R parity*, Phys. Rev. D **77** (2008) 046013 [0708.2691].

[302] K. Becker, M. Becker, M. Haack and J. Louis, *Supersymmetry breaking and alpha-prime corrections to flux induced potentials*, JHEP **06** (2002) 060 [hep-th/0204254].

[303] D. Cremades, L.E. Ibanez and F. Marchesano, *SUSY quivers, intersecting branes and the modest hierarchy problem*, JHEP **07** (2002) 009 [hep-th/0201205].

[304] R. Blumenhagen, D. Lust and S. Stieberger, *Gauge unification in supersymmetric intersecting brane worlds*, JHEP **07** (2003) 036 [hep-th/0305146].

[305] D. Lust, P. Mayr, R. Richter and S. Stieberger, *Scattering of gauge, matter, and moduli fields from intersecting branes*, Nucl. Phys. B **696** (2004) 205 [hep-th/0404134].

[306] T.W. Grimm and J. Louis, *The Effective action of $N = 1$ Calabi-Yau orientifolds*, *Nucl. Phys. B* **699** (2004) 387 [hep-th/0403067].

[307] H. Jockers and J. Louis, *The Effective action of D7-branes in $N = 1$ Calabi-Yau orientifolds*, *Nucl. Phys. B* **705** (2005) 167 [hep-th/0409098].

[308] A. Font and L.E. Ibanez, *SUSY-breaking soft terms in a MSSM magnetized D7-brane model*, *JHEP* **03** (2005) 040 [hep-th/0412150].

[309] M. Cicoli, M. Kreuzer and C. Mayrhofer, *Toric K3-Fibred Calabi-Yau Manifolds with del Pezzo Divisors for String Compactifications*, *JHEP* **02** (2012) 002 [1107.0383].

[310] M. Cicoli, F. Cunillera, A. Padilla and F.G. Pedro, *Quintessence and the Swampland: The Parametrically Controlled Regime of Moduli Space*, *Fortsch. Phys.* **70** (2022) 2200009 [2112.10779].

[311] M. Brinkmann, M. Cicoli, G. Dibitetto and F.G. Pedro, *Stringy multifield quintessence and the Swampland*, *JHEP* **11** (2022) 044 [2206.10649].

[312] M. Berg, M. Haack and B. Kors, *String loop corrections to Kahler potentials in orientifolds*, *JHEP* **11** (2005) 030 [hep-th/0508043].

[313] M. Dine, R. Rohm, N. Seiberg and E. Witten, *Gluino Condensation in Superstring Models*, *Phys. Lett. B* **156** (1985) 55.

[314] M. Berg, M. Haack and B. Kors, *Loop corrections to volume moduli and inflation in string theory*, *Phys. Rev. D* **71** (2005) 026005 [hep-th/0404087].

[315] S.R. Coleman and E.J. Weinberg, *Radiative Corrections as the Origin of Spontaneous Symmetry Breaking*, *Phys. Rev. D* **7** (1973) 1888.

[316] L. Dolan and R. Jackiw, *Symmetry Behavior at Finite Temperature*, *Phys. Rev. D* **9** (1974) 3320.

[317] K. Nakayama and F. Takahashi, *Cosmological Moduli Problem from Thermal Effects*, *Phys. Lett. B* **670** (2009) 434 [0811.0444].

[318] L. Anguelova, V. Calo and M. Cicoli, *LARGE Volume String Compactifications at Finite Temperature*, *JCAP* **10** (2009) 025 [0904.0051].

[319] D. Gallego, *Finite temperature effects in modular cosmology*, *JCAP* **09** (2020) 033 [2005.03939].

[320] K. Bamba, S. Capozziello, S. Nojiri and S.D. Odintsov, *Dark energy cosmology: the equivalent description via different theoretical models and cosmography tests*, *Astrophys. Space Sci.* **342** (2012) 155 [1205.3421].

[321] G.W. Horndeski, *Second-order scalar-tensor field equations in a four-dimensional space*, *Int. J. Theor. Phys.* **10** (1974) 363.

[322] C. Deffayet, X. Gao, D.A. Steer and G. Zahariade, *From k-essence to generalised Galileons*, *Phys. Rev. D* **84** (2011) 064039 [1103.3260].

[323] T. Kobayashi, M. Yamaguchi and J. Yokoyama, *Generalized G-inflation: Inflation with the most general second-order field equations*, *Prog. Theor. Phys.* **126** (2011) 511 [1105.5723].

[324] C. Charmousis, E.J. Copeland, A. Padilla and P.M. Saffin, *General second order scalar-tensor theory, self tuning, and the Fab Four*, *Phys. Rev. Lett.* **108** (2012) 051101 [1106.2000].

[325] L. Amendola, M. Kunz, I.D. Saltas and I. Sawicki, *Fate of Large-Scale Structure in Modified Gravity After GW170817 and GRB170817A*, *Phys. Rev. Lett.* **120** (2018) 131101 [1711.04825].

[326] E.J. Copeland, M. Kopp, A. Padilla, P.M. Saffin and C. Skordis, *Dark energy after GW170817, revisited*, *Phys. Rev. Lett.* **122** (2019) 061301 [1810.08239].

[327] M. Crisostomi and K. Koyama, *Self-accelerating universe in scalar-tensor theories after GW170817*, *Phys. Rev.* **D97** (2018) 084004 [1712.06556].

[328] J. Sakstein and B. Jain, *Implications of the Neutron Star Merger GW170817 for Cosmological Scalar-Tensor Theories*, *Phys. Rev. Lett.* **119** (2017) 251303 [1710.05893].

[329] J.M. Ezquiaga and M. Zumalacarregui, *Dark Energy After GW170817: Dead Ends and the Road Ahead*, *Phys. Rev. Lett.* **119** (2017) 251304 [1710.05901].

[330] T. Baker, E. Bellini, P.G. Ferreira, M. Lagos, J. Noller and I. Sawicki, *Strong constraints on cosmological gravity from GW170817 and GRB 170817A*, *Phys. Rev. Lett.* **119** (2017) 251301 [1710.06394].

[331] R. Kase and S. Tsujikawa, *Dark energy in Horndeski theories after GW170817: A review*, *Int. J. Mod. Phys. D* **28** (2019) 1942005 [1809.08735].

[332] C.-Q. Geng, Y.-T. Hsu, J.-R. Lu and L. Yin, *A Dark Energy model from Generalized Proca Theory*, Phys. Dark Univ. **32** (2021) 100819 [2104.06577].

[333] S. Nakamura, A. De Felice, R. Kase and S. Tsujikawa, *Constraints on massive vector dark energy models from integrated Sachs-Wolfe-galaxy cross-correlations*, Phys. Rev. D **99** (2019) 063533 [1811.07541].

[334] A. de Felice, L. Heisenberg and S. Tsujikawa, *Observational constraints on generalized Proca theories*, Phys. Rev. D **95** (2017) 123540 [1703.09573].

[335] C. Skordis and T. Złośnik, *New relativistic theory for modified newtonian dynamics*, Phys. Rev. Lett. **127** (2021) 161302.

[336] J. Zuntz, T.G. Zlosnik, F. Bourliot, P.G. Ferreira and G.D. Starkman, *Vector field models of modified gravity and the dark sector*, Phys. Rev. D **81** (2010) 104015.

[337] J.B. Jiménez and A.L. Maroto, *Cosmic vector for dark energy*, Phys. Rev. D **78** (2008) 063005.

[338] J. Beltran Jimenez and A.L. Maroto, *Cosmological electromagnetic fields and dark energy*, JCAP **03** (2009) 016 [0811.0566].

[339] J. Beltran Jimenez, R. Durrer, L. Heisenberg and M. Thorsrud, *Stability of Horndeski vector-tensor interactions*, JCAP **10** (2013) 064 [1308.1867].

[340] A. De Felice, L. Heisenberg, R. Kase, S. Mukohyama, S. Tsujikawa and Y.-l. Zhang, *Effective gravitational couplings for cosmological perturbations in generalized proca theories*, Phys. Rev. D **94** (2016) 044024.

[341] L. Heisenberg, *Scalar-Vector-Tensor Gravity Theories*, JCAP **10** (2018) 054 [1801.01523].

[342] A. Lewis, A. Challinor and A. Lasenby, *Efficient computation of CMB anisotropies in closed FRW models*, Astrophys. J. **538** (2000) 473 [astro-ph/9911177].

[343] D. Blas, J. Lesgourgues and T. Tram, *The Cosmic Linear Anisotropy Solving System (CLASS) II: Approximation schemes*, JCAP **1107** (2011) 034 [1104.2933].

[344] VIRGO Consortium collaboration, *Stable clustering, the halo model and nonlinear cosmological power spectra*, Mon. Not. Roy. Astron. Soc. **341** (2003) 1311 [astro-ph/0207664].

[345] G.-B. Zhao, L. Pogosian, A. Silvestri and J. Zylberberg, *Searching for modified growth patterns with tomographic surveys*, *Phys. Rev.* **D79** (2009) 083513 [0809.3791].

[346] A. Hojjati, L. Pogosian and G.-B. Zhao, *Testing gravity with CAMB and CosmoMC*, *JCAP* **1108** (2011) 005 [1106.4543].

[347] Z. Sakr and M. Martinelli, *Cosmological constraints on sub-horizon scales modified gravity theories with MGCLASS II*, *JCAP* **05** (2022) 030 [2112.14175].

[348] J.-h. He, *Testing $f(R)$ dark energy model with the large scale structure*, *Phys. Rev.* **D86** (2012) 103505 [1207.4898].

[349] G. Gubitosi, F. Piazza and F. Vernizzi, *The Effective Field Theory of Dark Energy*, *JCAP* **1302** (2013) 032 [1210.0201].

[350] B. Hu, M. Raveri, N. Frusciante and A. Silvestri, *Effective Field Theory of Cosmic Acceleration: an implementation in CAMB*, *Phys. Rev.* **D89** (2014) 103530 [1312.5742].

[351] R.A. Battye, B. Bolliet and J.A. Pearson, *$f(R)$ gravity as a dark energy fluid*, *Phys. Rev.* **D93** (2016) 044026 [1508.04569].

[352] R.A. Battye, B. Bolliet and F. Pace, *Do cosmological data rule out $f(\mathcal{R})$ with $w \neq -1$?*, *Phys. Rev.* **D97** (2018) 104070 [1712.05976].

[353] M. Zumalacárregui, E. Bellini, I. Sawicki, J. Lesgourgues and P.G. Ferreira, *hi_class: Horndeski in the Cosmic Linear Anisotropy Solving System*, *JCAP* **08** (2017) 019 [1605.06102].

[354] S. Capozziello, S. Nojiri, S.D. Odintsov and A. Troisi, *Cosmological viability of f(R)-gravity as an ideal fluid and its compatibility with a matter dominated phase*, *Phys. Lett.* **B639** (2006) 135 [astro-ph/0604431].

[355] S. Nojiri and S.D. Odintsov, *Introduction to modified gravity and gravitational alternative for dark energy*, *eConf* **C0602061** (2006) 06 [hep-th/0601213].

[356] R. Arjona, W. Cardona and S. Nesseris, *Unraveling the effective fluid approach for $f(R)$ models in the subhorizon approximation*, *Phys. Rev.* **D99** (2019) 043516 [1811.02469].

[357] R. Arjona, W. Cardona and S. Nesseris, *Designing Horndeski and the effective fluid approach*, *Phys. Rev. D* **100** (2019) 063526 [1904.06294].

[358] F. Pace, R.A. Battye, B. Bolliet and D. Trinh, *Dark sector evolution in Horndeski models*, *JCAP* **09** (2019) 018 [1905.06795].

[359] F. Pace, R. Battye, E. Bellini, L. Lombriser, F. Vernizzi and B. Bolliet, *Comparison of different approaches to the quasi-static approximation in Horndeski models*, *JCAP* **06** (2021) 017 [2011.05713].

[360] M. Lagos, E. Bellini, J. Noller, P.G. Ferreira and T. Baker, *A general theory of linear cosmological perturbations: stability conditions, the quasistatic limit and dynamics*, *JCAP* **03** (2018) 021 [1711.09893].

[361] A. Oliveros and C.J. Rodríguez, *Inflation in a scalar–vector–tensor theory*, *Gen. Rel. Grav.* **54** (2022) 9 [2201.03629].

[362] V.I. Sabla and R.R. Caldwell, *Microphysics of early dark energy*, *Phys. Rev. D* **106** (2022) 063526 [2202.08291].

[363] Virgo, LIGO Scientific collaboration, *GW170814: A Three-Detector Observation of Gravitational Waves from a Binary Black Hole Coalescence*, *Phys. Rev. Lett.* **119** (2017) 141101 [1709.09660].

[364] N. Frusciante, S. Peirone, S. Casas and N.A. Lima, *Cosmology of surviving Horndeski theory: The road ahead*, *Phys. Rev. D* **99** (2019) 063538 [1810.10521].

[365] R. McManus, L. Lombriser and J. Peñarrubia, *Finding Horndeski theories with Einstein gravity limits*, *JCAP* **1611** (2016) 006 [1606.03282].

[366] L. Lombriser and A. Taylor, *Breaking a Dark Degeneracy with Gravitational Waves*, *JCAP* **1603** (2016) 031 [1509.08458].

[367] J. Noller and A. Nicola, *Cosmological parameter constraints for Horndeski scalar-tensor gravity*, *Phys. Rev. D* **99** (2019) 103502 [1811.12928].

[368] C. de Rham and S. Melville, *Gravitational Rainbows: LIGO and Dark Energy at its Cutoff*, *Phys. Rev. Lett.* **121** (2018) 221101 [1806.09417].

[369] D.J.C. MacKay, *Information theory, inference, and learning algorithms*, Cambridge University Press (2003).

[370] A.E. Romano and S.A. Vallejo Pena, *The MESS of cosmological perturbations*, *Phys. Lett. B* **784** (2018) 367 [1806.01941].

[371] W. Cardona, L. Hollenstein and M. Kunz, *The traces of anisotropic dark energy in light of Planck*, *JCAP* **1407** (2014) 032 [1402.5993].

[372] S. Tsujikawa, *Matter density perturbations and effective gravitational constant in modified gravity models of dark energy*, Phys. Rev. **D76** (2007) 023514 [0705.1032].

[373] SDSS collaboration, *The 3-D power spectrum of galaxies from the SDSS*, Astrophys. J. **606** (2004) 702 [astro-ph/0310725].

[374] B. Sagredo, S. Nesseris and D. Sapone, *Internal Robustness of Growth Rate data*, Phys. Rev. D **98** (2018) 083543 [1806.10822].

[375] R. Bean and O. Dore, *Probing dark energy perturbations: The Dark energy equation of state and speed of sound as measured by WMAP*, Phys. Rev. **D69** (2004) 083503 [astro-ph/0307100].

[376] CANTATA collaboration, Y. Akrami et al., *Modified Gravity and Cosmology: An Update by the CANTATA Network*, Springer (2021), 10.1007/978-3-030-83715-0, [2105.12582].

[377] LIGO Scientific, Virgo collaboration, *GW170814: A Three-Detector Observation of Gravitational Waves from a Binary Black Hole Coalescence*, Phys. Rev. Lett. **119** (2017) 141101 [1709.09660].

[378] Planck collaboration, *Planck 2015 results. XIV. Dark energy and modified gravity*, Astron. Astrophys. **594** (2016) A14 [1502.01590].

[379] LIGO Scientific, Virgo collaboration, *Tests of general relativity with GW150914*, Phys. Rev. Lett. **116** (2016) 221101 [1602.03841].

[380] A. De Felice and S. Tsujikawa, *f(R) theories*, Living Rev. Rel. **13** (2010) 3 [1002.4928].

[381] L. Pogosian and A. Silvestri, *The pattern of growth in viable f(R) cosmologies*, Phys. Rev. D **77** (2008) 023503 [0709.0296].

[382] J. Pérez-Romero and S. Nesseris, *Cosmological constraints and comparison of viable $f(R)$ models*, Phys. Rev. D **97** (2018) 023525 [1710.05634].

[383] C. Álvarez Luna, S. Basilakos and S. Nesseris, *Cosmological constraints on γ-gravity models*, Phys. Rev. D **98** (2018) 023516 [1805.02926].

[384] S. Nesseris, *The Effective Fluid approach for Modified Gravity and its applications*, Universe **9** (2023) 2022 [2212.12768].

[385] J.K. Bloomfield, E.E. Flanagan, M. Park and S. Watson, *Dark energy or modified gravity? An effective field theory approach*, JCAP **08** (2013) 010 [1211.7054].

[386] N. Frusciante and L. Perenon, *Effective field theory of dark energy: A review*, *Phys. Rept.* **857** (2020) 1 [1907.03150].

[387] J. Noller, F. von Braun-Bates and P.G. Ferreira, *Relativistic scalar fields and the quasistatic approximation in theories of modified gravity*, *Phys. Rev. D* **89** (2014) 023521 [1310.3266].

[388] A. Silvestri, L. Pogosian and R.V. Buniy, *Practical approach to cosmological perturbations in modified gravity*, *Phys. Rev. D* **87** (2013) 104015 [1302.1193].

[389] S. Bose, W.A. Hellwing and B. Li, *Testing the quasi-static approximation in $f(R)$ gravity simulations*, *JCAP* **02** (2015) 034 [1411.6128].

[390] E. Bellini and I. Sawicki, *Maximal freedom at minimum cost: linear large-scale structure in general modifications of gravity*, *JCAP* **07** (2014) 050 [1404.3713].

[391] J. Gleyzes, D. Langlois and F. Vernizzi, *A unifying description of dark energy*, *Int. J. Mod. Phys. D* **23** (2015) 1443010 [1411.3712].

[392] I. Sawicki and E. Bellini, *Limits of quasistatic approximation in modified-gravity cosmologies*, *Phys. Rev. D* **92** (2015) 084061 [1503.06831].

[393] L. Pogosian and A. Silvestri, *What can cosmology tell us about gravity? Constraining Horndeski gravity with Σ and μ*, *Phys. Rev. D* **94** (2016) 104014 [1606.05339].

[394] A. De Felice, L. Heisenberg, R. Kase, S. Mukohyama, S. Tsujikawa and Y.-l. Zhang, *Effective gravitational couplings for cosmological perturbations in generalized Proca theories*, *Phys. Rev. D* **94** (2016) 044024 [1605.05066].

[395] A. de la Cruz-Dombriz, A. Dobado and A.L. Maroto, *On the evolution of density perturbations in f(R) theories of gravity*, *Phys. Rev. D* **77** (2008) 123515 [0802.2999].

[396] C. Llinares and D.F. Mota, *Cosmological simulations of screened modified gravity out of the static approximation: effects on matter distribution*, *Phys. Rev. D* **89** (2014) 084023 [1312.6016].

[397] T. Multamaki and I. Vilja, *Cosmological expansion and the uniqueness of gravitational action*, *Phys. Rev. D* **73** (2006) 024018 [astro-ph/0506692].

[398] A. de la Cruz-Dombriz and A. Dobado, *A f(R) gravity without cosmological constant*, *Phys. Rev. D* **74** (2006) 087501 [gr-qc/0607118].

[399] W. Hu and I. Sawicki, *A Parameterized Post-Friedmann Framework for Modified Gravity*, *Phys. Rev.* **D76** (2007) 104043 [0708.1190].

[400] S. Capozziello, V.F. Cardone and A. Troisi, *Reconciling dark energy models with f(R) theories*, *Phys. Rev. D* **71** (2005) 043503 [astro-ph/0501426].

[401] S. Nojiri and S.D. Odintsov, *Modified f(R) gravity consistent with realistic cosmology: From matter dominated epoch to dark energy universe*, *Phys. Rev. D* **74** (2006) 086005 [hep-th/0608008].

[402] S. Basilakos, S. Nesseris and L. Perivolaropoulos, *Observational constraints on viable f(R) parametrizations with geometrical and dynamical probes*, *Phys. Rev. D* **87** (2013) 123529 [1302.6051].

[403] S. Dodelson and F. Schmidt, *Modern Cosmology*, Elsevier Science (2020).

[404] L. Amendola, R. Gannouji, D. Polarski and S. Tsujikawa, *Conditions for the cosmological viability of f(R) dark energy models*, *Phys. Rev. D* **75** (2007) 083504 [gr-qc/0612180].

[405] D. Sapone and M. Kunz, *Fingerprinting Dark Energy*, *Phys. Rev. D* **80** (2009) 083519 [0909.0007].

[406] A.A. Starobinsky, *Disappearing cosmological constant in f(R) gravity*, *JETP Lett.* **86** (2007) 157 [0706.2041].

[407] D. Sapone, E. Majerotto, M. Kunz and B. Garilli, *Can dark energy viscosity be detected with the Euclid survey?*, *Phys. Rev. D* **88** (2013) 043503 [1305.1942].

[408] M. Kunz, *The phenomenological approach to modeling the dark energy*, *Comptes Rendus Physique* **13** (2012) 539 [1204.5482].

[409] I.D. Saltas and M. Kunz, *Anisotropic stress and stability in modified gravity models*, *Phys. Rev. D* **83** (2011) 064042 [1012.3171].

[410] W. Hu, *Structure formation with generalized dark matter*, *Astrophys. J.* **506** (1998) 485 [astro-ph/9801234].

[411] A.R. Liddle and D.H. Lyth, *Cosmological Inflation and Large-Scale Structure*, Cambridge University Press, New York (2000), 10.1017/CBO9781139175180.

[412] N.E. Groeneboom, L. Ackerman, I.K. Wehus and H.K. Eriksen, *Bayesian analysis of an anisotropic universe model: systematics and polarization*, Astrophys. J. **722** (2010) 452 [0911.0150].

[413] J. Kim and E. Komatsu, *Limits on anisotropic inflation from the Planck data*, Phys. Rev. **D88** (2013) 101301 [1310.1605].

[414] S.R. Ramazanov and G. Rubtsov, *Constraining anisotropic models of the early Universe with WMAP9 data*, Phys.Rev. **D89** (2014) 043517 [1311.3272].

[415] Planck collaboration, *Planck 2015 results. XVI. Isotropy and statistics of the CMB*, Astron. Astrophys. **594** (2016) A16 [1506.07135].

[416] Planck collaboration, *Planck 2013 results. XXII. Constraints on inflation*, Astron. Astrophys. **571** (2014) A22 [1303.5082].

[417] R. Namba, E. Dimastrogiovanni and M. Peloso, *Gauge-flation confronted with Planck*, JCAP **11** (2013) 045 [1308.1366].

[418] J.F. Rodriguez and Y. Rodriguez, *Analysis of Vector-Inflation Models Using Dynamical Systems*, Nucl. Part. Phys. Proc. **267-269** (2015) 257 [1504.02433].

[419] V.K. Oikonomou, *Autonomous dynamical system approach for inflationary Gauss–Bonnet modified gravity*, Int. J. Mod. Phys. D **27** (2018) 1850059 [1711.03389].

[420] WMAP collaboration, *Seven-Year Wilkinson Microwave Anisotropy Probe (WMAP) Observations: Cosmological Interpretation*, Astrophys. J. Suppl. **192** (2011) 18 [1001.4538].

[421] L. Heisenberg, R. Kase and S. Tsujikawa, *Anisotropic cosmological solutions in massive vector theories*, JCAP **11** (2016) 008 [1607.03175].

[422] D.H. Lyth and D. Wands, *Generating the curvature perturbation without an inflaton*, Phys. Lett. B **524** (2002) 5 [hep-ph/0110002].

[423] K. Dimopoulos, *Can a vector field be responsible for the curvature perturbation in the Universe?*, Phys. Rev. D **74** (2006) 083502 [hep-ph/0607229].

[424] K. Dimopoulos and M. Karciauskas, *Non-minimally coupled vector curvaton*, JHEP **0807** (2008) 119 [0803.3041].

[425] K. Dimopoulos, M. Karciauskas, D.H. Lyth and Y. Rodriguez, *Statistical anisotropy of the curvature perturbation from vector field perturbations*, *JCAP* **0905** (2009) 013 [0809.1055].

[426] K. Dimopoulos, M. Karciauskas and J.M. Wagstaff, *Vector Curvaton with varying Kinetic Function*, *Phys.Rev.* **D81** (2010.) 023522 [0907.1838].

[427] K. Dimopoulos, M. Karciauskas and J.M. Wagstaff, *Vector Curvaton without Instabilities*, *Phys.Lett.* **B683** (2010.) 298 [0909.0475].

[428] K. Dimopoulos, *Statistical Anisotropy and the Vector Curvaton Paradigm*, *Int.J.Mod.Phys.* **D21** (2012) 1250023 [1107.2779].

[429] A.A. Navarro and Y. Rodriguez, *The Vector Curvaton*, *AIP Conf.Proc.* **1548** (2013.) 277 [1305.7425].

[430] M. Karciauskas and D.H. Lyth, *On the health of a vector field with* $(RA^2)/6$ *coupling to gravity*, *JCAP* **1011** (2010) 023 [1007.1426].

[431] J.M. Wagstaff and K. Dimopoulos, *Particle Production of Vector Fields: Scale Invariance is Attractive*, *Phys.Rev.* **D83** (2011) 023523 [1011.2517].

[432] L. Ackerman, S.M. Carroll and M.B. Wise, *Imprints of a Primordial Preferred Direction on the Microwave Background*, *Phys.Rev.* **D75** (2007) 083502 [astro-ph/0701357].

[433] Planck collaboration, *Planck 2015 results. XVI. Isotropy and statistics of the CMB*, *Astron. Astrophys.* **594** (2016) A16 [1506.07135].

[434] A. Golovnev, V.F. Mukhanov and V. Vanchurin, *Vector Inflation*, *JCAP* **0806** (2008.) 009 [0802.2068].

[435] A. Golovnev and V. Vanchurin, *Cosmological perturbations from vector inflation*, *Phys.Rev.* **D79** (2009) 103524 [0903.2977].

[436] A. Golovnev, *Linear perturbations in vector inflation and stability issues*, *Phys.Rev.* **D81** (2010) 023514 [0910.0173].

[437] A. Golovnev, *On cosmic inflation in vector field theories*, *Class. Quant. Grav.* **28** (2011) 245018 [1109.4838].

[438] R. Emami, S. Mukohyama, R. Namba and Y.-l. Zhang, *Stable solutions of inflation driven by vector fields*, *JCAP* **03** (2017) 058 [1612.09581].

[439] A. Maleknejad, M. Sheikh-Jabbari and J. Soda, *Gauge Fields and Inflation*, Phys.Rept. **528** (2013) 161 [1212.2921].

[440] A. Maleknejad and M. Sheikh-Jabbari, *Non-Abelian Gauge Field Inflation*, Phys.Rev. **D84** (2011) 043515 [1102.1932].

[441] A. Maleknejad and M. Sheikh-Jabbari, *Gauge-flation: Inflation From Non-Abelian Gauge Fields*, Phys.Lett. **B723** (2013) 224 [1102.1513].

[442] B. Himmetoglu, C.R. Contaldi and M. Peloso, *Instability of anisotropic cosmological solutions supported by vector fields*, Phys.Rev.Lett. **102** (2009) 111301 [0809.2779].

[443] B. Himmetoglu, C.R. Contaldi and M. Peloso, *Instability of the ACW model, and problems with massive vectors during inflation*, Phys.Rev. **D79** (2009) 063517 [0812.1231].

[444] B. Himmetoglu, C.R. Contaldi and M. Peloso, *Ghost instabilities of cosmological models with vector fields nonminimally coupled to the curvature*, Phys.Rev. **D80** (2009) 123530 [0909.3524].

[445] S. Tsujikawa, M. Sami and R. Maartens, *Observational constraints on braneworld inflation: The Effect of a Gauss-Bonnet term*, Phys. Rev. D **70** (2004) 063525 [astro-ph/0406078].

[446] B.M. Carter and I.P. Neupane, *Towards inflation and dark energy cosmologies from modified Gauss-Bonnet theory*, JCAP **0606** (2006.) 004 [hep-th/0512262].

[447] M. Satoh and J. Soda, *Higher Curvature Corrections to Primordial Fluctuations in Slow-roll Inflation*, JCAP **0809** (2008) 019 [0806.4594].

[448] Z.-K. Guo and D.J. Schwarz, *Power spectra from an inflaton coupled to the Gauss-Bonnet term*, Phys.Rev. **D80** (2009) 063523 [0907.0427].

[449] J. Sadeghi, M.R. Setare and A. Banijamali, *Non-minimal Maxwell-Modified Gauss-Bonnet Cosmologies: Inflation and Dark Energy*, Eur.Phys.J. **C64** (2009) 433 [0906.0713].

[450] Z.-K. Guo and D.J. Schwarz, *Slow-roll inflation with a Gauss-Bonnet correction*, Phys.Rev. **D81** (2010) 123520 [1001.1897].

[451] M. Satoh, *Slow-roll Inflation with the Gauss-Bonnet and Chern-Simons Corrections*, JCAP **1011** (2010) 024 [1008.2724].

[452] P.-X. Jiang, J.-W. Hu and Z.-K. Guo, *Inflation coupled to a Gauss-Bonnet term*, Phys.Rev. **D88** (2013) 123508 [1310.5579].

[453] K. Nozari and N. Rashidi, *DBI inflation with a nonminimally coupled Gauss-Bonnet term*, Phys.Rev. **D88** (2013) 084040 [1310.3989].

[454] S. Koh, B.-H. Lee, W. Lee and G. Tumurtushaa, *Observational constraints on slow-roll inflation coupled to a Gauss-Bonnet term*, Phys. Rev. D **90** (2014) 063527 [1404.6096].

[455] N. Okada and S. Okada, *Simple inflationary models in Gauss–Bonnet brane-world cosmology*, Class. Quant. Grav. **33** (2016) 125034 [1412.8466].

[456] P. Kanti, R. Gannouji and N. Dadhich, *Gauss-Bonnet Inflation*, Phys. Rev. **D92** (2015) 041302 [1503.01579].

[457] C. van de Bruck and C. Longden, *Higgs Inflation with a Gauss-Bonnet term in the Jordan Frame*, Phys. Rev. D **93** (2016) 063519 [1512.04768].

[458] C. van de Bruck, K. Dimopoulos and C. Longden, *Reheating in Gauss-Bonnet-coupled inflation*, Phys. Rev. D **94** (2016) 023506 [1605.06350].

[459] S. Koh, B.-H. Lee and G. Tumurtushaa, *Reconstruction of the Scalar Field Potential in Inflationary Models with a Gauss-Bonnet term*, Phys. Rev. D **95** (2017) 123509 [1610.04360].

[460] J. Mathew and S. Shankaranarayanan, *Low scale Higgs inflation with Gauss–Bonnet coupling*, Astropart. Phys. **84** (2016) 1 [1602.00411].

[461] I.V. Fomin and S.V. Chervon, *A new approach to exact solutions construction in scalar cosmology with a Gauss–Bonnet term*, Mod. Phys. Lett. A **32** (2017) 1750129 [1704.07786].

[462] Z. Yi, Y. Gong and M. Sabir, *Inflation with Gauss-Bonnet coupling*, Phys. Rev. D **98** (2018) 083521 [1804.09116].

[463] L. Granda and D. Jimenez, *Slow-Roll Inflation with Exponential Potential in Scalar-Tensor Models*, Eur. Phys. J. C **79** (2019) 772 [1907.06806].

[464] D. Jimenez, L. Granda and E. Elizalde, *Cosmology in a model with Lagrange multiplier, Gauss–Bonnet and nonminimal kinetic couplings*, Int. J. Mod. Phys. D **28** (2019) 1950171 [1909.09746].

[465] K. Kleidis and V. Oikonomou, *A Study of an Einstein Gauss-Bonnet Quintessential Inflationary Model*, Nucl. Phys. B **948** (2019) 114765 [1909.05318].

[466] I. Fomin, *Gauss–Bonnet term corrections in scalar field cosmology*, Eur. Phys. J. C **80** (2020) 1145 [2004.08065].

[467] E.O. Pozdeeva, *Generalization of cosmological attractor approach to Einstein–Gauss–Bonnet gravity*, Eur. Phys. J. C **80** (2020) 612 [2005.10133].

[468] N. Rashidi and K. Nozari, *Gauss-Bonnet Inflation after Planck2018*, Astrophys. J. **890** (2020) 58 [2001.07012].

[469] K. Bamba and S.D. Odintsov, *Inflation and late-time cosmic acceleration in non-minimal Maxwell-$F(R)$ gravity and the generation of large-scale magnetic fields*, JCAP **0804** (2008) 024 [0801.0954].

[470] A. Oliveros, *Slow-roll inflation from massive vector fields non-minimally coupled to gravity*, Astrophys. Space Sci. **362** (2017) 19 [1612.06377].

[471] K. Dimopoulos, *Can a vector field be responsible for the curvature perturbation in the Universe?*, Phys.Rev. **D74** (2006) 083502 [hep-ph/0607229].

[472] A.A. Starobinsky, *Multicomponent de Sitter (Inflationary) Stages and the Generation of Perturbations*, *JETP Lett.* **42** (1985) 152.

[473] M. Sasaki and E.D. Stewart, *A general analytic formula for the spectral index of the density perturbations produced during inflation*, Prog.Theor.Phys. **95** (1996) 71 [astro-ph/9507001].

[474] D.H. Lyth, K.A. Malik and M. Sasaki, *A General proof of the conservation of the curvature perturbation*, JCAP **0505** (2005) 004 [astro-ph/0411220].

[475] D.H. Lyth and Y. Rodriguez, *The Inflationary prediction for primordial non-Gaussianity*, Phys.Rev.Lett. **95** (2005.) 121302 [astro-ph/0504045].

[476] S. Nojiri, S.D. Odintsov and M. Sasaki, *Gauss-Bonnet dark energy*, Phys. Rev. D **71** (2005) 123509 [hep-th/0504052].

[477] BOSS collaboration, *The clustering of galaxies in the completed SDSS-III Baryon Oscillation Spectroscopic Survey: cosmological analysis of the DR12 galaxy sample*, Mon. Not. Roy. Astron. Soc. **470** (2017) 2617 [1607.03155].

[478] S. Dodelson and F. Schmidt, *Modern Cosmology*, Elsevier Science (2020).

[479] D. Blas, J. Lesgourgues and T. Tram, *The cosmic linear anisotropy solving system (CLASS). part II: Approximation schemes*, *Journal of Cosmology and Astroparticle Physics* **2011** 034.

[480] J.M. Bardeen, J.R. Bond, N. Kaiser and A.S. Szalay, *The Statistics of Peaks of Gaussian Random Fields*, *Astrophys. J.* **304** (1986) 15.

[481] M.S. Turner, *The Road to Precision Cosmology*, *Annual Review of Nuclear and Particle Science* **72** (2022) 1 [2201.04741].

[482] D.J. Eisenstein and W. Hu, *Baryonic features in the matter transfer function*, *Astrophys. J.* **496** (1998) 605 [astro-ph/9709112].

[483] D. Boyanovsky, H.J. de Vega and N.G. Sanchez, *The dark matter transfer function: free streaming, particle statistics and memory of gravitational clustering*, *Phys. Rev. D* **78** (2008) 063546 [0807.0622].

[484] A. Dvornik et al., *KiDS-1000: Combined halo-model cosmology constraints from galaxy abundance, galaxy clustering and galaxy-galaxy lensing*, *A&A* **675** (2023) A189 [2210.03110].

[485] N. Schöneberg, L. Verde, H. Gil-Marín and S. Brieden, *BAO+BBN revisited — growing the Hubble tension with a 0.7 km/s/Mpc constraint*, *JCAP* **11** (2022) 039 [2209.14330].

[486] G. Carleo et al., *Machine learning and the physical sciences*, *Rev. Mod. Phys.* **91** (2019) 045002 [1903.10563].

[487] M. Schmidt and H. Lipson, *Distilling Free-Form Natural Laws from Experimental Data*, *Science* **324** (2009) 81.

[488] S.L. Brunton, J.L. Proctor and J.N. Kutz, *Discovering governing equations from data by sparse identification of nonlinear dynamical systems*, *Proceedings of the National Academy of Sciences* **113** (2016) 3932 [1509.03580].

[489] S.-M. Udrescu and M. Tegmark, *AI Feynman: a Physics-Inspired Method for Symbolic Regression*, *Sci. Adv.* **6** (2020) eaay2631 [1905.11481].

[490] Z. Liu and M. Tegmark, *Machine Learning Hidden Symmetries*, *Phys. Rev. Lett.* **128** (2022) 180201 [2109.09721].

[491] J. Koza and J. Koza, *Genetic Programming: On the Programming of Computers by Means of Natural Selection*, Bradford (1992).

[492] R. Arjona and S. Nesseris, *Hints of dark energy anisotropic stress using Machine Learning*, JCAP **11** (2020) 042 [2001.11420].

[493] EUCLID collaboration, *Euclid: Forecast constraints on the cosmic distance duality relation with complementary external probes*, Astron. Astrophys. **644** (2020) A80 [2007.16153].

[494] R. Arjona and S. Nesseris, *Novel null tests for the spatial curvature and homogeneity of the Universe and their machine learning reconstructions*, Phys. Rev. D **103** (2021) 103539 [2103.06789].

[495] EUCLID collaboration, *Euclid: Constraining dark energy coupled to electromagnetism using astrophysical and laboratory data*, Astron. Astrophys. **654** (2021) A148 [2105.09746].

[496] A. Aizpuru, R. Arjona and S. Nesseris, *Machine learning improved fits of the sound horizon at the baryon drag epoch*, Phys. Rev. D **104** (2021) 043521 [2106.00428].

[497] EUCLID collaboration, *Euclid: Forecast constraints on consistency tests of the ΛCDM model*, Astron. Astrophys. **660** (2022) A67 [2110.11421].

[498] G. Alestas, L. Kazantzidis and S. Nesseris, *Machine learning constraints on deviations from general relativity from the large scale structure of the Universe*, Phys. Rev. D **106** (2022) 103519 [2209.12799].

[499] B.C. Allanach, D. Grellscheid and F. Quevedo, *Genetic algorithms and experimental discrimination of SUSY models*, JHEP **07** (2004) 069 [hep-ph/0406277].

[500] Y. Akrami, P. Scott, J. Edsjo, J. Conrad and L. Bergstrom, *A Profile Likelihood Analysis of the Constrained MSSM with Genetic Algorithms*, JHEP **04** (2010) 057 [0910.3950].

[501] X.-L. Luo, J. Feng and H.-H. Zhang, *A genetic algorithm for astroparticle physics studies*, Comput. Phys. Commun. **250** (2020) 106818 [1907.01090].

[502] M. Ho et al., *A Robust and Efficient Deep Learning Method for Dynamical Mass Measurements of Galaxy Clusters*, Astrophys. J. **887** (2019) 25 [1902.05950].

[503] C. Bogdanos and S. Nesseris, *Genetic Algorithms and Supernovae Type Ia Analysis*, JCAP **05** (2009) 006 [0903.2805].

[504] S. Nesseris and A. Shafieloo, *A model independent null test on the cosmological constant*, Mon. Not. Roy. Astron. Soc. **408** (2010) 1879 [1004.0960].

[505] S. Nesseris and J. Garcia-Bellido, *A new perspective on Dark Energy modeling via Genetic Algorithms*, JCAP **11** (2012) 033 [1205.0364].

[506] S. Nesseris and J. García-Bellido, *Comparative analysis of model-independent methods for exploring the nature of dark energy*, Phys. Rev. D **88** (2013) 063521 [1306.4885].

[507] D. Sapone, E. Majerotto and S. Nesseris, *Curvature versus distances: Testing the FLRW cosmology*, Phys. Rev. D **90** (2014) 023012 [1402.2236].

[508] R. Arjona and S. Nesseris, *What can Machine Learning tell us about the background expansion of the Universe?*, Phys. Rev. D **101** (2020) 123525 [1910.01529].

[509] B.A. Reid. et al., *Cosmological constraints from the clustering of the Sloan Digital Sky Survey DR7 luminous red galaxies*, Mon. Not. Roy. Astron. Soc. **404** (2010) 60 [0907.1659].

[510] A. Díaz Rivero, C. Dvorkin, F.-Y. Cyr-Racine, J. Zavala and M. Vogelsberger, *Gravitational Lensing and the Power Spectrum of Dark Matter Substructure: Insights from the ETHOS N-body Simulations*, Phys. Rev. D **98** (2018) 103517 [1809.00004].

[511] S. Chabanier, M. Millea and N. Palanque-Delabrouille, *Matter power spectrum: from Lyα forest to CMB scales*, Mon. Not. Roy. Astron. Soc. **489** (2019) 2247 [1905.08103].

[512] J. Lesgourgues, G. Mangano, G. Miele and S. Pastor, *Neutrino Cosmology*, Cambridge University Press (2, 2013).

[513] KATRIN collaboration, *Direct neutrino-mass measurement with sub-electronvolt sensitivity*, Nature Phys. **18** (2022) 160 [2105.08533].

[514] D.J. Eisenstein and W. Hu, *Power spectra for cold dark matter and its variants*, Astrophys. J. **511** (1997) 5 [astro-ph/9710252].

[515] J.R. Bond and A.S. Szalay, *The collisionless damping of density fluctuations in an expanding universe*, Astrophys. J., Lett. Ed. **274** (1983) 443.

[516] J.R. Bond and G. Efstathiou, *Cosmic background radiation anisotropies in universes dominated by nonbaryonic dark matter*, Astrophys. J., Lett. Ed. **285** (1984) L45.

[517] E.W. Kolb and M.S. Turner, *The Early Universe*, vol. 69, Front. Phys. (1990), 10.1201/9780429492860.

[518] F. Renzi, N.B. Hogg, M. Martinelli and S. Nesseris, *Strongly lensed supernovae as a self-sufficient probe of the distance duality relation*, *Phys. Dark Univ.* **32** (2021) 100824 [2010.04155].

[519] R. Arjona, H.-N. Lin, S. Nesseris and L. Tang, *Machine learning forecasts of the cosmic distance duality relation with strongly lensed gravitational wave events*, *Phys. Rev. D* **103** (2021) 103513 [2011.02718].

[520] R. Arjona, A. Melchiorri and S. Nesseris, *Testing the* Λ*CDM paradigm with growth rate data and machine learning*, *JCAP* **05** (2022) 047 [2107.04343].

[521] D. Vallés-Pérez, S. Planelles, O. Monllor-Berbegal and V. Quilis, *On the choice of the most suitable indicator for the assembly state of dark matter haloes through cosmic time*, *Mon. Not. Roy. Astron. Soc.* **519** (2023) 6111 [2301.02253].

[522] J.-E. Campagne et al., *JAX-COSMO: An End-to-End Differentiable and GPU Accelerated Cosmology Library*, *Open J. Astrophys.* **6** (2023) 1 [2302.05163].

[523] G.C. Petter et al., *Host Dark Matter Halos of Wide-field Infrared Survey Explorer-selected Obscured and Unobscured Quasars: Evidence for Evolution*, *Astrophys. J.* **946** (2023) 27 [2302.00690].

[524] Euclid collaboration, *Euclid Preparation. XXVIII. Forecasts for ten different higher-order weak lensing statistics*, *Astron. Astrophys.* **675** (2023) A120 [2301.12890].

[525] L.R. Prole et al., *From dark matter halos to pre-stellar cores: high resolution follow-up of cosmological Lyman–Werner simulations*, *Mon. Not. Roy. Astron. Soc.* **520** (2023) 2081 [2301.00828].

[526] A. Variu et al., *Cosmic void exclusion models and their impact on the distance scale measurements from large-scale structure*, *Mon. Not. Roy. Astron. Soc.* **521** (2023) 4731 [2211.04328].

[527] G. Hütsi, M. Raidal, J. Urrutia, V. Vaskonen and H. Veermäe, *Did JWST observe imprints of axion miniclusters or primordial black holes?*, *Phys. Rev. D* **107** (2023) 043502 [2211.02651].

[528] E. Bellini, I. Sawicki and M. Zumalacárregui, *hi_class: Background Evolution, Initial Conditions and Approximation Schemes*, *JCAP* **02** (2020) 008 [1909.01828].

[529] T. Baker and P. Bull, *Observational signatures of modified gravity on ultra-large scales*, *Astrophys. J.* **811** (2015) 116 [1506.00641].

[530] D. Sapone and E. Majerotto, *Fingerprinting Dark Energy III: distinctive marks of viscosity*, Phys. Rev. D **85** (2012) 123529 [1203.2157].

[531] E. Bellini, A.J. Cuesta, R. Jimenez and L. Verde, *Constraints on deviations from ΛCDM within Horndeski gravity*, JCAP **02** (2016) 053 [1509.07816].

[532] DES collaboration, *Dark Energy Survey Year 1 Results: Constraints on Extended Cosmological Models from Galaxy Clustering and Weak Lensing*, Phys. Rev. D **99** (2019) 123505 [1810.02499].

[533] Euclid collaboration, *Euclid preparation. VII. Forecast validation for Euclid cosmological probes*, Astron. Astrophys. **642** (2020) A191 [1910.09273].